

THE EFFECTS OF PROGRAMME LOADING

ON

FATIGUE CRACK PROPAGATION

by

MIRZA KHAIRUZZAMAN, B.Sc.Engg.(Met.).

A thesis submitted for the degree of

DOCTOR OF PHILOSOPHY

of

The University of Aston in Birmingham

(U.K.)

THESIS
669.0192
KHA

28 Nov 73 167481

October 1973

Department of Metallurgy

SUMMARY

The object of the present research was to find and evaluate the effects of programme loading on fatigue crack propagation in EN24 steel. A potential drop technique was developed to measure very small changes in the crack length. The constant load amplitude test results, analysed on the basis of fracture mechanics, served as a basis for comparison with the results of the programme loading tests. The block programme loading schedules were designed to find the effects of load-interaction and stress levels on the crack propagation rate. Microscopic and fractographic examinations were conducted to understand the influence of micro-structures and strength levels on the fatigue fracture process.

The results showed that the micro-structural features of the three heat-treatments considered exerted a secondary influence on the crack growth rate. The capacity of the low strength ductile steels to accommodate large amount of strain at the crack-tip by plastic deformation and their ability to dissipate energy by numerous crack-branching and island formation were associated with the higher crack growth resistance of these steels as compared with the high strength martensitic steel. At any ΔK level, the crack growth rate was initially constant followed by a gradual slowing down which depended on the loading variables. With a growing fatigue crack at a constant ΔK , a decrease in the maximum stress caused a transient slow growth period whereas an increase in σ_{\max} did not show any appreciable acceleration of the crack growth rate. Based on a proposed mechanism of fatigue crack growth, an equation of the type $\frac{da}{dn} = \frac{A(\Delta K)^M}{R'}$, where $R' = \frac{\sigma_{ys}}{\sigma_{\max}}$, was found to unify the results of different loading conditions considered. This equation does not account for the slow growth periods and would, therefore, yield a conservative estimate of fatigue life.

<u>CONTENTS</u>		<u>Page</u>
1.	INTRODUCTION	1
2.	LITERATURE REVIEW	44
2.1	General Approach to Fatigue	4
2.1.1	Stress Approach	4
2.1.2	Fracture Mechanics Approach	5
2.1.2.1	The Plastic Zone Ahead of Crack Tip	9
2.2	Mechanisms of Crack Propagation	12
2.3	Laws of Crack Propagation	18
2.4	The Effects of Stress Level, Stress Ratio and Mean Stress	26
2.5	Micro-structural and Fractographic Aspects of Fatigue Crack Propagation	29
2.6	Fatigue Under Complex Load History	33
2.6.1	Introduction	33
2.6.2	Random Loading	35
2.6.3	Programme Loading	36
2.6.3.1	Effect of Load Interaction and Load Sequence	39
3.	EXPERIMENTAL WORK	51
3.1	Objectives	51
3.2	Material	51
3.2.1	Specimen Design and Testing Machine	51
3.2.2	Heat-treatments	53
3.2.3	Mechanical Properties	56
3.3	The Crack Growth Measurement Technique	58
3.4	Fatigue Crack Initiation	64
3.5	Constant Load Fatigue Tests	65
3.6	Programme Load Fatigue Tests	72

	<u>Page</u>	
3.7	General Method of Data Analysis	75
3.8	Other Experimental Work	75
3.9	Microscopic and Fractographic Study	77
4.	RESULTS	81
4.1	Initiation of Fatigue Crack	81
4.2	Constant Load Amplitude Test at Constant Mean Load	81
4.3	Programme Load Tests	82
4.3.1	Constant Load Amplitude with Varying Mean Load	82
4.3.2	Stepped Increase in Load Amplitude at Constant Mean Load	85
4.3.3	Two-Step Block Loading	93
4.3.4	Constant ΔK Tests at Constant K_{mean}	94
4.3.5	Constant ΔK Tests at Constant Mean Load	103
4.3.6	Constant ΔK Tests at Constant Maximum Load	103
4.3.7	Constant K_{max} with Increasing ΔK	108
4.3.8	Tests with ΔK Reductions at Constant Mean Load or Maximum Load	110
4.3.9	K_{mean} Reduction Tests	110
4.3.9.1	K_{mean} Reduction at Constant ΔK	110
4.3.9.2	K_{mean} Reduction Tests with Increased ΔK	118
4.3.10	Determination of Threshold ΔK	118
4.4	Other Results	120
4.5	Metallographic Observations	124
4.6	Fractographic Observations	133

	<u>Page</u>
5. DISCUSSION	147
5.1 Constant Load Tests	147
5.2 Constant Load Amplitude with Variable Mean Load	147
5.3 Stepped Increase in Load Amplitude	149
5.4 Two-Step Loading	149
5.5 Constant ΔK Tests at Constant K_{mean}	151
5.6 Constant ΔK Tests at Constant Mean Load and Maximum Load	161
5.7 Constant K_{max} with Increasing ΔK	163
5.8 ΔK Interaction Effect	163
5.9 K_{mean} Reduction Tests	164
5.10 COD Tests	171
5.11 The Effects of Stress Level	174
5.12 Microscopic and Fractographic Observations	178
5.13 A Proposed Mechanism of Fatigue Crack Propagation	182
5.14 Computer Prediction of Fatigue Life	201
6. CONCLUSIONS	205
RECOMMENDATIONS FOR FURTHER WORK	208
ACKNOWLEDGEMENTS	209
APPENDIX 1	210
APPENDIX 2	225
BIBLIOGRAPHY	227

1. INTRODUCTION

Fatigue failure of materials under fluctuating load has been a great concern to the designers of engineering components for a long time. A vast amount of research work has gone into evaluating the fatigue properties of a variety of metals and non-metals. The traditional approach to fatigue research is the determination of the fatigue strength of a material on the basis of number of cycles to failure under certain stress conditions. This merely tells the designer when the failure is going to occur. The major part of the fatigue life determined in this way might have been spent in crack initiation in some cases or in crack propagation in others.

In practice, all the commercially produced materials have inherent flaws such as cracks, inclusions and other stress-raisers and hence the crack initiation becomes of less importance. Many structures can be operated, with such flaws or fatigue cracks generated in them, until the cracks become long enough to cause failure. Thus, if it is possible to determine how far a crack has propagated in a structure, it could be possible to safeguard against failure. This fact, coupled with the advent of precise non-destructive testing methods, has given rise to the interest in evaluating the rate of propagation of a flaw in a component during fatigue loading and thence the total time available before catastrophic failure occurs. The inspection period can then be decided upon and any failure preventive measure can be taken. Consequently, investigations have been carried out on notched laboratory specimens and empirical equations developed to relate fatigue crack propagation rates with the stresses encountered by the specimens. However, these results could not be directly used in practical circumstances because of the geometrical differences between the real components and laboratory specimens.

In the past few years, the concept of Linear Elastic Fracture Mechanics (L.E.F.M.) has developed gradually. This considers K , the intensity of stress at a crack tip in a body as the singular factor determining the stress state for fracture. The fracture mechanics concept has been used to determine the crack propagation lives of notched specimens in the form of crack-growth-rate versus stress intensity range relations. A number of empirical equations based on the experimental data have thus been produced by different investigators. Some of these crack growth equations have found wide acceptance with the researchers in the field of fracture mechanics. The beauty of this approach is that the data generated on laboratory specimens can be related to real components through the use of a geometrical factor.

In general, the L.E.F.M. approach to fatigue crack propagation problems has shown a good deal of promise with a variety of steels and light aircraft materials under constant stress amplitude fatigue conditions.

The components in actual service generally undergo variable amplitude loading sequences. This random loading service spectrum can be approximated by a programmed loading sequence. ⁽⁹⁴⁾ This is done mainly for two reasons. Primarily, it enables to quantify the different variables involved in concrete terms. Secondly, the capabilities of ordinary fatigue machines can easily cope with it. Thus the programmed loading fatigue experiments are used to simulate the actual service conditions.

The present research was mainly aimed at evaluating the fatigue crack propagation characteristics of a low alloy steel under simple block programme loading using the fracture mechanics concept. The influence of interaction between different load amplitudes or mean loads on fatigue crack propagation life was the primary field of interest.

It was believed that if the mechanism of the fatigue crack propagation under programmed loading conditions could be well understood, then it could be easier to design against fatigue failures. With this view in mind, the detailed examination of the fracture surfaces and the fracture path in relation to the microstructural features were undertaken to understand the effects of heat-treatments and the resulting micro-structures on the fatigue crack-growth characteristics of the steel concerned.

2. LITERATURE REVIEW

2.1 General Approach to Fatigue

Through many years of investigation it has been well established that the fatigue failure of a structure or a component takes place in two stages, namely, fatigue crack initiation and its subsequent propagation. In the past, the design against fatigue failure was based on the number of cycles of stress required for crack initiation in a material. Recently the emphasis for the basis of design is shifting from crack initiation to the rate of propagation of crack in the material. This information helps in the determination of inspection intervals for a critical part of a structure and also in the calculation of the residual life before final failure would occur.

There are two general approaches to fatigue problems:

- (a) The stress approach.
- (b) The fracture mechanics approach.

The stress approach is the traditional approach to fatigue problems but the fracture mechanics approach is a fairly recent development.

2.1.1 Stress Approach

The stress approach to fatigue has been used for a good many years. It will be described only briefly. The data is generated on smooth or notched specimens and generally represented in the form of stress versus number of cycles to failure curves. The minimum stress amplitude at which the crack initiation does not occur in 10^7 cycles is considered as the *endurance* limit of the material and is applied to design with a factor of safety. The Goodman⁽¹⁾ diagram or different variations of it are used to take into account the effect of mean stress.

The crack propagation rates in notched specimens have also been related to the gross or net stress on the specimen through empirical equations. The basic disadvantage in this approach lies in the fact that the data generated on laboratory specimens cannot be directly related to the real service conditions.

2.1.2 Fracture Mechanics Approach

Sharp-crack fracture mechanics originated from a concept of crack propagation based on energy criterion put forward by A.A. Griffith⁽²⁾. Working with a brittle material, he postulated that a crack would propagate under the action of an external stress, if the energy used in creating new fracture surfaces is supplied from the released strain energy in the elastic solid. Thus, if a gross stress σ is applied at right angles to a centre crack of length $2a$ in a plate, the fracture stress under monotonic loading σ_f will be given by

$$\sigma_f = \left[\frac{2 E \gamma}{\pi a} \right]^{\frac{1}{2}} \quad \text{for plane stress} \quad \left. \vphantom{\sigma_f} \right\} \dots \quad (1)$$

$$\text{and } \sigma_f = \left[\frac{2 E \gamma}{\pi a (1-\nu^2)} \right]^{\frac{1}{2}} \quad \text{for plane strain}$$

Fracture will occur if $\sigma > \sigma_f$ or if $a > a_{\text{critical}}$ where a_{critical}

$$= \left[\frac{2 E \gamma}{\pi \sigma^2} \right]^{\frac{1}{2}} \quad \dots \text{ plane stress} \quad \text{or} \quad = \left[\frac{2 E \gamma}{\pi \sigma^2 (1-\nu^2)} \right]^{\frac{1}{2}} \quad \dots \text{ plane strain.}$$

Both Orowan⁽³⁾ and Irwin⁽⁴⁾ noted that in the case of ductile material, the Griffith type energy balance must be between the energy used in creating the new surface plus the work done in plastic deformation and the stored elastic energy in the solid. Since the work done in plastic deformation γ_p can greatly exceed the true surface energy γ , Irwin⁽⁵⁾ used the sum $\gamma + \gamma_p = G$, assuming that plastic working could be considered as a pseudo surface energy and hence the equation (1) can be written as :

$$\sigma = \left[\frac{E G}{\pi a} \right]^{\frac{1}{2}} \quad \dots \quad (2)$$

where G is the total work done per unit of crack extension and is called the strain energy release rate. For a certain crack length,

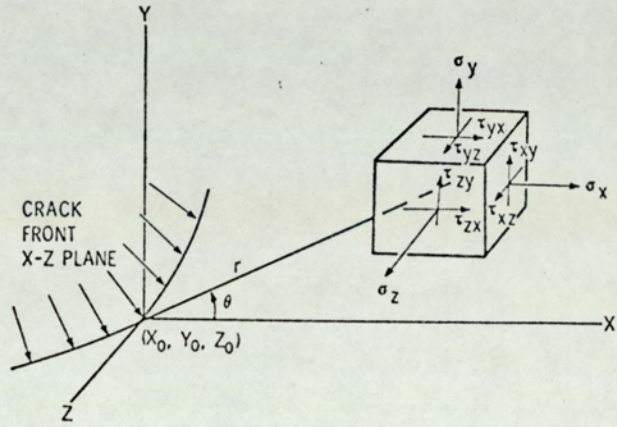
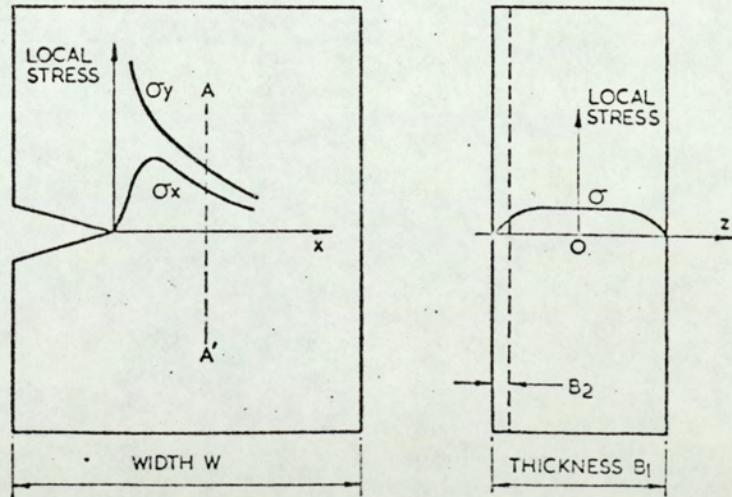


Fig 1—Stresses acting on element of material near a crack front.

(After Ref.74)



Variation of σ_y and σ_x across width. Elastic condition.

Section at AA', $\sigma_z = \nu(\sigma_y + \sigma_x)$. Variation of σ_z through the thickness at section AA'. Elastic condition.

Fig. 2

(After Ref.96)

at a certain critical value of $\sigma = \sigma_c$, instability will occur and G will be equal to G_c , the critical strain energy release rate which is a material property.

(6)

Paris and Sih **noted** that for the tensile mode of crack tip deformation, the stress field near the end of a centre crack of length $2a$ in an elastic solid (Fig.I) could be given by the equations

$$\left. \begin{aligned} \sigma_x &= \frac{K}{(2\pi r)^{\frac{1}{2}}} \cos \theta/2 (1 - \sin \theta/2 \cdot \sin 3\theta/2) \\ \sigma_y &= \frac{K}{(2\pi r)^{\frac{1}{2}}} \cos \theta/2 (1 + \sin \theta/2 \cdot \sin 3\theta/2) \\ \tau_{xy} &= \frac{K}{(2\pi r)^{\frac{1}{2}}} \cos \theta/2 \cdot \sin \theta/2 \cdot \cos 3\theta/2 \end{aligned} \right\} \dots (3)$$

$$\tau_{xz} = \tau_{yz} = 0, \quad \sigma_z = 0 \quad (\text{generalised plane stress})$$

$$\sigma_z = \nu (\sigma_x + \sigma_y) \quad (\text{Plane strain, } \nu \text{ is Poisson ratio})$$

In the above equation (r, θ) signifies the polar co-ordinates of a point in the stress field taking the crack tip as origin and K is called the stress intensity factor which is equal to $(EG)^{\frac{1}{2}}$ for plane stress and $(\frac{EG}{1-\nu})^{\frac{1}{2}}$ for plane strain. The elastic stress distribution is shown in (Fig. 2).

If $K = (EG)^{\frac{1}{2}}$ is substituted in equation (2), we get the stress intensity factor in a panel of infinite width

$$K = \sigma (\pi a)^{\frac{1}{2}} \quad \text{for plane stress} \quad \dots (4)$$

Since K is independent of the co-ordinates r and θ , it controls the intensity of the stress field but not the distribution, which is constant in the near tip region for all cracks.

For a specimen of finite width, the equation (4) is modified as

$$K = Y \sigma (a)^{\frac{1}{2}} \quad \dots (5)$$

where Y is called the compliance function and depends upon the crack length and specimen geometry. Through the work of Brown and Srawley⁽⁷⁾ boundary collacation approaches are now available to determine Y values for different specimen geometries. Experimental compliance calibration (8, 9, 10) is also possible. Through the use of this geometrical factor, the data generated from the laboratory tests can be used in the practical situations.

Subsequent to the development for montonic loading, L.E.F.M. found its application to fatigue as well. Substituting the σ term in the equation (5) by $\sigma_{min.}$, σ_{mean} , σ_{max} and $\Delta \sigma$, the corresponding stress intensity terms can be obtained. It has been demonstrated through works of different people⁽¹¹⁾ that the fatigue crack propagation rates in a variety of materials could be related to stress intensity factors by means of simple equations. The fracture mechanics approach is now widely used to evaluate the resistance of materials to fatigue crack propagation.

Linear Elastic Fracture Mechanics can be applied in cases of less ductile material where only small scale yielding occurs at the crack tip. To encompass the cases where the materials are very ductile and general yield has occurred in the specimen so that the measurement of applied stress has no meaning, an alternative measurable parameter called the crack opening displacement (C.O.D.) has been suggested by Wells⁽¹²⁾ and Cottrell⁽¹³⁾. Critical C.O.D. is the amount by which a crack opens before a final fracture and depends only on the local fracture ductility of the material. It is thus considered a material property and is directly related to a critical stress intensity factor.

Wells⁽¹⁴⁾ has shown that the basic equation relating to the linear elastic fracture mechanics and the general yield fracture mechanics is given by :

$$G = \sigma_{ys} \delta \dots (6)$$

where $\delta =$ C.O.D. at the crack tip.

Later Wells⁽¹⁵⁾ proposed that for monotonic loading condition

$$G_c = n \sigma_{ys} \delta_c \dots\dots (7)$$

where subscript c stands for the critical values and n is a plastic stress intensification factor at the crack tip which is approximately 1 for plane stress and 2 for plane strain condition.

By substituting the value of G_c in terms of stress intensity factor K_c in equation (7), we get,

$$\delta_c = \frac{K_c^2}{n E \sigma_{ys}} \dots\dots (8)$$

The critical C O D is measured by clip gauge or photographic method some times aided by a crack growth detection technique, such as ultrasonic⁽¹⁶⁾ or electrical potential method⁽¹⁷⁾.

More and more research workers are now using C O D as a parameter for evaluating fatigue crack propagation rates, but proper theoretical analysis for fatigue situations is not available as yet.

2.1.2.1. The plastic zone ahead of crack tip

Since the intensity of stress at the very crack tip approaches infinity according to the equation (3), localised yielding takes place as the stress reaches the yield level. A plastic zone thus develops, the shape and size of which depends on the stress system and the material properties. Depending on whether the specimen containing the crack is under plane stress or plane strain, the size of the plastic zone varies. Under plane stress conditions, yielding will occur when the applied stress reaches the yield stress of the material in uniaxial tension.

Thus substituting σ_{ys} in the equation (3) at $\theta = 0$, we get

$$r_y = \frac{1}{2 \pi} \left(\frac{K}{\sigma_{ys}} \right)^2 \text{ for plane stress} \dots\dots (9)$$

However, according to Rice⁽¹⁸⁾ due to stress redistribution, the plastic zone extends to a size w which is approximately equal to $2 r_y$.

In the case of plane strain conditions, due to the presence of σ_z stress, yielding criterion dictates that yielding would occur at a higher stress than the uniaxial yield stress. Irwin⁽¹⁹⁾ states that yield stress in plane strain can be approximated by $\sqrt{3} \sigma_{ys}$. Hence the equation (9) becomes,

$$r_y = \frac{1}{6\pi} \left(\frac{K}{\sigma_{ys}} \right)^2 \quad \text{for plane strain} \quad \dots \quad (10)$$

Paris⁽²⁰⁾ and Rice⁽¹⁸⁾ independently stated that the equations (9) and (10) do not apply to fatigue situations. Due to the presence of extreme stress concentration at the crack tip, plasticity is always present in the material. When the load is reversed as in the case of fatigue, plasticity occurs at the crack tip in the reversed sense. The new plastic zone starts to form within the old plastic zone from the maximum load.

Since to cause plasticity in the reversed direction the yield stress should be doubled, the new fatigue plastic zone size is approximated by

$$\left. \begin{aligned} r_y &= \frac{\Delta K^2}{2\pi (2\bar{\sigma}_{ys})^2} = \frac{1}{8\pi} \left(\frac{\Delta K}{\sigma_{ys}} \right)^2 \quad \text{for plane stress} \quad \dots \\ \text{and } r_y &= \frac{\Delta K^2}{2\pi (\sqrt{3} 2\sigma_{ys})^2} = \frac{1}{24\pi} \left(\frac{\Delta K}{\sigma_{ys}} \right)^2 \quad \text{for plane strain} \quad \dots \end{aligned} \right\} \quad (11)$$

For fatigue cycling with a stress amplitude of ΔP , the cyclic plastic zone depends on ΔP only and is independent of the maximum stress provided that no crack closure occurs during compressive part of the load cycle. The formation of the cyclic plastic zone within the maximum plastic zone is shown schematically in (Fig. 3).

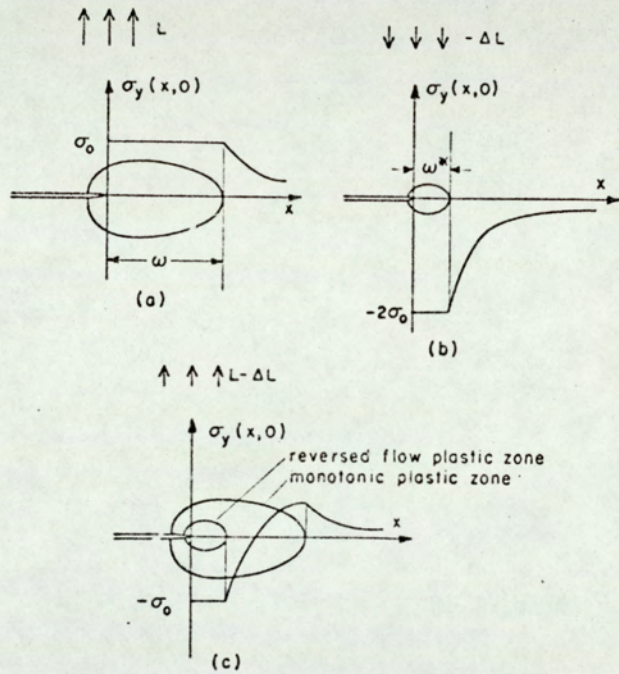


Fig. 3 —Plastic superposition for unloading. Adding (b) for load $-\Delta L$ with a doubled yield stress to (a) gives the solution (c) resulting after unloading from L to $L-\Delta L$. Reloading, $L-\Delta L$ to L , restores (a).

(After Ref.18)

Frost and Dugdale⁽²¹⁾ carried out fatigue tests on centrally cracked sheet specimens and concluded that the ratio of the length of the plastic zone to the crack length i.e. w/a is related to the maximum stress by smooth curve implying that the region at the yield stress during the maximum stress of ^{the} cycle will be dependent on the maximum stress. The same data was replotted by McClintock⁽²²⁾ as w/a against the ratio of applied stress to yield stress in shear and found that a functional relation existed. He concluded that if the fatigue crack growth is by progressive damage or renucleation ahead of the crack tip, the crack growth rate is proportional to the square of the plastic zone radius but if the propagation is by irreversible plastic deformation, the growth rate would vary as the first power of the plastic zone radius.

In cases of very ductile material, especially in plane stress situations, because of the presence of appreciable plasticity at the tip of a fatigue crack, a plastic zone correction factor equal to the radius of the plastic zone, needs to be added to the crack length to get an effective crack length. In a fatigue test, the size of the plastic zone can change depending on the geometry and the properties of the material tested if the state of stress changes from plane strain to plane stress as usually happens with sheet materials.

2.2 Mechanisms of Crack Propagation

Any metallic structure subjected to cyclic loading, undergoes considerable damage leading to final catastrophic failure. This fatigue failure has been found to take place in three stages.

- a) The initial damage occurring at a defect or a source of stress concentration leading to the nucleation of crack;
- b) The propagation of the crack
- c) The final failure through very fast fracture when the crack length reaches a critical size.

Each of these stages are effected by a number of variables, such as mechanical and physical properties of the material, the state, magnitude and interaction of the stresses. Since the initiation of fatigue crack is beyond the scope of this research, it will be only briefly dealt with.

The crack initiation is associated with cyclic slip (23, 24) and occupies a large percentage of fatigue life depending upon the stress amplitude for an un-notched specimen. The fatigue crack appears from the intensification of slip bands near the surface. The initiation of fatigue cracks from defects, inclusion or notches arises from the high stress concentration in those areas and constitutes a relatively shorter proportion of fatigue life. Yokobori et al⁽²⁵⁾ have reported a number of mechanisms of micro-crack formation. They observed that the number of micro-cracks initiated depended on the stress level.

The propagation of a fatigue crack takes place in two stages (26, 27).

(a) Stage I - micro-crack growth and (b) Stage II - macro-crack growth. The stage I crack growth occurs in crystallographic planes in response to the resolved shear stress. The growth tends to occur on planes approximately at 45° to the stress axis and the direction varies slightly from grain to grain. The micro-cracks generated during initiation period undergo a process of joining at stress level, which in turn determines the rate of Stage I crack propagation (25). The stage I crack propagation persists only through a few grains after which Stage II takes over.

The Stage II crack propagation occurs at 90° to the stress axis and fracture surface may have striation markings, characteristic to fatigue crack growth only, running more or less parallel to the crack front. The mechanisms for Stage II growth and the striation formation

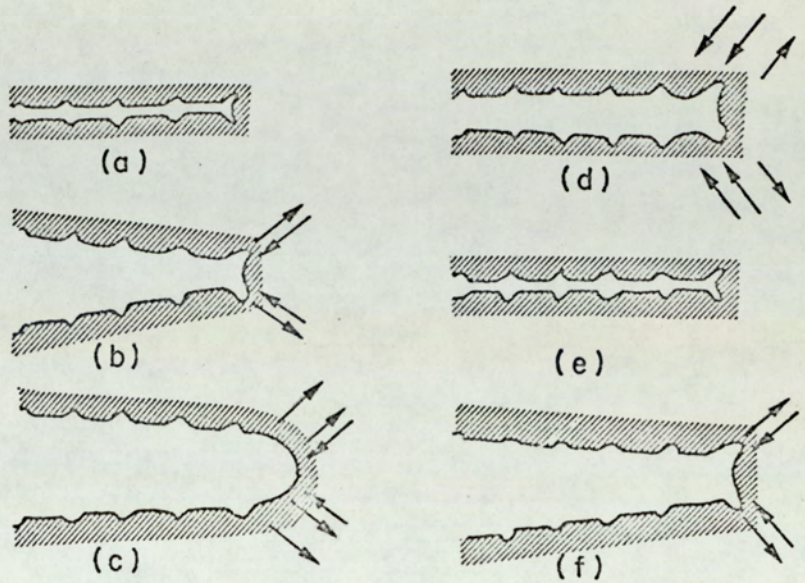


Fig. 4a—The plastic blunting process of fatigue crack propagation in the stage II mode: (a) zero load, (b) small tensile load, (c) maximum tensile load, (d) small compressive load, (e) maximum compressive load, and (f) small tensile load. The double arrowheads in (c) and (d) signify the greater width of slip bands at the crack in these stages of the process. The stress axis is vertical.

(After Ref.28)

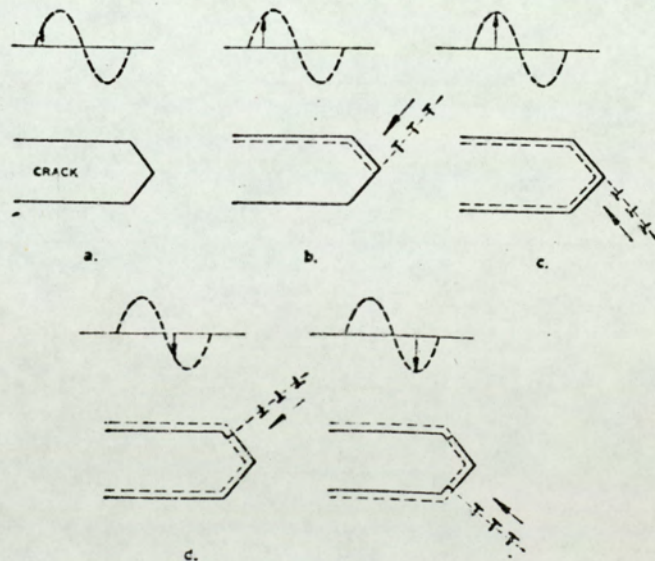


Fig. 4b—Crack extension in one load cycle by dislocation movements on two different sets of crystallographic planes

(After Ref.29)

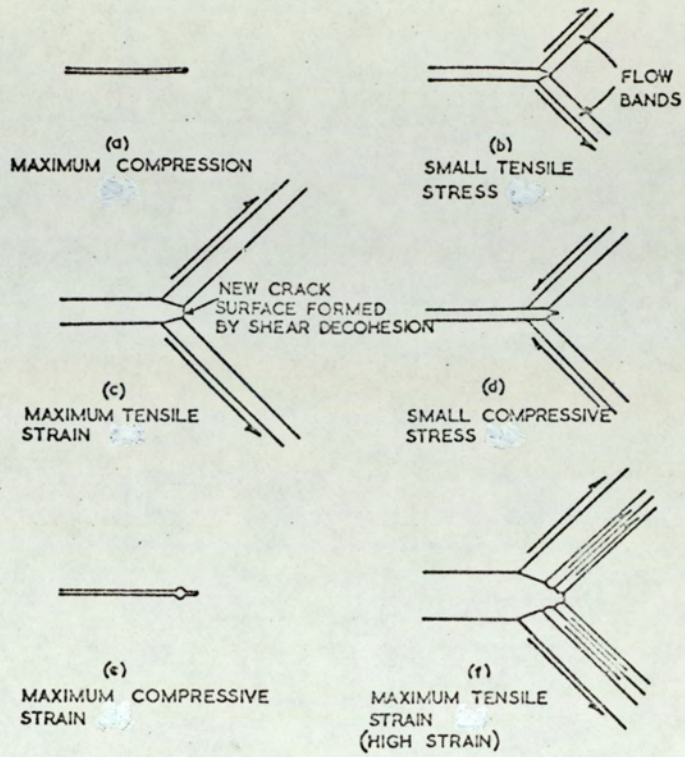


Fig. 4 C - Shear decohesion mechanism for Stage II crack growth.

(After Ref.32)

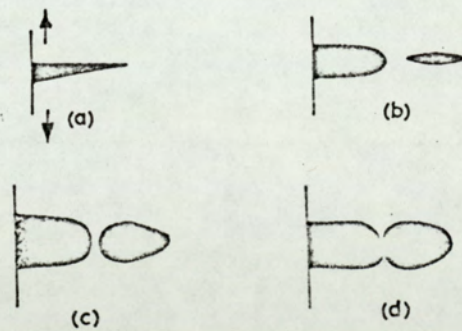


Fig. 4d - Fatigue crack growth during one cycle of stress : (a) end of compressive half cycle, which may have cracked inclusions ahead of crack tip; (b) tensile half cycle blunts crack tip and produces void ahead of crack in region of triaxial tension; (c) thinning of unfractured bridge under biaxial tension; (d) final separation of bridge by thinning.

(After Ref.33)

have been explained in different ways. A few of them are noted below:

- (a) Plastic blunting process at crack tip (28)
- (b) Cyclic slip and movement of dislocations (29, 30)
- (c) By shear and decohesion (31, 32)
- (d) Void coalescence and growth (33)

Fig. 4_{a-d}

All the models for crack propagation are based on the damage due to cycling at the immediate vicinity of the crack tip. They differ only in the way in which the damage occurs.

Laird,⁽²⁸⁾ in his plastic blunting process assumes that a small double notch exists at the crack tip from prior damage. On application of a small tensile load, the double notch serves to concentrate the slip bands along planes at 45° to the crack plane and thus maintains a square geometry of the tip. When the maximum tensile load is applied, the crack tip blunts and assumes a semicircular shape due to broadening of the slip bands. As the compressive load is applied, reversed slip occurs and the new crack surface formed during tensile portion of the load is forced into the plane of the crack and partly folded due to the buckling of the very front surface of the crack. The process then repeats and crack growth occurs. Depending on the inclusions, grain boundaries etc. in the material, the slip zones may not remain symmetric. Moreover, variation of the positions of the slip planes with respect to the stress axis for different orientation of crystals at the crack tip, may cause asymmetry of the notch. Subsequent loading may induce plastic blunting process in the most advanced part of the notch. Therefore, in ductile polycrystalline material, different types of striation can be observed.

Schijve⁽²⁹⁾ considers the Stage II crack propagation as an extension of the Stage I crack propagation. On cycling, dislocation movement occurs on one or two sets of crystallographic planes at 45° .

to the crack plane. The crack tip may act as source or sink depending on the stress condition. Thus the crack extension occurs in each cycle as a consequence of a "sliding off" mechanism. Broek⁽³⁰⁾ suggests that depending on the orientation of the slip planes, striation depth could be larger on one fracture surface than on its mating part.

Pelloux⁽³¹⁾ considers that deformation at the crack tip may take place either by alternate shears or simultaneous shear on the two shear bands. The fatigue crack propagation can then occur only by alternate shear on the two slip bands. If shear starts on one plane and strain hardening occurs, it could be easier to shear on the other plane. This process may alternate. Thus, the notch length is extended by a rupture process and the amount of crack extension will be equal to half the COD. If the material is non-hardening or if the hardening is saturated, simultaneous shear may occur and the crack blunting will take place. Due to the presence of high strain ahead of the crack tip, void nucleation and growth may occur which will sharpen the crack and lead to further blunting. Tomkin⁽³²⁾, on the other hand, considers that the shear decohesion along the inner edges of both the flaw bands occurs during the tensile part of the fatigue cycle. During compression, the reversed slip occurs, the crack closes but without significant re-cohesion of the newly cracked surface. Tomkin considers that ^{the} familiar fatigue fracture surfaces ripple pattern can form due to this process (Fig. 4c) and suggests that the same mechanism occurs in Stage I growth as well but only on one plane.

Forsyth and Ryder⁽³³⁾ argued that dimple type fracture observed in tensile fracture surfaces can also be formed in fatigue. The tensile stress applied to a notched specimen will cause plastic

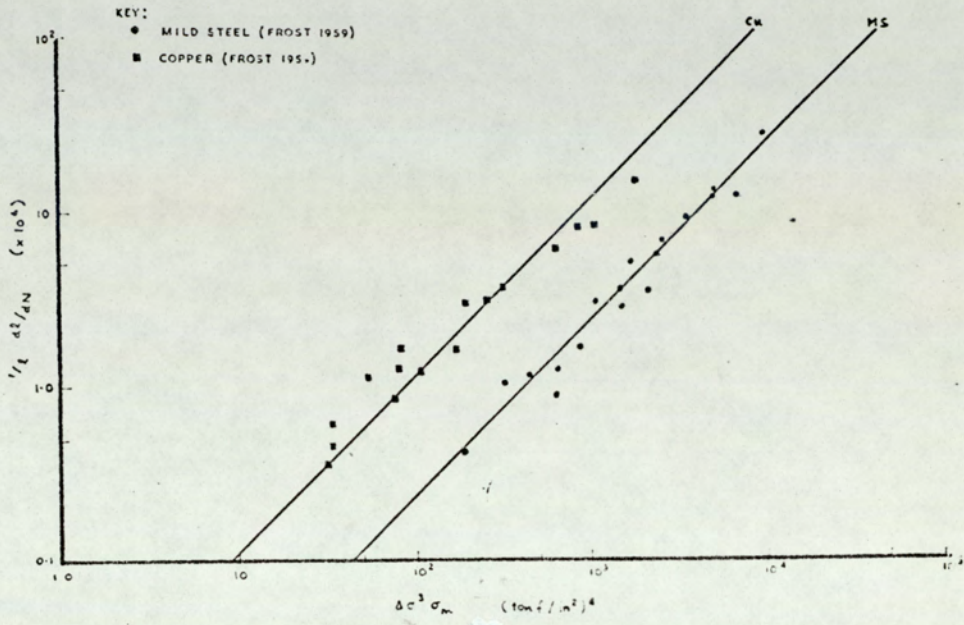
deformation at the tip of the notch. Due to plastic deformation, a redistribution of the stress gradient ahead of the crack will occur. The maximum root stress will diminish and the crack will blunt. This, by virtue of the plastic strain involved and the increase in the effective root radius, causes an increase in the mean stress in an increased volume of material ahead of the crack tip. This constrained volume of material is being hydrostatically stressed in tension; therefore the tensile stress to shear stress ratio is high. Voids nucleate due to tensile stress usually at the brittle second phase particles, but due to the shape of the crack tip, the affected region lies ahead of and parallel to the crack front. In the next step, thinning of the unfractured bridge between the crack and the void will occur resulting in crack extension. Striations can form on the fracture surfaces by this mechanism.

2.3 Laws of Crack Propagation

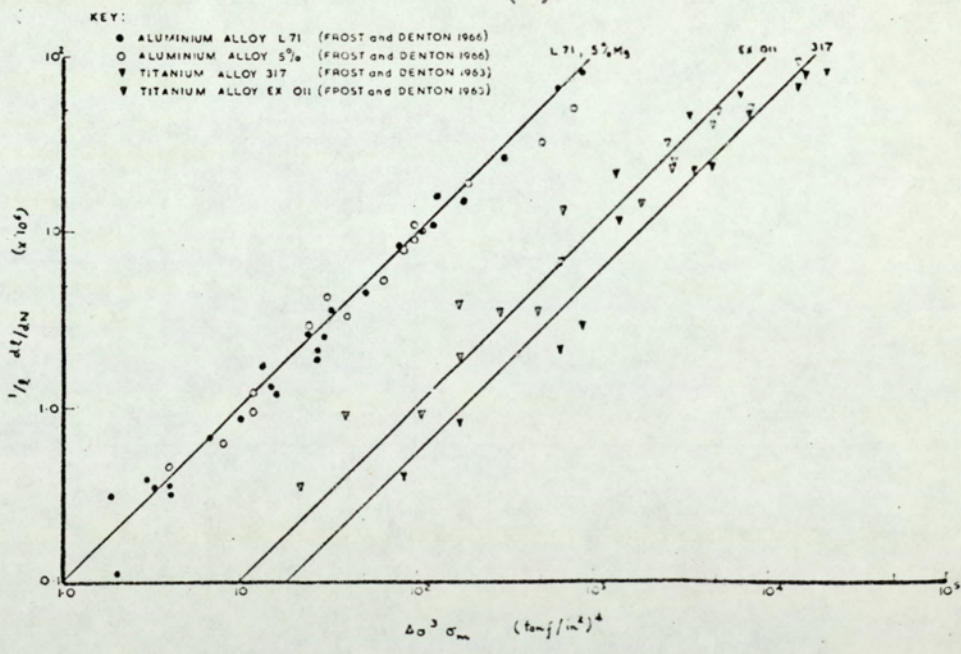
To provide adequate description of the manner in which a fatigue crack grows in a material, a number of empirical laws have been proposed based on the experimental evidences. These laws consider the ratio of the incremental increase in crack length to the incremental increase in the load cycle as a continuous function of different variables such as load range, specimen dimensions and material properties. Christensen and Harmon⁽³⁴⁾ have listed a number of such crack propagation laws originated by different persons during the years 1935 to 1965. A critical analysis of these laws is also given by Paris and Erdogan⁽³⁵⁾ and Rice⁽¹⁸⁾.

One of the earliest continuum fatigue crack growth equations was given by Head⁽³⁶⁾ who showed that,

$$\frac{da}{dn} = \frac{C \Delta\sigma^3 a^{3/2}}{(\sigma_{ys} - \Delta\sigma) r_y^{1/2}} \dots (12)$$



(a)



(b)

Confirmation of low stress crack propagation law—eqn. 15
(a) cold worked metals, (b) alloys.

Fig. 5

(After Ref.32)

where $\frac{da}{dn}$ is the crack growth per cycle, C is a constant, $\Delta\sigma$ is the stress range, a is the crack length, σ_{ys} is the material yield strength and r_y is the plastic zone size at the crack tip. In his equation Head assumed that the plastic zone size is constant irrespective of the crack length. Later Frost and Dugdale⁽²¹⁾ showed that the plastic zone size is proportional to the crack length. They proposed that the fatigue crack growth rate is proportional to $\Delta\sigma^3$ and the length of the crack.

$$\text{Therefore, } \frac{da}{dn} = A \Delta\sigma^3 a \quad \dots \quad (13)$$

where A is a constant.

In a subsequent paper Frost et al⁽³⁷⁾ incorporated a mean stress term σ_m in the equation and hence gave

$$\frac{da}{dn} = \Delta\sigma^3 a (P + Q \sigma_m) \quad \dots \quad (14)$$

where P and Q are material constants.

Using saturation of hysteresis energy absorption as a criterion for fatigue crack propagation, Liu⁽³⁸⁾ argued that the power of ^{the} stress range in equation (13) should be 2. However, recently Tomkins⁽³²⁾ put forward a continuum theoretical model of crack propagation and showed that the crack growth rate can be given by the equation

$$\frac{da}{dn} = A \Delta\sigma^3 \sigma_m a \quad \dots \quad (15)$$

He verified the equation by plotting $\frac{da}{dn} \frac{1}{a}$ versus $\Delta\sigma^3 \sigma_m$ values from Frost et al's data on different materials (Fig.5.)

Hardrath and McEvily⁽³⁹⁾ analysed the results of aluminium alloys and found that a plot of $\log \frac{da}{dn}$ Vs $\log a$ deviated from a straight line of unit slope. This is in contradiction to Frost and Dugdale's result. They also showed that the crack growth rate was a function of $\Delta\sigma \left(\frac{a}{\rho}\right)^{\frac{1}{2}}$ where ρ is the radius of curvature of the crack tip.

Paris and Erdogan⁽³⁵⁾ critically analysed different crack propagation laws and showed that

$$\frac{da}{dn} = \frac{\Delta\sigma^m a^n}{C} \dots (16)$$

where C is a constant and m = 4 and n = 2.

They concluded that, in terms of fracture mechanics, equation (16) can be written as

$$\frac{da}{dn} = A (\Delta K)^m \dots (17)$$

where A is a constant and m = 4.

Paris⁽²⁰⁾ argued that the value of the exponent m should be 4 on the assumption that the crack growth rate is proportional to the plastic work done per cycle for unit length of crack front, which in turn is proportional to the volume of the plastic zone size per unit crack front.

According to Liu's analysis⁽³⁸⁾, the value of m = 2. Liu argued that this value holds good for results with equimaximum stress levels. Since the elastic strain energy released is a function of maximum stress, the maximum stress should give reasonable correlation. Liu admitted that the value of m will be modified if σ_{max} is not the same.

Although a good fit for a variety of experimental data is observed with Paris type equation, it has been noted that m can vary from 2 to 6 (40,41).

Forman et al⁽⁴²⁾ have observed that Paris's equation was not a good fit for higher load ratios and crack growth rates. The instability of the crack growth rate when K_{max} approaches K_c has not been considered. To incorporate the effects of these factors, they proposed that

$$\frac{da}{dn} = \frac{C (\Delta K)^m}{(1 - R) K_c - \Delta K} \dots (18)$$

where C is a constant, $R = \frac{K_{min}}{K_{max}}$ and K_c = fracture toughness value.

The data from 2024-T3 and 7075-T6 aluminium alloys fitted nicely to the equation (18). For 2024-T3, the data were found to be a good fit even at $R = -1$ (43).

Pearson (44) tested different 12.7 mm.thick aluminium alloy specimens at different R values and found that Forman's equation did not fit well to the results. He modified Forman's equation by raising the denominator to a power $\frac{1}{2}$ and using $K_c = K_{max}$ (limit) obtained during the fatigue tests showed that a better fit could be obtained. He argued that Forman et al and Hartman and Schijve (43) obtained good agreement with equation (18) perhaps because the ΔK values used were much smaller than K_c values.

The primary purpose of including ^{the} R term in a crack growth equation was to account for mean or maximum stress effect. This could as well be done by including K_{mean} or K_{max} term in an equation containing ΔK . As a result Heald et al (45) proposed an equation of the type

$$\frac{da}{dn} = A \left[\frac{\Delta K^4}{\sigma_{uts}^2 (K_c^2 - K_{max}^2)} \right]^n \dots (19)$$

where A is a constant, σ_{uts} is the strength of the material and n lies between 0.5 to 1.

They showed that fatigue crack growth results obtained from heat-treating a one percent carbon steel to different micro-structures were in good agreement with the equation (19).

Arad et al (46) working on a polymer (PMMA) found a mean stress effect and put forward an equation of the form

$$\frac{da}{dn} = \beta (K_{max}^2 - K_{min}^2)^n \dots (20)$$

where β is a constant. He found the value of $n = 2.5$.

Roberts and Erdogan⁽⁴⁷⁾ analysed the results of Broek and Schijve on 2024-T6 aluminium sheet specimens in tension and some of their own results on 2024-T3 in bending and showed that the dependency of crack growth rate on mean stress and ΔK can be satisfactorily represented by an equation of the type

$$\frac{da}{dn} = B (K_{max})^m (\Delta K)^n \dots (21)$$

where B is a constant. They found the value of both m and n to be equal to 2.

Recently some attention has been given to the threshold value of ΔK at which no crack propagation takes place. This is considered as a fracture mechanics equivalent of the fatigue limit of an S-N curve. Klensil and Lucas⁽⁴⁸⁾ carried out experiments on steels of three different carbon contents. By giving proper consideration to the fact that residual stress may develop at the tip of the crack when load is lowered from a high to low value, they found that the basic threshold stress intensity factor was a constant and was equal to $4.02 \text{ MNm}^{-3/2}$ ($410 \text{ Kp cm}^{-3/2}$). They therefore proposed an equation

$$\frac{da}{dn} = A (\Delta K_a^n - \Delta K_{at}^n) \dots (22)$$

where ΔK_{at} is the threshold stress intensity value following a stress intensity of ΔK_a .

It was shown that ΔK_{at} is dependent on ΔK_a by the equation

$$\Delta K_{at} = \Delta K_{atb}^{1-\alpha} \cdot \Delta K_a^\alpha \dots (23)$$

where ΔK_{atb} is the basic threshold value of stress intensity and α is a material constant dependent on the strength.

Cooke and Beevers⁽⁴⁹⁾ have also found threshold stress intensities for five medium carbon steels and concluded that ΔK_{at} depends on load ratio R.

To encompass the effect of threshold stress intensity at low ΔK values and the influence of strength, constraint and mean stress for conditions approaching failure, Richards and Lindley⁽⁵⁰⁾ have suggested the following equation

$$\frac{da}{dn} = A' \left\{ \frac{(\Delta K - \Delta K_0)^4}{\sigma_{uts}^2 (K_c^2 - K_{max}^2)} \right\}^n \dots (24)$$

where A' is a constant and ΔK_0 is the threshold stress intensity value. Using this equation they found good correlation with crack growth rate results on three different heat-treatments and strength levels of 1% carbon steel. The value of the exponent in these cases was found to be 0.73.

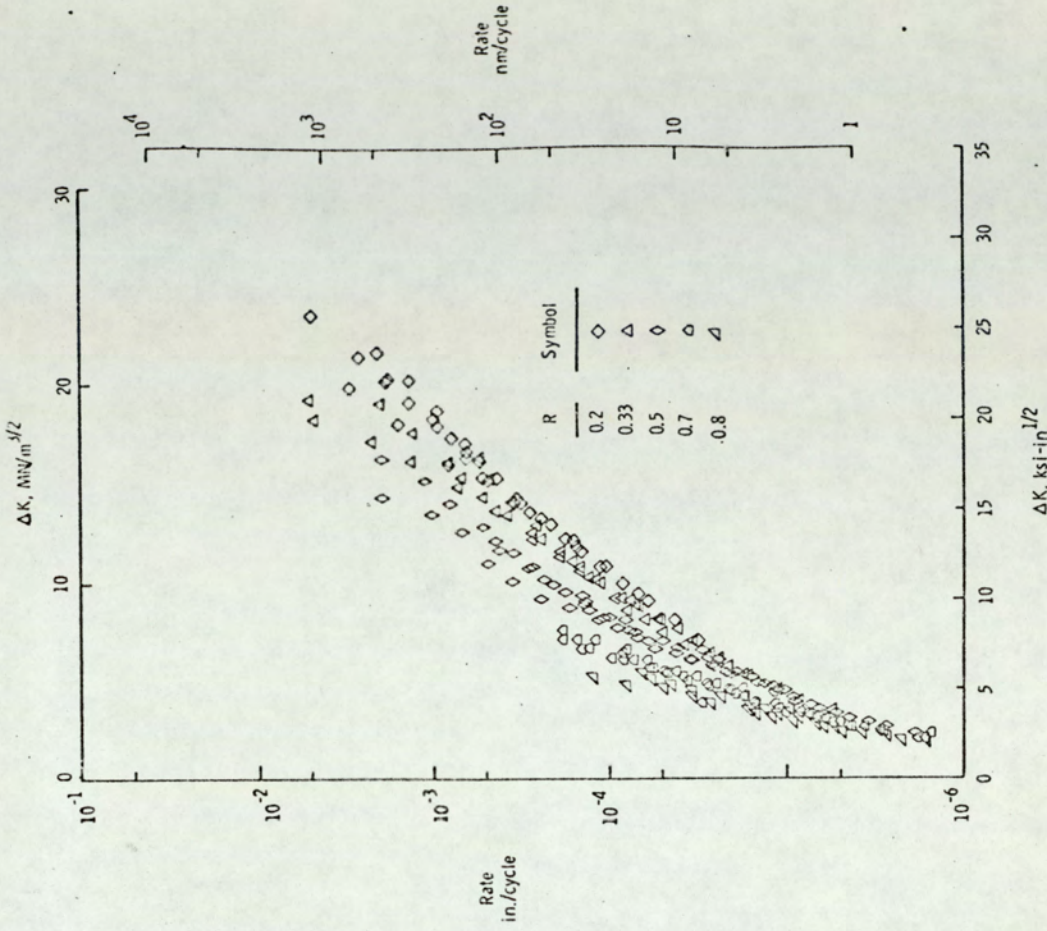
In the case of high strain fatigue, to accommodate the effects of cyclic hardening or softening, efforts are being made to incorporate different variables such as plastic strain, plastic zone size, strain hardening exponent and COD in the crack growth equations. In the light of the present growing interest in the crack opening displacement, a few researchers have tried to correlate crack propagation rate with COD.

Pelloux⁽³¹⁾ has plotted the crack opening displacement value corresponding to different stress intensity values against the rate of crack propagation for 4340 steel, 2024-T3 and 7075-T6 aluminium alloys and also for titanium alloys. He observed that a unique relation exists between the two parameters. He put the relation in the form

$$\frac{da}{dn} = A (\text{COD})^2 \dots (25)$$

where A is a constant.

Dover⁽⁵¹⁾ performed high strain fatigue tests on mild steel and measured COD by clip gauge and transducer meter. He converted the clip gauge COD values to crack tip COD values through an equation and established a relation of the type,



Variation of fatigue crack growth rate with ΔK for $R > 0$.

Fig. 7

After Ref. 56.

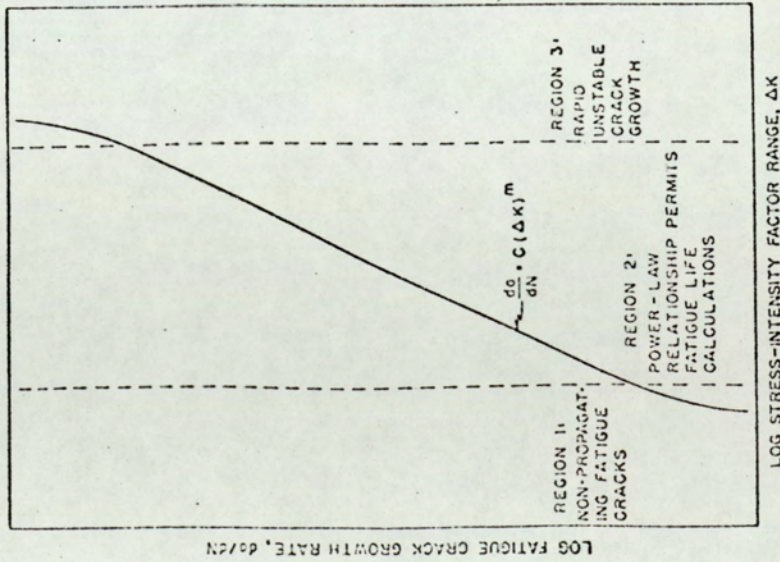


Fig. 6

After Ref. 95.

$$\frac{da}{dn} = A (\text{COD range})^n \dots \dots (26)$$

where A is a material constant. The value of n was determined to be 3.26.

It can be seen from all the crack propagation 'laws' described above that the fatigue crack growth rate can be expressed as a function of the crack tip stress intensity factor. It has been observed that for simple zero-to-tension cycling in air or inert environments, the crack-growth-rate versus stress intensity range relationship generally, follows a sigmoidal shape consisting of three regions (Fig.6). Most of the equations given above describe the linear middle portion of the sigmoidal curve. Incorporation of the threshold stress intensity factor has been done in a few 'laws' to cover the portion of the sigmoidal curve at very low ΔK levels. Similarly, the introduction of K_c term in the crack propagation 'laws' is meant to cover the portion of the sigmoidal curve close to catastrophic failure at very high values of ΔK .

2.4 Effect of Stress Level, Stress Ratio and Mean Stress

Though the stress amplitude or ΔK is the main variable in determining fatigue crack propagation rate, various people have found that stress level, stress ratio or mean stress exert a secondary influence in various materials.

Early work of Frost and Dugdale⁽²¹⁾ showed a dependence of crack-growth rate on mean stress in aluminium alloys. In the case of mild steel they found very little mean stress dependence. Later Frost and Denton⁽⁵²⁾ examined a variety of metals and alloys and confirmed that aluminium alloys had marked dependence on mean stress. They showed that the mean stress dependency was reflected through changes in the value of A in equation (13). They believed that this dependency on

mean stress was associated with the spasmodic elements of fast fracture known to occur in these alloys. They postulated that the fast fracture could have been due to the presence of brittle inclusions, intermetallics or second phase particles which do not permit the crack tip blunting. Thus the contribution of the fast fracture element would be dependent on the size and distribution of the inclusions. They also argued that if during the loading cycle, the maximum tensile stress ahead of the crack tip is not high enough to operate the fast fracture sources, the dependency on mean stress will not be noticed. Hence, for a particular load cycle, there is a minimum crack length at which the fast fracture contribution to the crack-growth occurs.

Frost and Greenan⁽⁵³⁾ tested double-edge-notched mild steel sheets and observed that under certain loading conditions non-propagating cracks may occur. They found that whether or not an edge crack of length a , small compared to the plate width, grows under loading cycle $\sigma_{\text{mean}} + \sigma_{\text{alt}}$, where $\sigma_m \geq \sigma_a$ and $\sigma_m + \sigma_a < \sigma_{\text{yield}}$ depends on the value of $\sigma_a^3 \cdot a$. They noted that a certain factor C_m existed such that if $\sigma_a^3 \cdot a > C_m$, a crack will grow and if $\sigma_a^3 \cdot a < C_m$, it will be dormant, the value of C_m depending on material and $\frac{\sigma_m}{\sigma_a}$. At $\frac{\sigma_m}{\sigma_a} = 1$, C_m had a value of 0.7 and decreased linearly with increasing $\frac{\sigma_m}{\sigma_a}$ according to the equation $C_m = 0.7 - 0.27 \left(\frac{\sigma_m}{\sigma_a} - 1 \right)$ to a value of 0.15 at $\frac{\sigma_m}{\sigma_a} = 3$ and then remained constant.

Gurney⁽⁵⁴⁾ carried out fatigue tests on mild steel and plotted his crack growth rate data as a function of K_{max} . A point of transition of slope in the data was observed. He found that below the knee of transition, the crack growth rate was a function of mean stress and could be described by a series of straight lines. Above the point of transition, all data were encompassed into a narrow scatter band showing no significant effect of mean stress.

Newman⁽⁵⁵⁾ analysed the results on 7075-T6 Al alloy and a titanium alloy at stress ratios from 0 to 0.85 obtained by C.M. Hudson of the NASA Langley Research Centre and showed the influence of mean stress on transition of $\Delta K - \frac{da}{dn}$ slope. The transition occurred at lower values of ΔK as the stress ratio R is increased. He also observed that the transition points occurred at very nearly the same crack growth rate for a given material.

Hudson and Scardina⁽⁵⁶⁾ tested 7075-T6 Al alloy at stress ratios ranging from -1 to 0.8 and at maximum stresses from 34.5 to 345 MNm⁻². They found that in the plot of $\frac{da}{dn}$ Vs ΔK , data from negative R values and that from R = 0 fell within a narrow scatter band indicating that the compressive part of the load cycle did not significantly effect the crack growth. For given R values, the data fell into discrete bands and the higher was the stress ratio the greater was the rate of crack growth for a given ΔK . As ΔK is increased, the spread between the rates for different values of R became larger (Fig.7). For tests with negative R values, the value of ΔK at which the fracture mode changed from normal to shear was approximately constant. Forman et al's crack growth law (Equation 18) was found to give good fit to the data.

Dahlberg⁽⁵⁷⁾ tested SAE 4340 steel and observed that if the maximum to minimum load ratio is changed from 5:4 to 5:1, the growth rate increases by 2 orders of magnitude. This effect was not observed in wet atmospheres. In contrast to this Ryder and Gallahar⁽⁵⁸⁾ found no effect of mean stress in inert atmosphere but observed that corrosion fatigue growth rate increased with increasing Kmean.

Miller⁽⁴⁰⁾ investigated a variety of high strength steels and observed that the crack growth rate was dependent on stress intensity level. For low stress intensity levels ($K_{max} < 18.7 \text{ MNm}^{-3/2}$), the rate of crack propagation was nearly similar for all the steels examined despite wide variations in mechanical properties.

At high K_{max} levels, the growth rates were different and the value of m in equation (17) was different. Yokobori et al⁽⁵⁹⁾ working on steel used the same mean load but different load amplitudes and found the value of m to vary with amplitude. This perhaps shows the effect of R .

Carman and Katlin⁽⁶⁰⁾ using various thicknesses of high strength steels, observed that for ΔK values below 0.7 to 0.8 K_c , the 4th power law of Paris was valid but after that transition occurred and higher growth rates were obtained. A similar observation has been made by Barsom⁽⁶¹⁾ with high strength steels. His data showed that the deviation from the equation of the form $\frac{da}{dn} = A(\Delta K)^n$ occurred and a higher growth rate obtained when $\left(\frac{\Delta K_1}{E \sigma_{ys}}\right)^2$ is approximately equal to $4.07 \times 10^{-2} \text{ mm}$. He concluded that this transition may occur at a slightly higher or lower value of ΔK if the fracture toughness of the material is higher or lower respectively.

2.5 Micro-structural and Fractographic Aspects of Fatigue Crack Propagation

Most workers on fatigue seem to agree that the influence of micro-structure is generally masked by the predominant influence of stress amplitude or ΔK on the macroscopic growth rate. Nevertheless, a better understanding of micro-structural and fractographic aspects of crack propagation can lead to the development of materials having better fatigue crack growth resistance.

A recent survey by Richards and Lindley⁽⁵⁰⁾ on the influence of stress intensity and micro-structure in steels, has summarised the different mechanisms of crack growth in fatigue. They concluded that depending on the mechanical properties and micro-structures, the crack growth can take place by (a) striation formation; (b) micro-cleavage; (c) micro-void coalescence and (d) intergranular separation or by a mixture of them.

Well defined striations are usually observed in non-ferrous metals and alloys. Striations in ferritic and bainitic structures are less clearly visible. In martensitic structure, the presence of striations has not been confirmed. The growth rate due to a striation mechanism is generally less than that due to the other three mechanisms mentioned. ~~The~~ Striation formation occurs at low and medium values of K_{max}

Micro-cleavage has been observed in steels and high strength aluminium alloys. Micro-cleavage may occur in materials containing brittle second phase particles. Micro-void coalescence, on the other hand, seems to operate in structural metal and alloys having fine micro-structures and high toughness. This mechanism is favoured by high ΔK and K_{max} values. Fatigue crack propagation by intergranular separation is common in quenched and tempered steels. The separation takes place along prior austenitic grain boundaries. Impurity elements and moisture encourage intergranular fracture during fatigue in high strength steels.

An interesting observation has been made by Inckle⁽⁶²⁾ on three different carbon steels. He found that the stage II crack propagation took place in two sub-stages which he designated stage IIa and stage IIb. The first part, stage IIa occurred at low ΔK values and was structure sensitive, the crack path changing at ferrite grain boundaries. The crack also tended to follow ferrite-pearlite interface. Whether the crack would go through the pearlite colony or not depended on the orientation of the cementite lamellae to the crack path. The stage IIa fracture surface was characterised by markings roughly parallel to the direction of crack propagation, representing a 'hill and valley' structure. Ill-defined striation markings were also present.

The stage IIb was insensitive to micro-structure. The crack propagated without regard to detailed micro-structure of the steel.

The fracture surface was characterised by well defined striations and crack branching.

Kawasaki et al⁽⁶³⁾ observed striations in fatigued fracture surface of a structural carbon steel. They could associate tearing type of fracture as the crack passed through ferrite grains and a brittle type of fracture through the pearlitic region.

Heald et al⁽⁴⁵⁾ found that crack growth rate in spheroidised steel was less than that in the pearlitic steel. The fatigue crack passed around the spheroidised particles which in general did not fracture or de-cohere. The striation markings were distorted and no void-coalescence occurred. The crack growth rate was not dependent on K_{max} level, whereas in pearlitic steel it was. In pearlitic steel, complex fracture surfaces were observed which were dependent on the orientation of the carbide lamellae in the pearlite colonies. Occasional micro-cleavage regions present were perhaps due to the fracturing of the grain boundary carbides. The crack path was found to propagate through the pearlite colonies fracturing the carbide lamellae. The higher growth rate was attributed to the micro-cleavage mechanism operating when K_{max} approaches K_C value.

Wei⁽⁶⁴⁾ could not find any obvious correlation between the fracture path and the micro-structure of a low alloy steel. However, he found that the crack path seemed to follow the martensite plate boundaries. He also observed the cracking of the prior-austenitic grain boundaries in humid argon atmosphere. Quasi-cleavage type fracture was present in ^{the} case of low toughness material and dimple rupture type fracture along with some isolated intergranular cracking were observed in high toughness material.

Griffiths et al⁽⁶⁵⁾ working on a bainitic weld metal and Crooker et al⁽⁶⁶⁾ on alloy steel, found that at low values of ΔK , the fracture surfaces had tear ridges with striations in isolated patches.

At medium ΔK values, the predominant features were shallow dimples and tear ridges, but at high ΔK , micro-void coalescence was extensive. Griffiths et al associated micro-void coalescence and higher growth rates with the second phase particles. In the regions where striation mechanism was working, the second phase particles were visible but they took very little part in the crack growth process.

Heiser and Hertzberg⁽⁶⁷⁾ studied different heat-treated hot rolled steel plates in three different orientations. The micro-structural constituents and their orientation and direction with respect to the fracture plane was important in determining crack growth rates at different stress levels. The macroscopic growth rate was due to the combined effect of a predominant striation mechanism and inclusion-matrix interfacial failure or cleavage. Depending on the orientation of the inclusions, the inclusion-matrix interfacial failure could either locally accelerate or retard the crack propagation rate.

The observation that the mechanism of fatigue crack propagation changes from a striation mechanism to a progressive micro-cleavage and/or void-coalescence as the stress intensity is raised, has also been made in Al-alloys^(68, 69). Pelloux⁽⁷⁰⁾ and Kershaw and Liu⁽⁶⁹⁾ consider the micro-cleavage mechanism to be dependant on the size of the plastic zone. The higher the ΔK , the bigger is the plastic zone and the more will be the fracture prone brittle particles within the zone and therefore the growth rate will be higher. Gerberich and Hartbower⁽⁷¹⁾ related dimple size on fatigue fracture surfaces of a steel to the stress intensity values on a plot of $\log \Delta K$ versus \log dimple size and noticed that a slope of 2.3 existed. They argued that if there is a relationship between the dimple size associated with microvoid coalescence and the region of fracture instability, then a relationship between dimple size and COD is expected.

Since COD is proportional to K^2 (equation 8), then the result showed that direct relationship exists between dimple size and COD. Since plastic zone size is also proportional to K^2 (equation 9), on the basis of the above work, it can also be argued that dimple size should be directly proportional to the plastic zone size as well or vice versa.

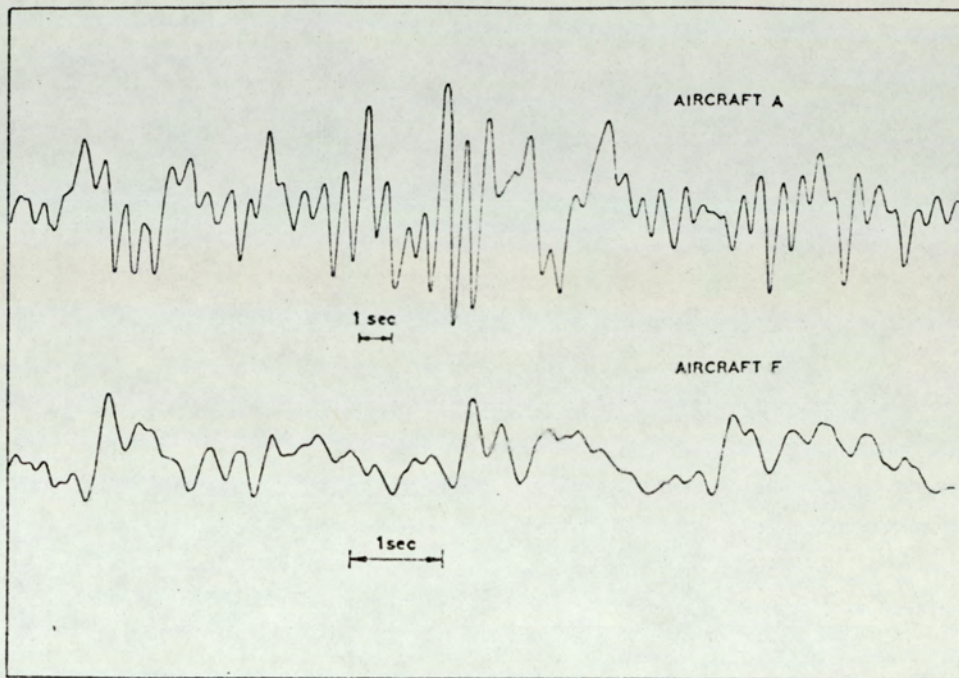
2.6 Fatigue Under Complex Load History

2.6.1 Introduction:-

The S-N curves produced on the basis of pure sinusoidal stress histories depend on the values of mean stress σ_m and the stress amplitude σ_a . The magnitude of fatigue life determined in this way is also dependent on the specific material tested, the temperature of test, the severity of notch and in the case of un-notched specimens, on the surface finish of the material. Frequency and stress wave forms have insignificant effect on S-N diagram except at high temperature or in aggressive environments.

In the practical service conditions, a member or a component undergoes complicated stress patterns. The S-N curves based on pure sinusoidal test results cannot predict the failure life under these circumstances. On the other hand, because of the multitude of possible load patterns, it is not feasible to compile S-N data for complex load histories similar to that accumulated for pure sinusoidal loading. Consequently, a number of fatigue "damage laws" were developed which made use of the sinusoidal S-N data but still could reasonably predict life for complex load histories.

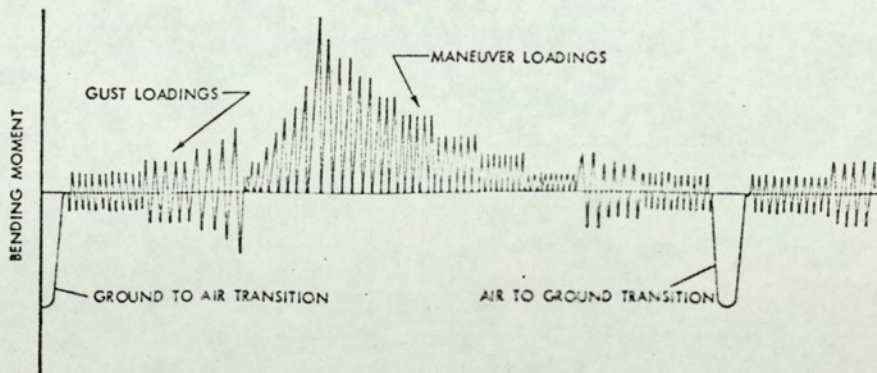
The most commonly used law is the one put forward by Miner in 1945⁽⁷²⁾. He assumed that the cumulative damage under cyclic loading was related to the net work absorbed by the specimen. The number of cycles applied, expressed as a percent of the number of cycles to failure at a given



—Samples of Two Load-Time Histories.

Fig-8

(After Ref.75)



Flight-by-flight sequence of test loading—F-104A wing fatigue test.

Fig-9

(After Ref.97)

stress level, would be a proportion of useful life expended. When the total damage derived from different stress level would reach 100 percent, the fatigue failure will occur. Hence, this hypothesis applied to variable amplitude loading can be expressed as:-

$$\sum \frac{n_i}{N_i} = 1 \quad \dots \quad (27)$$

where n_i is the number of cycles at a given stress level at which N_i number of cycles are required for failure.

It was subsequently found that Miner's Rule based on a concept of linear damage generally over-estimates life. Main criticism against Miner's hypothesis is that the parameters such as mean stress, loading sequence, notch effect and static loading prior to fatiguing, are not included in the treatment. Because of the inherent simplicity of the Miner's Rule, it has found widespread application in design.

2.6.2. Random Loading

Components in service usually undergo random load histories. It is not ^{easily} possible to define a random load-time history by a ^{simple} mathematical function and it is not easy either to give a complete definition of it. An example of this type of loading is given in fig.(8). Usually the distribution function of the peak loads is presented but it does not show the sequence in which these peak loads are applied. It is possible to describe certain types of random loadings by means of power spectrums. The results of the random load fatigue tests are generally evaluated in terms of Miner's Rule or are compared with constant amplitude fatigue data. A comprehensive survey of random load testing is given by Swanson in reference ⁽⁷³⁾.

Paris ⁽²⁰⁾ showed that by using a power spectrum approach and with some modification of crack growth laws, it is possible to use fracture mechanics to correlate fatigue crack propagation data under random loadings. In case of aluminium alloys, he found that a good correlation

exists between the average rises in the quasi-stationary K-time history and the average extension of crack per rise. Paris admitted that in his approach, the sequence effects of rises and falls in the load-time history has been ignored. He pointed out that the sequence effect could be a minor variable compared to the effects of rises and falls and the mean. Smith⁽⁷⁴⁾ used the same approach to find the fatigue crack growth behaviour of aluminium and titanium alloys. He compared the sinusoidal and random loading crack growth rate data on the basis of average of the greatest rise and fall in stress intensity between mean level crossings. The data showed a cross over between constant amplitude and random loading behaviour; at low stress intensity level, random loading exhibited faster crack propagation rates than constant amplitude loading and at high stress intensity level, the growth rate for random loading was slower. He also compared the fatigue crack growth behaviour of the alloys under narrow and broad band spectrum loading. The narrow band spectrum is the one where the range of frequencies is small compared to the spectral height, whereas in the broadband spectrum, the range and the spectral height are of the same order of magnitude. No significant difference in fatigue crack growth was found between the two types.

2.6.3 Programme Loading

The constant amplitude fatigue testing is an over simplification of the actual service condition and the random load testing, on the other hand, is too complicated to use and analyse. The programme loading is thus a reasonable solution to these difficulties. It usually contains sinusoidal loading at different mean levels with different amplitudes (Fig.9). Programme loadings are usually derived from random load-time histories generated in service. The loading in a programme-fatigue test is established such that it contains the same distribution of peak loads (or some other characteristic

-Cycle counting methods.

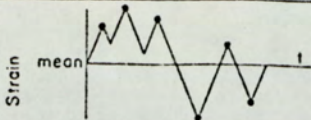
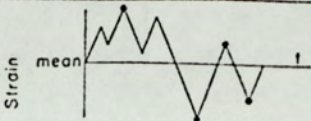
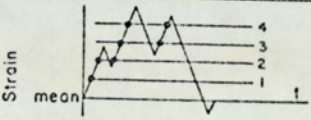
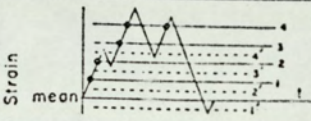
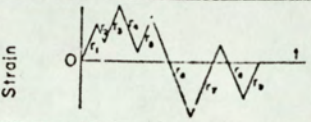
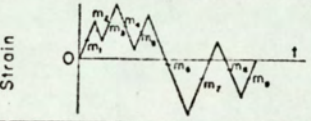
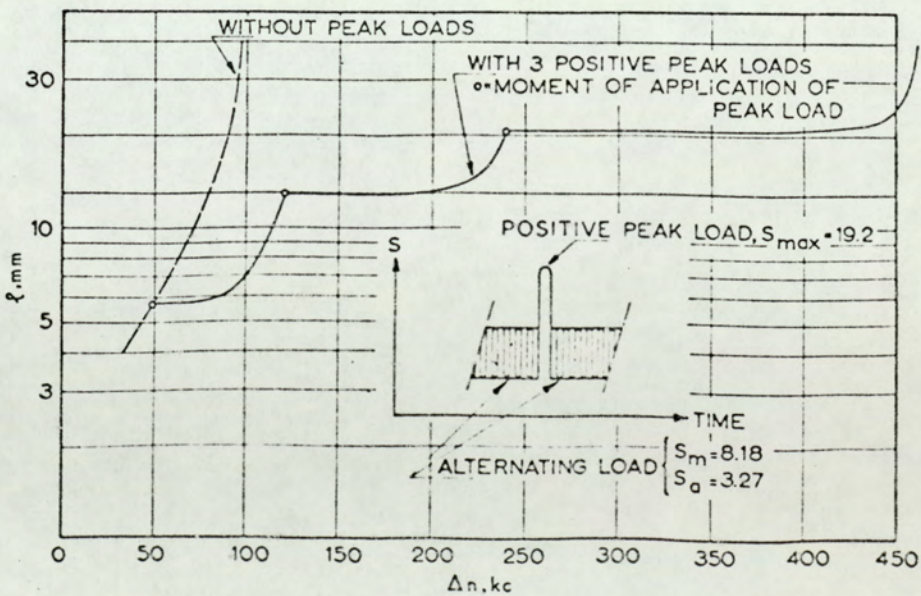
Name	Example	Description
Peak		All maximums above the mean and all minimums below the mean are counted.
Mean crossing peak		Only the largest peak between successive crossings of the mean is counted.
Level crossing		All positive slope level crossings above the mean, and negative slope level crossings below the mean, are counted.
Fatigue - meter		Similar to level crossing except that only one count is made between successive crossings of a lower level associated with each counting level.
Range		Each range, i.e. the difference between successive peak values, is counted as 1/2 cycle, the amplitude of which is half the range.
Range - mean		Ranges are counted as above and the mean value of each range is also considered.

Fig-10

(After Ref.94)



-Effect of Positive Peak Loads on Crack Propagation under Constant-Amplitude Loading.

Fig. 11

(After Ref.81)

measure for the load history) as the random load. However, some variables need to be selected arbitrarily. These variables are the number of cycles in one period or block, the sequence of loading, the number of load levels, and the highest and the lowest load amplitude to be included. All of these may have some influence on the overall fatigue behaviour.

Different methods of reducing random load-time history to a collection of cyclic loads are at present practised.^(75, 92) These are; (1) Peak count method; (2) mean crossing peak count method; (3) range count method; (4) range mean count method; (5) range pair count method; (6) fatigue-meter count method and (7) level crossing count method. A brief description of these methods is given in Fig. (10).

Arrangement of load blocks in a programme loading can be done in different manners, viz. (a) increasing load amplitude; (b) decreasing load amplitude; (c) increasing-decreasing load amplitude or (d) randomised sequence of load amplitudes. Sometimes, occasional high positive or negative stresses are included to simulate conditions characteristic to an aircraft-flight. Most of the present programme loading tests are done to evaluate life of a structure in terms of Miner's rule, though the load interaction and sequence effects on crack growth behaviour are noted. Many workers^(73, 75, 76) have used programme and random loading fatigue tests and have found either adequacy or inadequacy of Miner's rule or evaluated the usefulness of using a particular programme. Limited literature is available correlating fatigue crack propagation rates with load interaction, load sequencing or such other phenomenon in programme loading.

2.6.3.1 Effect of Load Interaction and Load Sequence

The earliest work on load sequence effect that could be traced in the literature, was the one done on un-notched specimens by D.R. Kibbey at Ohio State University in 1949. He found that in the case of ascending load amplitude tests $\sum \frac{n_i}{N_i}$ was greater than one and in/case of descending load amplitude tests $\sum \frac{n_i}{N_i}$ was less than one. Marco and Starkey⁽⁷⁷⁾ followed this work using SAE4340 steel and an aluminium alloy. Their data confirmed Kibbey's observation. The argument put forward in support of this behaviour was that at low initial load amplitude, lesser number of crack nuclei were contributing to the accumulation of damage whereas at high initial load, greater number of crack nuclei were operative and the actual accumulation of fatigue damage was non-linear and contrary to Miner's rule. In the light of the present understanding of fatigue crack initiation from unnotched specimens, it seems obvious that the number of cycles required for actual initiation of cracking will be more in the case of ascending load amplitude giving rise to the result as observed.

The effect of load interaction on crack growth rate was observed by Christensen⁽⁷⁸⁾ in steel and nickel alloy under stepped programme loading. A decrease in stress level caused a transient delay in the crack growth whereas an increase caused a momentary acceleration. Crack growth rate data for a steel tested at different constant load amplitudes with different temperatures and cyclic frequency were shown to follow a unique relation when plotted against stress intensity range. Programmed loading tests performed on similar material gave results which could be reasonably predicted from the constant load cycle growth data. It could be noted from the results given that the maximum change in load level in low-high sequence was 34 percent and that in high-low sequence was about 20 percent.

In two-step load tests on 2024-T3 and 7075-T6 aluminium sheet specimens, Hardrath and McEvily⁽⁷⁹⁾ observed a similar delay effect when a high load was followed by a low load. No appreciable accelerating effect was noticed when a low load was followed by a high load. In one test, after high-low sequence, the crack did not grow at all although the stress at the lower level was enough to grow the crack if it were a constant load test. The larger was the stress level change and the higher was the preceding level of stress, the greater was the delay. Hardrath and McEvily presumed that probably the introduction of compressive residual stress reduced the local mean stress such that the local stress range remained below the minimum value required for crack propagation. On examining the fracture surface, they observed alternate dark and light bands due to programming. Donaldson and Anderson⁽⁸⁰⁾ also found local interaction effect in two-step programme loading at zero stress ratio. The crack length at the end of each step was used to calculate stress intensity values. Integration of the crack growth rate data in low-high and high-low sequence gave essentially the same result indicating negligible effect of analytical sequencing. It was observed that somewhat conservative results could be obtained if the load interaction effect is ignored. Since the final crack lengths resulting from the above integration were not compared with the actual crack lengths obtained in the tests, the picture of sequencing is not very clear from the literature.

Schijve et al⁽⁸¹⁾ did two-step programme loading tests and tests with occasional positive and negative peak loads on aluminium alloys. They noted the retardation effect of high-low sequence of load cycle (Fig.11). They also observed that occasional application of negative peak loads did not show any visible effect on the crack growth rate. If a positive peak load was followed by a negative peak load, the

favourable retardation effect of the positive peak load was greatly reduced and a small acceleration followed by a retardation was observed. They reasoned that formation of negative residual stress at crack tip was responsible for the crack delay in two-step load test. When positive-negative peaks were applied, a small tensile residual stress formed inside the bigger compressive residual stress field resulting in a momentary acceleration of growth rate followed by retardation. When only negative peaks were applied, the crack closed partly, thus reducing the stress concentration at the tip and therefore positive residual stress could not form easily.

McMillan and Pelloux⁽⁸²⁾ attempted to find the influence of maximum load, load amplitude and load sequence on crack propagation rates in 2024-T3 aluminium alloy. They used two basic load programmes:

- (a) constant maximum load with variable load amplitude, and
- (b) constant load amplitude with variable maximum load.

Crack growth and striation spacing measurements were used to explain the effect of programming. In cases of constant maximum load tests, though the crack growth rates varied with different types of programmes used, there was no marked acceleration or retardation due to the load amplitude change. In constant load amplitude tests where maximum stress values were varied, marked transient acceleration or retardation in crack growth rates were observed depending on whether the stress level was increased or decreased respectively. The acceleration of growth rate was assumed to be related to the radius of the crack tip which is sharper at lower load levels. Sudden application of high load to a sharp crack was believed to cause the crack acceleration until the crack tip attained a stable radius. The retardation in crack propagation rate in a high-low maximum load sequence was considered to be due to work softening of the plastic zone ahead of the crack tip. Excellent electron-micrographs showing evidence of crack jumps due to

low-high sequence have been produced, but no evidence pertinent to the retardation effect has been presented. The electron micrographs also showed the variation of striation spacing with the changes of maximum load level in constant amplitude load tests.

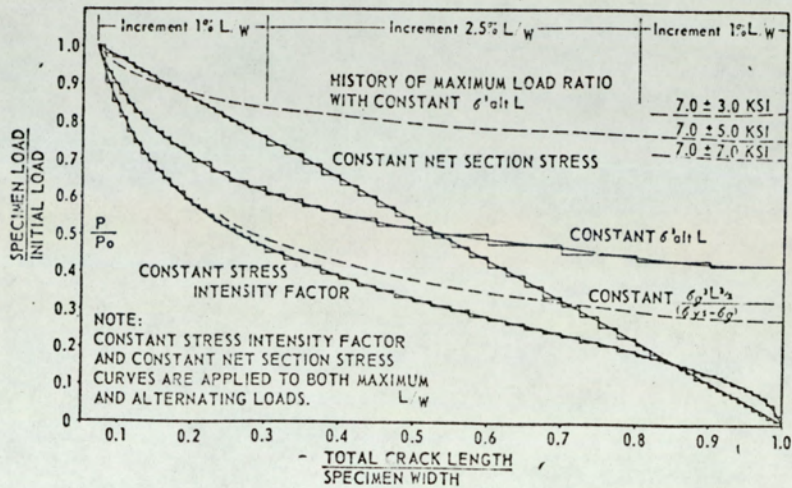
Morrow et al⁽⁸³⁾ approached the problem of high-low sequence in a different manner. They tested 2024-T3 notched aluminium alloy specimens in completely reversed loading. They used two types of high pre-stress amplitudes consisting of single cycle of the same stress range. The only difference between the two types was that type A started in tension and ended after a compressive peak, whereas the type B started in compression and ended after a tensile peak. They found that at lives shorter than 10^4 cycles i.e. when nominal stress range used was high, application of the two different pre-stresses had no effect on life, but at long lives, i.e. when the stress range used was small, type B loading gave much longer life than type A. The reason given was that with type A which goes through compressive peak test, local tensile residual stresses are formed at the tip, which contribute to the fatigue damage at subsequent cycling. The type B loading, on the other hand, produces local compressive residual stress which is beneficial. If the subsequent cycling is at high stress range, sufficient plastic strain is present which causes the relaxation of the residual stresses and the effect of prestress does not show up. A similar observation was made by Breyan⁽⁸⁴⁾ on aluminium alloy box-beams. Application of a single static preload or periodic overloads of 100 percent or more of the limit load, increased the fatigue life provided nominal fatigue loading was 60 percent or less of the limit load. The increased fatigue life was attributed to the introduction of beneficial compressive residual stresses at the rivet holes due to overloads. It appears from these results that Morrow's⁽⁸³⁾ argument regarding relaxation of

residual stresses could be applicable here also. Inckle⁽⁶²⁾ also believed in the role of residual stress and its decay, on the observation of transient growth after a high-low load sequence. Structure sensitive stage IIa type of fracture was observed to occur after a high-low load change even though the maximum stress intensity at low load level was greater than the transition value and structure insensitive stage IIb was supposed to occur. Inckle reasoned that the compressive residual stress formed was responsible for lowering the actual K_{max} value at the crack tip. He also noted that the extent of unstable growth region or in other words the rate of decay of the residual stress, was dependent on ΔK values at the low load level. Higher ΔK values were associated with shorter lengths of induced unstable growth region.

Impellizzeri⁽⁸⁵⁾ summarised the effect of residual stress on fatigue life due to spectrum loading. He noted that periodic application of high tensile stress is more beneficial to fatigue life than a single application. This happens because the favourable compressive residual stress induced by high peak load decays gradually on cycling. The application of negative high stress is detrimental to fatigue life because it either:-

- (a) introduces unfavourable tensile residual stresses, or
- (b) nullifies the compressive residual stresses induced from previous high-low sequence.

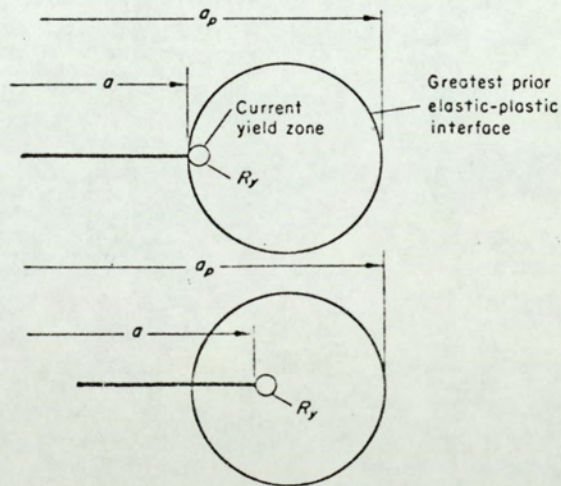
The negative peak stress is also more detrimental when used at the end of a low-high sequence. The order of application of load, whether low-high, high-low or high-low-high, or random, that would give the lowest life depends on the exact detail of each particular spectrum. In the absence of beneficial compressive residual stress, the low stress levels have no detrimental effect to fatigue life, but their ability to cause relaxation of the compressive residual stress field is the main reason for shortened fatigue life.



—Theoretical curves and experimental increments of load ratio versus crack length to specimen width ratio for load shedding tests.

Fig-12

(After Ref.86)



Schematic showing relative sizes of plastic zones in retardation model proposed by Wheeler.

Fig-13

(After Ref.92)

Swanson et al⁽⁸⁶⁾ studied crack propagation in aluminium alloy square panels under programmed and random loading. In the programme loading tests, all done at constant amplitudes, incremental load shedding procedure (Fig.12) was applied to keep either K_{max} , or net stress, or some other variable constant. It was possible to correlate all the crack growth rate data obtained from programme and random loading with the maximum stress intensity levels. They found no effect of prior load history when the programme and random loading data were compared with the constant amplitude test data without load shedding. It is understandable from these results that the residual stresses would have no effect because the changes in load levels were very small.

Schijve et al⁽⁸⁷⁾ have listed some of the arguments for interaction effects during fatigue crack propagation, these are:-

- (1) Residual stresses;
- (2) Crack blunting or sharpening;
- (3) Cyclic strain hardening (or softening) and associated influence on the material structure;
- (4) Mismatch between the macroscopic fracture planes as a consequence of different states of stress at the crack tip.

Schijve concluded that with the exception of influence of residual stresses, the qualitative understanding of the other arguments is still partly speculative and therefore requires further study.

A very recent reason put forward to explain interaction effect is the crack closure under positive stresses during fatigue. Elber^(88, 89) showed that as a result of permanent plastic deformation left in the wake of a propagating fatigue crack, it is possible to have at least partial crack closure during the loading cycle, even though loading may be in tension. Adams⁽⁹⁰⁾ supported Elber's view through experimental observations. Measurements of COD and strains

near the crack surface of aluminium alloy sheets both displayed a two stage behaviour. In the first stage occurring at the lower portion of the load cycle, both measurements agreed with those predicted for an uncracked sheet. In the second stage which occurred at the upper portion of the load cycle, both measurements agreed with those predicted for a cracked sheet. This implied that the crack was at least partially closed for the lower portion of the load cycle. Elber postulated that due to crack closure during zero to maximum fatigue cycling, there should exist a minimum stress at which the crack will open and hence the effective stress range for fatigue will be the difference between the maximum stress, σ_{max} and the crack opening stress, σ_{op} . Hence, the effective stress ratio U will be $\frac{\Delta\sigma_{eff}}{\Delta\sigma}$ where $\Delta\sigma_{eff}$ is the effective stress range and $\Delta\sigma$ is the applied stress range. Hence, if the crack propagation rate is described as a function of effective stress intensity, it will take the form

$$\frac{da}{dn} = C (\Delta K_{eff})^n = C (U \Delta K)^n \dots (28)$$

It was found that in the case of 2024-T3 aluminium alloy, the effective stress ratio was a function of R . Thus using equation (28), it was found that a better fit to the crack growth data could be obtained.

Elber also observed that crack closure phenomenon can account for the load interaction effects in variable amplitude loading. Experiments suggested that the variation of the crack opening stress after a high-low load sequence, can cause delayed retardation observed in the crack growth rate. When the change of maximum load was 50 percent, the crack became non-propagating after a period of delayed retardation. Elber argued that it was the residual deformation left behind the crack tip that caused the retardation. When low-high load

sequence was used, the crack opening load dropped substantially causing an acceleration of growth rate. After a few cycles, the crack opening stress rose to the level compatible with the new load level and a normal growth rate was obtained.

Corbly and Packman⁽⁹¹⁾ have compared different models that have been presented to-date to account for the crack growth retardation due to the high-low load sequence. They are as follows:-

- (a) Elber's crack closure model^(88, 89)
- (b) Wheeler's model⁽⁹²⁾
- (c) Willenborg et al's model⁽⁹¹⁾ (Developed at Air Force Flight Dynamics Laboratory (AFFDL)).

Elber's model based on effective stress intensity value resulting from crack closure has been described before. Wheeler's model gives the retarded crack growth rate after high-low sequence as

$$\frac{da}{dn} \text{ (retard)} = C_{pi} \cdot C (\Delta K)^n \dots (29)$$

where C_{pi} is the retardation parameter bounded by zero and unity.

C_{pi} increases monotonically according to the equation

$$C_{pi} = \left(\frac{r_y}{a_p - a} \right)^m \dots (30)$$

where r_y is the plastic zone size at lower stress level, $(a_p - a)$ is the distance from the crack tip to the boundary of the last plastic zone formed due to high stress, and m is a shaping exponent.

Wheeler's model is shown schematically in Fig.13. The retardation is assumed to be proportional to the distance the crack has to pass through the initial plastic zone. The retardation disappears and normal growth rate is obtained when the current plastic zone touches the initial peak plastic zone. Wheeler chose a value of $m = 1.3$ for the steel he investigated to suit his results. This model predicts

retardation for all values of the ratio between high and low stress.

AFFDL model given by Willenborg et al assumes that the retardation is obtained due to the change of ΔK value at lower stress levels to a reduced value ΔK_{eff} . In fact the reduction is effective on K_{max} and K_{min} . According to this model, initial maximum plastic zone size can be calculated at the high stress level, but when the load is reduced from σ_2 to σ_3 , the equivalent applied stress will be less than σ_3 by an amount σ_{red} . The maximum σ_{red} will be given by $\sigma_{\text{red}}(\text{max}) = \sigma_2 - \sigma_3$ and the minimum reduction will be zero. The values of maximum and minimum effective stress are then calculated by subtracting the respective σ_{red} values from the applied maximum and minimum stresses. These values are used to calculate effective stress intensity ranges.

AFFDL model predicts that a reduction of peak stress by 50 percent or more produces no crack growth. The decrease in effectiveness of the retardation for a high-low sequence is monotonic and dependent upon some measure of the equivalent difference in plastic zone sizes produced by the high and low stresses. The retardation ceases, as in the case of Wheeler's model, when the two plastic zones touch each other.

Corbly and Packman⁽⁹¹⁾ performed fatigue tests on 7075-T6511 aluminium alloy and compared their results in the light of different models. They found that complete cessation of crack growth at 50 percent reduction of peak stress as suggested by Elber and AFFDL models did occur only in cases where secondary ΔK was small; but the retarded growth occurred if the secondary ΔK was high. The amount of retardation by a sequence of high-low was strongly dependent on the number of applications of the high loads, the retardation increasing with increasing number of load application. On low-high sequence, the crack growth rate first rose above that predicted for

the secondary level and then gradually returned back to normal. The acceleration was associated with the formation of a stretch zone in the fracture surface. The crack-growth rates were related to ΔK levels by ^{only} fractographic measurement of striation spacing in the above investigation. The validity and accuracy of the rate of crack-growth measurements are therefore in doubt.

Von Euw et al⁽⁹³⁾ used constant stress intensity tests on 2024-T3 aluminium sheet material to investigate load-interaction effects. A single peak load was found to cause delayed retardation of the crack growth rate, which became more pronounced as the percentage overload or baseline stress intensity level, or both, is increased. The minimum growth rate did not occur immediately after the single overload. The delayed crack length was found to be equivalent to the plastic zone size formed due to the peak load. When multiple peak loads or high-low block loading sequences were applied, the retardation was greater, but the minimum growth rate was obtained immediately after the high-low load change. Fracto-graphic examination revealed stretch zones associated with peak-overload. The crack growth acceleration effect was observed with low-high loading sequence. All the interaction effects were explained in the light of Elber's^(88, 89) crack closure concept.

Summarising the findings on load interaction and sequence effects, the following conclusions can be drawn:-

- 1) Short range interaction effects on the fatigue crack growth exist in variable amplitude loading.
- 2) High-low load interaction produces transient crack-growth retardation. The extent of retardation depends upon the magnitudes of the interacting loads. The condition of the crack tip and the material immediately ahead of it seems to be the controlling factor in crack-growth retardation. The nature of retardation is not very clear.

- 3) The interaction effect due to low-high load is not very well understood.
- 4) The findings on the effects of repeated load sequencing are contradictory in nature and no firm conclusions could be drawn

It is interesting to note that most of the programme loading work, particularly that pertinent to the load interaction effects, has been done on aluminium alloys. This particular line of work was initiated by the problems encountered in the variable loading situations with components in the aircraft industry. Because of the relatively small amount of work done on this particular aspect of fatigue and also because of the fact that only aluminium alloys have been investigated, the overall picture is not very clear at the present stage. It was therefore an obvious decision that a different material should be selected for the present investigation. Two materials were initially considered. They were titanium alloys and EN24 steel (SAE4340). The latter was finally selected for two reasons.

- (a) EN24 steel is a general purpose steel used for a wide range of engineering parts. It is widely used for different moving parts in automobile and machine tool industries where variable loading situations are encountered.
- (b) EN24 steel can be heat-treated to produce different strength levels with widely different micro-structures.

Since the aim of the present investigation was to evaluate the effects of programme loading and micro-structures on the fatigue crack propagation, EN24 steel seemed to be an ideal choice.

3. EXPERIMENTAL WORK

3.1 Objectives

It could be observed from the available literature that the effects of load-interaction and load-sequencing in programme loading tests, are not very clear. The object of the present research was to investigate this aspect of fatigue by using very simple block programme loadings on a structural steel. The effects of different micro-structures on fatigue crack propagation in programme loading also needed to be evaluated. It was believed that the constant load fatigue test results would serve as a basis for the comparison of the programme load fatigue test data on the crack propagation rates.

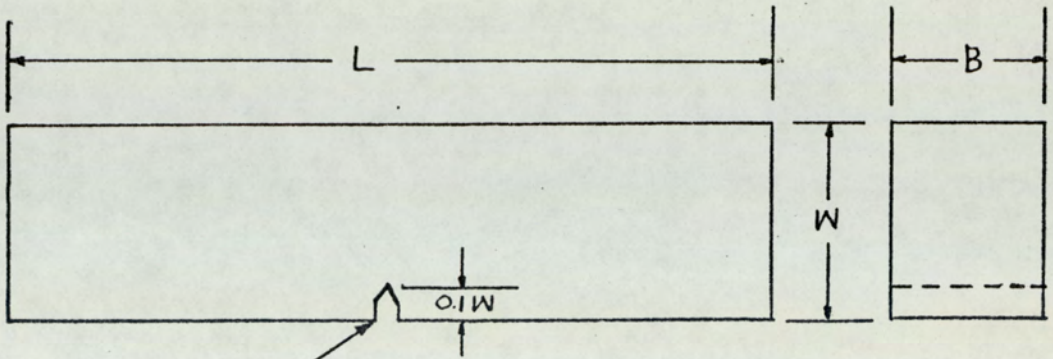
3.2 Material

Some work has been done on load-interaction and sequencing effects, particularly in aluminium alloys. It was thought that similar investigations needed to be done on a different material. With this view in mind, EN24 steel was chosen for investigation. This steel has got a wide range of engineering applications. The material was obtained in the form of 48.1 x 19.1 mm ($1\frac{1}{2}$ " x $\frac{3}{4}$ ") rolled bars. The analysis of the material is given below (wt%).

C	: 0.41;	Si	: 0.26;	S	: 0.024;	P	: < 0.01
Mn	: 0.61;	Ni	: 1.33;	Cr	: 1.08;	Mo	: 0.21
Sn	: 0.02;	Sb	: 0.005;	As	: <0.01;	Pb	: < 0.002
Bi	:< 0.0002.						

3.2.1 Specimen Design and Testing Machine

It was decided that 3 point bend specimens would be suitable for the present investigation. The following points were considered in the selection of the specimen type and dimensions.



1.59 mm. wide notch with 60° included angle and 0.127 mm. root radius.

Fig. 14. Bend Specimen.

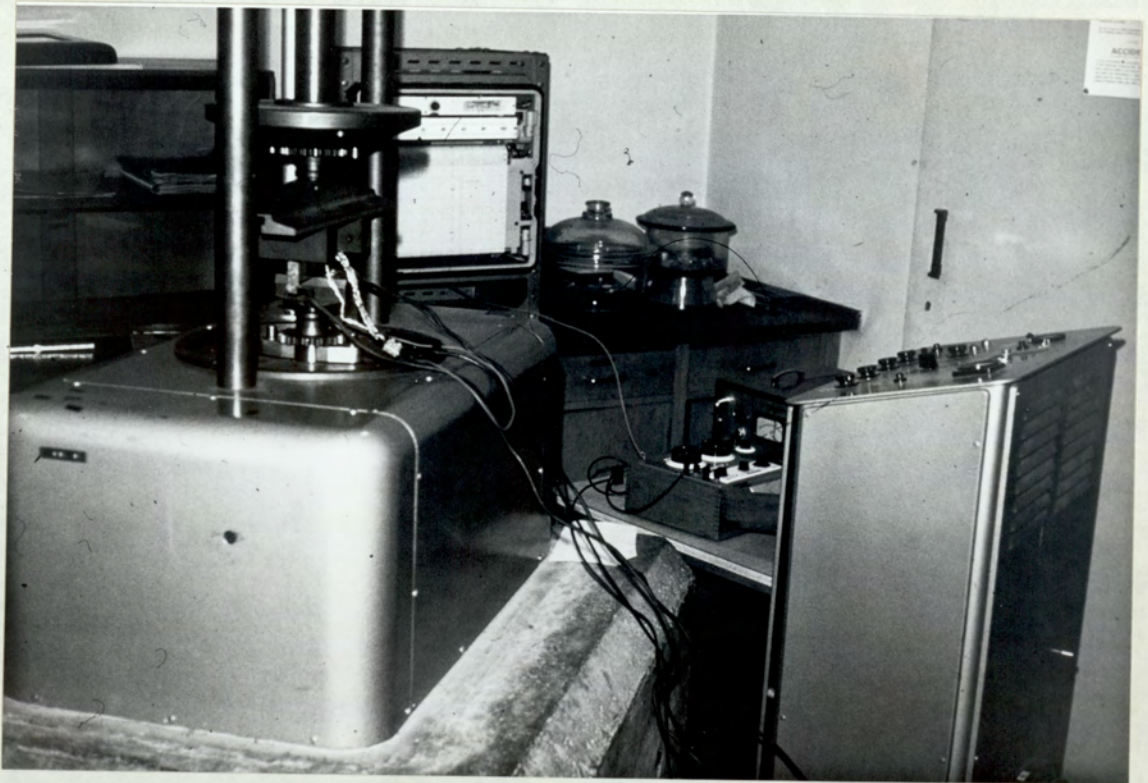


Fig. 15. Amsler Fatigue Testing Machine And The Potential Technique Equipment.

- (a) Minimum amount of material required;
- (b) Maximum testing capacity available;
- (c) Convenience in preparation;
- (d) Availability of K-calibration data;
- (e) Availability of enough width for crack growth measurement.

Four lots of specimens were prepared during the investigation.

They had the following dimensions:-

- (a) B = 12.7 mm, W = 25.4 mm, L = 127 mm.
- (b) B = 12.5 mm, W = 25.0 mm, L = 125 mm.
- (c) B = 11.93 mm, W = 23.86 mm, L = 120 mm.
- (d) B = 11.43 mm, W = 22.86 mm, L = 115 mm.

Each specimen had an initial notch-length of $0.1 W$ with a root-radius of 0.127 mm. (Fig. 14). The notches were cut perpendicular to the rolling direction. The specimens were to be loaded in span to width ratio of 4 : 1.

A two ton (≈ 20 KN) Amsler Vibrophore fatigue machine (Fig.15) was used for the crack propagation tests under sinusoidal loading at room temperatures. The test frequency varied from 175 Hz at low crack lengths to 150 Hz at high crack lengths. In the case of block programme loading tests, the machine was stopped after each block of load and the testing conditions were changed to suit the new block of load. The automatic load change mechanism was not used because it entails a gradual change of load amplitude from one block to another. The crack growth measurements were made using a potential drop technique which will be described later.

3.2.2.2. Heat-treatments

Roughly finished notched specimens were given three different heat-treatments to produce different micro-structures and strength levels.

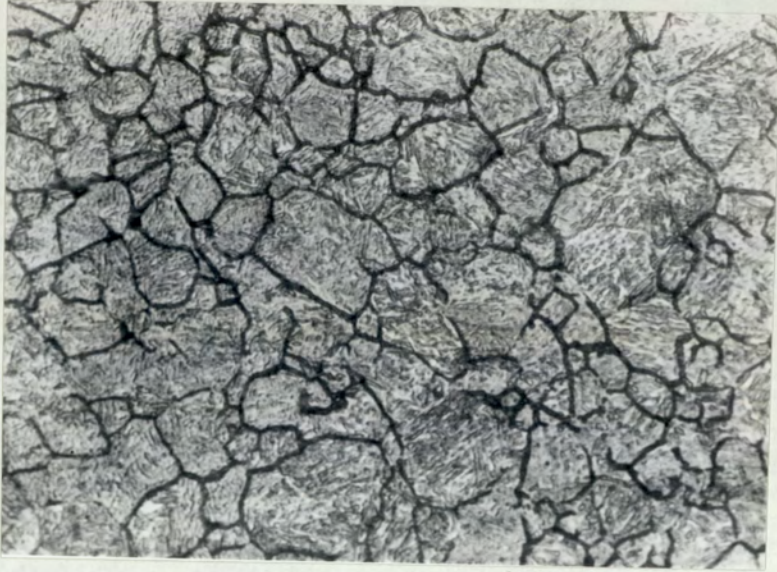


Fig.16. Typical Micro-structure of QT-A Steel.
(x 300)



Fig.17. Typical Micro-structure of QT-B Steel.
(x 400)

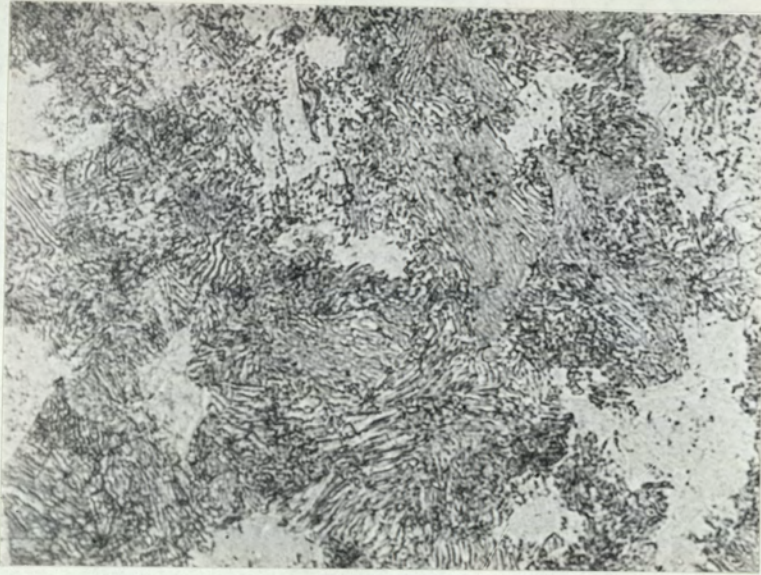


Fig.18. Typical Micro-Structure of IS Steel.
(x 750)

(a) Heat-treatment QT-A

Austenised at 840°C for 1 hour, quenched in oil, and tempered at 200°C for 2 hours.

(b) Heat-treatment QT-B

Austenised at 840°C for 1 hour, quenched in oil. Heated to 650°C , held for 15 hours at temperature and then air cooled.

(c) Heat-treatment IS

Austenised at 840°C for 1 hour, transferred instantly to a salt bath at 670°C , held for 15 hours at temperature and then air cooled.

After the heat-treatments, the specimens were ground to size. The micro-structures resulting from the above heat-treatments are shown in Figs. 16 - 18. The general etchant used was nital. Alcohol saturated with picric acid (with a few ml. of teepol) at 70°C was used to etch prior austenitic grain boundaries in the cases of QT-A and QT-B steels.

The material QT-A was quenched and tempered martensite. The material QT-B was very finely spheroidised and the material IS was a mixture of isothermally transformed ferrite and somewhat spheroidised fine pearlite.

3.2.3 Mechanical Properties

Tensile tests were carried out with No. 11 tensile test specimens by a Hounsfield tensometer. Hardness tests were done on a Vickers hardness testing machine.

Fracture toughness tests were performed on an Instron Universal testing machine. The recommended procedure for plane-strain fracture toughness testing was followed⁽⁹⁸⁾ for the material QT-A. For the materials QT-B and IS, the test geometry did not yield valid plane-strain fracture toughness values. For these two materials, a COD

C.O.D. Calibration Curves
Bend Specimens

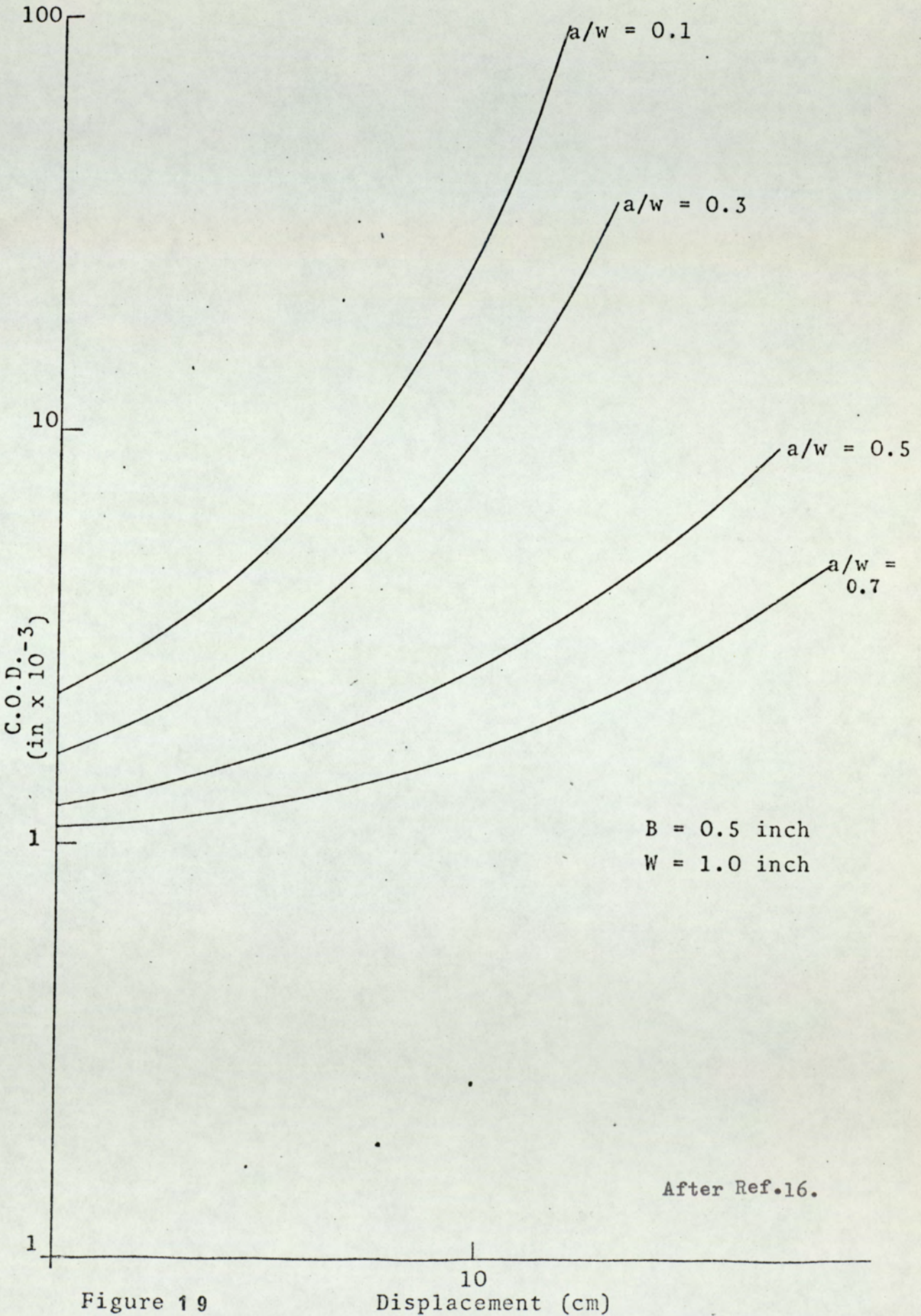


Figure 19

Displacement (cm)

approach was used⁽¹⁶⁾. Following the procedure in ref.(16) and using the calibration curves therein, (Fig.19), COD values at maximum load positions were determined. The fracture toughness values were then calculated by using the equation (8).

Average grain sizes were measured by using the linear intercept method and checked by Quantimet.

Various mechanical properties of the materials used in this investigation are given in Table I.

TABLE I Room Temperature Mechanical Properties.

Material	σ_{ys} MNm ⁻²	U.T.S. MNm ⁻²	Elong %	Area Red %	Hardness Vhn	Grain size μm	K_{lc} value MNm ^{-3/2}
QT-A	1637	1867	14	28	550	28	51.8 *
QT-B	687	841	28	60	250	39	68.2
IS	386	696	29	52	200	-	94

* Valid K_{lc} value.

3.3 The Crack-Growth Measurement Technique.

Different methods of crack extension measurement have been described by Srawley and Brown in ref.(99). The use of any of these techniques depends on its speed of operation; accuracy, reproducibility cost; probability of automation and the ease of application. A visual method with a maximum accuracy around 0.1 mm is used widely and also as a check to other methods used. In the present days the ultrasonic and the electrical potential methods are gaining popularity because of their high sensitivity (around 0.025 mm) and reproducibility and ease of continuous monitoring of crack-growth in a fatigue situation.

The electrical potential method involves passing a stabilised direct current through the specimen and measuring the increases in the

potential drop across the crack as it propagates. The increases in the potential drop can be calibrated against the crack length by using the visual method. The sensitivity of the system can be changed by different mode and amount of current application, the positioning of the potential measuring points and their distance of separation. The sensitivity also depends on the instruments used to measure the potentials which are usually of micro-volt range. Different aspects of the electrical potential method have been dealt with by Jack and Yeldham⁽¹⁰⁰⁾ and Ritchie⁽¹⁰¹⁾. Various features in the system which could cause inaccuracy in the results are as follows:-

- (a) Instability of constant current supply.
- (b) Thermo-electric E.M.F. generated due to dissimilar metal connection between potential leads and the specimen.
- (c) Inefficient earthing and screening of wiring.
- (d) Temperature variation in the specimen.

Any of these factors can cause instability of the system and give rise to spurious results.

In the present investigation, a highly stabilised Farnell constant power source of maximum 50 amp. capacity was used. Two methods were used to apply current to the specimens:-

- (a) Through brass strips soldered at the ends of the specimen, and
- (b) Through brass strips screwed at the ends of the specimens with silver-dag-layer in between.

It was found that if proper contacts were not made between the brass strips and the specimen ends, instability of the potential drop measurement results. A 0.28 mm screened iron wire was used for the potential leads which were spot welded on to the specimen. The potential drop was measured by a Rikadenki D.C. micro-voltmeter before being recorded by a Kent three-speed chart recorder. The apparatus gave a 100 micro-volt full-scale deflection. As the potential drop increases with the growth

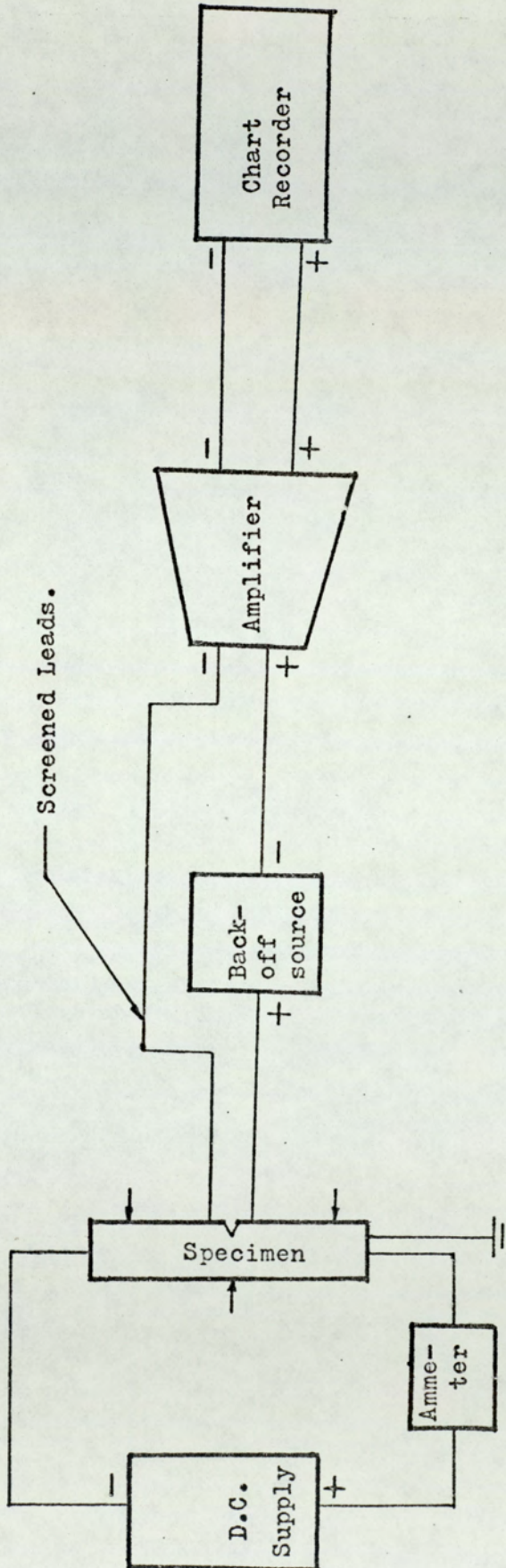


Fig.20. A Schematic Diagram Of The Electrical Potential Method.

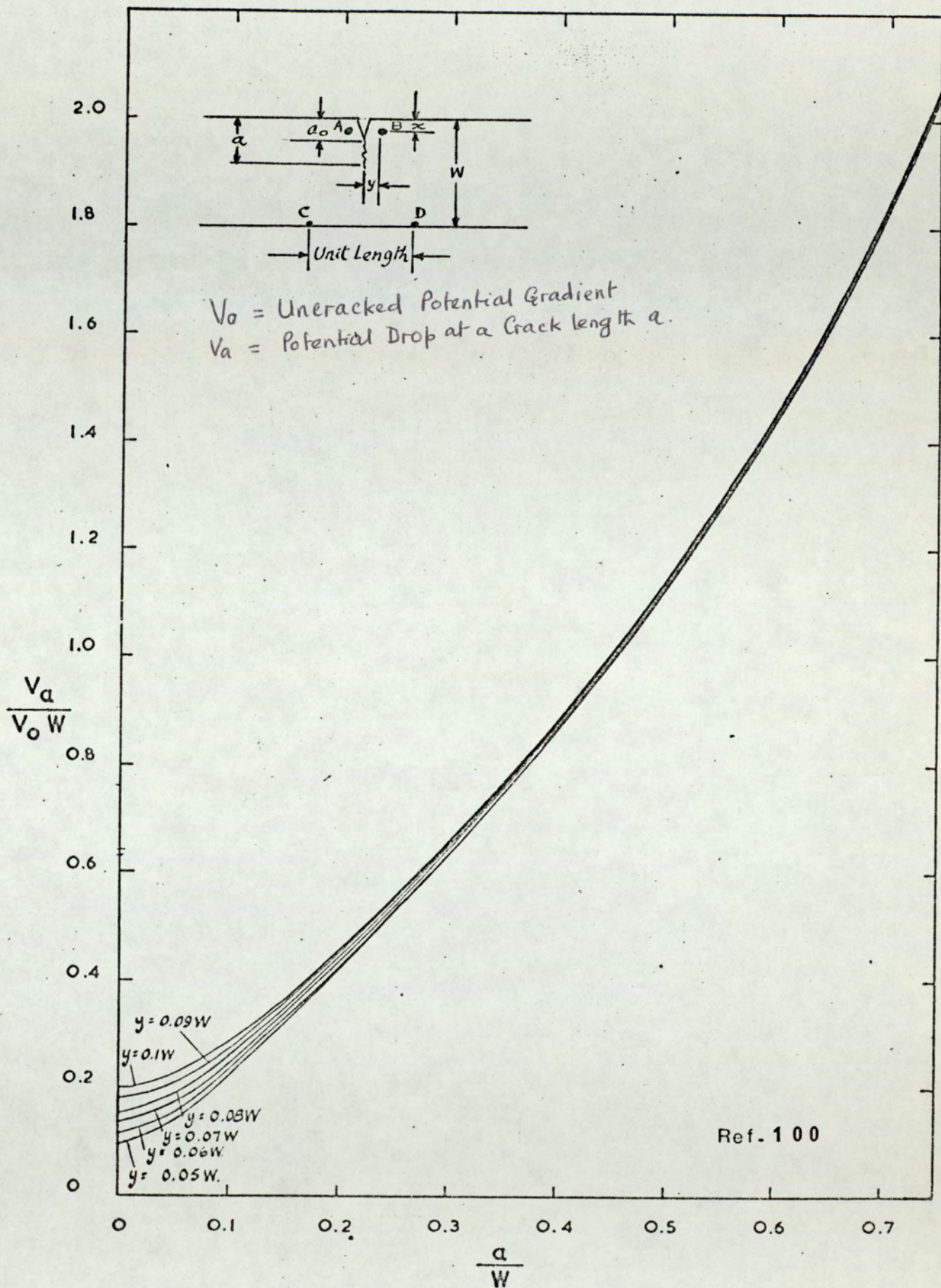


FIG.21 GRAPH OF $\frac{V_a}{V_0 W}$ VERSUS $\frac{a}{W}$ FOR POTENTIAL MEASURING POINTS AT $x = 0$, $y = \pm$ VALUES SHOWN.

of the crack, a back-off voltage was required to maintain 100 micro-volt full-scale deflection on the chart recorder. The back-off voltage was supplied from a potentiometric source. A schematic diagram of the apparatus is shown in Fig.(20).

Gilby and Pearson⁽¹⁰²⁾ used a theoretical calibration between the potential drops and the crack lengths for different applications of the current and for different positioning of the potential measuring leads yielding good correlation with visual measurements. An example of the typical calibration curves from ref.(100) is shown in Fig.(21). It was noted that the maximum sensitivity of the potential method could be obtained if the potential leads were placed at the position where the crack length was zero. The uncracked potential gradient V_0 was approximated by measuring the potential at the back surface of the notched specimen. The ICL 1903 computer was used to fit polynomials to the theoretical calibration curves derived for different positioning of the potential leads (i.e. y values) as shown in Fig.(21). The values of a/W at different values of $\frac{V}{V_0 W}$ were tabulated at intervals of 0.001 (Appendix I). The values of the co-efficients of the polynomials for different values of y are given below:-

For $y = 0.090 W$;

$C_0 = -0.081389,$	$C_1 = 0.76142,$
$C_2 = -0.37229,$	$C_3 = 0.20344,$
$C_4 = -0.07420,$	$C_5 = 0.010734.$

For $y = 0.095 W$;

$C_0 = 0.091324,$	$C_1 = 0.79260,$
$C_2 = -0.41581,$	$C_3 = 0.23376,$
$C_4 = -0.084474,$	$C_5 = 0.012080.$

For $y = 0.10 W$;

$C_0 = -0.10178,$	$C_1 = 0.82574,$
$C_2 = -0.46218,$	$C_3 = 0.26608,$
$C_4 = -0.095415,$	$C_5 = 0.013513.$

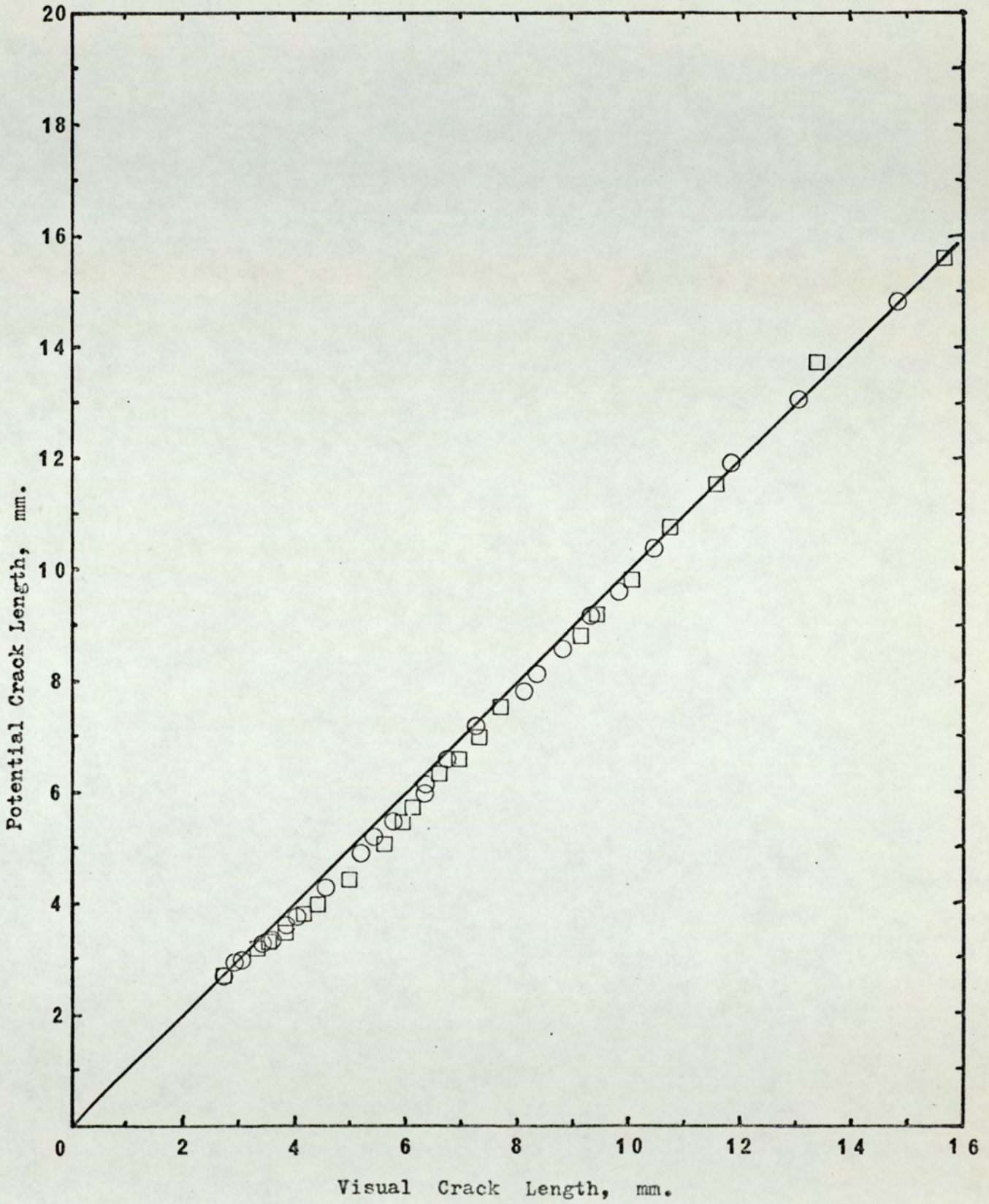


Fig.22. Comparison Of Potential Method With Visual Method.

For $y = 0.105 W$;

$C_0 = -0.11319,$	$C_1 = 0.86173,$
$C_2 = -0.51264,$	$C_3 = 0.30142,$
$C_4 = -0.10744,$	$C_5 = 0.015094.$

For $y = 0.11 W$;

$C_0 = -0.12501,$	$C_1 = 0.89882,$
$C_2 = -0.56406,$	$C_3 = 0.38713,$
$C_4 = -0.11957,$	$C_5 = 0.016694.$

Knowing the initial notch length a_0 at the start of each test and the value of $\frac{V}{V_0} \frac{a_0}{W}$, it was possible to follow the right calibration curve. This would eliminate any inaccuracy in positioning of the potential leads. A representative check by the visual method (using travelling microscope) on the potential method, is shown in Fig.(22).

By passing a current of 20 Amps through the specimen, the sensitivity of the potential crack growth monitoring system was of the order of 0.001 W i.e. about 0.025 mm. In terms of measurement of absolute crack length, a maximum difference of about 0.50 mm (i.e. about 0.02 a/W) between the visual and the potential drop measurement was observed at low a/W values. This would represent only a small change in the specimen compliance value and hence a relatively small inaccuracy in the absolute value of the stress intensity at the crack tip. The potential method was capable of detecting the crack initiation long before the crack was visible on the surface.

3.4 Fatigue Crack Initiation

Since a machined notch is less sharp than a fatigue crack, the load required for the initiation of a fatigue crack from a notch is higher than that required for its propagation. The initiation load was therefore calculated as follows:-

As laid down in the BISRA open report on plane strain fracture toughness⁽¹⁰³⁾, for the propagation of a reasonably sharp fatigue crack by 1.27 mm (0.05 inch) in 50,000 cycles, we need:-

$$\Delta K = 0.0005 E \quad \dots \quad (31)$$

where E is the Young's modulus of the material.

Now for a 3 point bend specimen (span : width = 4:1),

$$\Delta K = \frac{Y \cdot \Delta P}{B \cdot W^{\frac{1}{2}}} \quad \dots \quad (32)$$

where ΔP is the load range and Y is a geometrical factor given as a function a/W ⁽¹⁰⁴⁾.

For a certain crack length a (e.g. notch length), Y is known and hence equating equations (31) and (32), we can write:

$$\Delta P = \frac{(0.0005 E) (B W^{\frac{1}{2}})}{Y} \quad \dots \quad (33)$$

The equation (33) gives the load range required for the propagation of an existing fatigue crack by 0.127 mm in 50,000 cycles. It was found that for the initiation of a fatigue crack from the machined notch in a reasonable number of cycles (say 50,000), a load range of about 140 percent of that given by equation (33) was necessary. It was also noted from the reference⁽¹⁰³⁾ that to maintain a sharp crack tip, the load range should not be less than 75 percent of the maximum load in the case of tension-tension loading and if the load alternates through zero, the load range should not be greater than twice the maximum load.

3.5 Constant Load Fatigue Tests:

A suitable load range was selected to give a wide range of ΔK values over the range of crack lengths for which compliance function was available. After the initiation of the fatigue crack from the

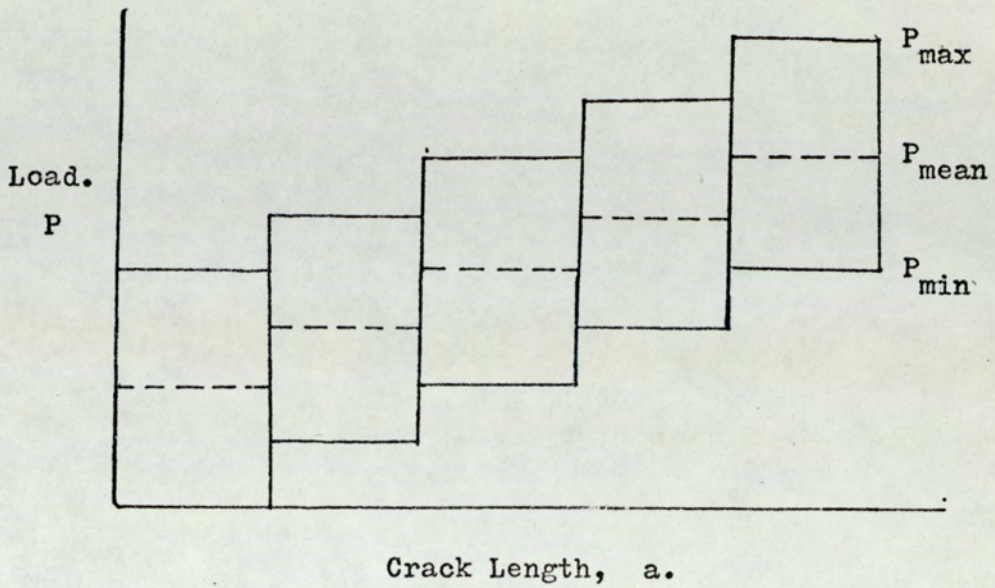


Fig.23a. Constant Load Amplitude With Increasing Mean Load.

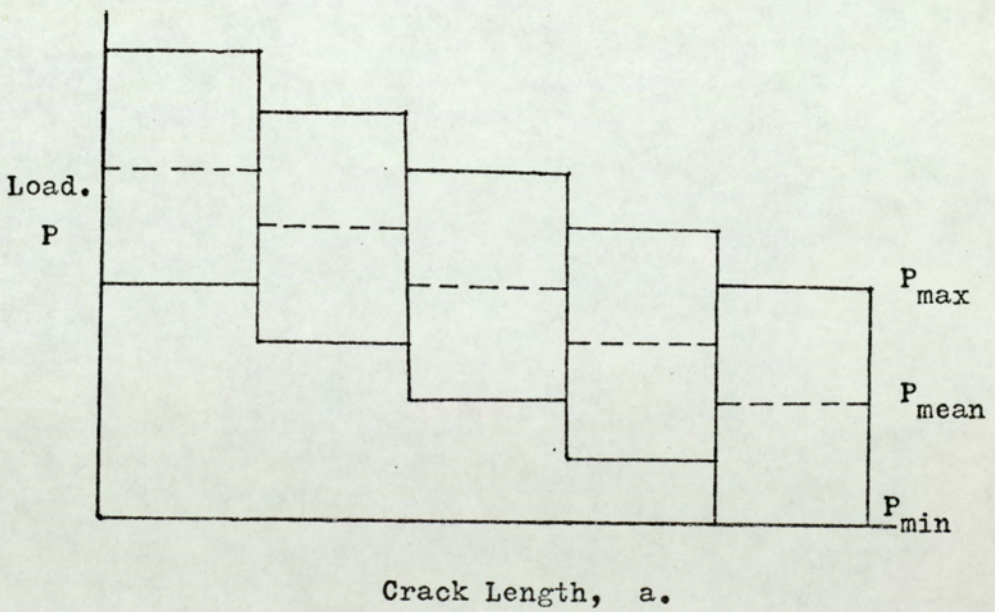


Fig.23b. Constant Load Amplitude With Decreasing Mean Load.

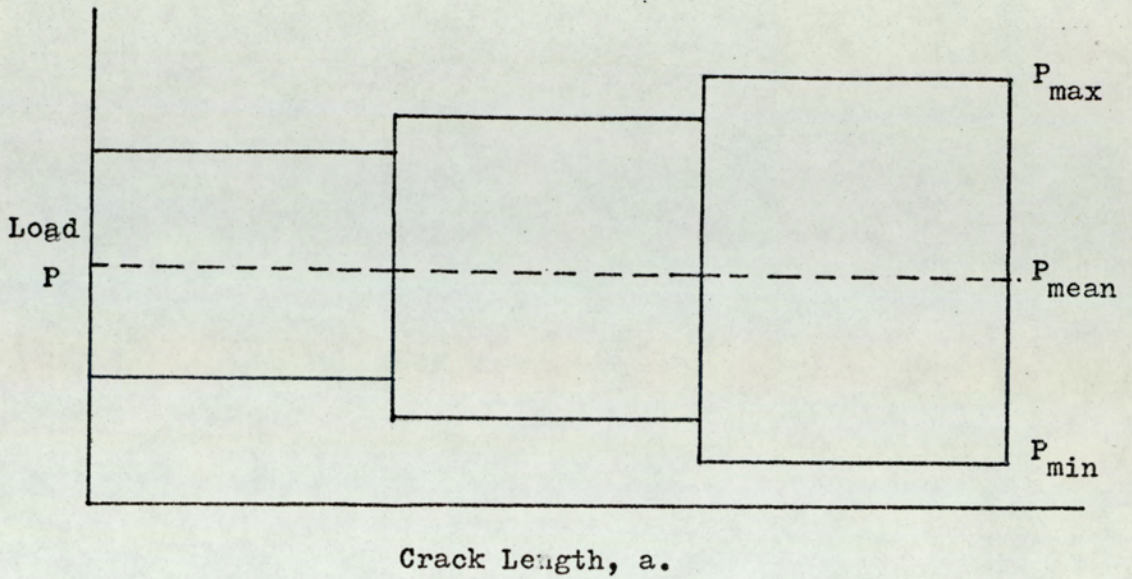
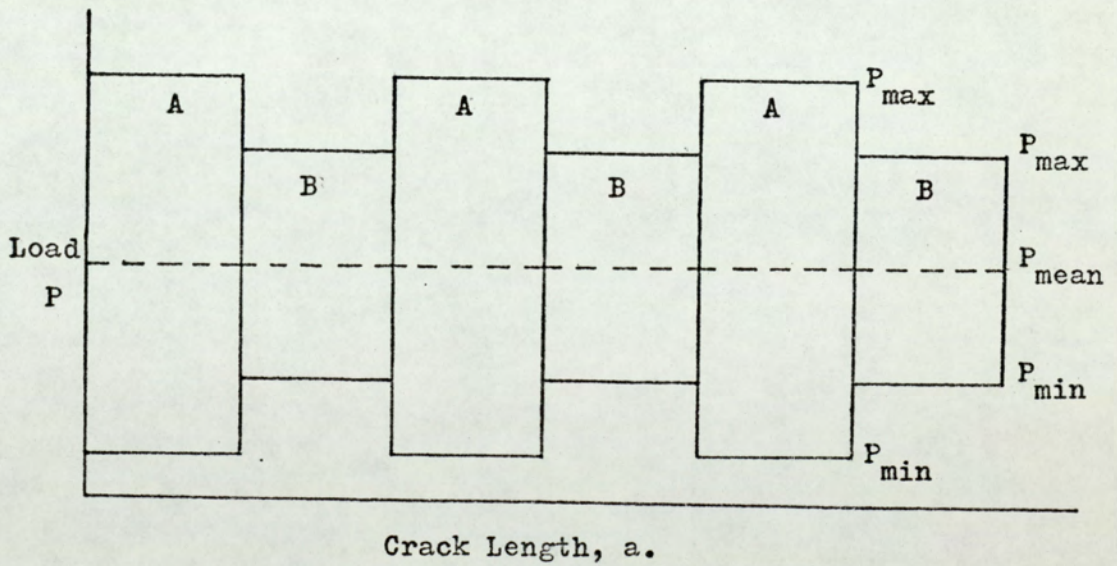


Fig.23c. Stepped Increase In Load Amplitude At Constant Mean Load.



A=High Load Block. B=Low Load Block.

Fig.23d. Two-Step Load Amplitudes At Constant Mean Load.

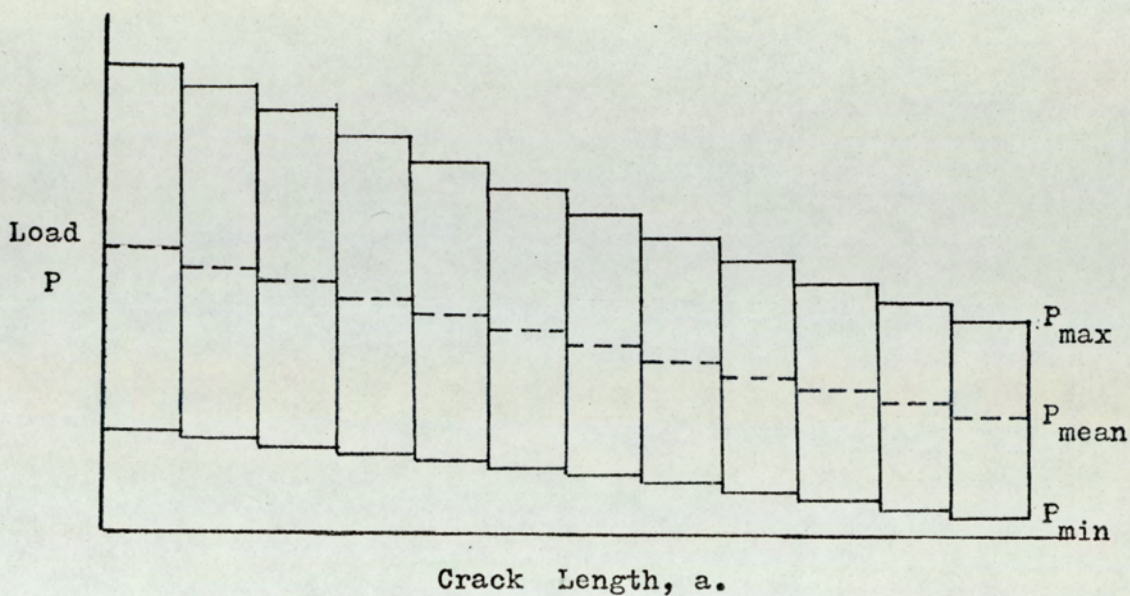


Fig.23e. Constant ΔK At Constant K_{mean} .

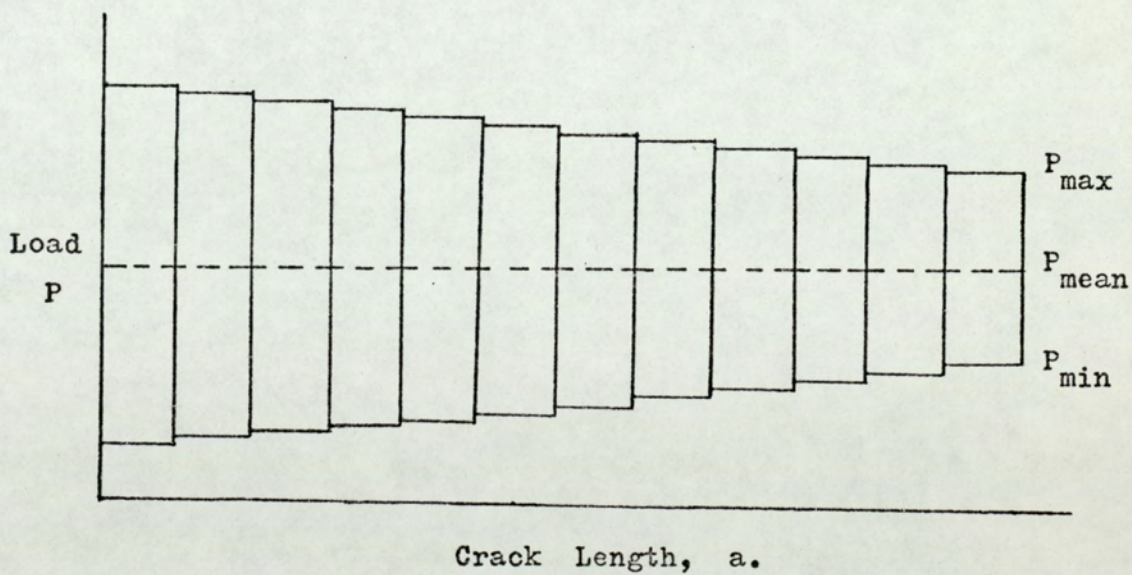


Fig.23f. Constant ΔK At Constant Mean Load.

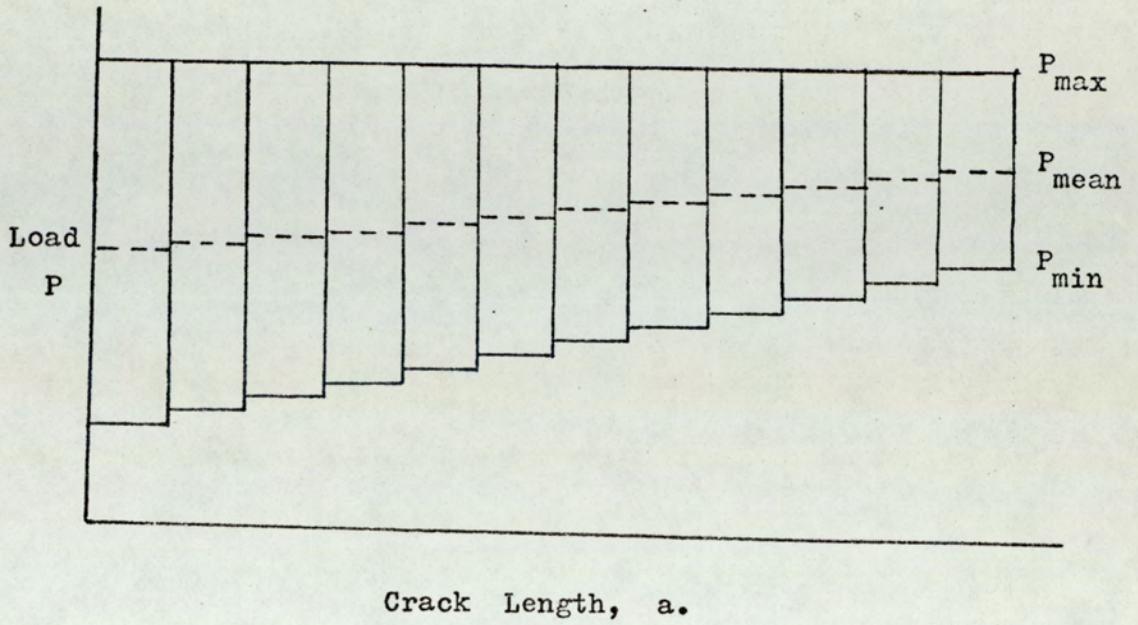


Fig.23g. Constant ΔK At Constant Maximum Load.

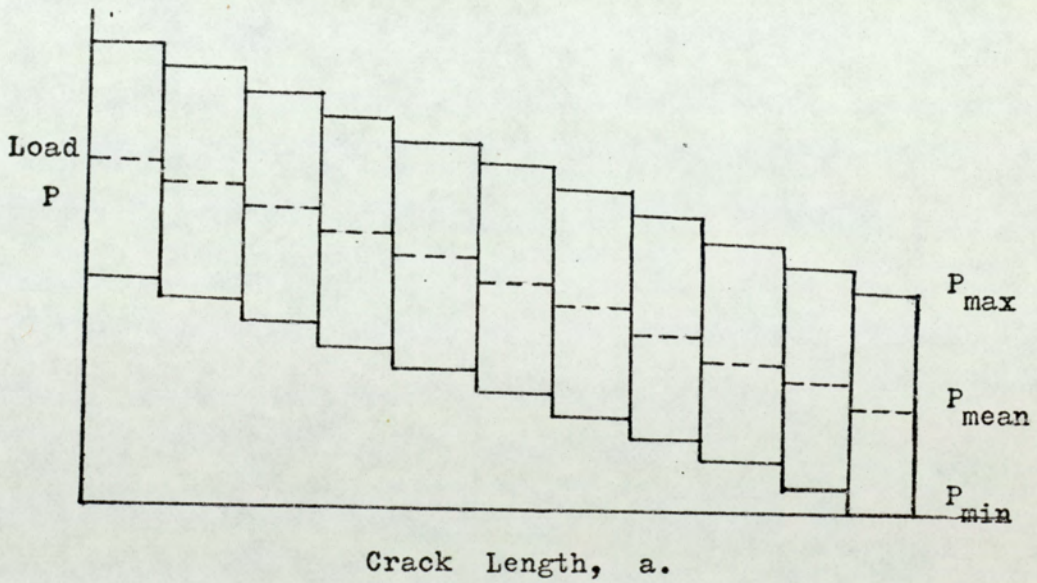


Fig.23h. Constant K_{max} With Increasing ΔK .

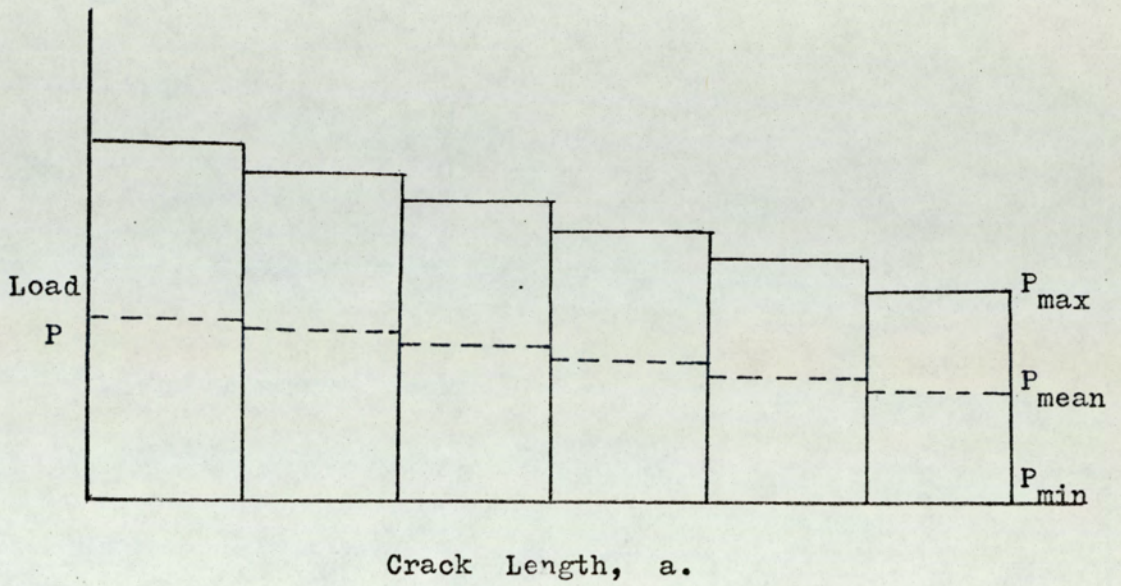
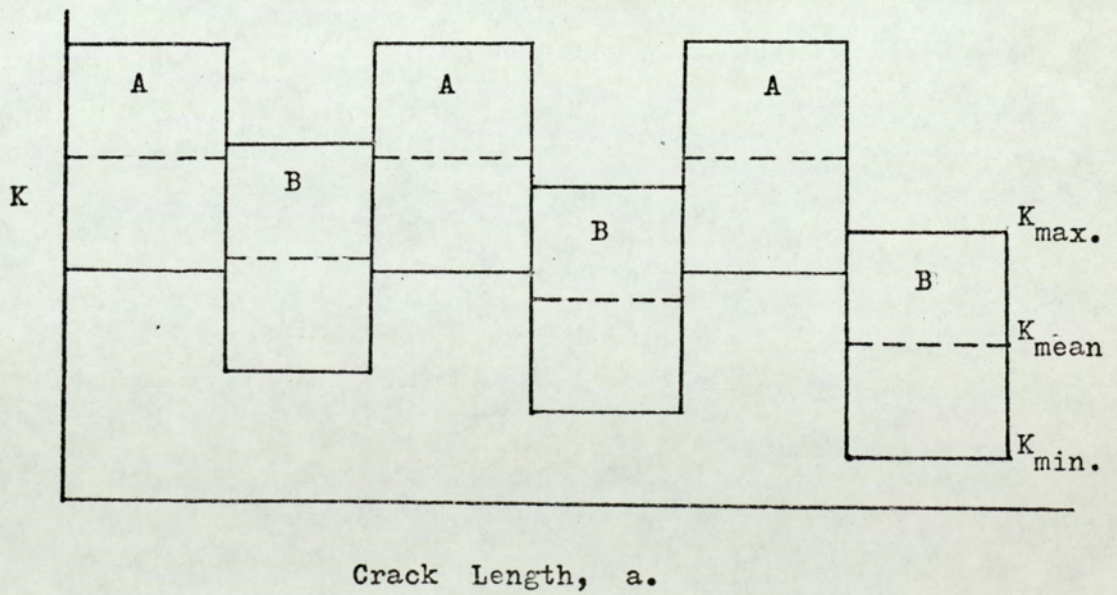


Fig.23i. Constant ΔK And K_{max} With Zero K_{min} .



A=Control Blocks.

B=Test Blocks.

Fig.23j. K_{mean} Reduction By Steps.

A=Control Blocks.

B=Test Blocks.

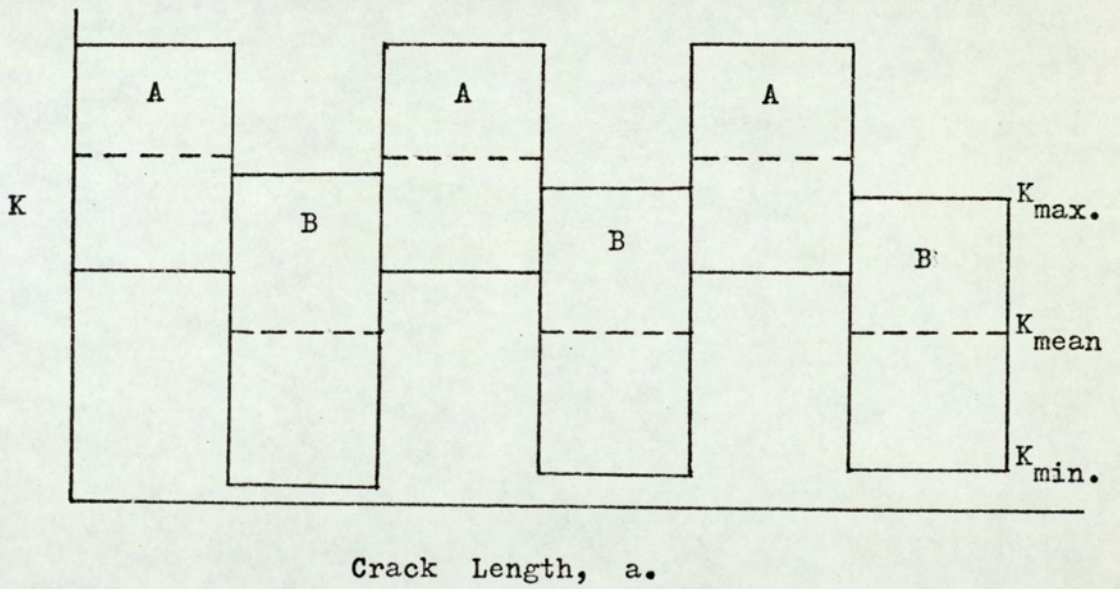


Fig.23k. 50% K_{mean} Reduction And ΔK Increase.

machined notch ($a = 0.1 W$) at high load, the test load was applied and the crack growth measurement started at about $0.15 W$. It was found that with the Amsler Vibrophore, the constant load amplitude could be maintained to a maximum crack length of about $0.65 W$.

3.6 Programme Load Fatigue Tests

The loading programmes used in this investigation were aimed at finding out the effects of mean load, maximum load, stress ratio, load-interaction and load-sequence and also the effect of overall load history on the crack propagation. Some of these programmes were designed to follow up the results of a preceding programme. The designs of the load programmes were such that the controlling variables were either stresses or stress intensities. Sometimes mixed design was used. The load programmes used in this investigation are briefly described below:-

- (a) Constant load amplitudes in blocks with increasing or decreasing mean load.

A constant step of increase or decrease of mean load was used thus changing the stress ratio in each block.

- (b) Stepped increase in load amplitudes in blocks at constant mean load.

The increase in load amplitude was about 40 percent of the preceding load.

- (c) Two-step block load test at constant mean load.

In this programme high-low-high-low sequence was used. the difference in the magnitude of load amplitude was 20 percent in one test and 40 percent in another. The load ranges selected were such that the stress intensity ranges corresponding to them during total crack propagation upto a/W of about 0.6 would be within the overall stress

intensity range of the constant load amplitude tests.

The crack was allowed to grow by a constant amount equal to 0.05 W in each block.

(d) Constant ΔK test at constant K_{mean} .

In these tests, as the crack grew, load shedding similar to fig.(12) was used to keep both ΔK and K_{mean} constant. The value of R which is defined as $\frac{K_{\text{min}}}{K_{\text{max}}}$ was therefore constant throughout a particular test. The amount and frequency of load shedding was determined by the following:-

- i) The minimum value of Amsler load-scale reading.
- ii) The rate of crack-growth which determined the time available between load shedding.
- iii) The sensitivity of the crack growth measuring equipment.

Three different values of ΔK and K_{mean} were chosen to give three different R values. The Olivetti Programmer 101 was used to determine the values of the crack lengths at which load shedding had to be done. This procedure, therefore, resulted in a 'semi-continuous' load shedding.

(e) Constant ΔK at constant P_{mean}

In these cases semi-continuous load shedding was not used. The crack was allowed to grow by amounts equal to 0.05 W. At the end of each block, the load was reduced to keep the average ΔK constant. The average ΔK was calculated by using the Y values at the mid-point of each block. This procedure of keeping the stress intensity approximately constant can be termed as 'block load shedding' method. Different ΔK and mean load levels were used in these tests.

(f) Constant ΔK at constant P_{max}

In these cases both the semi-continuous load shedding and the block load shedding described before were used to keep ΔK constant. Different ΔK and maximum load levels were used.

(g) Constant K_{max} with increasing ΔK

In these tests semi-continuous load shedding was used.

Three different levels of K_{max} were chosen.

(h) Constant ΔK and K_{max} with zero K_{min}

In these tests block load shedding was used. Stress ratio R in this programme was zero.

(i) K_{mean} reduction tests

In these tests block load shedding was used to keep ΔK and K_{mean} constant. A control block of ΔK and K_{mean} was applied to grow the crack by an amount equal to 0.05 W and then K_{mean} was reduced by a certain percentage of the control K_{mean} , keeping the ΔK as before. The crack was then allowed to grow by another 0.05 W at the end of which the K_{mean} was raised to the control value. This procedure was repeated in a test with different percentage reductions of K_{mean} . A follow up programme of the above test was done by increasing the ΔK level by a certain percentage of the control ΔK after the K_{mean} was reduced by 50 percent.

(j) Determination of threshold value of ΔK

A low ΔK value was chosen which would give a reasonable crack growth. The maximum load was kept constant and ΔK was reduced in blocks by steps of 10 percent. The load programme used in this test was somewhat similar to that given in Fig.23g. All the load programmes used in this investigation are shown schematically in Fig.(23 a-k)

3.7 General Method of Data Analysis

In order to obtain consistent and accurate results, almost all the tests were duplicated except in cases where the test procedure was too cumbersome to permit duplication. The constant load amplitude tests which would serve as a basis for comparison with other programme load results were triplicated.

The initial crack growth data were plotted as the crack length versus number of cycles curve. The crack propagation rates were obtained graphically by taking tangents to the curves at different points. The stress intensity values for the corresponding points were calculated from the equation (32). No plastic zone correction was used. For some of the programme load tests, specially the K-controlled tests, average crack-growth rate was calculated by dividing the crack increment in a block by the number of cycles taken to grow that increment. The stress intensity value was calculated at mid-point of the block. Wherever possible, a regression line was fitted to the crack propagation data to show the general trend.

3.8 Other Experimental Work

Because of the present interest in COD approach to fatigue and also to explain some of the results obtained in the programme fatigue tests, the measurements of COD in fatigued specimen were carried out. The main difficulty in doing this was the non-availability of proper instrumentation for measuring COD in actual fatigue situations. Following the argument put forward by Elber⁽⁸⁹⁾ that the plastic deformation left in the wake of a propagating fatigue crack contributes to the displacement at the crack tip, an approximate method of COD measurement was employed. The method involved stopping the fatigue cycling and measuring COD at the crack tip under monotonic loading over one cycle. It was assumed that frequency of loading would have negligible effect on actual measurement. Micro-hardness marks were placed on either side of the crack at a distance of

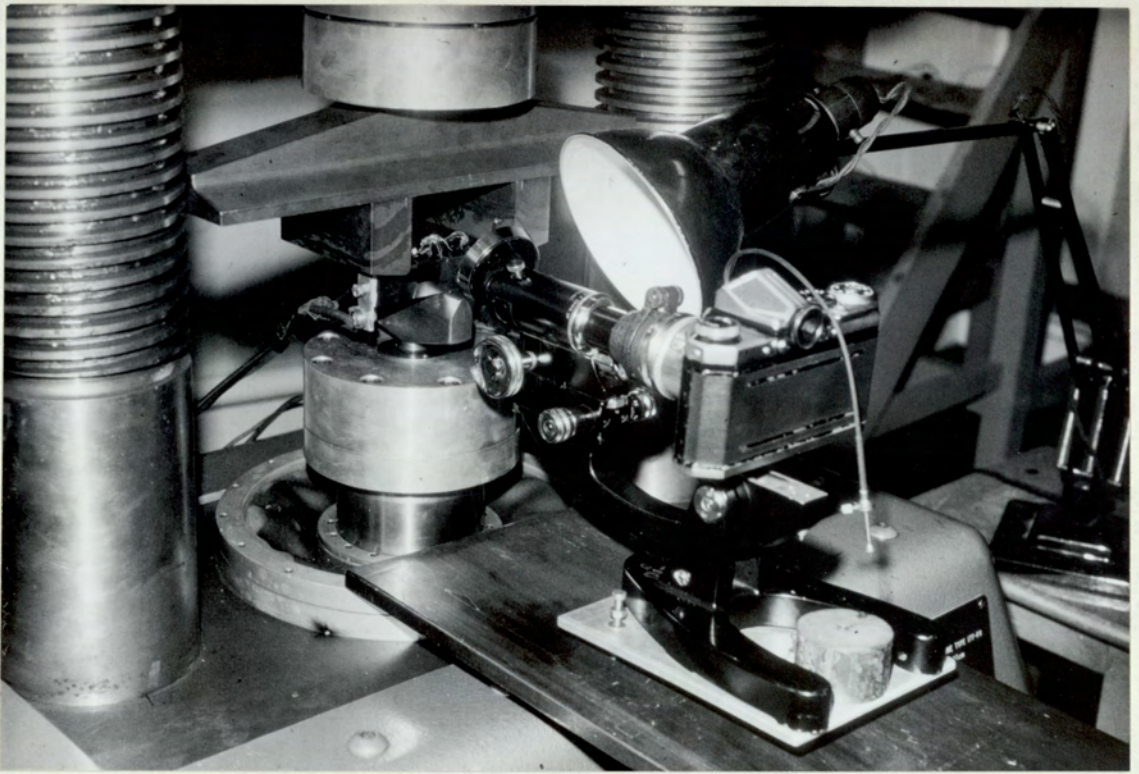


Fig.23x. Experimental Set-up for C O D Measurement.

0.1 mm. The marks at the crack tip were photographed by a 35 mm. camera with microscope attachment (Fig.23x). The film was projected on to a screen by a slide projector to get a total magnification of about 700. The distances between the micro-dots were measured and COD obtained with reference to the datum distance at no load condition. Two types of COD tests were done:-

- (a) COD values were measured for different loads below K_c after propagating the crack to different lengths.
- (b) The specimen was cracked under constant K conditions to a crack length of 0.3 W. The K_{mean} was then reduced by 30 percent and fatiguing was continued under the same ΔK as before. The crack opening displacements were measured at maximum and minimum loads by stopping the fatigue cycling at intervals of 3000 cycles.

3.9 Microscopic and Fractographic Study

The specimens were sectioned, polished, etched and optical micrographs of the fracture path taken to reveal the effects of micro-structures on the fatigue crack propagation. The fracture surfaces from constant load tests and from different programme loadings were also studied extensively under a scanning electron microscope.

The micro-meter attached to the stereoscan specimen-holder was used to locate different load change positions and also to determine the value of the stress intensity at the area under examination. In cases where demarcation lines of the load change position were visible by the naked eye, hardness marks were given to locate such positions under the stereoscan.

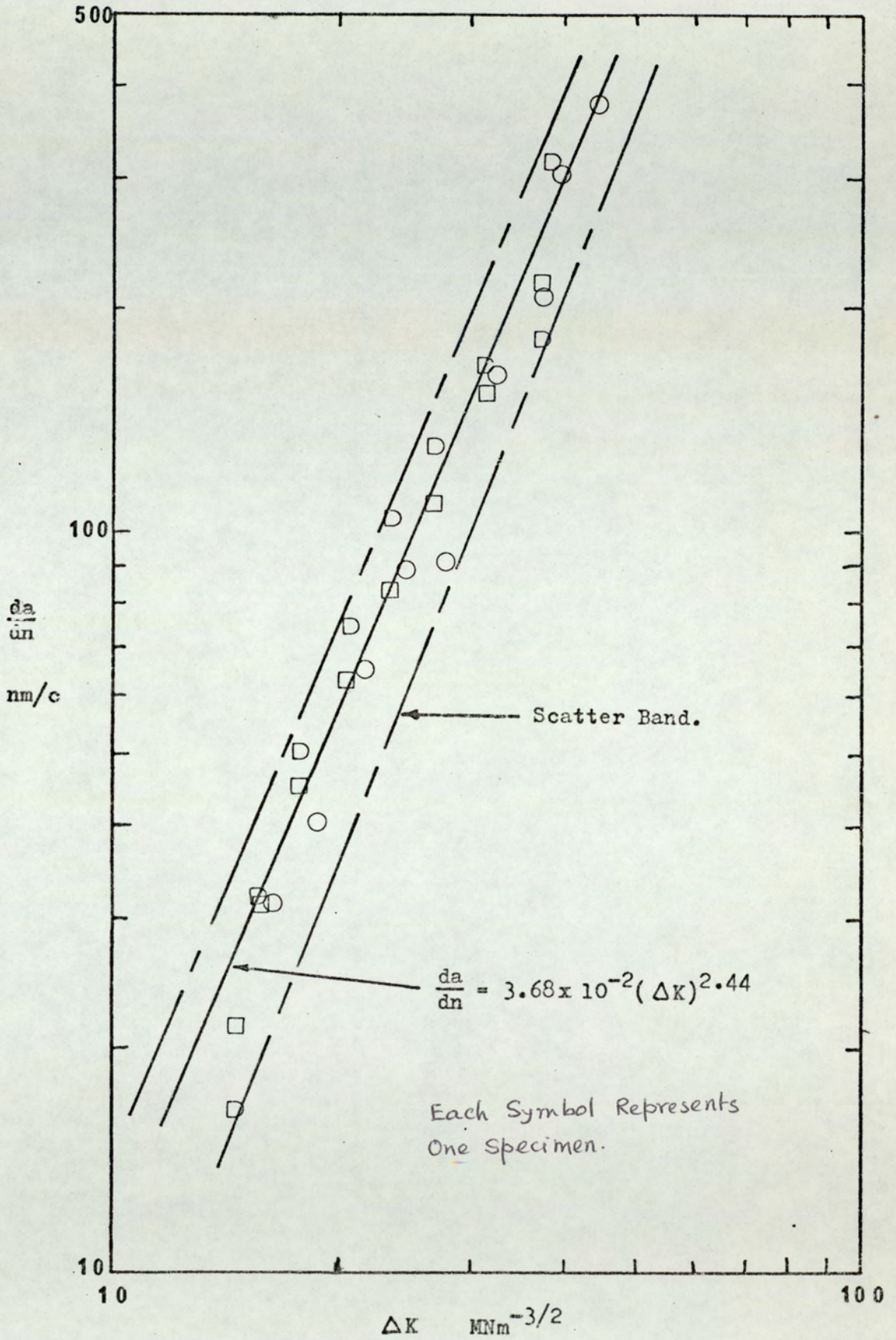
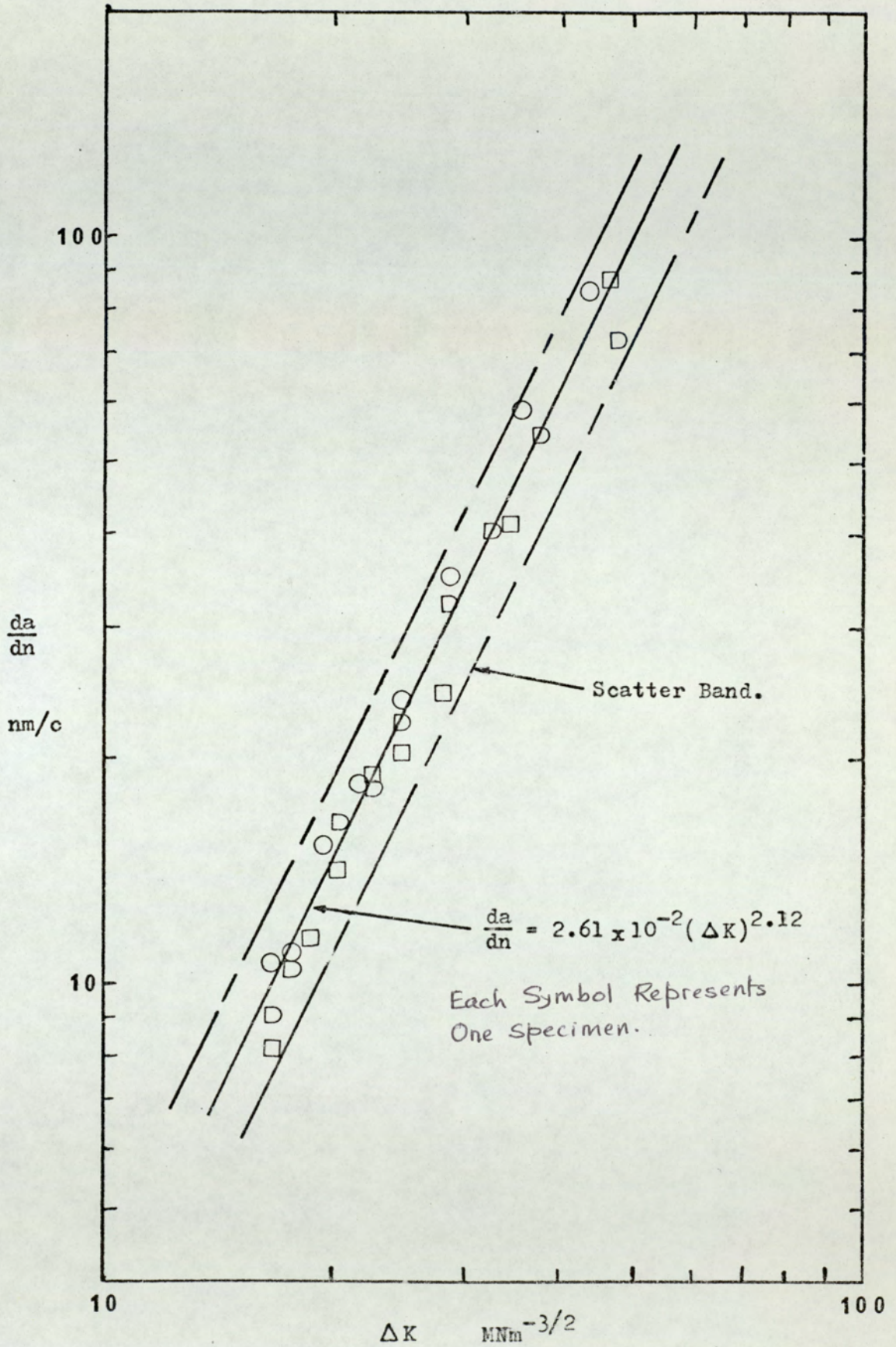


Fig.24a. Crack Growth Curve For Constant Load Amplitude Tests At Constant Mean Load. (QT-A).



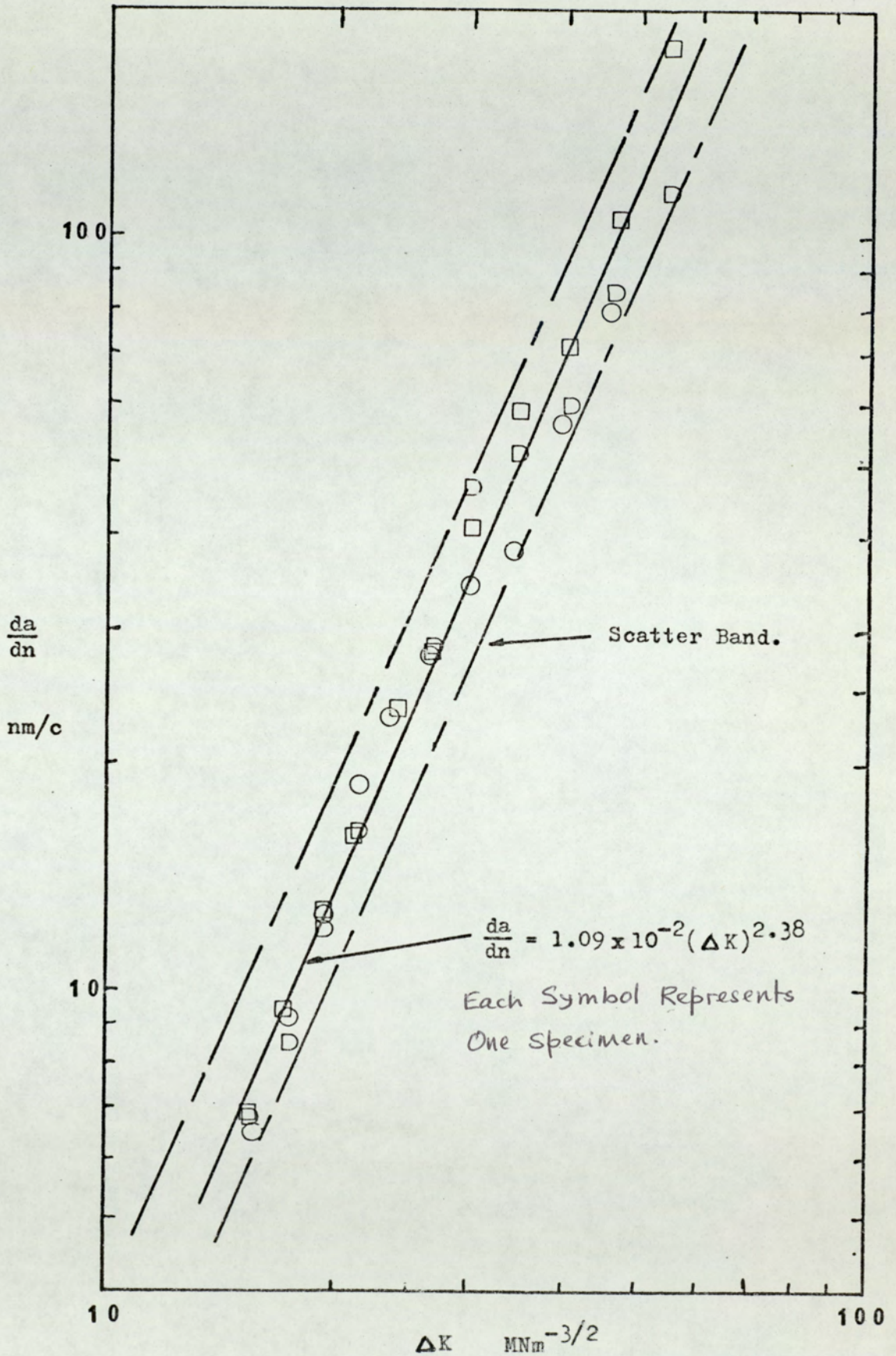


Fig.24c. . Crack Growth Curve For Constant Load Amplitude Tests At Constant Mean Load. (IS).

4. RESULTS

4.1 Initiation of Fatigue Crack

Under the initiation condition described in section (3.4), the fatigue cracks initiated from the machined notch within 50,000 cycles in almost all the specimens. The initial fatigue crack front was straight in most of the specimens with the exception of a few where slant crack fronts were observed. It was found that the slanting occurred due to the rough edges of the machined specimens. A very slight rounding of the specimen edges eliminated crack front slanting. However, a little slanting occurred in almost all the specimens at the start of the tests, but it evened out before the crack growth measurements were started for the purpose of analysis. The variation in duplicate results in some cases was due to the persistent slant crack front. These results were therefore discarded. The crack initiation was easier in the case of martensitic steel as compared to the other two structures, but it was more prone to crack slanting.

4.2 Constant Load Amplitude Tests at Constant Mean Load

The constant load amplitude tests were done at a stress ratio of 0.2 on all the three heat-treatments. The rates of crack propagation obtained graphically from a-N curve were plotted as a function of stress intensity ranges. The relationship between $\log \Delta K$ and $\log \frac{da}{dn}$ was linear as predicted by the equation (17). The plots are shown in Figs. 24a-c. The regression line fitted to the results of three specimens was regarded as the master curve for each heat-treatment. All regressions of $\log \frac{da}{dn}$ on $\log \Delta K$ showed high degrees of positive correlation.

In the case of material QT-A, the values of crack growth exponent m varied from 2.35 to 2.48 and the pre-exponent A varied from 3.12×10^{-2} to 4.57×10^{-2} when the growth rate was in nm/cycle and the

stress intensity in $\text{Mnm}^{-3/2}$. Henceforth all the A values of equation (17) will be quoted for these units. In QT-B, the values of m varied from 1.99 to 2.19 and A varied from 1.88×10^{-2} to 3.77×10^{-2} . The material IS showed a variation of m from 2.27 to 2.52 and a variation of A from 7.15×10^{-3} to 1.50×10^{-2} . The values of m and A for the master curves for the three heat-treatments are given in table 2.

Material	micro-structure	m	A x 10 ⁻²
QT-A	Martensitic	2.44	3.68
QT-B	Spheroidised	2.12	2.61
IS	Pearlitic	2.38	1.09

Table 2. Values of Crack Growth Exponent & Pre-exponent

The crack growth rates in material QT-B and IS were identical and fell nearly on the same scatter band. The growth rates in QT-A, on the other hand, were about 3 to 5 times faster over the range of ΔK considered (10 to 50 $\text{Mnm}^{-3/2}$). Though the values of m and A seemed to be very close for the three heat-treatments, the crack-growth data fell into two distinctly separate scatter bands.

4.3. Programme Load Tests

4.3.1 Constant Load Amplitude with Varying Mean Load

Two types of varying mean load tests were done on materials QT-A and IS (Figs. 23a-b). In one case, the mean load was increased by a constant step between the blocks in such a way that the stress ratio increased from zero at the start of the test to about 0.3 at the end. In the other case, the reverse procedure was followed. About seven

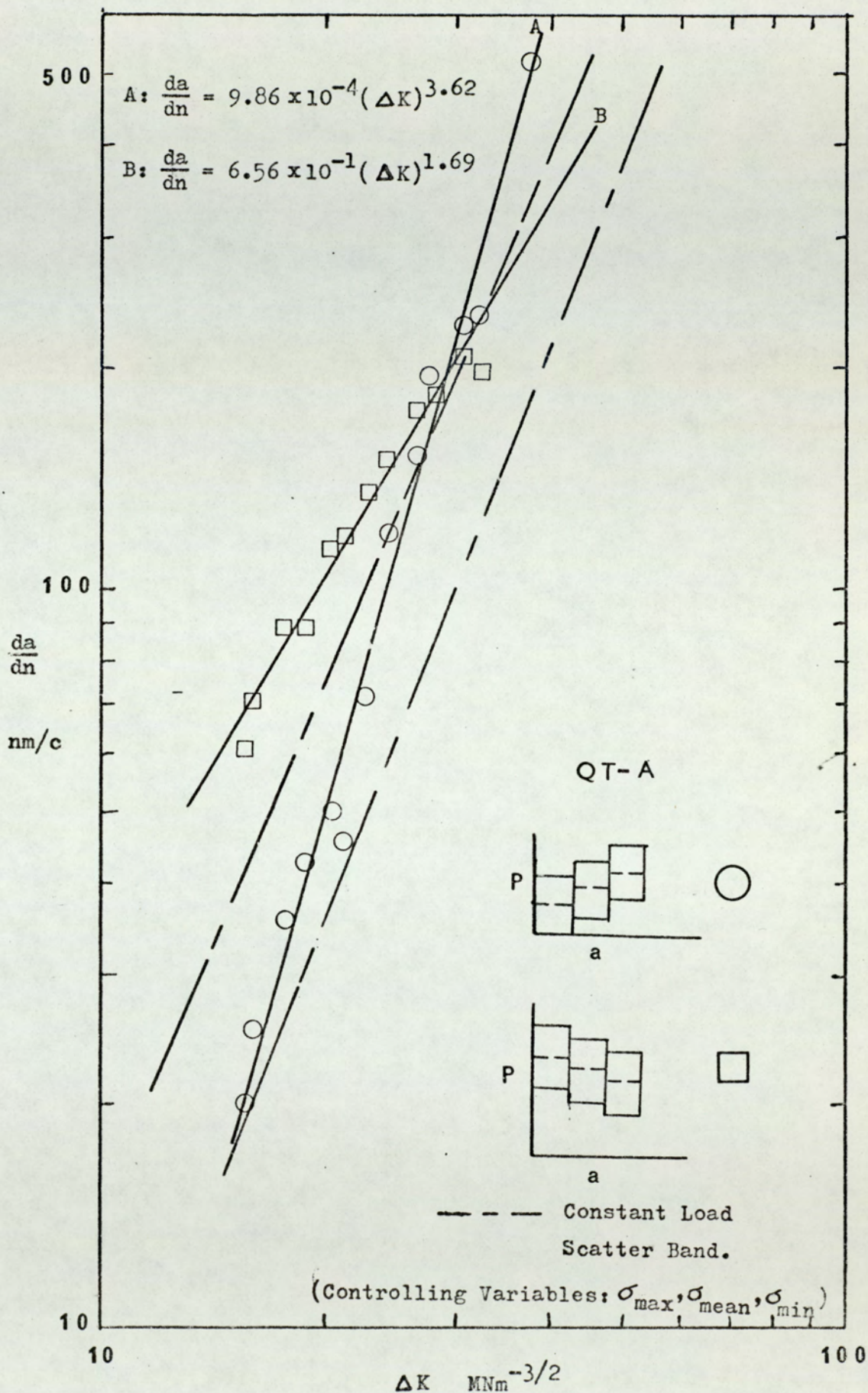


Fig.25a. Crack Growth Curves For Constant Load Amplitude Tests With Increasing And Decreasing Mean Load.

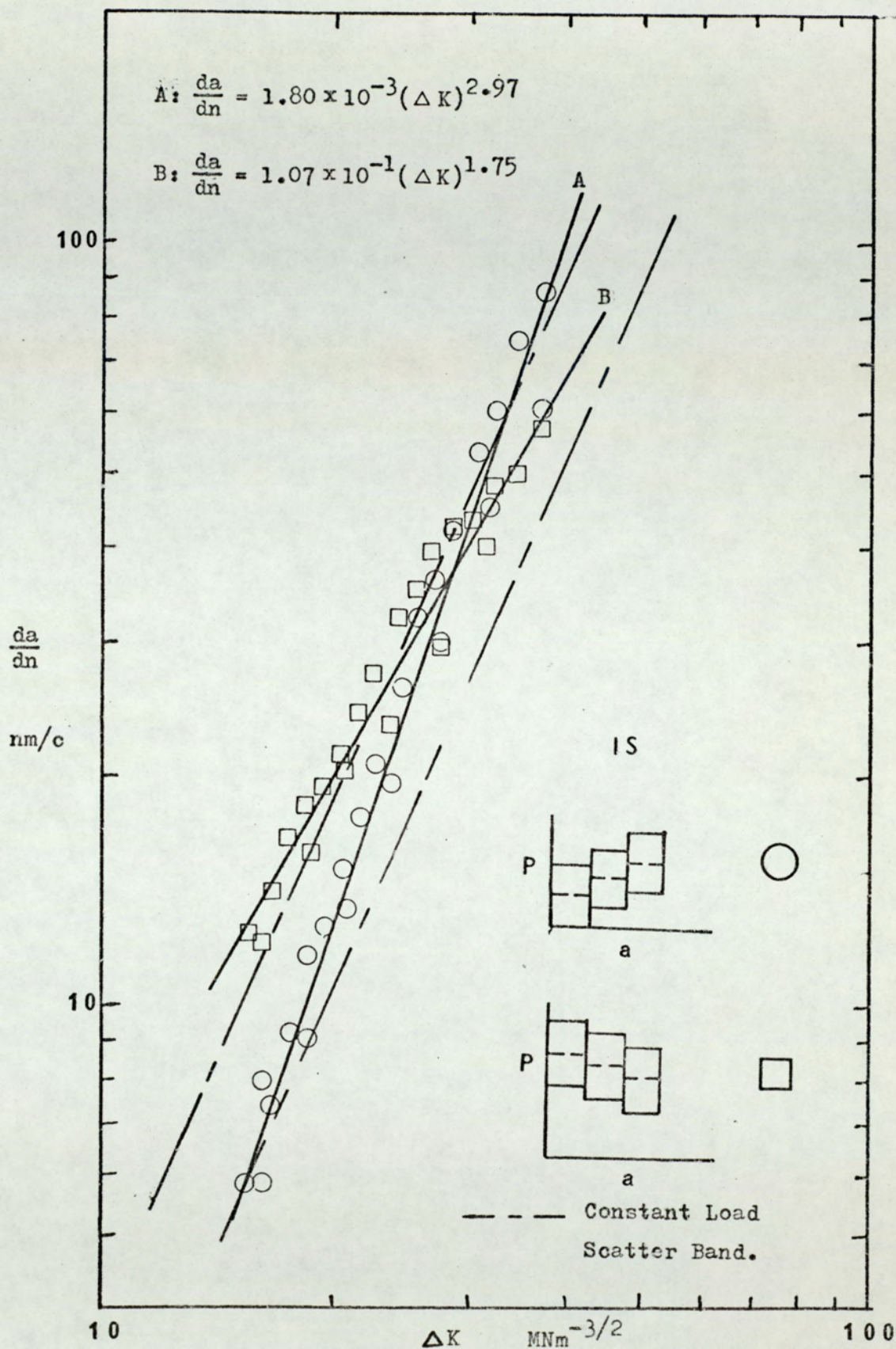


Fig.25b. Crack Growth Curves For Constant Load Amplitude Tests With Increasing And Decreasing Mean Load. (Controlling Variables: σ_{max} , σ_{mean} , σ_{min})

blocks were used in each test. In each block, the crack was allowed to grow by $0.05 W$ under a constant stress amplitude. The a-N data from each test produced a smooth curve. The crack-growth rates obtained graphically were related to stress intensity range as shown in Figs. (25a-b). In both the materials tested, the overall life was shorter in the case where the mean load was decreasing than where the mean load was increasing. The values of m and A are shown in table 3.

Material	Load Programme	m	A
QT-A	Increasing Mean Load	3.62	9.86×10^{-4}
QT-A	Decreasing Mean Load	1.69	6.56×10^{-1}
IS	Increasing Mean Load	2.97	1.80×10^{-3}
IS	Decreasing Mean Load	1.75	1.07×10^{-1}

Table 3. Values of Crack Growth Exponent & Pre-exponent

4.3.2 Stepped Increase in Load Amplitude at Constant Mean Load

In this case the tests were done at a constant mean load, but the load amplitude was increased by about 40%, thereby increasing σ_{max} and decreasing σ_{min} after each $0.1 W$ of crack growth (Fig. 23c). Thus three load blocks were used for growth between $0.2 W$ to $0.5 W$. These three load blocks were at stress ratios of 0.333, 0.177 and 0.053 in the case of material QT-A. With material IS, the stress ratios were 0.385, 0.233 and 0.069. The a-N curves showed a sudden and discrete change in slope at starts of a new load amplitude level. This was more pronounced in the case of material IS than QT-A. Within each block, the a-N curve was smooth as can be seen from Fig. 26. The

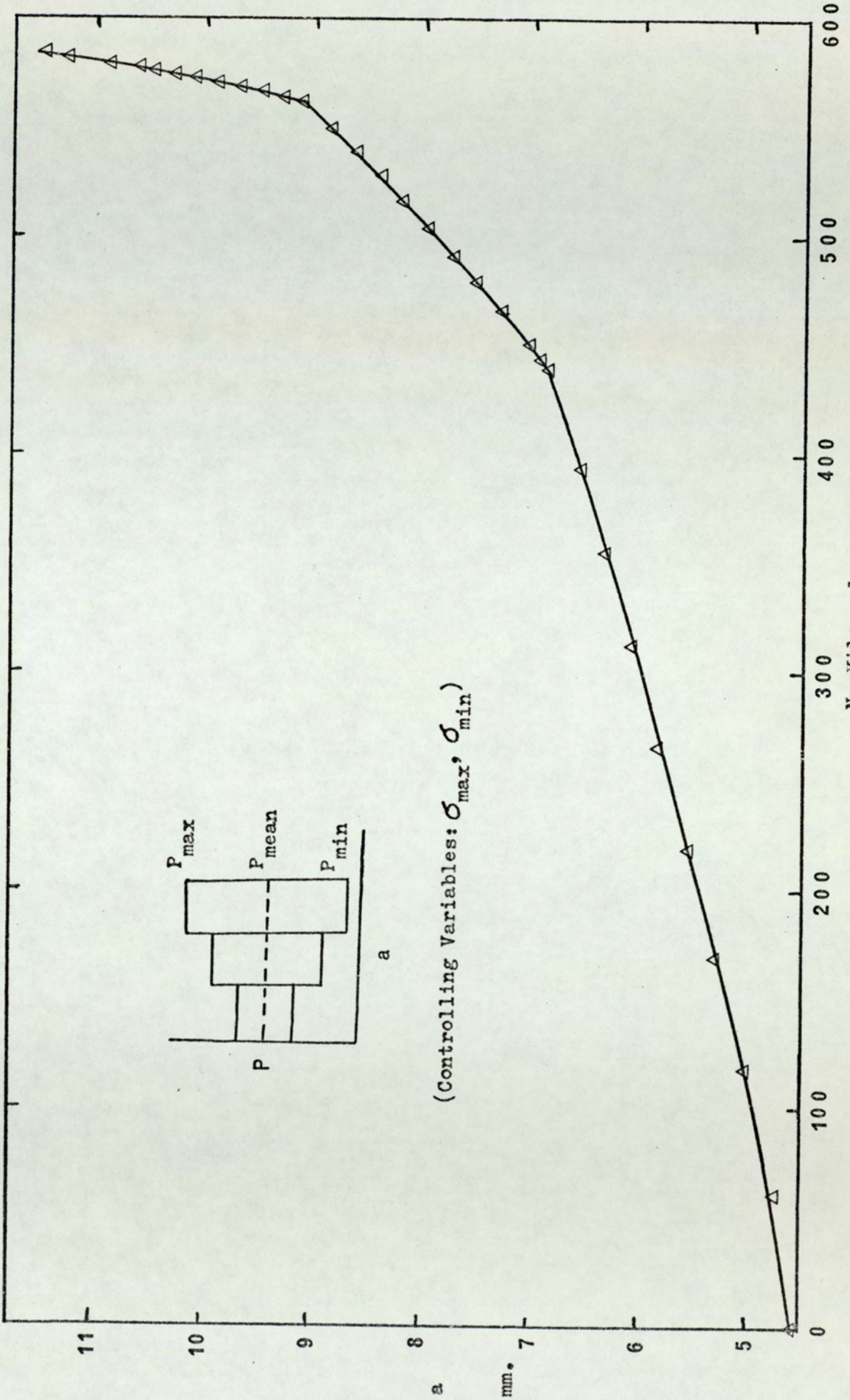


Fig.26. a-N Curve For a Stepped Increase In Load Amplitude Test At Constant Mean Load.

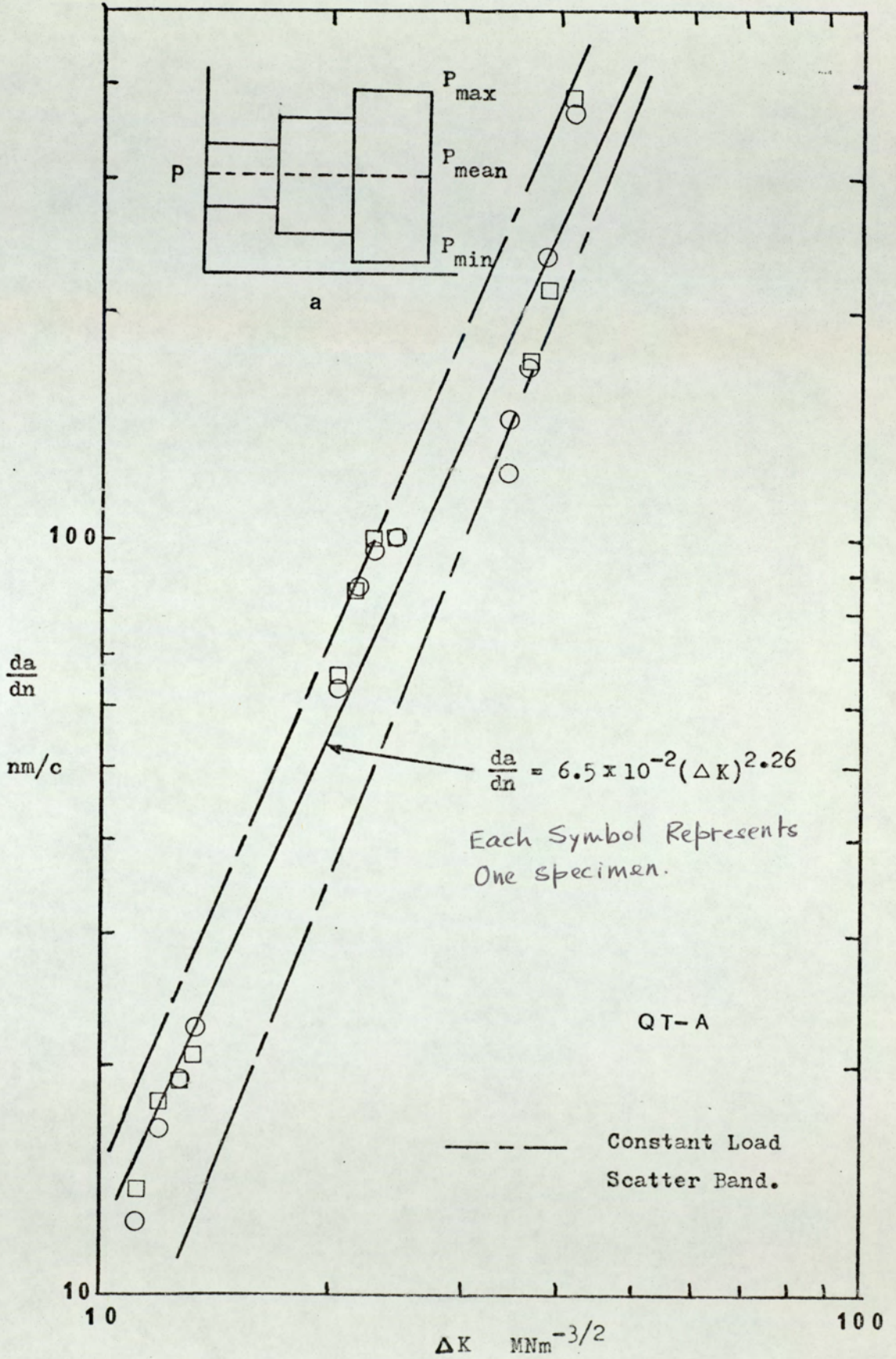


Fig. 27a. Crack Growth Curve For Stepped Increase In Load Amplitude Tests At Constant Mean Load. (Controlling Variables: σ_{max} , σ_{min})

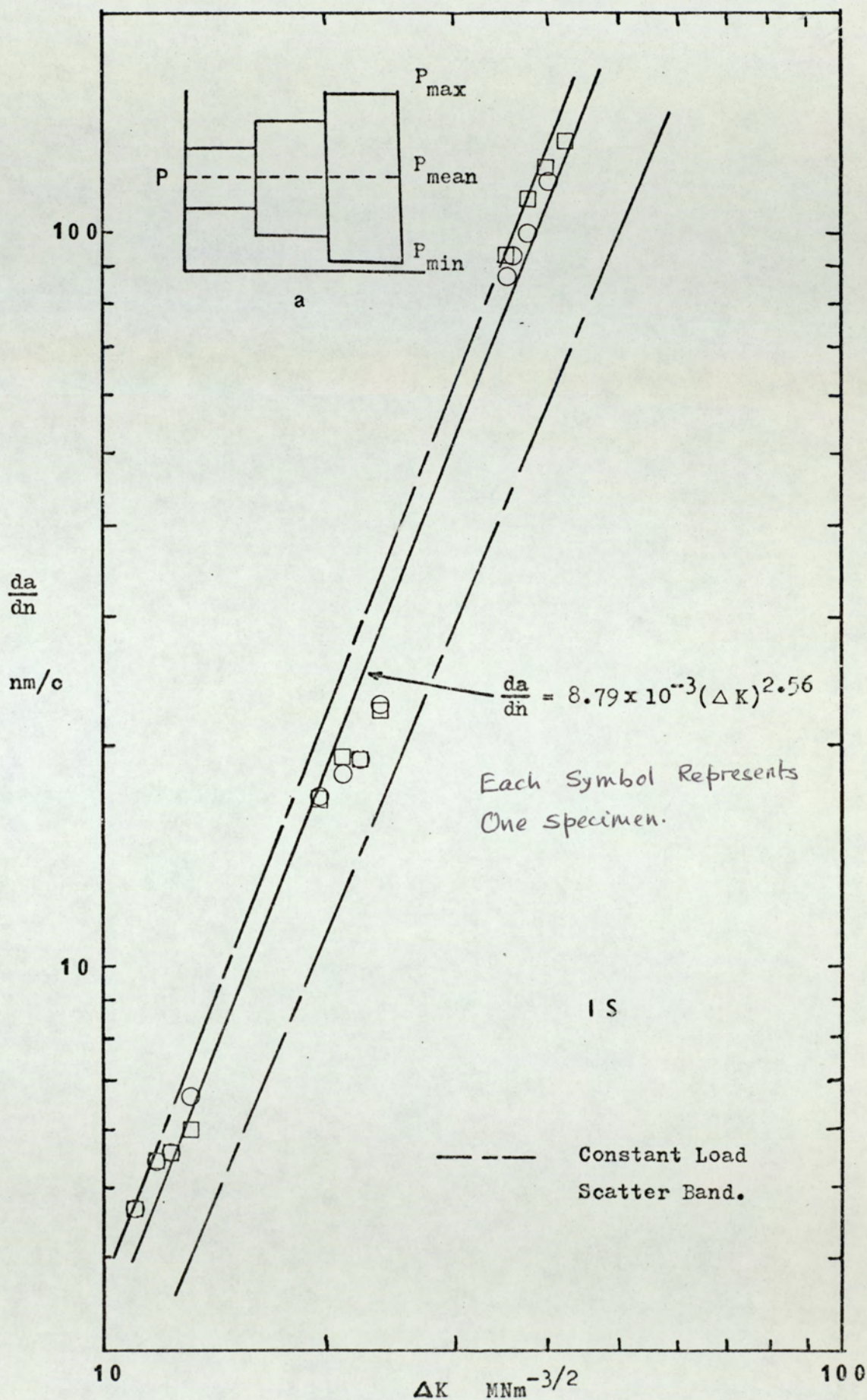


Fig.27b. Crack Growth Curve For Stepped Increase In Load Amplitude Tests At Constant Mean Load. (Controlling Variables: σ_{max} , σ_{min})

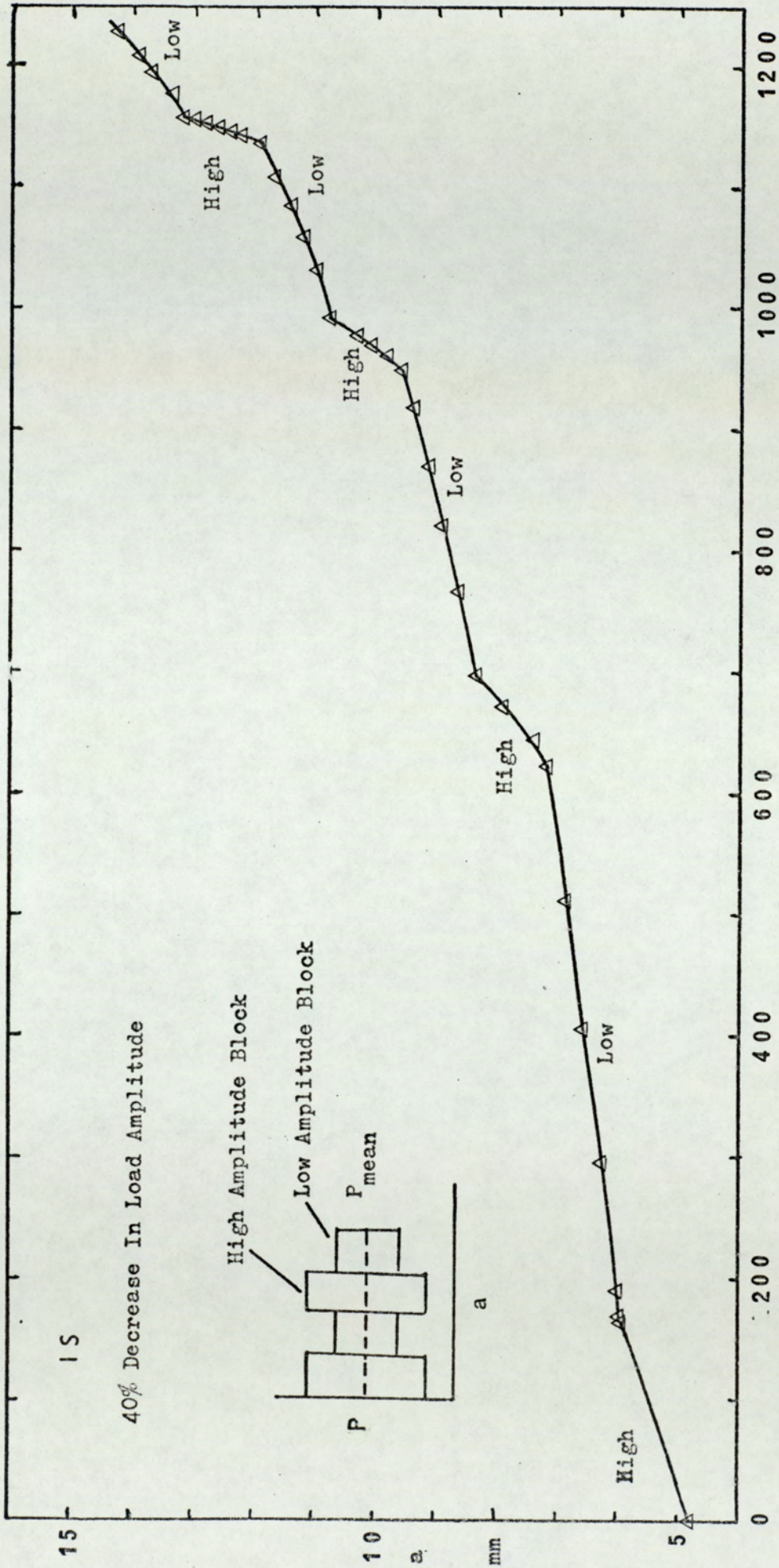


Fig.28. a-N Curve For a Two-Step Load Test.
(Controlling Variables: σ_{max} , σ_{min})

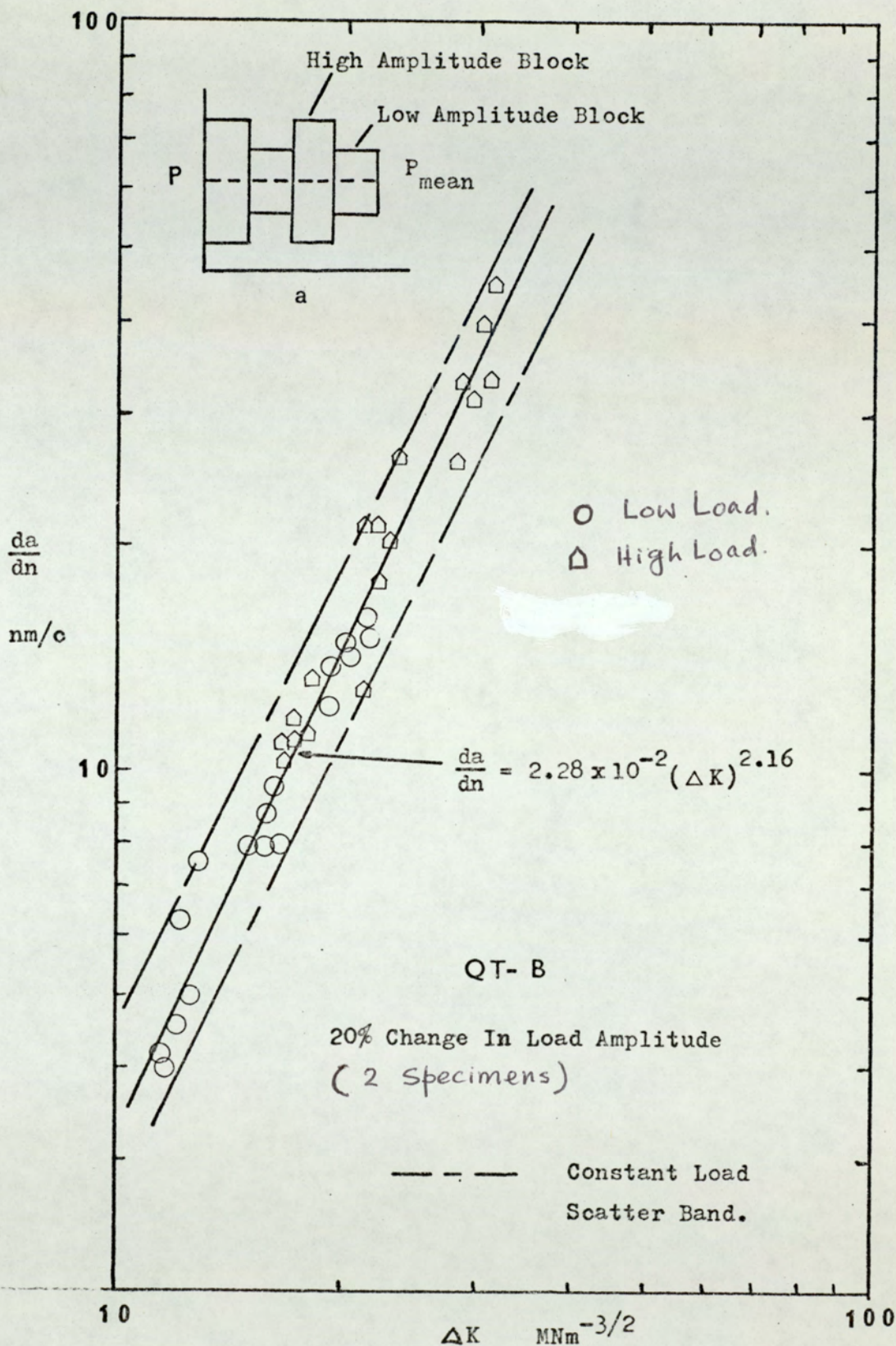


Fig.29a. Crack Growth Curve For Two-Step Load Tests.
(Controlling Variables: σ_{max} , σ_{min})

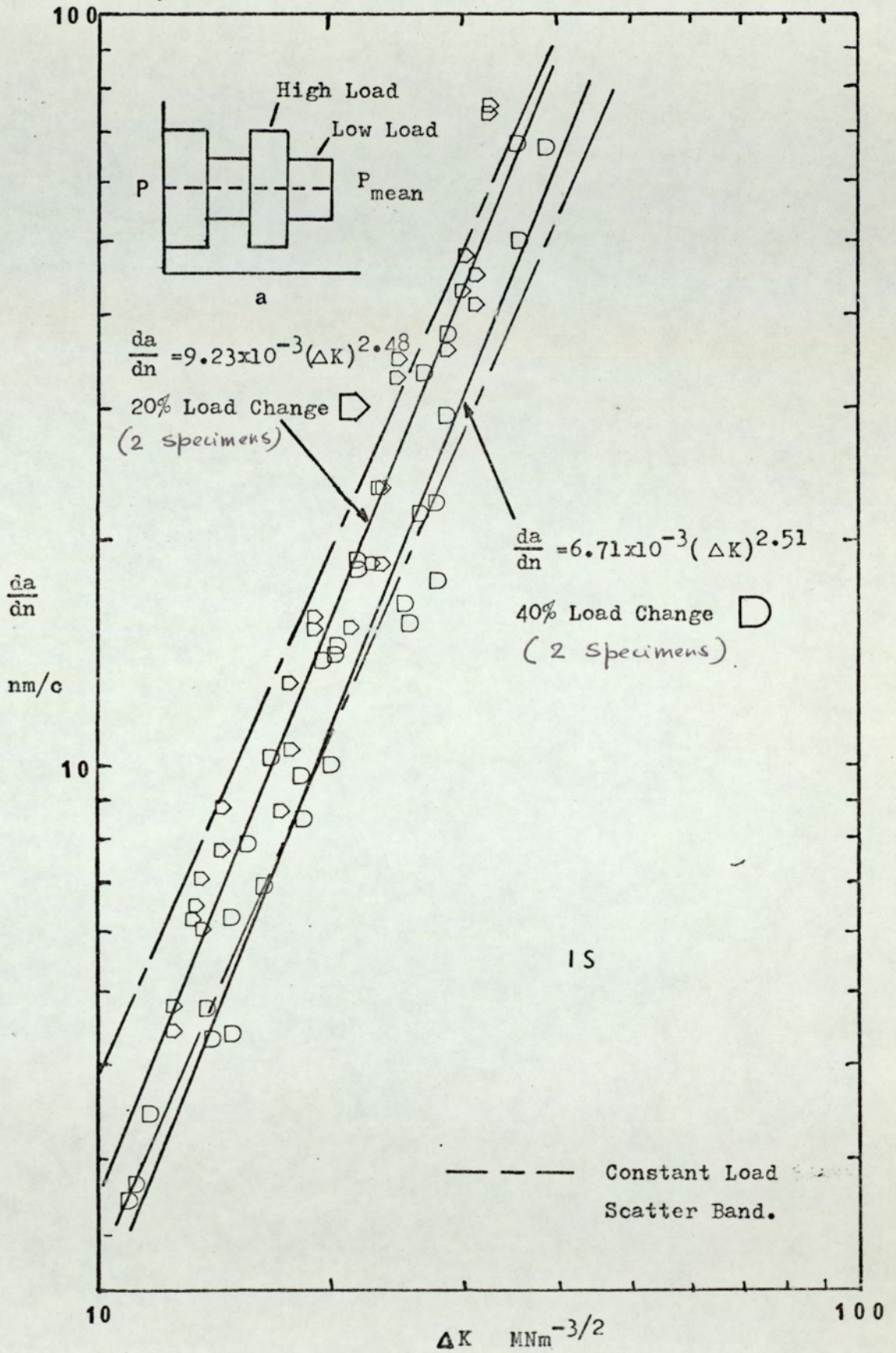


Fig.29b. Crack Growth Curve For Two-Step Load Tests.
(Controlling Variables: σ_{max} , σ_{min})

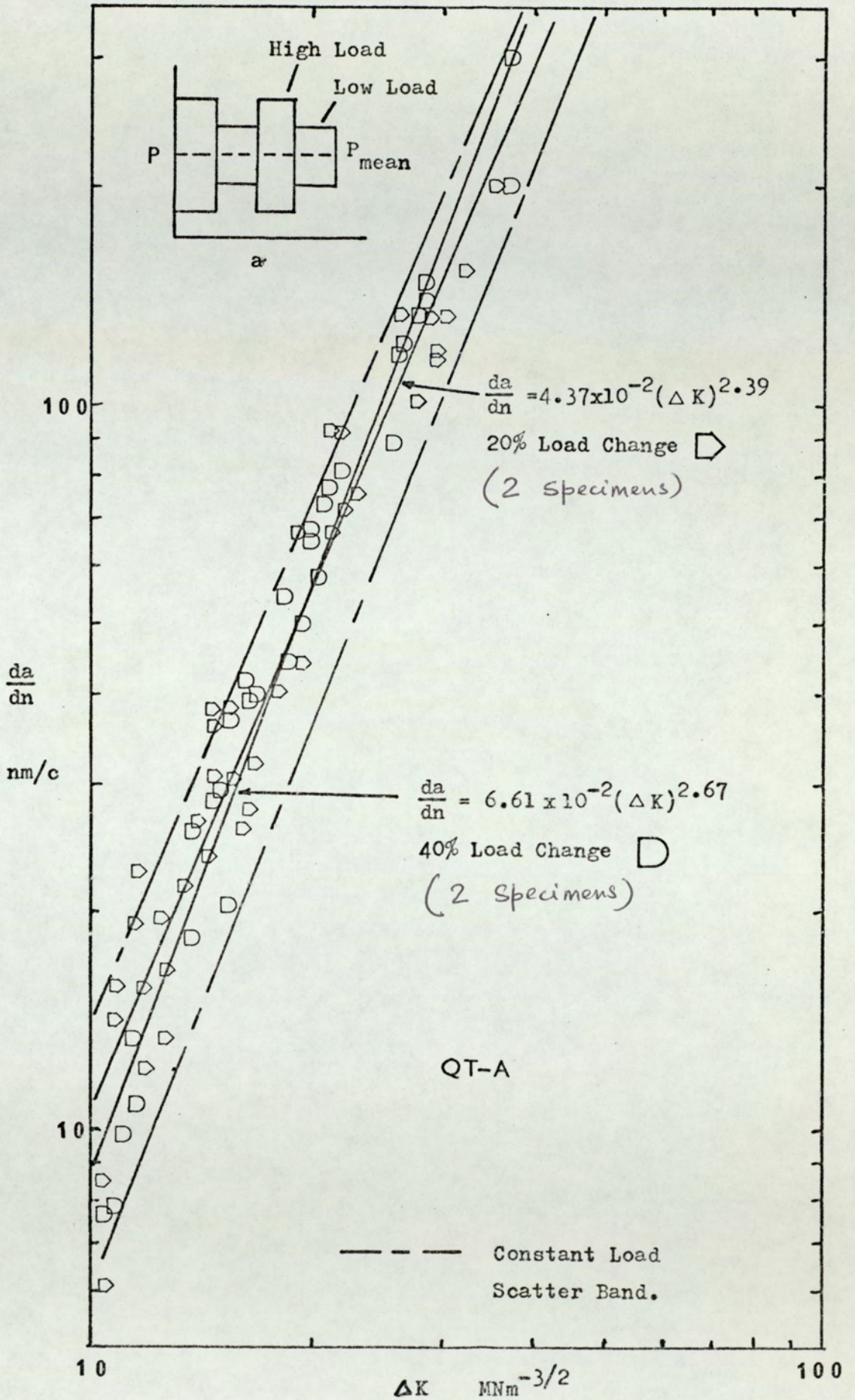


Fig.29c. Crack Growth Curve For Two-Step Load Tests.
(Controlling Variables : $\sigma_{max}, \sigma_{min}$)

crack propagation rates obtained in each test were related to stress intensity ranges (Figs. 27a,b). The crack growth rate seemed to conform to the higher stress intensity level as the change was made from a low to a high stress amplitude. The crack growth rate curve was thus broken down into three separate regions. Ignoring this effect, regression line was fitted to the overall data. In the case of QT-A steel, m and A values were 2.26 and 6.5×10^{-2} respectively and for material IS, the values were 2.56 and 8.79×10^{-3} respectively.

4.3.3 Two Step Block Loading

Two-step block loading tests were done at constant mean load level (Fig. 23d). After a high load amplitude block, σ_{\max} was decreased and σ_{\min} increased to obtain a low amplitude block. The difference between the high and the low amplitude was 20% in one test and 40% in another. In the case of 20% difference in the load amplitude, the high and the low load block had stress ratios of 0.2 and 0.304 respectively and in the case of 40% difference, 0.2 and 0.428 respectively. The tests were started at a high load block and ended with a low load block following a high-low-high-low sequence of loading. In the case of material QT-B, tests were done with only 20% load amplitude change. A representative a-N curve obtained from these tests is shown in Fig. 28. In the case of 40% load amplitude change tests, a slight slowing down of growth rate after a high-low load sequence was observed. This effect was more pronounced in material IS than QT-A. The crack growth curves for these tests are shown in Figs. (29a-c). The values of m and A are shown in table 4.

Material	Load Programme	m	A
QT-A	Two step-20%	2.39	4.37×10^{-2}
QT-B	Two step-20%	2.16	2.28×10^{-2}
IS	Two step-20%	2.48	9.23×10^{-3}
QT-A	Two step-40%	2.67	6.61×10^{-2}
IS	Two step-40%	2.51	6.71×10^{-3}

Table 4. Values of Crack Growth Exponent & Pre-exponent

4.3.4 Constant ΔK Tests at Constant K_{mean}

According to the equation $\frac{da}{dn} = A(\Delta K)^m$, for any constant ΔK condition the crack propagation rate should be constant. The effects of stress ratios and other minor variables would be reflected through the values of the pre-exponent A. Thus to investigate the effects of stress ratios, tests were done keeping both ΔK and K_{mean} constant by reducing the load amplitude and mean stress with the increase in the crack length (Fig. 23e). Different levels of K_{mean} and ΔK were chosen to give different stress ratios. A variation of this test was done to obtain a zero stress ratio as shown in Fig. 23i by keeping zero σ_{min} and reducing σ_{max} only. Table 5 shows the different programmes used. (See page 102)

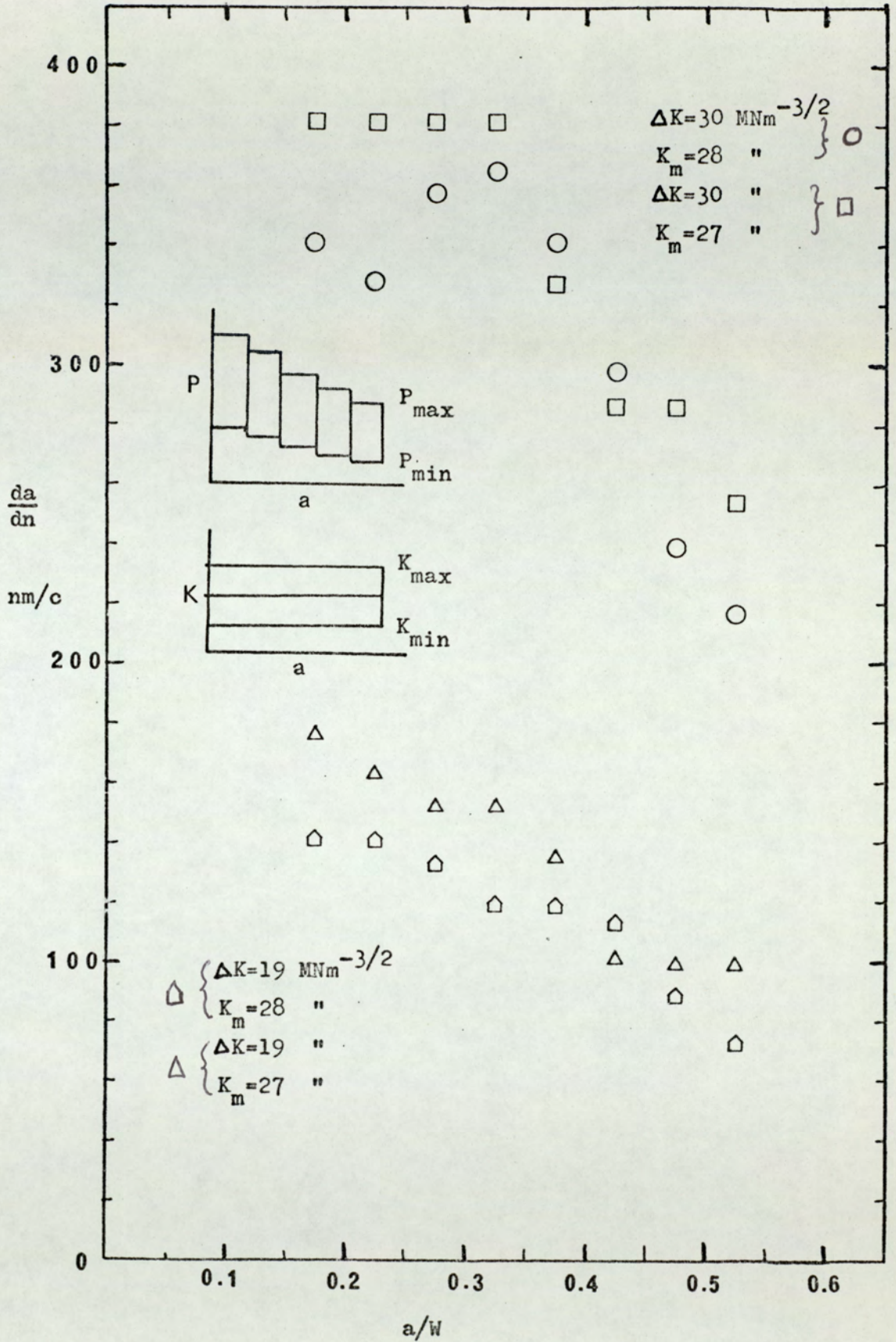


Fig.30a. Dependence Crack Growth Rate On a/W For Constant K Tests. QT-A. (Controlling Variables: σ_{max} , σ_{mean} , σ_{min})

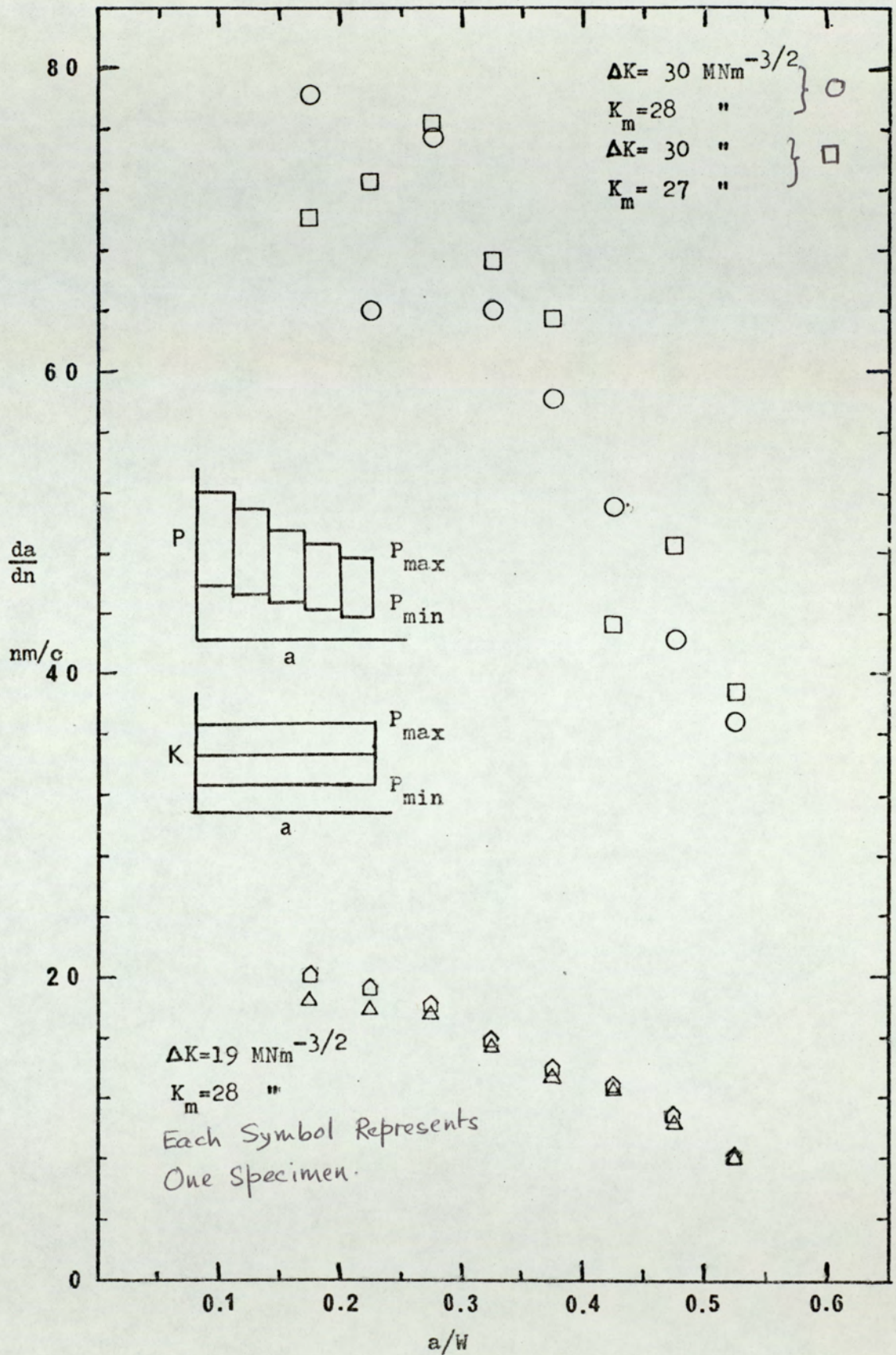


Fig. 30b. Dependence Of Crack Growth Rate On a/W For Constant K Tests. IS. (Controlling Variables: σ_{max} , σ_{mean} , σ_{min})

Material	ΔK $\text{MNm}^{-3/2}$	Initial a/w	Initial $\frac{da}{dn}$ nm/c	Final a/w	Final $\frac{da}{dn}$ nm/c	Red. in $\frac{da}{dn}$ $\%$	Transition Data			W mm
							$\frac{a}{W}$	$\frac{K_{\text{max}}}{K_C}$	R	
QT-A	19	0.15	140.3	0.55	72.3	48.5	0.3	0.725	0.493	23.86
	19	0.15	176.0	0.55	99.4	43.5	0.3	0.705	0.480	22.86
	25	0.15	265.0	0.55	133.0	49.8	0.3	0.782	0.383	23.86
	25	0.15	269.0	0.55	143.0	46.8	0.3	0.763	0.367	22.86
	30	0.15	341.0	0.55	217.0	36.4	0.3	0.830	0.302	23.86
	30	0.15	381.0	0.55	254.0	33.3	0.35	0.830	0.286	22.86
IS	19	0.15	20.0	0.55	12.13	38.5	0.3	0.55	0.493	25.0
	19	0.15	18.4	0.55	8.33	54.8	0.3	0.55	0.493	25.0
	19	0.15	19.85	0.55	10.0	49.6	0.25	0.55	0.493	25.0
	19	0.15	19.00	0.55	10.23	46.2	0.3	0.55	0.493	25.0
	25	0.15	43.1	0.55	18.0	58.2	0.3	0.432	0.367	25.0
	25	0.15	50.0	0.55	21.0	57.0	0.25	0.432	0.367	22.86
	30	0.15	78.2	0.55	36.8	53.0	0.35	0.615	0.286	25.0
	30	0.15	70.0	0.55	38.8	44.7	0.3	0.615	0.286	22.86
	19	0.15	13.16	0.55	3.11	76.5	0.2	0.279	0	25.0

Table 6. Crack Growth Data from Constant ΔK and K_{mean} Tests

(Controlling Variables: σ_{max} , σ_{mean} , σ_{min})

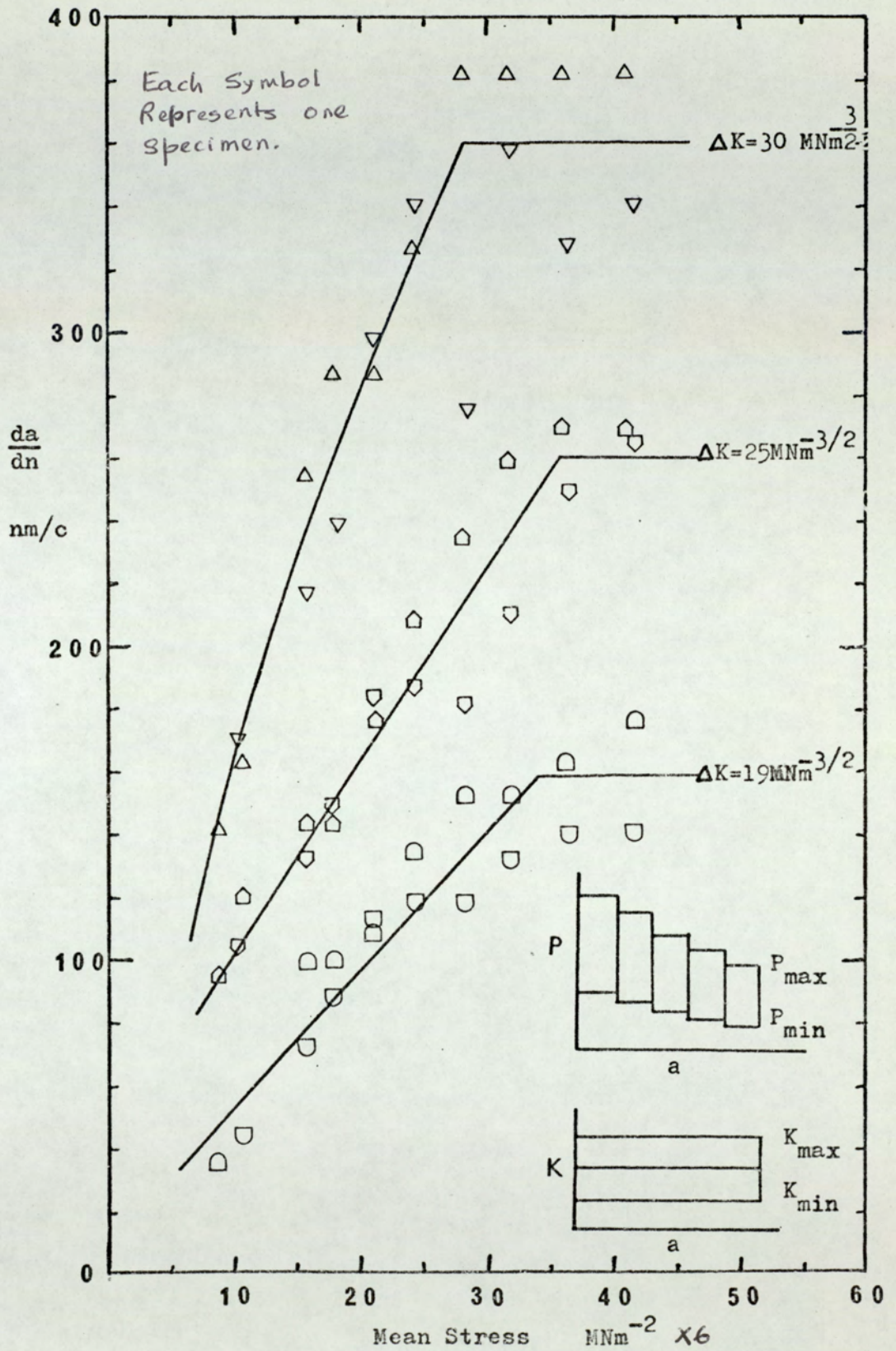


Fig.31a. Crack Growth Rate Versus Mean Stress Curves For Constant K Tests. QT-A. (Controlling Variables: σ_{max} , σ_{mean} , σ_{min})

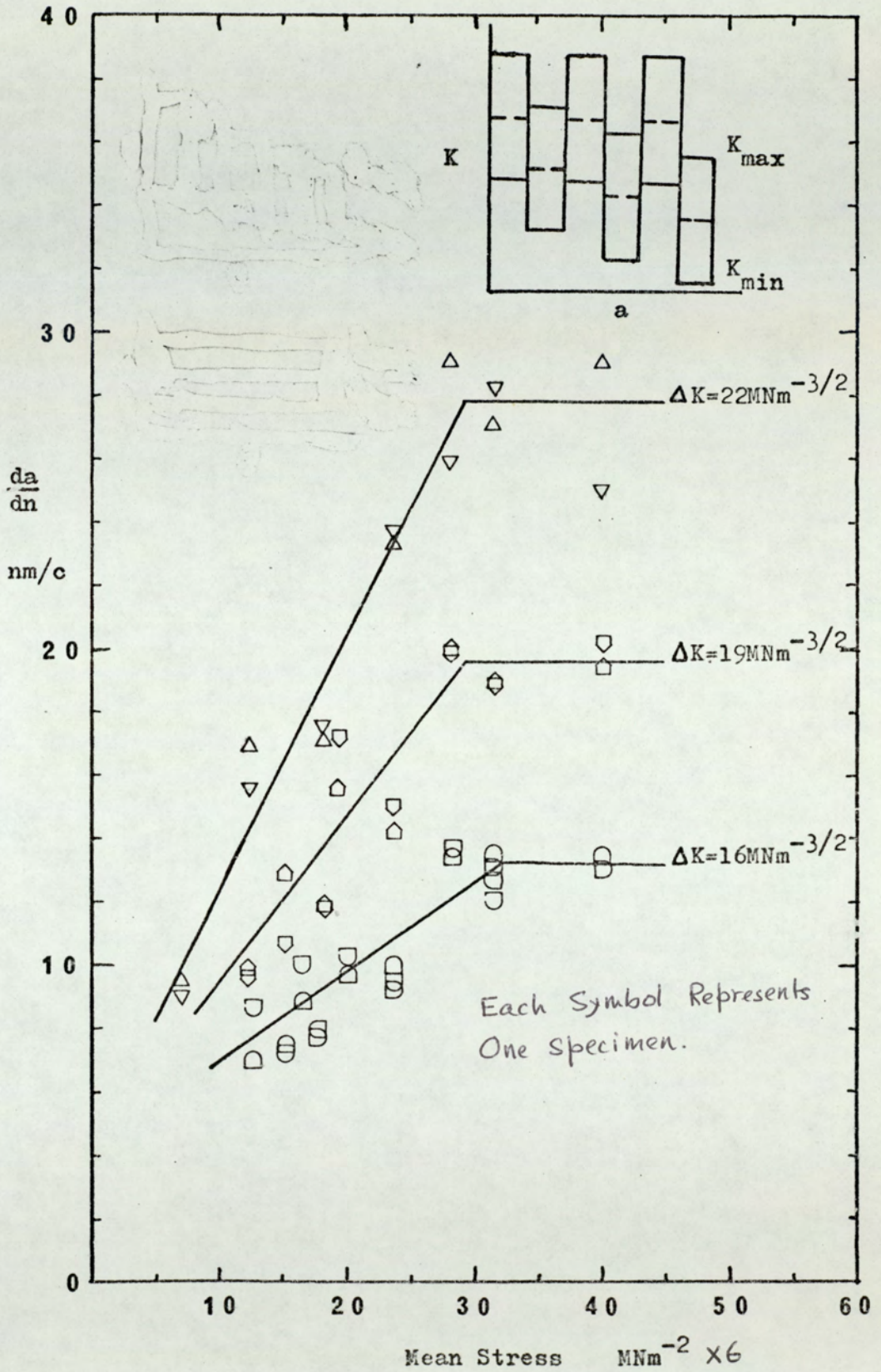


Fig.31b. Crack Growth Rate Versus Mean Stress Curves For Constant K tests. QT-B. (Controlling Variables: σ_{\max} , σ_{mean} , σ_{\min})

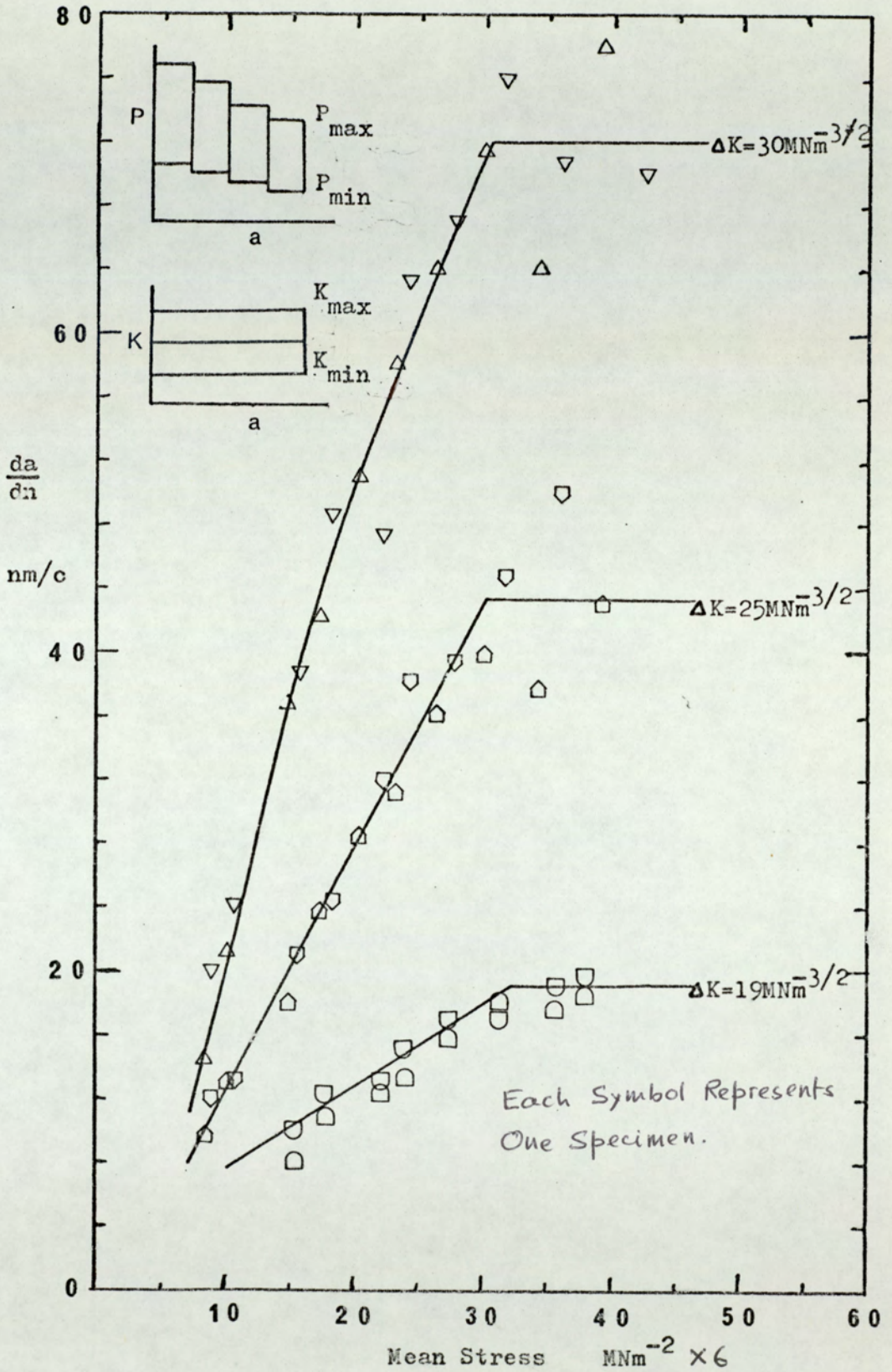


Fig.31c. Crack Growth Rate Versus Mean Stress Curves For Constant K tests. IS. (Controlling Variables: σ_{max} , σ_{mean} , σ_{min})

Mat.	ΔK MNm ^{-3/2}	σ_m MNm ⁻² x6	K_{\max} Kc (From To)	R (From To)	$\frac{a}{W}$ (i)	Initial $\frac{da}{dn}$ nm/c	$\frac{a}{W}$ (f)	Final $\frac{da}{dn}$ nm/c	Red. in $\frac{da}{dn}$ %	Transition Data			W mm
										$\frac{a}{W}$	$\frac{K_{\max}}{Kc}$	R	
	22	23.1	0.512 0.891	0.17 0.58	0.15	149.0	0.50	170.4	Incr.	-	-	-	23.86
QT-A	22	23.1	0.503 0.873	0.16 0.515	0.15	152.5	0.50	282	Incr.	-	-	-	22.86
	30	23.1	0.589 0.968	0 0.465	0.15	217.0	0.50	398	Incr.	-	-	-	23.86
	30	23.1	0.582 0.863	0 0.326	0.15	346.0	0.45	320	0.81	-	-	-	22.86
	19	14.0	0.279 0.515	0 0.467	0.15	12.38	0.55	9.08	26.7	0.3	0.325	0.143	25
	19	27.4	0.418 0.873	0.334 0.687	0.15	19.23	0.55	9.37	51.3	0.3	0.502	0.446	25
IS	19	30.0	0.44 0.94	0.373 0.71	0.15	19.54	0.55	10.16	48.0	0.3	0.536	0.48	25
	22	15.4	0.379 0.744	0.165 0.573	0.15	24.0	0.55	11.7	51.3	0.3	0.456	0.293	25
	30	15.4	0.447 0.933	0 0.527	0.15	64.1	0.55	34.7	45.8	0.35	0.555	0.208	25
	30	30.0	0.379 0.742	0.158 0.57	0.15	73.6	0.55	48.2	34.5	0.3	0.447	0.286	25

Table 7. Crack Growth Data for Constant ΔK at Constant Mean Load Tests

(Controlling Variables: σ_{\max} , σ_{\min})

Material	ΔK MNm ^{-3/2}	K_{mean} MNm ^{-3/2}	$R = \frac{K_{\text{min}}}{K_{\text{max}}}$
QT-A	19	28	0.493
QT-A	19	27	0.48
QT-A	25	28	0.383
QT-A	25	27	0.367
QT-A	30	28	0.302
QT-A	30	27	0.286
IS	19	28	0.493
IS	25	27	0.367
IS	30	27	0.286
IS	19	9.5	0

Table 5. Test Programmes for Constant ΔK & K_{mean} .
(Controlling Variables: σ_{max} , σ_{mean} , σ_{min})

The results obtained in the above tests did not show a constant crack growth rate for a constant ΔK . The growth rate remained constant for a certain length of crack and then a transition occurred leading to a gradual slowing down. The maximum reduction in crack growth rate was obtained in material IS at a constant ΔK of 19 MNm^{-3/2} at zero stress ratio. The reduction was 76.5% over a crack length of 0.15 W to 0.55 W. The minimum reduction observed over the same crack length was 33% with the QT-A steel at a constant ΔK of 30 MNm^{-3/2} and a stress ratio of 0.286. The data obtained from different tests are shown in table 6. The crack growth rates are also shown as a function of a/W in Figs. 30a-b and as a function of mean stress in

Figs. 31a-c. (The data for QT-B had been obtained for tests described in section 4.3.9.1.)

4.3.5 Constant ΔK Tests at Constant Mean Load

These tests were done at a constant mean load but with gradually decreasing load amplitude to keep ΔK constant (Fig. 23f). Different levels of ΔK and mean loads were used. In each case K_{\min} and K_{\max} gradually increased as the crack became longer. The value of the stress ratio also increased over a certain range during the test. With the increase in crack length during the test, a reduction in growth rate was observed in the case of IS steel. In the case of QT-A steel, the crack growth rate was reasonably constant over most of the crack length, but increased gradually at high a/W values. The results of these tests are shown in table 7.

4.3.6 Constant ΔK Tests at Constant Maximum Load

These tests were done according to the programme shown in Fig. 23g. Different levels of constant ΔK values were used. The tests were started at a stress ratio of about zero. Since P_{\max} and ΔK were kept constant throughout the test, the value of R increased as the crack became longer. The final value of R was about 0.6 in QT-B and IS steels, but was about 0.35 in the case of QT-A. As K_{\max} increased with the test, the ratio of K_{\max} to ΔK increased from 1 to about 2.5 with materials QT-B and IS, and to about 1.55 with the material QT-A. The crack growth rate in the high strength QT-A steel remained fairly constant over the crack length tested. In fact, the growth rate had a tendency to increase at longer crack lengths. In contrast, the crack growth rates in low strength QT-B and IS steels were constant up to a/W value of about 0.45, but tended to decrease after that. These decreases were much smaller in comparison with those obtained

Test Condition	$\frac{a}{W}$	$\frac{da}{dn}$ nm/c
$\Delta K = 16 \text{ MNm}^{-3/2}$ $\sigma_{\text{max}} = 6 \times 12.35 \text{ MNm}^{-2}$	0.40 - 0.45	13.6
	0.45 - 0.50	13.8
	0.50 - 0.55	20.0
	0.55 - 0.60	19.8
$\Delta K = 25 \text{ MNm}^{-3/2}$ $\sigma_{\text{max}} = 6 \times 19.7 \text{ MNm}^{-2}$	0.40 - 0.45	85.0
	0.45 - 0.50	85.6
	0.50 - 0.55	93.2
	0.55 - 0.60	97.5
$\Delta K = 32 \text{ MNm}^{-3/2}$ $\sigma_{\text{max}} = 6 \times 26.0 \text{ MNm}^{-2}$	0.40 - 0.45	163.0
	0.45 - 0.50	228.0
	0.50 - 0.55	155.0
	0.55 - 0.60	200.0

Table 8a. Crack Growth Rates for Constant ΔK and Constant P_{max} .

Tests (QT-A).

(Controlling Variables: $\sigma_{\text{mean}}, \sigma_{\text{min}}$)

Test Condition	$\frac{a}{W}$	$\frac{da}{dn}$ nm/c
$\Delta K = 16 \text{ MNm}^{-3/2}$ $\sigma_{\max} = 6 \times 25.5 \text{ MNm}^{-2}$	0.20 - 0.25	9.98
	0.25 - 0.30	10.56
	0.30 - 0.35	9.13
	0.35 - 0.40	10.5
	0.40 - 0.45	10.85
	0.45 - 0.5	8.7
$\Delta K = 25 \text{ MNm}^{-3/2}$ $\sigma_{\max} = 6 \times 39.5 \text{ MNm}^{-2}$	0.20 - 0.25	39.7
	0.25 - 0.30	43.3
	0.30 - 0.35	39.7
	0.35 - 0.40	36.4
	0.40 - 0.45	33.1
	0.45 - 0.50	26.0
$\Delta K = 32 \text{ MNm}^{-3/2}$ $\sigma_{\max} = 6 \times 51.0 \text{ MNm}^{-2}$	0.20 - 0.25	77.4
	0.25 - 0.30	81.0
	0.30 - 0.35	75.0
	0.35 - 0.40	72.3
	0.40 - 0.45	68.0
	0.45 - 0.50	50.7

Table 8b. Crack Growth Rates for Constant ΔK and Constant P_{\max} Tests (QT-B)

(Controlling Variables: σ_{mean} , σ_{min})

Test Condition	$\frac{a}{W}$	$\frac{da}{dn}$ nm/c
$\Delta K = 19 \text{ MNm}^{-3/2}$ $\sigma_{\max} = 6 \times 27.8 \text{ MNm}^{-2}$	0.15 - 0.20	11.47
	0.20 - 0.25	11.73
	0.25 - 0.30	12.82
	0.30 - 0.35	11.78
	0.35 - 0.40	10.25
	0.40 - 0.45	10.15
	0.45 - 0.50	11.42
	0.50 - 0.55	7.38
$\Delta K = 19 \text{ MNm}^{-3/2}$ $\sigma_{\max} = 6 \times 28.3 \text{ MNm}^{-2}$	0.20 - 0.25	16.23
	0.25 - 0.30	14.11
	0.30 - 0.35	13.10
	0.35 - 0.40	14.72
	0.40 - 0.45	14.03
	0.45 - 0.50	11.58
$\Delta K = 25 \text{ MNm}^{-3/2}$ $\sigma_{\max} = 6 \times 36.7 \text{ MNm}^{-2}$	0.15 - 0.20	36.8
	0.20 - 0.25	38.5
	0.25 - 0.30	43.2
	0.30 - 0.35	40.3
	0.35 - 0.40	35.7
	0.40 - 0.45	32.1
	0.45 - 0.50	29.1
	0.50 - 0.55	31.3
$\Delta K = 25 \text{ MNm}^{-3/2}$ $\sigma_{\max} = 6 \times 37.2 \text{ MNm}^{-2}$	0.15 - 0.20	44.18
	0.20 - 0.25	45.88
	0.25 - 0.30	45.88
	0.30 - 0.35	43.38
	0.35 - 0.40	38.48
	0.40 - 0.45	30.58
	0.45 - 0.50	26.21
	0.50 - 0.55	30.58

Table 8c. Crack Growth Rates for Constant ΔK and Constant P_{\max} Tests (IS)
 (Controlling Variables: $\sigma_{\text{mean}}, \sigma_{\text{min}}$)

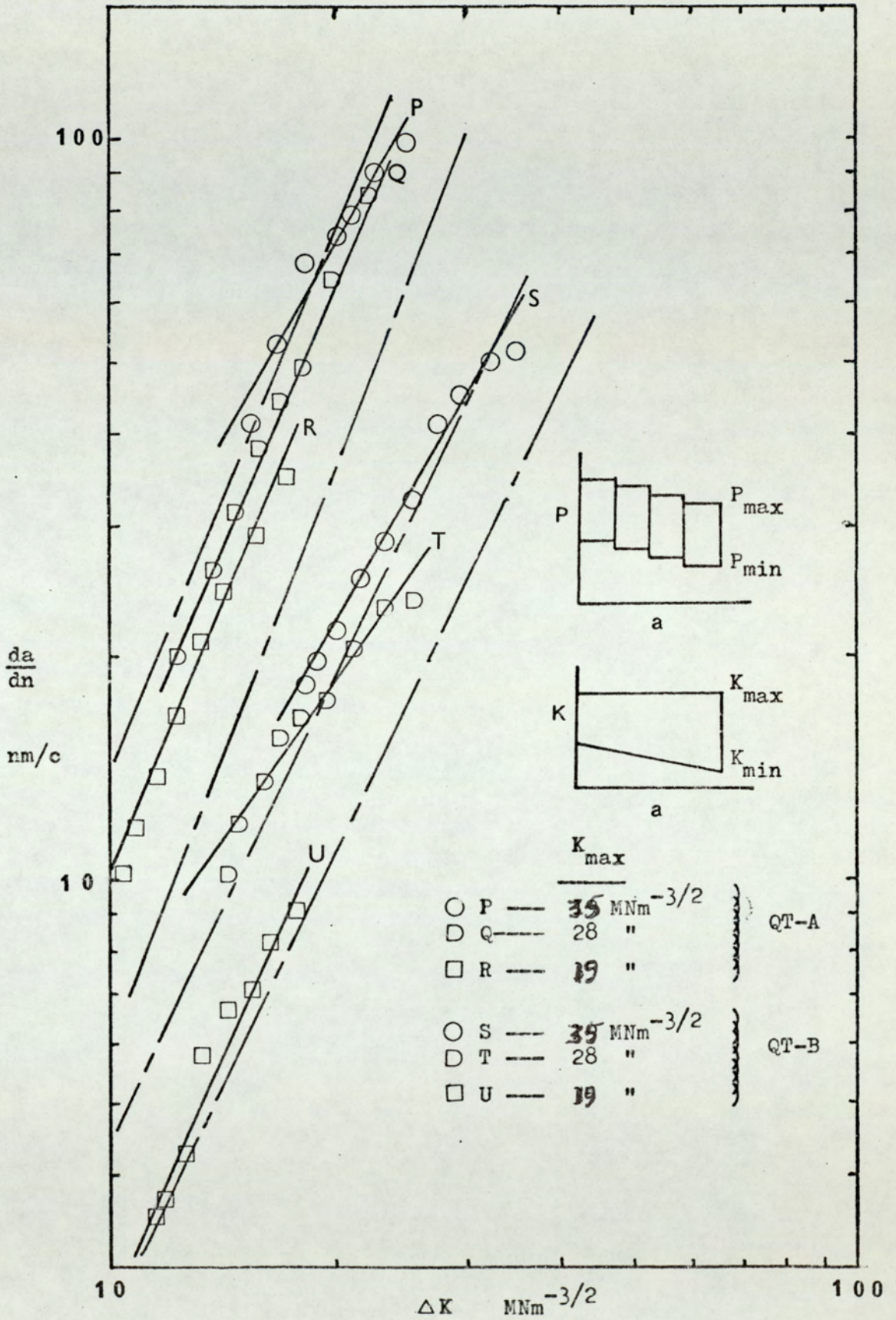


Fig.32. Crack Growth Results Of Constant K_{\max} Tests With Increasing ΔK . (Controlling Variables: σ_{\max} , σ_{mean} , σ_{\min} , $\Delta\sigma = \text{Const.}$)

with constant ΔK and constant K_{max} tests. The results are shown in table 8a-c.

4.3.7 Constant K_{max} with Increasing ΔK

In these tests the load amplitude was kept constant but the maximum load was decreased with the increase in crack length to keep K_{max} constant (Fig. 23h). Three different levels of K_{max} were investigated. The load range values were so chosen that a reasonable range of ΔK values could be obtained during the test. The crack growth data in each test resulted in a smooth a-N curve. The crack growth rates obtained graphically are plotted against ΔK as shown in Fig. 32. The value of R changed from about 0.55 at the start of the test to about zero at the end of the test resulting in the change of K_{max} to ΔK ratio of about 2.25 to 1. The values of m and A of the crack growth equations obtained for the tests are given in table 9.

Material	Constant K_{max} MNm ^{-3/2}	m	A
QT-A	35	1.74	3.81×10^{-1}
	28	2.43	4.57×10^{-2}
	19	2.53	2.87×10^{-2}
	19,28,35	2.74	1.86×10^{-2}
QT-B	19	2.28	1.38×10^{-2}
	28	1.43	2.57×10^{-1}
	35	1.75	1.18×10^{-1}
	19,28,35	2.52	9.55×10^{-3}

Table 9. Crack Growth Exponent and Pre-exponent Values for Tests with Constant K_{max} and Increasing ΔK .
(Controlling Variables: σ_{max} , σ_{mean} , σ_{min} .
 $\Delta\sigma = \text{Constant}$)

Test Conditions	Block	ΔK MNm ^{-3/2}	Red. in ΔK %	$\frac{da}{dn}$ nm/c	R
QT-A	1	25	-	125.5	0
W = 23.86 mm	2	17.5	30	70.0	0.243
Base $\Delta K =$ 25 MNm ^{-3/2}	3	25	-	133.0	0.136
Const. σ_{mean}	4	15	40	43.4	0.427
6X 18.6 MNm ⁻²	5	25	-	183.5	0.259
	6	12.5	50	19.5	0.593
	7	25	-	183.5	0.391
	8	10	60	4.84	0.738
IS	1	25	-	35.1	0
W = 23.86 mm	2	17.5	30	15.0	0.386
Base $\Delta K =$ 25 MNm ^{-3/2}	3	25	-	41.8	0.239
Const. $\sigma_{max.}$	4	15	40	8.84	0.599
6X 37.2 MNm ⁻²	5	25	-	30.6	0.412
	6	12.5	50	4.24	0.745
	7	25	-	24.9	0.563
	8	10	60	1.4	0.85

Table 10. Crack Growth Data for ΔK Reduction Tests
(Controlling Variables: σ_{max} , σ_{mean} , σ_{min})

4.3.8 Tests with ΔK Reductions at Constant Mean Load or Maximum Load

These tests were designed on the basis of the results obtained in sections 4.3.5 and 4.3.6 with a view to find the effects of ΔK reductions on the crack growth rate. A constant mean stress of $6 \times 18.6 \text{ MNm}^{-2}$ was chosen for the test with QT-A steel and a maximum stress of 47.3 MNm^{-2} was selected for the test with material IS. For both the cases, a base ΔK value of $25 \text{ MNm}^{-3/2}$ was used. At constant mean stress or maximum stress level as the case might be, the crack was allowed to grow by $0.05 W$ at the base ΔK value. Then ΔK was reduced by a certain percentage of the base value and the crack grown by another $0.05 W$ before returning to the original test conditions. This was repeated for different percentage reductions of the base ΔK value. Average crack growth rate was calculated for each test block. The crack growth rate data are shown in table 10. No appreciable deceleration or acceleration of growth rates was observed with the decrease or increase of ΔK respectively. It was observed with both the steels that at about 60% reduction of ΔK i.e. at ΔK value of $10 \text{ MNm}^{-3/2}$, the crack growth rate was discontinuous and occurring in jumps.

4.3.9 K_{mean} Reduction Tests

These tests were performed according to the block programme outlined in section 3.6 (i) and Fig. 23j.

4.3.9.1 K_{mean} Reduction at Constant ΔK

The base K_{mean} selected for the tests was $28 \text{ MNm}^{-3/2}$. Three different levels of ΔK were investigated with material QT-B but only two levels were tested with QT-A and IS. With the growth of the crack, the required ΔK and K_{mean} levels were maintained in each load block

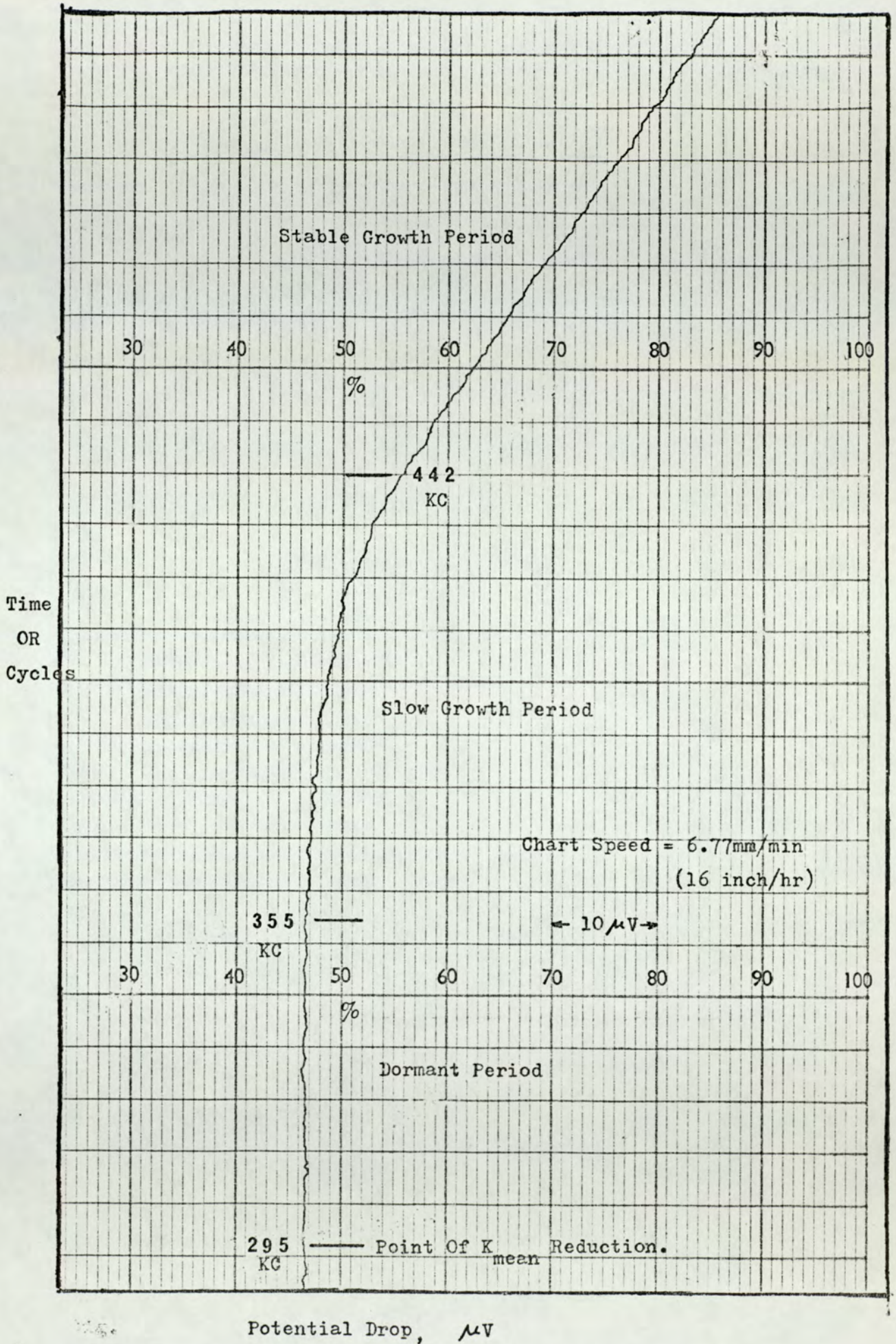


Fig.33. Potential Chart Record Showing Transient Growth.

Test Conditions	Block No.	$\Delta\sigma$ MNm ⁻² x6	σ_{mean} MNm ⁻² x6	K_{mean} MNm ^{-3/2}	$\frac{da}{dn}$ (1) nm/c	$\frac{da}{dn}$ (2) nm/c	R
QT-B W = 25 mm. Const. $\Delta K =$ 16 MNm ^{-3/2} Crack Growth from 0.15 W to 0.55 W	1	23.0	40.08	28	13.44	13.02	0.556
	2	20.4	28.4	22.4	13.62	13.58	0.473
	3	17.85	31.25	28	13.51	12.13	0.556
	4	14.67	16.6	16.8	8.84	10.20	0.355
	5	13.38	23.6	28	10.00	9.53	0.556
	6	12.13	21.05	28	9.75	10.34	0.556
	7	10.20	12.73	19.6	7.03	8.77	0.42
	8	8.93	15.3	28	7.44	7.30	0.556
QT-B W = 25 mm Const. $\Delta K =$ 19 MNm ^{-3/2} Crack Growth from 0.15 W to 0.55 W	1	27.4	40.08	28	19.40	20.20	0.48
	2	24.2	28.4	22.4	20.00	20.00	0.404
	3	21.35	31.25	28	18.93	18.93	0.48
	4	18.5	19.1	19.6	15.71	17.35	0.347
	5	15.9	23.6	28	14.26	15.06	0.48
	6	14.3	12.4	16.8	9.88	9.80	0.278
	7	12.13	17.85	28	11.90	11.90	0.48
	8	10.20	15.3	28	12.90	10.68	0.48
QT-B W = 25 mm Const. $\Delta K =$ 22 MNm ^{-3/2} Crack Growth from 0.15 W to 0.60 W	1	31.9	40.08	28	29.06	25.00	0.436
	2	28.1	28.4	22.4	29.04	25.94	0.341
	3	24.2	31.25	28	27.17	28.40	0.436
	4	21.7	19.1	19.6	26.13	26.15	0.281
	5	19.15	23.6	28	23.46	23.65	0.436
	6	16.6	12.4	16.8	16.96	15.66	0.209
	7	14.0	17.85	28	17.12	17.60	0.436
	8	12.13	15.3	28	13.69	13.64	0.436
	9	10.20	7.0	15.4	9.54	9.03	0.167

Table 11a. Stabilized Crack Growth Rate Data for K_{mean} Reduction Tests

(Controlling Variables: σ_{max} , σ_{mean} , σ_{min})

Test Conditions	Block No.	$\Delta\sigma$ MNm ⁻² x6	σ_{mean} MNm ⁻² x6	$K_{mean}^{-3/2}$ MNm ^{-3/2}	$\frac{da}{dn}$ (1) nm/c	$\frac{da}{dn}$ (2) nm/c	R
QT-A W = 23.86 mm Const. $\Delta K =$ 16 MNm ^{-3/2} Crack Growth from 0.2 W to 0.55W	1	21.0	36.4	28	91.8	119.3	0.556
	2	18.2	22.4	19.6	70.2	88.3	0.42
	3	16.1	28	28	91.8	102	0.556
	4	14	14.7	16.8	60.7	98.2	0.355
	5	11.9	21.4	28	70.2	83.6	0.556
	6	10.5	9.1	14	52.5	119.2	0.273
	7	9.1	15.75	28	85.2	199	0.556
QT-A W = 23.86 mm Const. $\Delta K =$ 22 MNm ^{-3/2} Crack Growth from 0.2 W to 0.55 W	1	28.7	36.4	28	219	188	0.436
	2	25.2	22.4	19.6	232	177	0.281
	3	21.7	28	28	262	167	0.436
	4	18.9	14.7	16.8	215	155	0.209
	5	17.5	21.4	28	253	167	0.436
	6	14.7	9.1	14	119.2	66	0.120
	7	12.6	15.75	28	153.8	167	0.436
IS W = 22.86 mm Const. $\Delta K =$ 16 MNm ^{-3/2} Crack Growth from 0.15 W to 0.55 W	1	24.4	42.7	28	14.67	-	0.556
	2	21.2	39.6	22.4	12.77	-	0.473
	3	18.6	32.5	28	12.1	-	0.556
	4	16.4	20	19.6	10.77	-	0.42
	5	14.3	25.05	28	10.64	-	0.556
	6	12.5	13.13	16.8	6.88	-	0.355
	7	10.8	18.9	28	7.7	-	0.556
	8	9.14	16.1	28	6.12	-	0.556
IS W = 22.86 mm Const. $\Delta K =$ 22 MNm ^{-3/2} Crack Growth from 0.15 W to 0.5 W	1	33.4	42.7	28	35.2	-	0.436
	2	29.1	39.6	22.4	31.6	-	0.341
	3	25.5	32.5	28	30.9	-	0.436
	4	22.5	20	19.6	29	-	0.281
	5	19.7	25.05	28	24.3	-	0.436
	6	17.2	13.13	16.8	13.9	-	0.209
	7	14.77	18.9	28	16.8	-	0.436

Table 11b. Stabilized Crack Growth Rate Data for K_{mean} Reduction Tests

(Controlling Variables: σ_{max} , σ_{mean} , σ_{min})

Test Conditions	K _{mean} Red. %	K _{mean} MNm ^{-3/2}	σ _{max} (Base) MNm ⁻² x 6	σ _{max} (Test) MNm ^{-3/2} x 6	σ _{max} change %	Trans. Growth (1) Kilo Cycles		Trans. Growth (2) Kilo Cycles		Average Growth Kilo Cycles		Total Transient Growth Kilo Cycles
						Stop	Slow	Stop	Slow	Stop	Slow	
QT-B W = 25 mm Const. ΔK = 16 MNm ^{-3/2} Base K _{mean} = 28 MNm ^{-3/2}	20 30 40 43 50 60	22.4 19.6 16.8 16.0 14.0 11.2	52.23 27.07 40.13 19.75 19.75 30.26	38.54 17.84 24.21 11.79 10.19 14.33	26.2 34.1 39.6 40.3 48.3 52.6	0 30 73 210 546 801	10 15 76 - - -	0 27 60 500 530 900	15 15 87 - - -	0 28.5 66.5 - - -	12.5 15 81.5 - - -	12.5 43.5 148 - - -
QT-B W = 25 mm Const. ΔK = 19 MNm ^{-3/2} Base K _{mean} = 28 MNm ^{-3/2}	20 30 40 45 50	22.4 19.6 16.8 15.4 14.0	54.46 41.72 31.53 23.89 20.38	40.75 28.35 19.43 13.38 10.51	25.7 32.0 38.3 44.0 48.4	0 2 24 800 1000	6 17 80 - -	0 0 37 825 1150	8 18 54 - -	0 1 30.5 - -	7 17.5 67 - -	7 18.5 97.5 - -
QT-B W = 25 mm Const. ΔK = 22 MNm ^{-3/2} Base K _{mean} = 28 MNm ^{-3/2}	20 30 40 45 50	22.4 19.6 16.8 15.4 14.0	56.69 43.32 33.12 21.34 24.84	42.36 29.94 20.70 12.10 13.70	25.2 30.8 37.4 43.2 44.8	0 3 22 293 1000	5 10 34 242 -	0 3 20 453 -	10 15 46 213 -	0 3 21 373 -	7.5 12.5 40 227.5 -	7.5 15.5 61 600.5 -

Table 12a. Transient Growth Data for K_{mean} Reduction Tests
(Controlling Variables: σ_{max}, σ_{mean}, σ_{min})

Test Conditions	K _{mean} Red. %	K _{mean} MNm ^{-3/2}	σ _{max} (Base) MNm ⁻² × 6	σ _{max} (Test) MNm ⁻² × 6	σ _{max} change %	Trans. Growth (1) Kilocycles		Trans. Growth (2) Kilocycles		Average growth Kilocycles		Total Transient Growth Kilocycles
						Stop	Slow	Stop	Slow	Stop	Slow	
QT-A W = 23.86mm Const. ΔK = 16 MNm ^{-3/2} Base K _{mean} = 28 MNm ^{-3/2}	30	19.6	46.90	34.30	32.84	0	0	0	4	0	2	2
	40	16.8	36.05	24.15	39.81	8.5	30.5	2	18	5.25	24.25	29.5
	50	14.0	27.30	16.45	47.44	286	39	160	28	223	33.5	256.5
	60	11.2	20.30	10.50	55.18	1050	-	1010	-	-	-	-
QT-A W = 23.86mm Const. ΔK = 22 MNm ^{-3/2} Base K _{mean} = 28 MNm ^{-3/2}	30	19.6	50.75	35.00	31.03	0	1	0	1	0	1	1
	40	16.8	38.85	24.15	37.84	0	6	0	4	0	5	5
	50	14.0	29.75	16.45	44.71	0	45	58	27	29	36	65
	60	11.2	22.05	10.50	52.38	643	65	513	91	578	78	656
IS W = 22.86mm Const. ΔK = 16 MNm ^{-3/2} Base K _{mean} = 28 MNm ^{-3/2}	20	22.4	54.86	40.23	26.60	0	24	-	-	-	-	24
	30	19.6	41.83	28.23	32.50	7.5	39	-	-	-	-	46.5
	40	16.8	32.23	19.39	39.80	37	170	-	-	-	-	207
	50	14.0	24.30	12.54	48.40	1010.5	-	-	-	-	-	-
IS W = 22.86mm Const. ΔK = 22 MNm ^{-3/2} Base K _{mean} = 28 MNm ^{-3/2}	20	22.4	59.4	44.20	25.50	0	9.5	-	-	-	-	9.5
	30	19.6	45.3	31.28	30.90	0	22	-	-	-	-	22
	40	16.8	34.94	21.76	37.70	8	89	-	-	-	-	97
	50	14.0	26.29	14.36	45.30	1030	-	-	-	-	-	-

Table 12b. Transient Growth Data for K_{mean} Reduction Tests

(Controlling Variables: σ_{max}, σ_{mean}, σ_{min})

by adjusting the load amplitude and the mean load respectively. At any ΔK level, a reduction in K_{mean} after a base block was achieved by a proportionate reduction in σ_{mean} , thereby reducing σ_{max} and σ_{min} . The load amplitude was adjusted to obtain the constant ΔK for that block. It was observed with all the three heat-treatments that above 20% K_{mean} reduction, a transient period of crack growth occurred immediately after the reduction. The transient period consisted of a slow crack growth region sometimes preceded by a dormant period. The extent of this transient period depended on the amount of K_{mean} reduction, increasing with increased reduction. It was also observed that a total dormancy of the crack could occur at about 50% K_{mean} reduction in the case of low strength QT-B and IS steels. With high strength QT-A steel, about 60% reduction in K_{mean} caused total dormancy only in the case where ΔK was low ($16 \text{ MNm}^{-3/2}$). In tests with higher ΔK values, 60% reduction did not stop the crack totally but induced a long dormant period followed by a slow growth. About a million cycles were allowed before deciding on the total dormancy of a crack.

After the transient growth period, the crack growth rate was observed to attain somewhat constant stabilized value commensurate to the constant ΔK value of the test. The extent of the transient growth period was determined in each case by locating the point of deviation of the potential drop chart record from the straight line which was characteristic of the constant growth rate. A typical example of the potential drop chart record is shown in Fig. 33. The crack growth results for the stabilized part of the growth in each block for different tests are shown in table 11(a-b). The transient crack growth results are also shown in Figs. 12(a-b).

$K_{mean}^{-3/2}$ MNm	ΔK MNm ^{-3/2}	Increase in ΔK %	R	$\frac{da}{dn}$ nm/c (1)	$\frac{da}{dn}$ nm/c (2)	σ_{max}^{-2} MNm ⁻² x6	Change in σ_{max} %	Trans. Growth (1) Kilocycles		Trans. Growth (2) Kilocycles		Average Growth Kilocycles		Total Transient Growth Kilo- Cycles
								Stop	Slow	Stop	Slow	Stop	Slow	
28	16	-	0.556	13.15	12.75	40.2	-	-	-	-	-	-	-	-
14	24	50	0.077	19.44	21.0	25.5	36.6	0	26	0	24	0	25	25
28	16	-	0.556	9.39	9.46	30.3	-	-	-	-	-	-	-	-
14	20.8	30	0.148	10.32	11.52	18.2	40.0	64	60	68	59	66	59.5	125.5
28	16	-	0.556	7.66	7.96	23.0	-	-	-	-	-	-	-	-
14	19.2	20	0.186	-	-	12.8	44.3	1010	-	1010	-	-	-	-

Table 13. Crack Growth Rate Data for K_{mean} Reduction Tests with Increasing ΔK (QT-B)

(Controlling Variables: σ_{max} , σ_{mean} , σ_{min})

4.3.9.2 K_{mean} Reduction Tests with Increased ΔK

It was observed in the K_{mean} reduction tests that a total dormancy of the crack growth could be obtained in QT-B and IS steels by more than 50% reduction in K_{mean} under constant ΔK conditions. In order to investigate the role of ΔK under the reduced K_{mean} condition, the following test was done.

A constant base K_{mean} and ΔK condition was used to grow the crack by 0.05 W in a block. In the next block, K_{mean} was reduced by 50% by reducing the mean load. This would cause the dormancy of the crack if the base ΔK was used by reducing σ_{max} and σ_{min} . However, the ΔK used in the test block was actually bigger by a certain percentage of the base ΔK . This was achieved by using a bigger load amplitude than that would be required to maintain the base ΔK . When the crack grew under this condition, it was allowed to grow by the same amount as in the base block. The testing conditions of the base block were then applied again and the process repeated with different percentage increases in ΔK . In this test only QT-B steel was used. The results of these tests are shown in table 13. It was observed that more than 20% increase in ΔK was required to allow the crack to grow. It should also be noted that even 50% increase in ΔK could not totally overcome the effect of K_{mean} reduction, some transient growth still existed.

4.3.10 Determination of Threshold ΔK

In order to determine threshold value of ΔK below which no crack growth would occur, it was necessary to take into account the findings that any abrupt and large change in mean or maximum stress could cause a transient growth and would give rise to a false threshold value. Therefore, starting with a small value of ΔK which would give

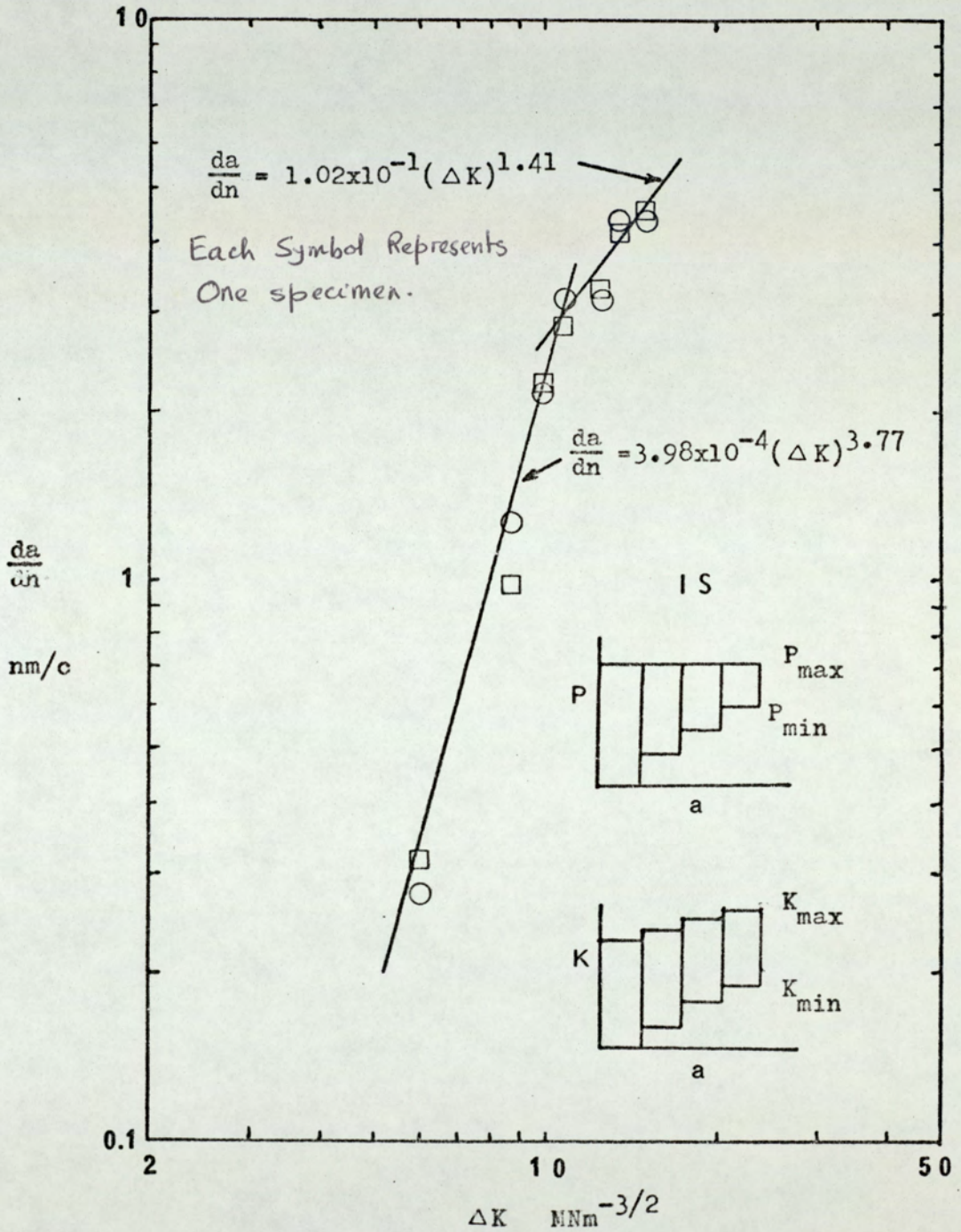


Fig.34. Crack Growth Curve For The Threshold Determination Tests. (Controlling Variables: σ_{mean} , σ_{min})

reasonable crack growth, the block loading test was continued with only 10% reduction of ΔK after each block by reducing σ_{\min} . The material IS was tested and hence to avoid any slowing down of the crack growth rate, the maximum stress was kept constant. The results of the test are shown in Fig. 34. It was observed that starting with an initial ΔK of $15 \text{ MNm}^{-3/2}$ and stepping down to as low a value as $6 \text{ MNm}^{-3/2}$, no crack arrest was obtained. At low ΔK value, the crack growth was very slow and discontinuous. The crack growth rate at the ΔK value of $6 \text{ MNm}^{-3/2}$ was of the order of 0.3 nm/cycle. Fig.34 shows that a crack growth transition existed at a ΔK value of about $11 \text{ MNm}^{-3/2}$ where crack growth rate was around 3 nm/cycle. Before the transition, the crack growth exponent and pre-exponent values were 3.77 and 3.98×10^{-4} respectively and after transition these values were 1.41 and 1.02×10^{-1} respectively. The later coefficient values did not agree with those obtained in the constant load tests, presumably because a lower value of σ_{\max} was used in the threshold determination tests.

4.4 Other Results

The Crack Tip Opening Displacements (CTOD) were measured by a photographic method ⁽¹⁶⁾ in fatigue cracked specimen following the procedure given in section 3.8. Two types of tests performed were as follows:

Test A: The fatigue cycling was stopped after the crack had attained a certain length. The crack opening displacements at the crack tip were measured at different load levels under monotonic loading condition. This was repeated for different crack lengths.

Test B: After stopping fatigue cycling at constant ΔK condition at a certain crack length, CTOD was measured at static loads equivalent to the minimum and the maximum stress of the constant ΔK used. The

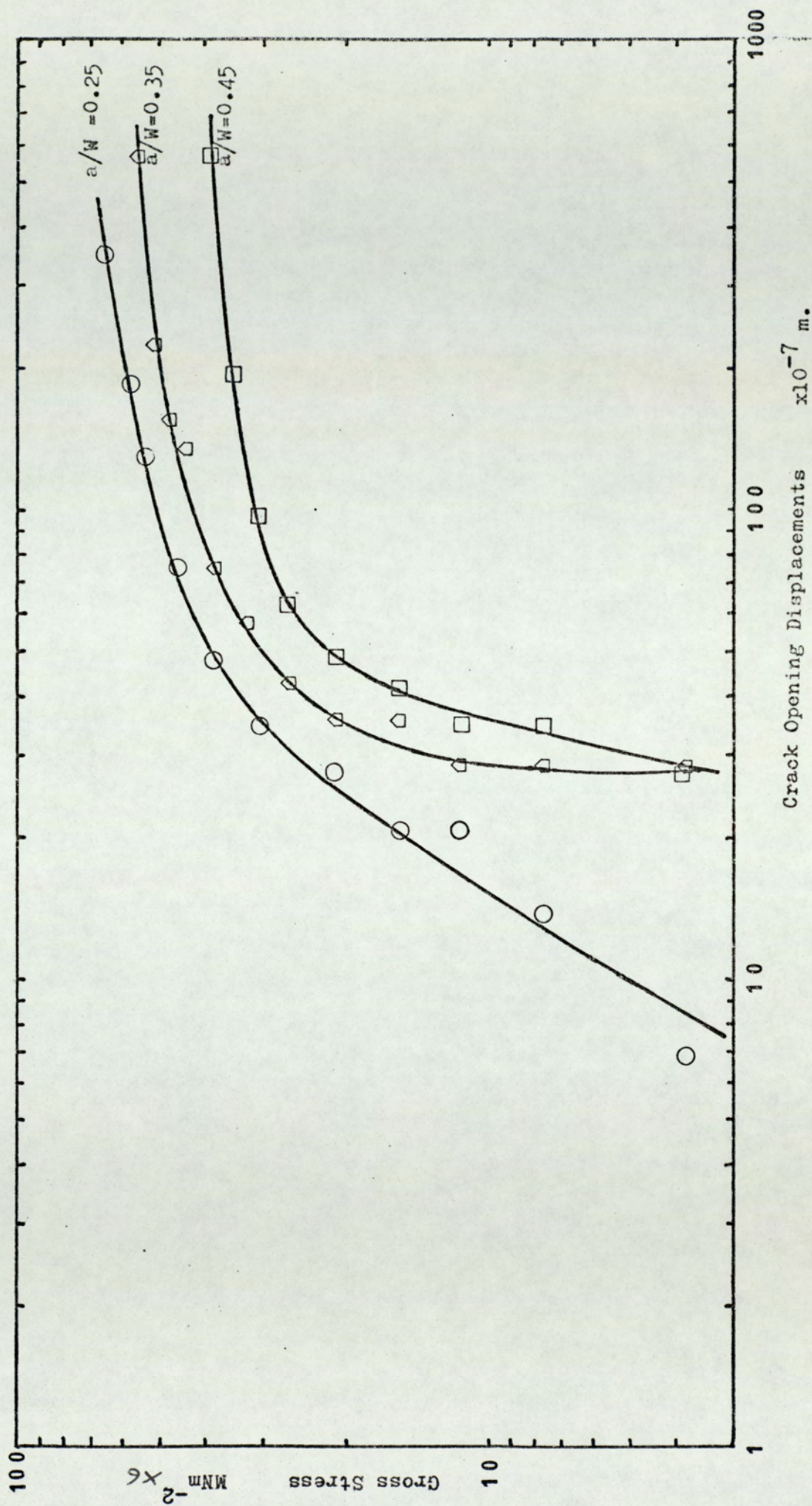
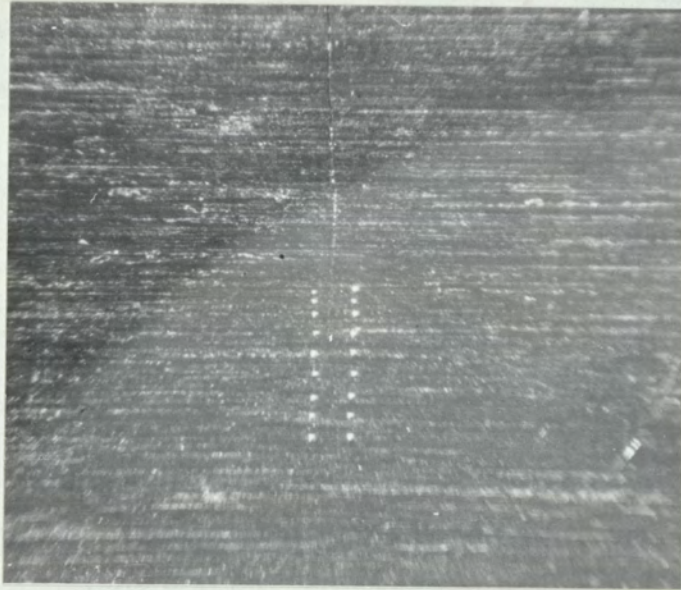


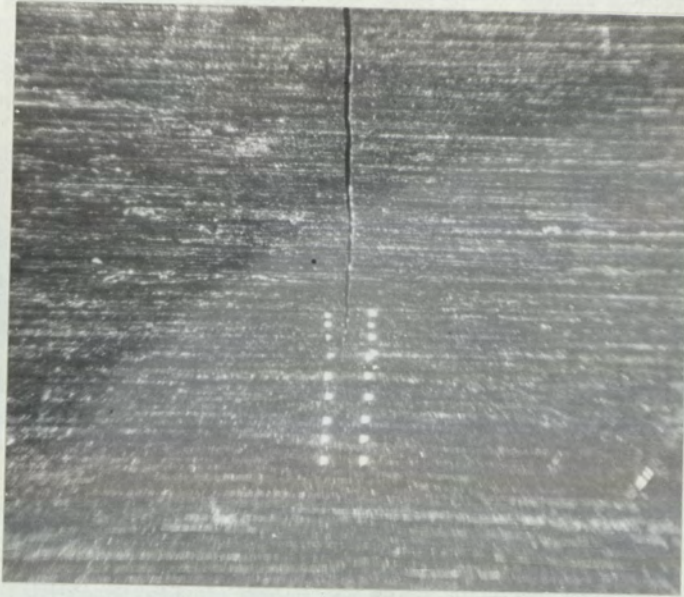
Fig.35. The Dependence Of Static COD On Gross Stress at Different Fatigue Crack Lengths.
(COD Measured at Static Stress After Stopping Fatigue Cycling.)



Stress= 0



Stress=26.7 MNm⁻²



Stress=38.2 MNm⁻²

Fig.36. Examples of C O D Photographs taken under Static Stress after Stopping Fatigue Cycling.
(x 50 approx.)

K Condition	No. of Cycles	Max. COD 10^{-3} mm	Min. COD 10^{-3} mm	COD Range 10^{-3} mm
$28 \pm 16 \text{ MNm}^{-3/2}$	0	4.48	2.99	1.49
$19.6 \pm 16 \text{ MNm}^{-3/2}$	3070	2.99	0.75	2.24
" "	6010	1.49	0.75	0.74
" "	9050	2.24	0	2.24
" "	12070	2.24	0.75	1.49
" "	15160	2.24	0.75	1.49
" "	18110	2.24	0.75	1.49
" "	21130	2.24	0.75	1.49
" "	24120	2.24	0.75	1.49
" "	29120	2.24	0.75	1.49
" "	39120	2.24	0.75	1.49
" "	49130	2.99	0.75	2.24
" "	69120	4.48	0.75	3.74
" "	89060	14.90	7.5	7.4

Table 14. COD Results in K_{mean} Reduction Test

(Controlling Variables: σ_{max} , σ_{mean} , σ_{min})

K_{mean} was then lowered by 30% by lowering σ_{mean} and hence σ_{max} and σ_{min} had to be lowered to maintain the same base ΔK . The CTOD measurement was performed as before after stopping fatiguing at intervals of 3,000 cycles.

Both the tests were performed at a frequency of 60 Hz. For test A the crack was grown under constant K conditions with ΔK and K_{mean} at $19 \text{ MNm}^{-3/2}$ and $27 \text{ MNm}^{-3/2}$ respectively. The results of the CTOD measurements are shown in Fig. 35 as the maximum stress versus CTOD curves. Fig. 36 shows typical examples of COD photographs taken at the crack tip.

For test B, the crack was grown with constant ΔK and K_{mean} of $16 \text{ MNm}^{-3/2}$ and $28 \text{ MNm}^{-3/2}$ respectively. When the crack grew to 0.3 W, the K_{mean} was reduced to $19.6 \text{ MNm}^{-3/2}$ and the test was continued at constant ΔK as before. The results of the CTOD measurements are shown in table 14. The last two measurements shown on the table were taken when the crack tip had gone well past the micro-hardness marks given near the crack tip.

4.5 Metallographic Observations

The general micro-structures of the three heat-treatments used in this investigation have been shown in Figs. 16-18. In QT-A and QT-B steels, banding was observed perpendicular to the cracking direction (Fig. 37). The distance between the bands was about $100 \mu\text{m}$. The banding did not exert any noticeable influence on the crack path or the macroscopic growth rate.

In general, the crack path was not much influenced by the micro-structural features. The crack path was fairly straight in the case of QT-A steel. The main crack generally passed through the grains, but tended to follow the grain boundary if its orientation with respect to the direction of crack growth was suitable (Fig. 38).

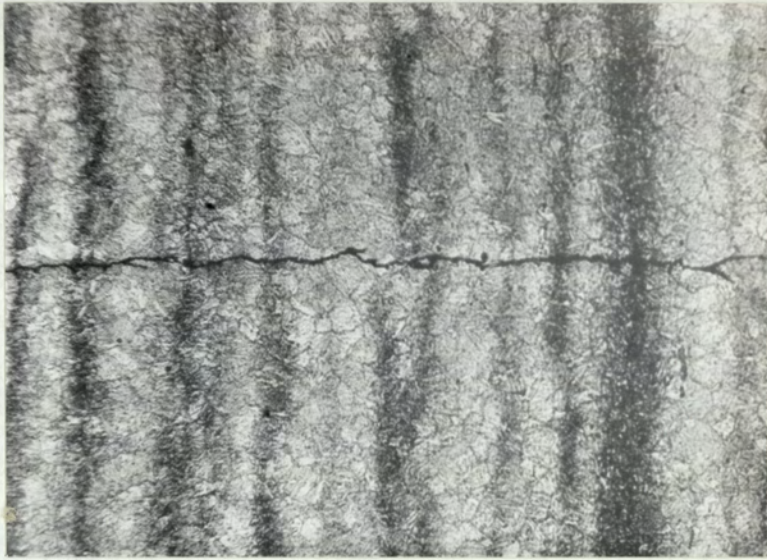


Fig.37. Banding Perpendicular to Crack Propagation
Direction. (x 100)

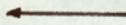
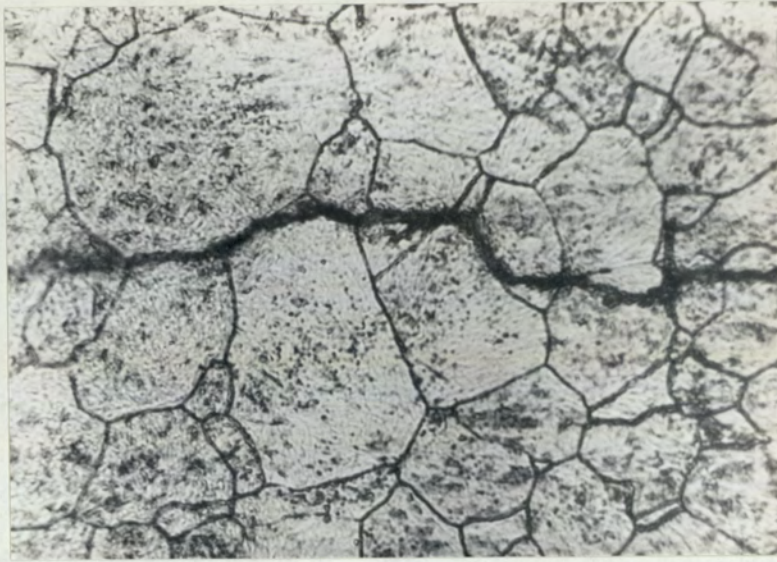


Fig.38. Grain Boundary Cracking in QT-A Steel.
(x 700)



Fig.39. Deep Branch Crack Following G.B. in QT-A Steel.
(x 400)

$$\Delta K = 10.7 \text{ MNm}^{-3/2}$$

$$K_{\max} = 18.4 \text{ MNm}^{-3/2}$$



Fig.40. Numerous Branch Cracks in IS Steel. (x 400)

$$\Delta K = 42.3 \text{ MNm}^{-3/2}$$

$$K_{\max} = 52.8 \text{ MNm}^{-3/2}$$

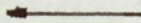
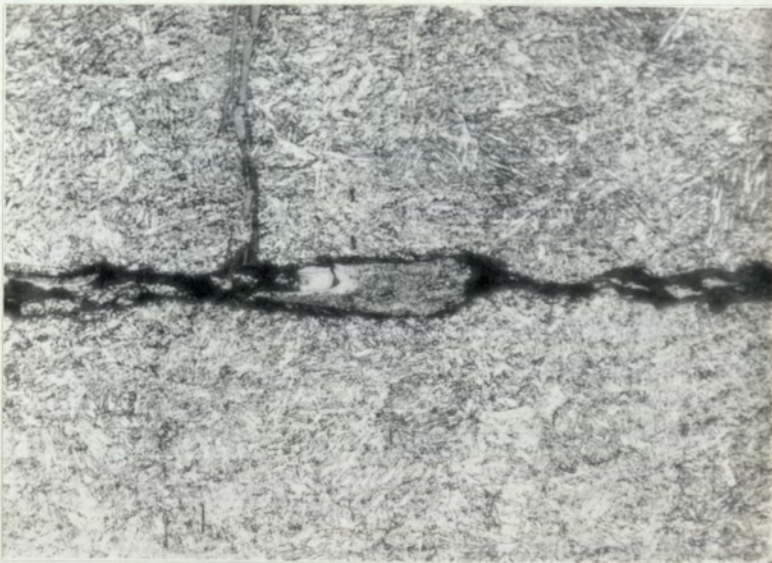


Fig.41. Crack Branching along a MnS Inclusion in QT-B Steel. (x300)

$$\Delta K = 24.2 \text{ MNm}^{-3/2}$$

$$K_{\max} = 28.3 \text{ MNm}^{-3/2}$$

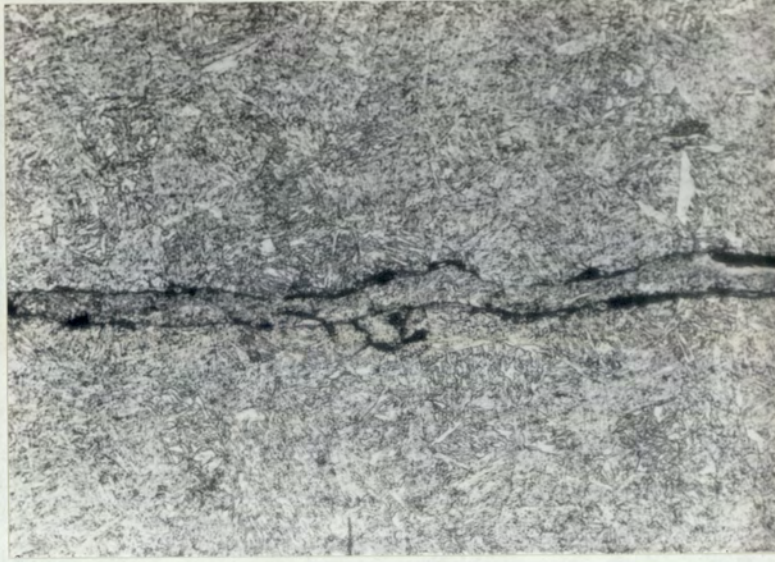


Fig.42. Parallel Cracks in QT-B Steel. (x 300)

$$\Delta K = 14.1 \text{ MNm}^{-3/2}$$

$$K_{\max} = 17.6 \text{ MNm}^{-3/2}$$

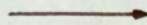


Fig.43. Forked Crack and Joining of Micro-cracks
in IS Steel. (x 400)

$$\Delta K = 15.4 \text{ MNm}^{-3/2}$$

$$K_{\max} = 19.2 \text{ MNm}^{-3/2}$$

Occasional fairly deep branch cracks were also observed (Fig. 39). The branch cracks generally followed the grain boundaries. The presence of stringer type MnS inclusions which were perpendicular to the cracking direction did not seem to have any influence on the rate and direction of crack growth.

The crack paths in the heat-treatments QT-B and IS were not as straight as in the case of QT-A. In both the materials, numerous branch cracks were observed (Fig. 40). These branches were smaller compared to those in QT-A and were generally trans-granular in nature. In contrast to QT-A, the branch cracks in QT-B and IS were found to be influenced by the presence of MnS inclusions and tended to follow them though they were at right angles to the general crack growth direction (Fig. 41). In both QT-B and IS steels, the extent of crack branching was such that it very frequently caused the formation of islands on the crack path (Fig. 41). At some places this crack branching even gave the impression that as if two main cracks were running parallel to each other (Fig. 42). In some cases the main crack forked and then one of the forks became dormant while the other continued growing (Fig. 43). Fig. 43 also shows that micro-cracks were being formed ahead of the main crack and crack growth was continued by a process of joining the micro-cracks. The formation of forked crack was also observed in QT-A steel.

The effect of programme loading on the directionality of the crack path or on the rate of crack growth process did not show up conclusively. In the case of two-step loading, extensive measurements on the crack path showed that some deviations of the crack path occurred at the points of load changes. The deviation was gradual and possibly represents the transient growth after the load change.

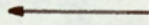


Fig.44. Mixed Transgranular and Intergranular Fracture
in QT-A Steel. (x 1400)

$$\Delta K = K_{\max} = 16 \text{ MNm}^{-3/2}$$

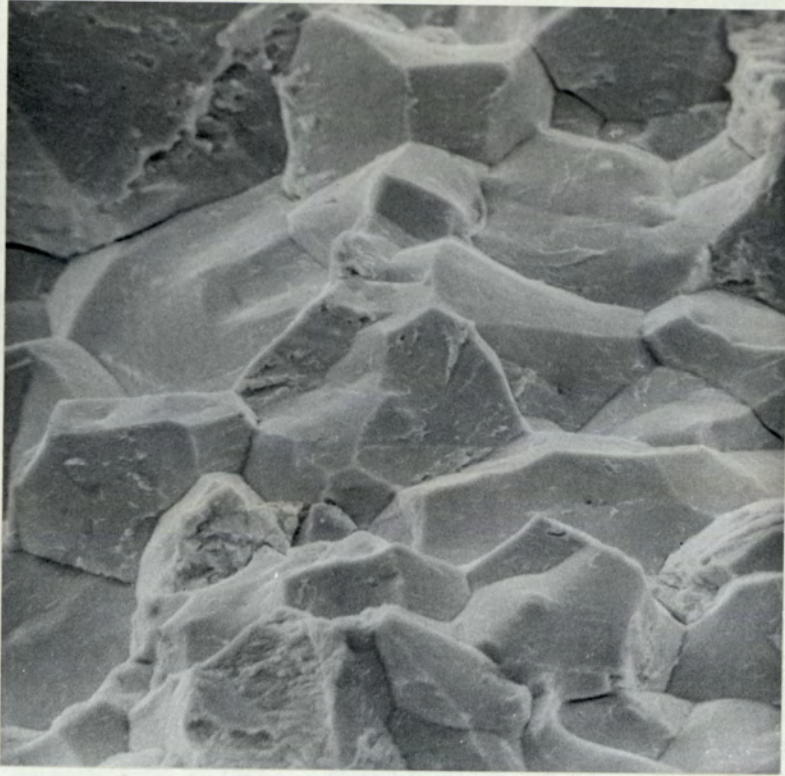


Fig.45. Region of Intergranular Fracture in QT-A Steel.

(x 1400) $\Delta K=16 \text{ MNm}^{-3/2}$ $K_{\text{max}}=25 \text{ MNm}^{-3/2}$



Fig.46. Region of Transgranular Fracture in QT-A Steel.

(x 1350) $\Delta K=9 \text{ MNm}^{-3/2}$ $K_{\text{max}}=17.8 \text{ MNm}^{-3/2}$

Specimen 1				Specimen 2			Specimen 3		
ΔK MNm ^{-3/2}	K_{\max} MNm ^{-3/2}	Intergranular crack %		ΔK MNm ^{-3/2}	K_{\max} MNm ^{-3/2}	Intergranular crack %	ΔK MNm ^{-3/2}	K_{\max} MNm ^{-3/2}	Intergranular crack %
10.97	19.00	39		14.05	28.00	41	14.82	35.00	56
12.19	19.00	45		17.33	28.00	22	15.91	35.00	49
13.45	19.00	72		18.25	28.00	36	17.90	35.00	8
15.23	19.00	52		20.91	28.00	53	18.82	35.00	27
16.00	16.00	42		25.00	25.00	45	22.65	35.00	29
16.00	18.97	50		25.00	31.70	29	23.85	35.00	34
16.00	22.61	69		25.00	39.82	34	32.00	32.00	42
16.00	24.72	87		25.00	41.15	39	32.00	37.63	38
16.00	25.07	95		25.00	46.54	18	32.00	43.17	50
16.00	25.15	71		25.00	49.65	12	32.00	52.27	31
16.00	30.56	83		25.00	55.61	8	-	-	-
16.00	33.14	51		-	-	-	-	-	-
16.00	36.33	25		-	-	-	-	-	-

Table 15. Extent of Intergranular Cracking at Various K Levels

After these slight deviations, the crack path again followed the general direction of crack growth. These deviations were only noticeable in the case of 40% difference in load amplitude levels.

4.6 Fractographic Observations

The fracture surfaces obtained in different types of tests were closely examined under a scanning electron microscope. The predominant mode of cracking that has been observed in QT-A steel was a mixture of intergranular and transgranular fractures (Fig. 44). However, with different specimens investigated, it was noticed that certain regions of fracture surfaces could be located where nearly 100% intergranular (Fig. 45) or 100% transgranular fracture (Fig. 46) existed. A point counting method was applied to the series of pictures taken from different fracture surfaces to determine the extent of each mode of fracture and its relation to the stress intensity values. The results of this investigation are given in table 15. This did not show any definite trend of a particular type of cracking to be associated with a particular stress intensity level. The evidence of the maximum extent of intergranular cracking has been found at around a stress intensity range of 16 to 20 $\text{MNm}^{-3/2}$. It could also be noticed that the maximum intergranular cracking occurred when $\frac{K_{\text{max}}}{K_{\text{mean}}}$ was around 1.6 to 1.7 provided that $\frac{\Delta K}{K_{\text{mean}}}$ was greater than unity. On the other hand, when $\frac{\Delta K}{K_{\text{mean}}}$ was less than unity, the maximum extent of either of the two fracture types occurred at $\frac{K_{\text{max}}}{K_{\text{mean}}}$ value of about 1.4. In the case of QT-A steel, no definite striation markings were observed.

In the QT-B and IS steels, transgranular fractures predominated. These were of a ductile tearing type (Fig. 47). No striation was observed on the fracture surfaces. On high magnifications, furrows



Fig.47. General Transgranular Fracture in QT-B Steel.

(x 1300) $\Delta K=22.3 \text{ MNm}^{-3/2}$ $K_{\text{max}}=27.8 \text{ MNm}^{-3/2}$



Fig.48. Furrows Running Parallel to Crack Growth Direction in QT-B Steel. (x 13,000)

$\Delta K= 27.4 \text{ MNm}^{-3/2}$ $K_{\text{max}}= 34.2 \text{ MNm}^{-3/2}$

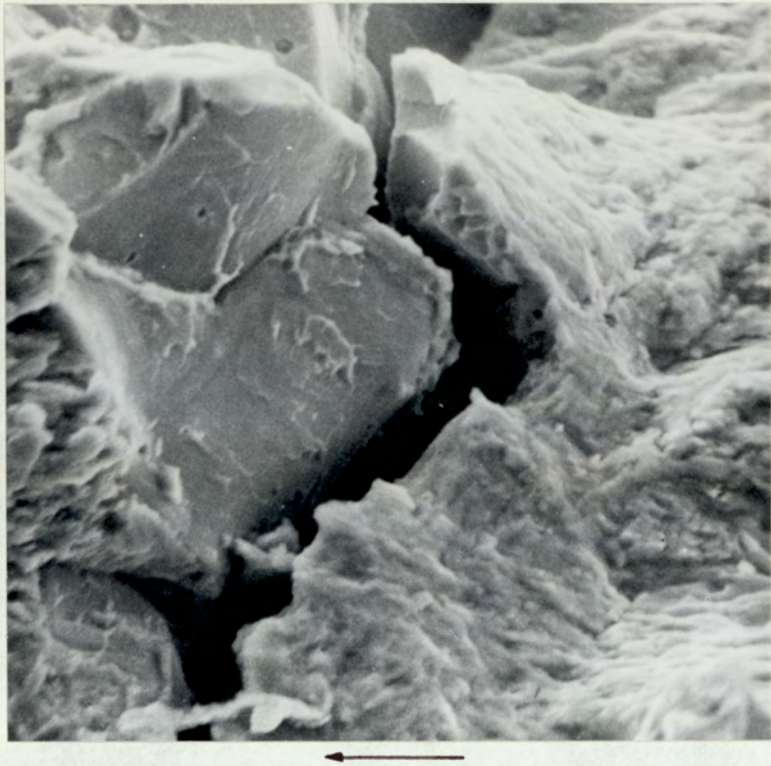


Fig.49. Intergranular Branch Crack in QT-A Steel. (x 2600)

$$\Delta K = 33.4 \text{ MNm}^{-3/2}$$

$$K_{\max} = 52.3 \text{ MNm}^{-3/2}$$



Fig.50. Transgranular Branch Crack in IS Steel. (x 7000)

$$\Delta K = 19 \text{ MNm}^{-3/2}$$

$$K_{\max} = 37.5 \text{ MNm}^{-3/2}$$

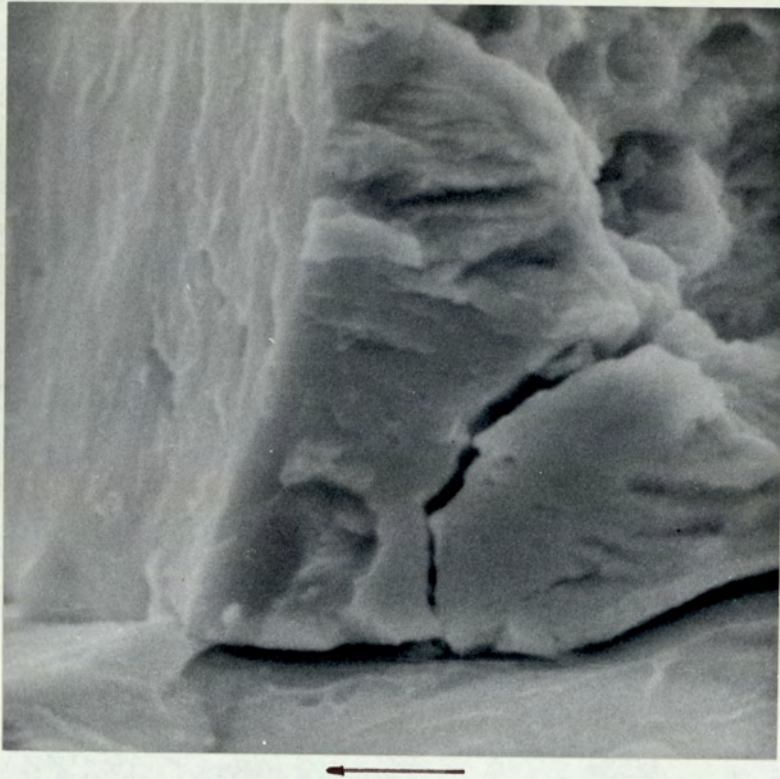


Fig.51. Transgranular Branch Crack in QT-A Steel. (x 7000)

$$\Delta K = 16.8 \text{ MNm}^{-3/2}$$

$$K_{\text{max}} = 30.6 \text{ MNm}^{-3/2}$$

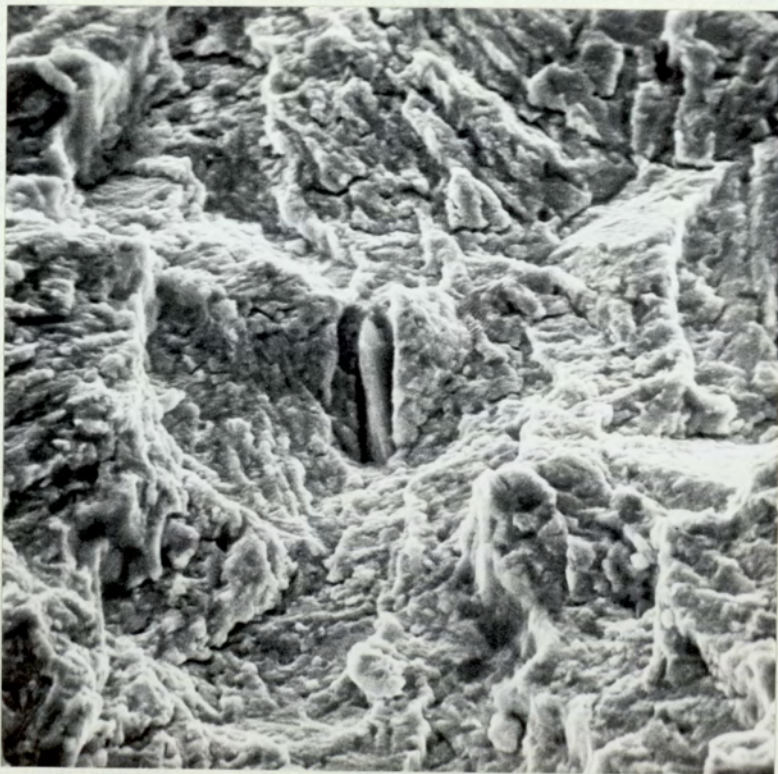


Fig.52. Decohesion of a MnS Particle in QT-B Steel.

(x 1600)

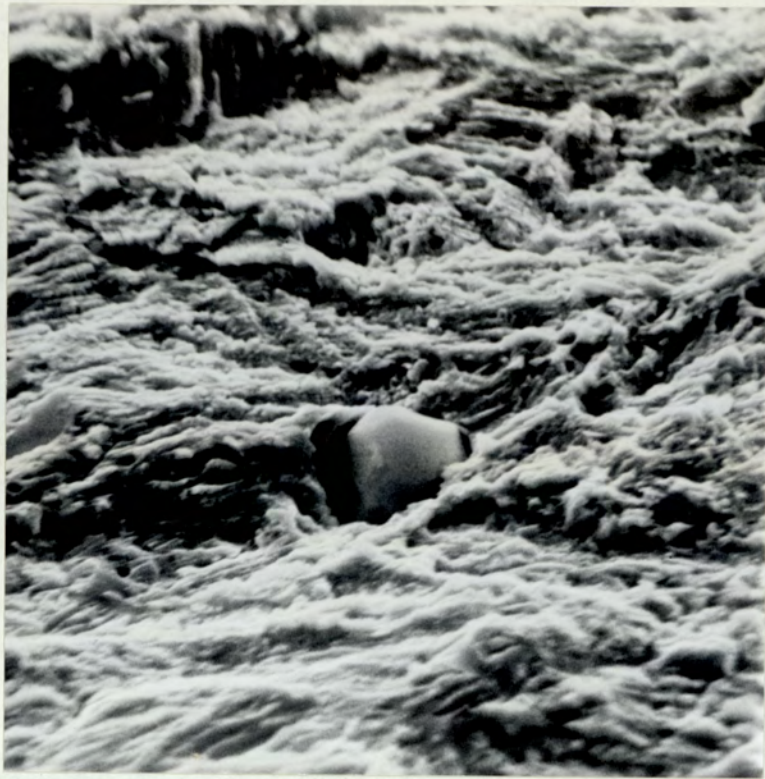


Fig.53. Decohesion of a Cr-rich Particle in IS Steel.

(x 2800) $\Delta K=6 \text{ MNm}^{-3/2}$ $K_{\text{max}}=30.9 \text{ MNm}^{-3/2}$

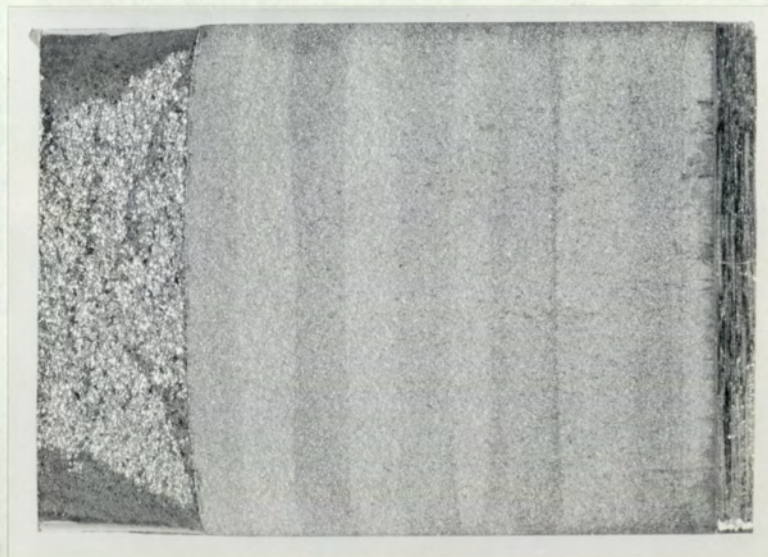


Fig.54. Photograph Showing Dark and Light Bands on Fracture Surface of a Two-Step Load Test.

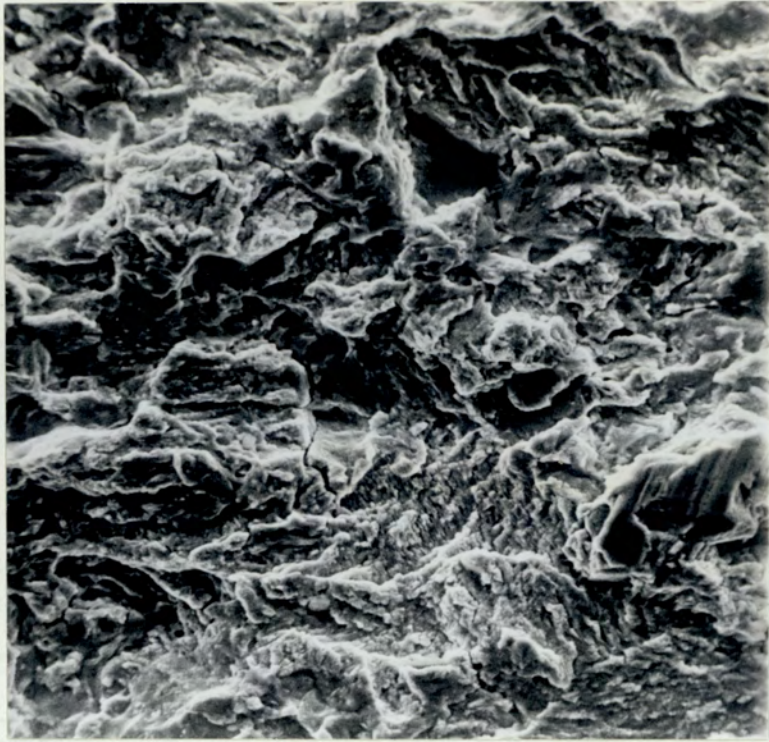
(x 5.8)

running parallel to the crack growth direction were observed (Fig.48) on the transgranular fractures. The furrows were also found in QT-A steel in the fully transgranular portions of the fracture surfaces.

In all the three types of steel, branch cracks were observed under the stereoscan. The evidence of intergranular branch cracks in QT-A steel is shown in Fig. 49 and a representative fractograph of a transgranular type of branch crack found in QT-B and IS steels is shown in Fig. 50. In QT-A steel, the crack branching was not only observed along the grain boundaries but also through the grain in some cases (Fig. 51). The fracture surfaces also revealed a bigger number of branch cracks in the QT-B and IS steels as compared to QT-A steel.

The inclusions and the second phase particles seemed to play a secondary role in the process of fracture. Decohesion of the inclusions and the second phase particles from the matrix was observed. Fig. 52 shows a MnS particle and Fig. 53 shows a chromium rich particle separated from the matrix by decohesion during the fatigue crack growth process. These particles were identified by an energy dispersive x-ray analysis equipment (Keevex-Ray) coupled with the stereoscan.

The fracture surfaces of the two-step loading tests showed alternate light and dark bands corresponding to the high and low load levels of the test. The bands were generally clearer in the tests where the difference between the high and low loads was 40%. Again these bands were more prominent in the QT-B and IS steels than in the QT-A steel. A typical picture of the fracture surface is shown in Fig. 54. When the fracture surface of IS steel was closely examined under the stereoscan at about 0° tilt angle, it was found that the fracture consisted of ill-defined large cellular structures.

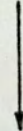


(a) Low Load Region. (x 1250)

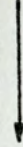


(b) High Load Region. (x 1250)

Fig.55. Comparison of Fracture Surfaces on Adjacent Dark and Light Band of IS Steel.

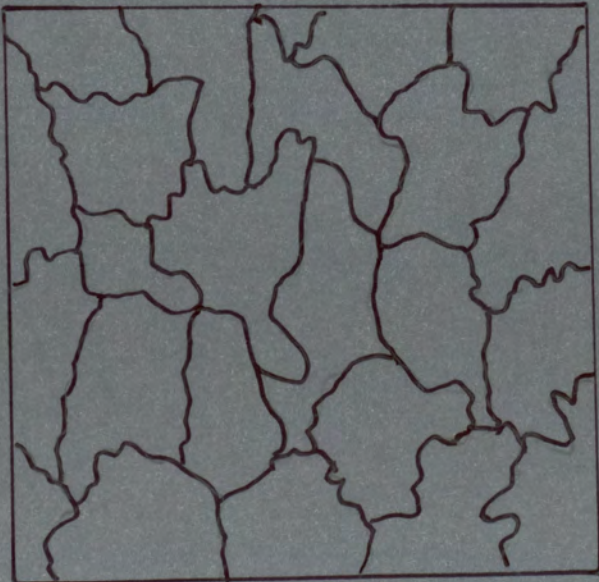
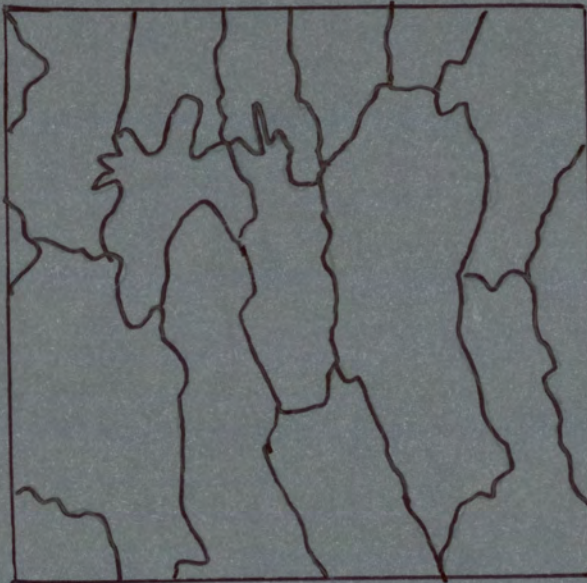
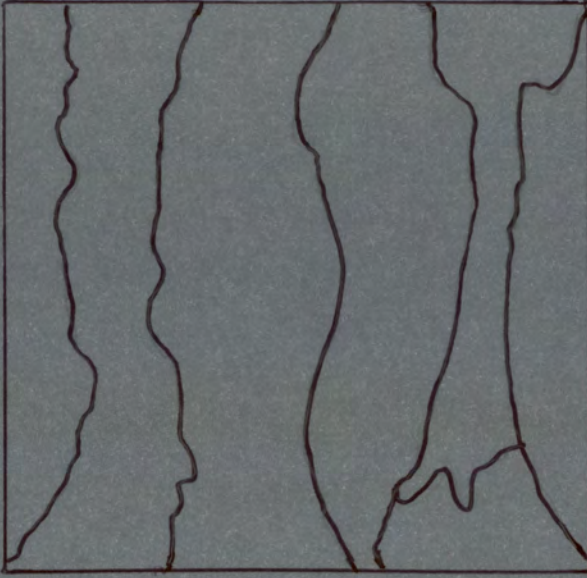


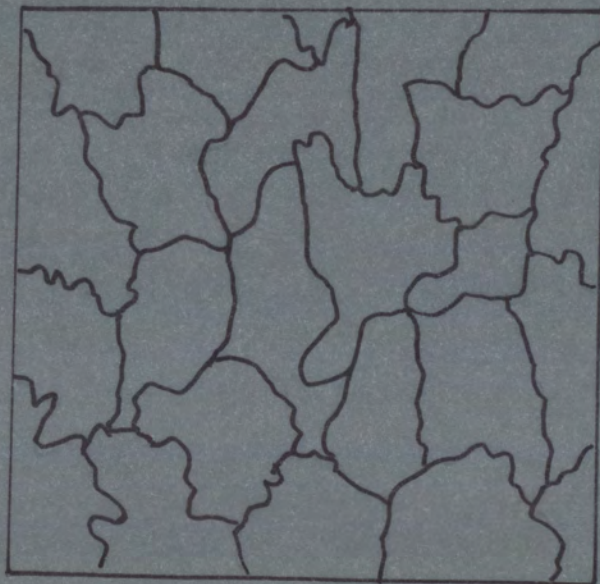
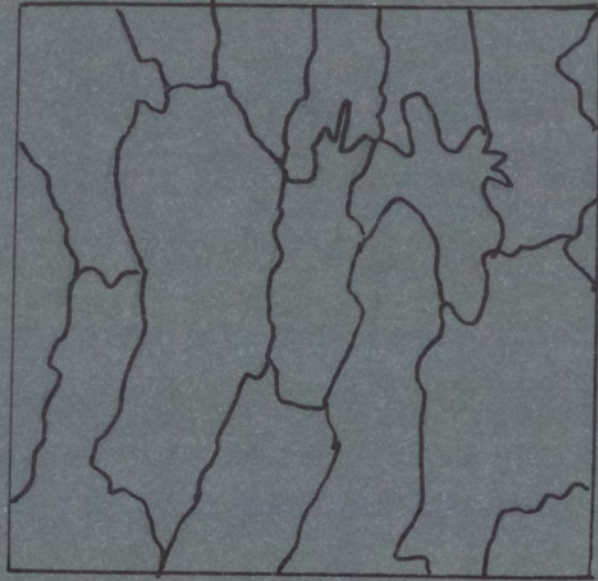
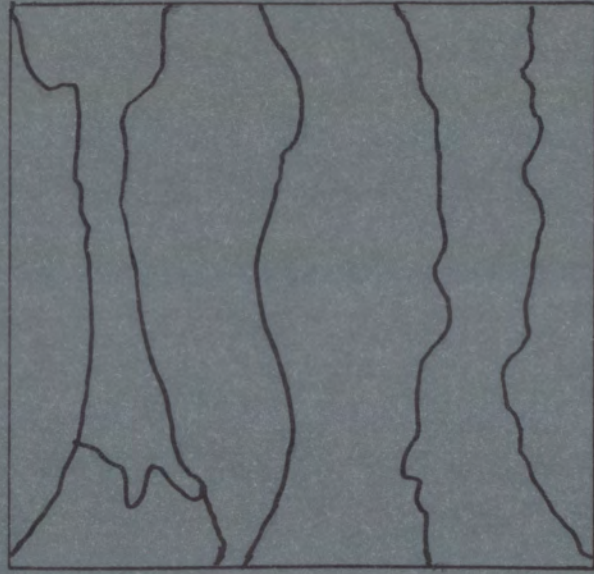
(a) Low Load Region.



(b) High Load Region.

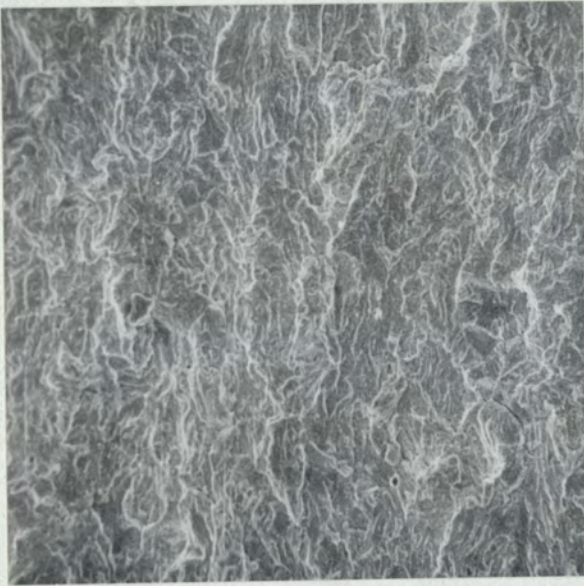
Fig.56. Comparison of Fracture Surfaces on Adjacent Dark and Light Bands in QT-A Steel.
(x 525)



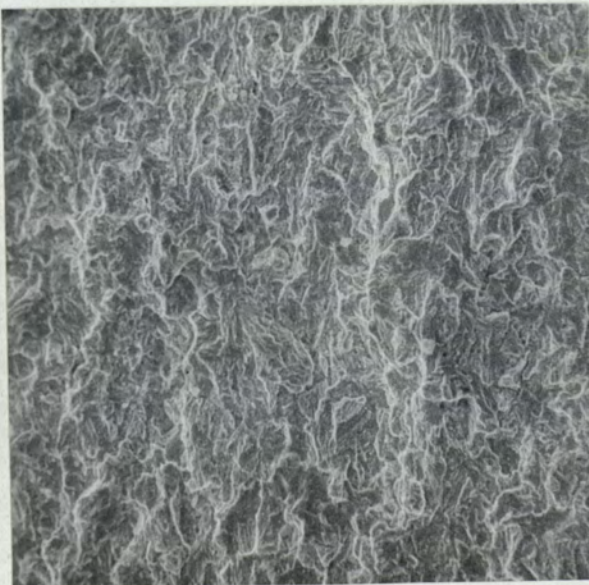




$\Delta K = 27.5 \text{ MNm}^{-3/2}$



$\Delta K = 16.2 \text{ MNm}^{-3/2}$



$\Delta K = 11.1 \text{ MNm}^{-3/2}$

Fig.57. Comparison of Fracture Surfaces Arranged in the Increasing Order of ΔK in IS Steel.
(x 375)

Inside the large cells, there were smaller cells. Comparison of the adjacent light and dark band showed that the light band, i.e. the high load fracture surface, had more elongated cells than the dark band. The cells were drawn out in the direction of crack propagation. This is shown in Figs. 55a-b. Similar behaviour was observed with QT-B steel. In the case of QT-A steel, the cellular structure was not visible. The fracture had an appearance of flow in the crack growth direction. The high load band showed a more flowed fracture surface than the adjacent low load band (Fig. 56a-b).

When the fractographs taken from the IS specimen were arranged in the ascending order of ΔK (Fig. 57), the gradual elongation of the cell structure with the increase of ΔK became more prominent. In the case of QT-A, the fracture surface became more flowed with the transgranular portions becoming more fibrous in the direction of crack growth as ΔK was increased. No noticeable pattern was observed when the fractographs were arranged in the ascending order of K_{max} .

No special features of the fracture surfaces were found which could be related to small changes of load amplitude or mean load. However, the examination of the fracture surfaces of K_{mean} reduction tests, where crack stopping and transient growth behaviour were observed, revealed one interesting feature. It was found that generally the region of K_{mean} change was marked by the appearance of a ridge-like structure running perpendicular to the crack growth direction. At positions where K_{mean} change was large, the ridge-like structure was accompanied by branch cracks. The branch cracks were found to be in a discontinuous line running nearly along the

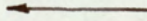


Fig.58. Ridge-like Structure at the Position of High
 K_{mean} Change in QT-B Steel.
(x 1250)



Fig.59. Static Fracture Surface of QT-B Steel.
(x 1300)



Fig.60. Static Fracture Surface of IS Steel.
(x 1300)

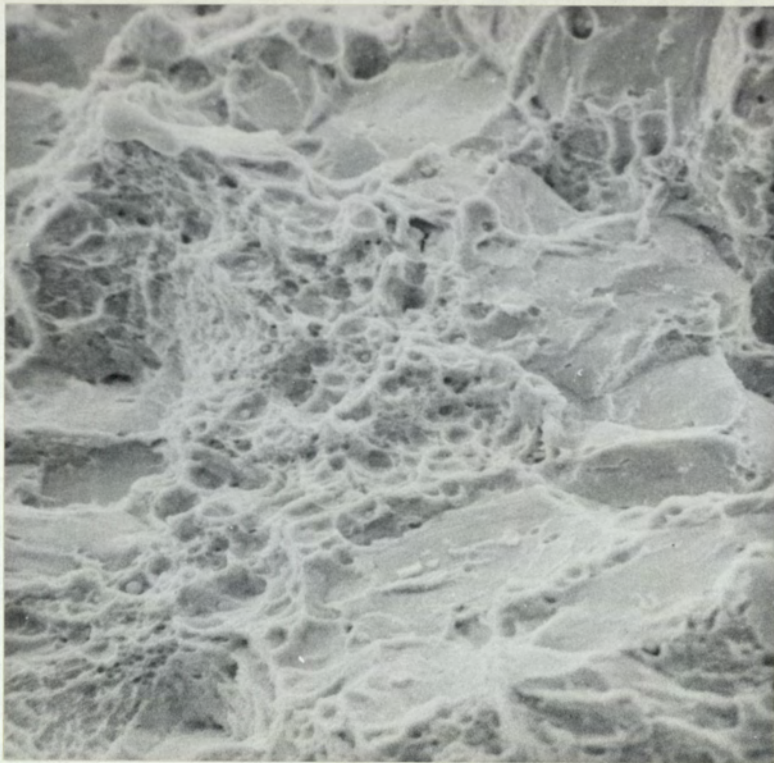


Fig.61. Static Fracture Surface of QT-A Steel.
(x 1250)

whole width of the fracture surface, (Fig. 58).

The static fracture surfaces of the three steels were also examined. The fracture surfaces of QT-B and IS steels showed ductile dimple type of fracture (Figs. 59 and 60). The fracture surface of the QT-A steel, on the other hand, showed a mixture of ductile dimples and intergranular cracking (Fig. 61). In all the static fracture surfaces, the inclusions and the second phase particles were found to be associated with the dimple sites.

5. DISCUSSION

5.1 Constant Load Tests

The results of the constant load amplitude tests at constant mean load show that the rate of crack propagation was dependant on the heat-treatment and the general mechanical properties obtained. The materials QT-B and IS have nearly similar mechanical properties (Table 1) and similar crack growth rates. The material QT-A, on the other hand, has a much higher hardness and strength level and a much lower ductility. The crack growth rate in this steel is 3-5 times higher than that of the other two. It should be noted that the values of the crack growth exponent m , on their own, do not reveal the difference in the rates of crack propagation. The values of m for the three heat-treatments lie between 2 to 2.5 and their differences are marginal (Table 2). In actual fact, it is the combination of the values of m and the value of the pre-exponent A which determines the crack growth rate in each of these materials. The values of m and A do not show any significant correlation with the fracture toughness values obtained in the three heat-treatments. Therefore, the fracture toughness value cannot be used as an indicator of the rate of fatigue crack propagation. In general, the scatter of the results on the crack growth curve was more in the case of QT-A (Fig. 24a) than in QT-B and IS (Figs. 24b-c). The scatter bands of the constant load tests for the three materials will be used as the basis for the comparison of crack growth rates with the results of the programme loading tests.

5.2 Constant Load Amplitude with Variable Mean Load

The results of both QT-A and IS steels show that the test with gradually decreasing mean load gave an overall higher growth rate than

the corresponding test with increasing mean load. The value of R was changed over the same range in both the cases. The test with decreasing mean load started with a high R value and a corresponding high crack growth rate. Though the R value was decreased with the progress of the test, the growth rate did not decrease in proportion to the R value since ΔK was increasing. On the other hand, with the increasing mean load test, the initial crack growth rate was low at the low R value, but the rate did not increase in proportion as the R value was increased. This indicates that the sequence of load application has an effect on the overall crack propagation rate even though the range of R value during the test could be the same. In the increasing mean load case the value of m was higher and A lower than the values of m and A in the corresponding decreasing mean load case (Table 3).

Figs. 25a-b show that the results of the decreasing mean load tests are mostly lying outside the scatter band of the constant load test results indicating a much higher overall crack growth rate. This effect is more pronounced in the case of QT-A steel. It is possible that in this case of low toughness material, a static mode of fracture was operative in addition to the usual fatigue damage. Ritchie (105) has observed that the static mode of fracture such as cleavage or intergranular cracking could be dependent on the magnitude of the maximum tensile stress. He associated intergranular cracking with the higher growth rates in a low alloy embrittled steel tested at high R values. In the decreasing mean load test of QT-A steel, the analysis of the first load block showed an average $\frac{K_{max}}{K_{min}}$ ratio of about 1.56 and $\frac{\Delta K}{K_{mean}}$ ratio of greater than unity, average ΔK being around $16 \text{ MNm}^{-3/2}$. This condition, as observed in section

(4.6), was associated with the highest percentage of intergranular cracking. Thus the higher growth rates in the decreasing mean load test on QT-A steel could be due to the static component of fracture.

5.3 Stepped Increase in Load Amplitude

The results of these tests show that there was no noticeable transient acceleration of crack growth rate at the point of increase in load amplitude when the mean load was kept constant. The rate of crack propagation after the load amplitude change seems to conform to the higher ΔK level experienced by the crack tip. Though the respective m and A values for QT-A and IS materials were different from those obtained in the constant load tests, the crack growth rate results fell within the scatter bands of the constant load tests for the two materials (Figs. 27a-b). When the crack growth curve for any of the two heat-treatments were examined closely, it could be noticed that the results of each load block had a different slope than the other ones. For both the heat-treatments, the slope for the individual load blocks became steeper with the increase in R value. This tendency was stronger for QT-A steel which is possibly more susceptible to the static mode of fracture.

If the overall growth rate for each test is considered, there does not seem to be any effect of the interaction between the load amplitudes in the adjacent blocks in either of the heat-treatments.

5.4 Two Step Loading

The crack growth rate results of the two step block loading indicate that there was no transient acceleration effect on crack growth rate due to the low-high load amplitude change. The high-low load amplitude change, on the other hand, showed some transient delay effect on the crack propagation rate. This effect became

more noticeable if the difference between the high and the low load amplitudes were increased. Moreover, this transient slowing down effect seems to be related to the yield strengths of the materials, being prominent in the case of low strength material such as IS. Let us now compare the constant load crack growth results with the two step load test results (Figs. 29a-c). It can be noticed that in the case where the difference between the high-low amplitudes was 20%, the crack growth results for the two step load test fell within the constant load scatter band for each of the heat-treatments. The values of m and A obtained with the three heat-treatments also correspond to those obtained in corresponding constant load tests. This implies that the load interaction effect is not operative in cases where load amplitude difference is low. This observation agrees with the conclusion drawn by Christensen ⁽⁷⁸⁾ in two-step load tests.

In the case of 40% load amplitude difference between the high and the low load blocks, the results of QT-A material were within the scatter band for the constant load test. Thus even for a considerable difference in load amplitudes, the load interaction effect does not show up clearly in the case of high strength material. In fact, the values of m and A , when compared with the constant load results, indicate a slightly higher overall crack growth rate. This increase could be due to the effect of higher R values of the load blocks as compared to the constant load test. On the other hand, for the low yield strength IS material, part of the crack growth rate results of the two-step load test with 40% amplitude difference lay outside the scatter band for the constant load test. This indicates an overall slower crack growth rate. Thus, a big difference in load amplitudes for high-low loading causes the transient delay effect in low strength

material. From the equation (10), it can be seen that the lower the yield strength, the bigger will be the maximum plastic zone size. If the maximum plastic zone size were related to the delayed crack growth rate ^(91,92), it seems reasonable that the lower strength IS material would be subjected to a bigger load-interaction effect than the high strength QT-A material.

5.5 Constant ΔK Tests at Constant K_{mean}

It was quite surprising to find that with both QT-A and IS steels, a gradual reduction of the crack growth rate occurred with the increase in crack length even though ΔK and K_{mean} were kept reasonably constant. It was hypothesised that the load-interaction due to block-load shedding could have caused this slowing down. A test was, therefore, performed with IS steel using semi-continuous load shedding where the difference between the adjacent load amplitude was only about 4%. The stress intensity range was kept constant at $19 \text{ MNm}^{-3/2}$ at $R = 0.493$. A reduction of 46.2% in crack growth rate was observed between a/W of 0.15 to 0.55. This result eliminated the possibility of load-interaction. Next it was thought that the current passing through the specimen for the crack growth measurement purpose might have some effect. Therefore, the above test was again performed without the potential method and using travelling microscope only. The slowing down was again obtained. Next, it was considered that the atmospheric moisture might have been increasing the crack growth rates at low a/W values, whereas at high crack lengths, due to the difficulty of penetration, the moisture had no effect. The test was, therefore, performed by sealing off the possible fracture path from the outside atmosphere by means of a small container built around the specimen. The

reduction of the crack growth rate was observed once again. The fracture surface was considerably cleaner than that usually obtained with tests in atmospheric condition. This showed that the moisture was not responsible for slowing down.

The constant K condition tests were performed at different ΔK values. The tests showed a reduction of the crack growth rate by about 50% between crack length of 0.15 W to 0.55 W. Recently Von Euv et al ⁽⁹³⁾ reported a similar effect in aluminium alloy. He observed a reduction of about 15% for crack lengths between 0.25 W to 0.45 W, but he could not explain the reason for it.

Dowse and Richards ⁽¹⁰⁶⁾ found a reduction of crack growth rate by a factor of 2 in tests with a welded low alloy steel under constant K conditions. They observed this gradual slowing down when the crack was grown from the parent metal towards the heat-affected zone, the H.A.Z. being at 75° to the tensile axis. They argued that the increased hardness of the H.A.Z. did reduce the plastic zone size at the crack tip with a consequent reduction in COD and the crack growth rate. In contrary to their arguments, the hardness and $\frac{da}{dn}$ curves given in the paper showed that the slowing down occurred long before the crack tip reached the hard H.A.Z. By considering the extreme case of a plane stress condition, if we calculate the plastic zone radius r_y (Equation 11), using the data given in the paper, we get $r_y = 1.15$ mm. The slowing down started at a distance of 5 mm from the hard H.A.Z. Thus the explanation put forward for the reduction of the plastic zone size by the hard H.A.Z. does not seem to be a very sound one.

On the basis of the evidence of the present investigation and the examination of the available literature it seems reasonable to

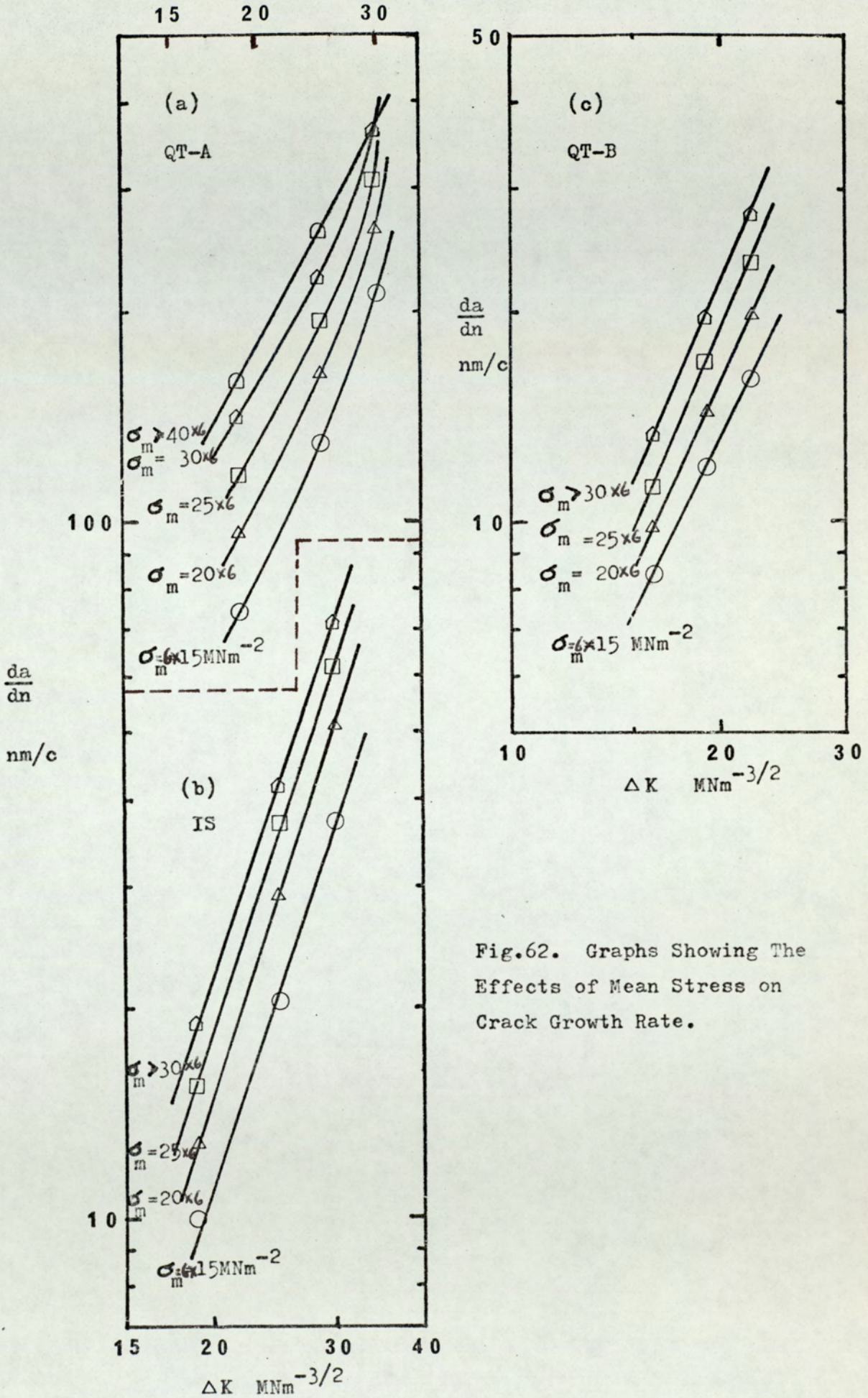


Fig.62. Graphs Showing The Effects of Mean Stress on Crack Growth Rate.

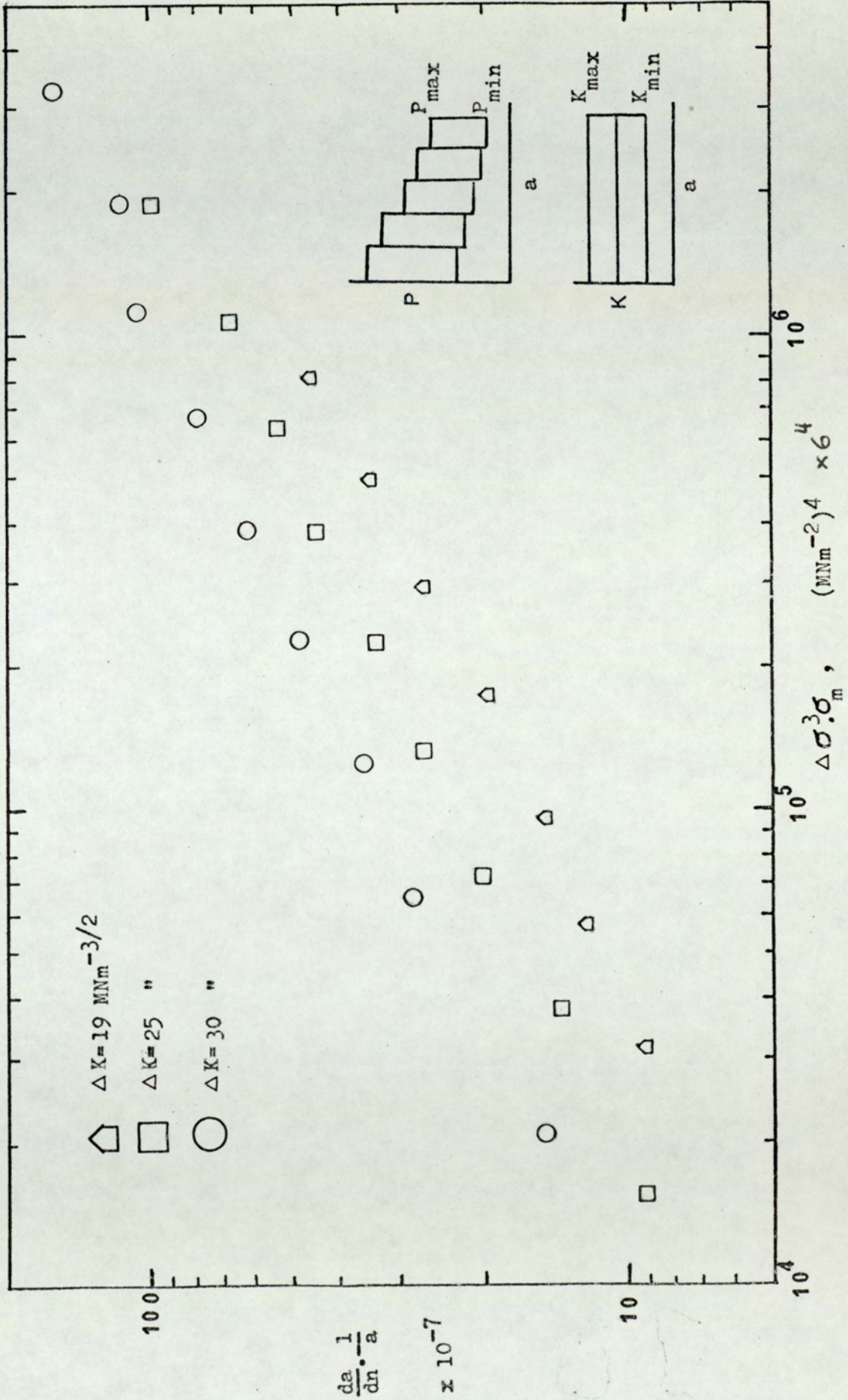


Fig. 63a. The Effect Of Mean Stress On Crack Growth Rate (Const. K/IS)
 (Controlling Variables: σ_{max} , σ_{mean} , σ_{min} .)

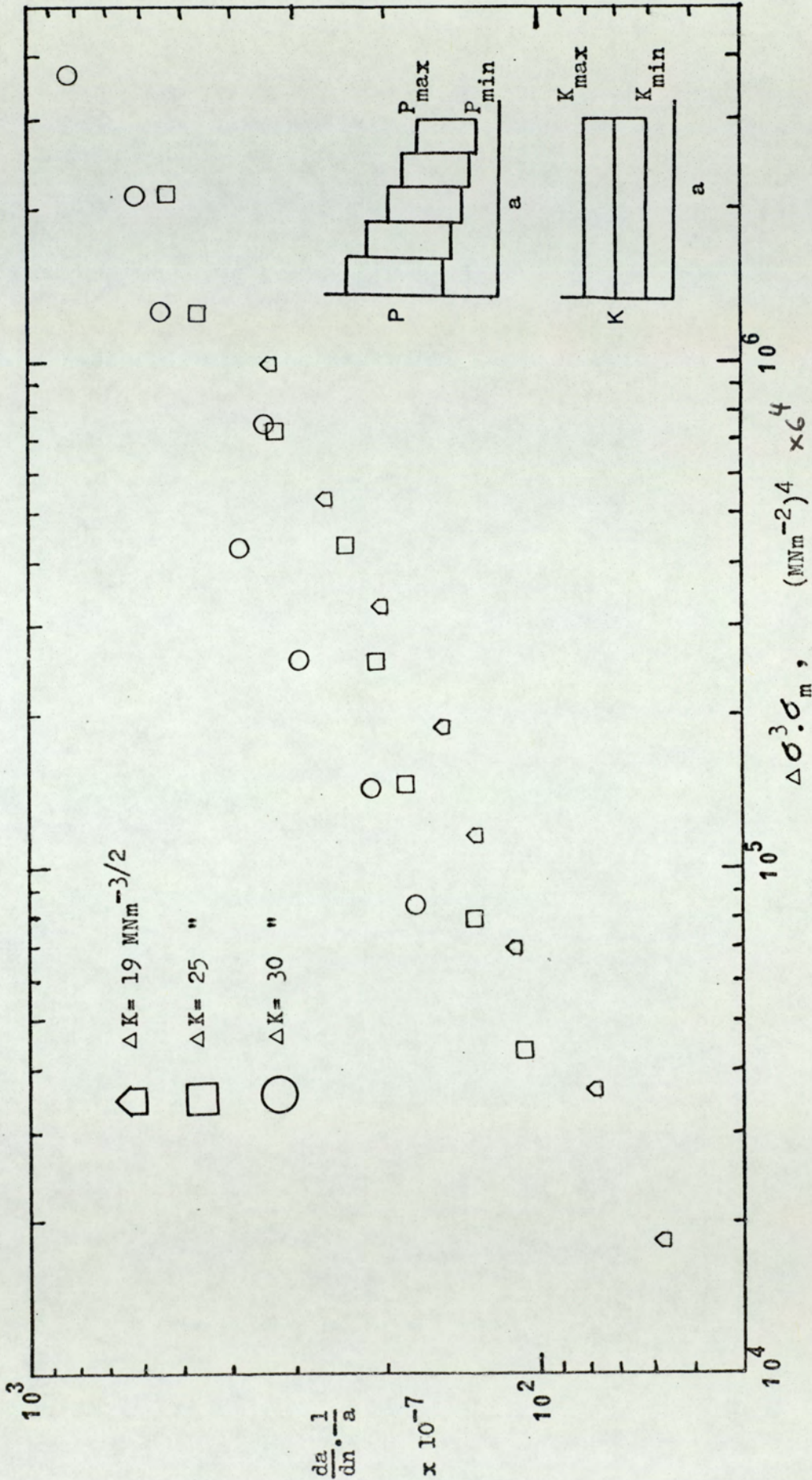


Fig.63b. Effects Of Mean Stress On Crack Growth Rate (Const. K/QT-A)
 (Controlling Variables: σ_{\max} , σ_{mean} , σ_{\min})

conclude that the reduction of the crack growth rate at constant K conditions is a material property and does not depend on the specimen geometry.

It can be seen from table 6 and Fig. 30a-b that the gradual and systematic reduction in crack growth rate started at about $a/W = 0.3$. The crack growth rate values before that show scatter, but can be approximated by a mean constant value. The scatter is more at high ΔK than at low ΔK .

In constant K tests, the mean load was reduced gradually to keep K_{mean} constant. The crack growth rates were therefore plotted against mean stress (Fig. 31a-c) which showed that a relation between the two variables existed for each ΔK value. If the crack growth rates at different ΔK values for a constant mean stress are plotted against ΔK , we obtain Fig. 62a-c. These curves show the effect of mean stress on the crack propagation rates of the three materials. In each case, at a constant ΔK , if σ_m increases, $\frac{da}{dn}$ increases; a factor of 2 increase in mean stress causing an increase in $\frac{da}{dn}$ by a factor of 1.5. In the case of QT-A steel at constant mean stress, the rate of increase in $\frac{da}{dn}$ increased at very high ΔK levels. It could also be noted from Figs. 31a-c that for each ΔK value, there is a saturation mean stress level at which the crack growth rate is virtually constant.

Tomkins⁽³²⁾, through his theory of crack growth by shear and decohesion, has shown that the crack growth rate could be a function of $\Delta\sigma$, σ_m and a (equation 15). Since the constant K condition tests showed an effect of mean stress and crack length on the crack growth rate, it would be interesting to find how well equation 15 fits the present data. The data replotted in terms of this equation are shown in Figs. 63a-b. It could be seen that 1:1 slope between

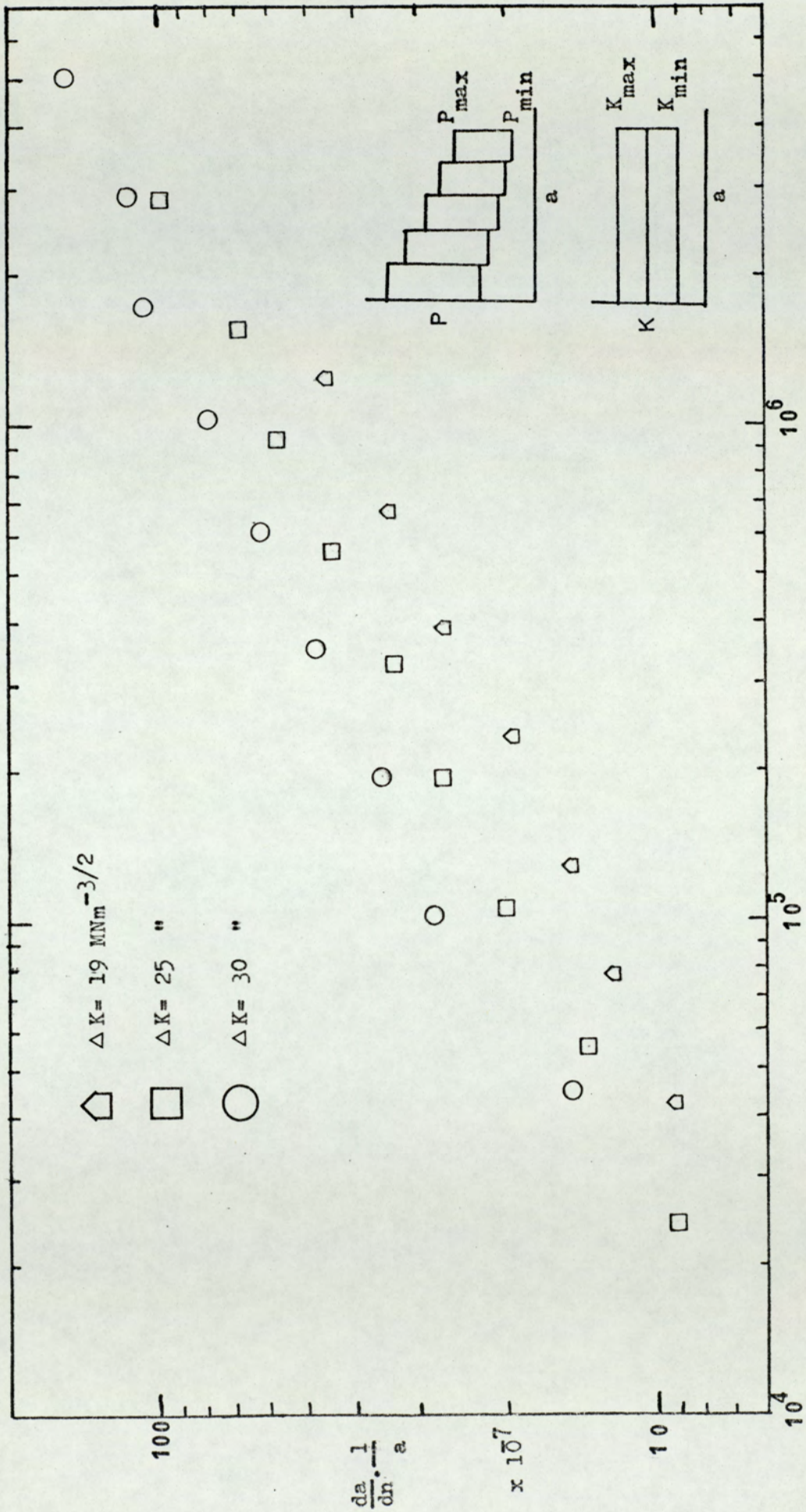
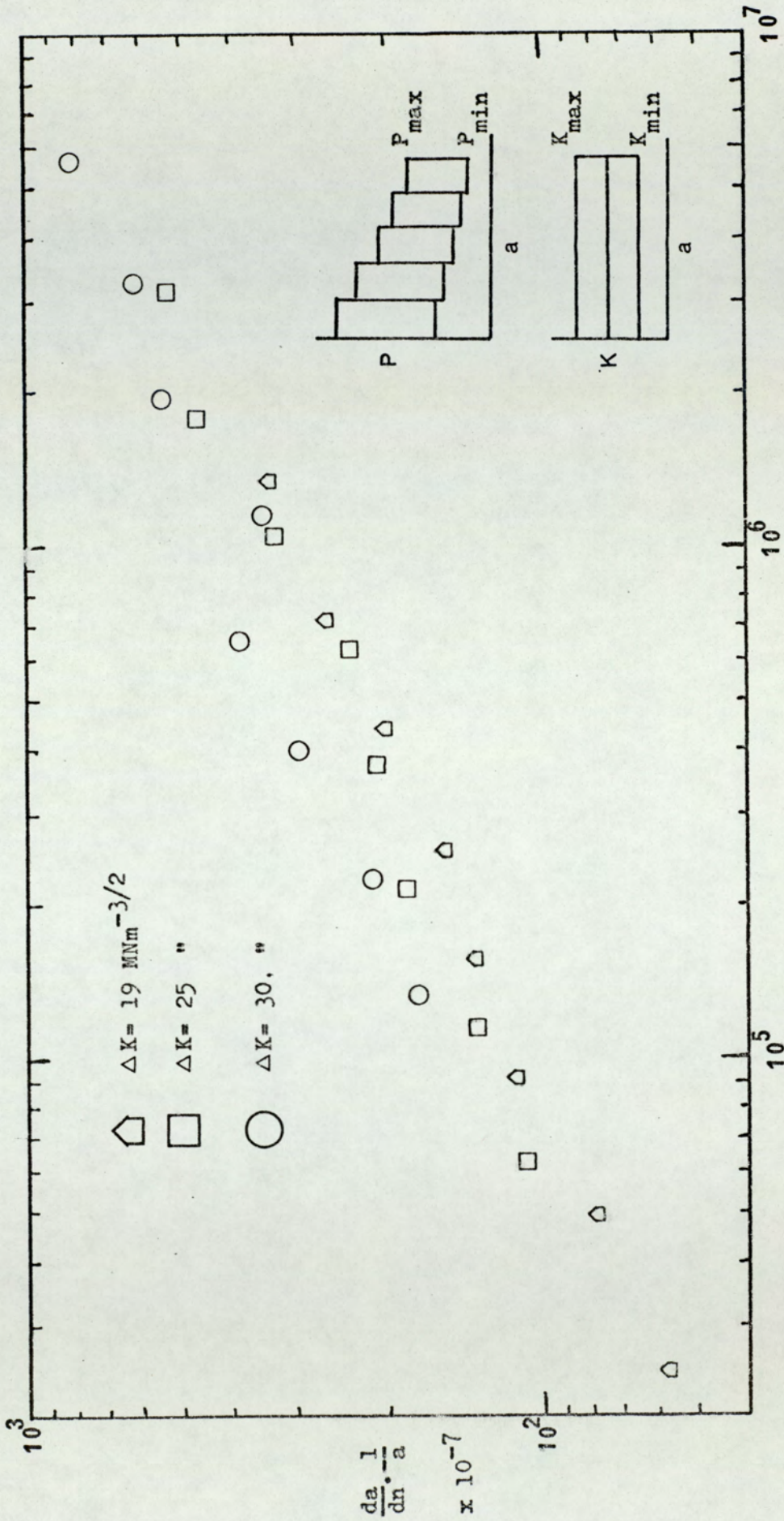


Fig.64a. Effects Of Maximum Stress On Crack Growth Rate (Const.K/ IS)
 (Controlling Variables: $\sigma_{\max}, \sigma_{\text{mean}}, \sigma_{\min}$)



$$\Delta \sigma^3 \cdot \sigma_{\max}^4 \quad (\text{MNm}^{-2})^4 \times 6^4$$

Fig. 64b. The Effect Of Maximum Stress On Crack Growth Rate (Const.K/ QT-A)
 (Controlling Variables: σ_{\max} , σ_{mean} , σ_{\min})

$\Delta\sigma^3 \cdot \sigma_m$ and $\frac{da}{dn} \cdot \frac{1}{a}$ as predicted by equation 15 does not hold. For the present data, the slope observed had a value of roughly 1:2. Thus an equation of the following type resulted:

$$\frac{da}{dn} = A(\Delta\sigma)^m \cdot \sigma_m^n \cdot a \quad (34)$$

where A, m and n are constants.

The values of m and n for the present data are about the half of those obtained by Tomkins who used Frost and his co-workers' data on different materials. The constant K condition data, though it followed equation 34, showed a layering effect which depended on ΔK values, the data of each ΔK level having a A value of its own.

A similar correlation can be obtained by replacing σ_m by σ_{max} in equation 34. The layering effect still existed, but the overall scatter is reduced (Figs. 64a-b). Thus the use of the maximum stress is advantageous over the use of σ_{mean} and the maximum stress seems to be a better controlling factor for the crack growth rates.

The equation of the crack growth rate obtained in this investigation on the basis of maximum stress was of the type:

$$\frac{da}{dn} = A(\Delta\sigma)^{1.5} \cdot \sigma_{max}^{0.5} \cdot a \quad (35)$$

When $\sigma_{max} = \Delta\sigma$, the above equation reduces to:

$$\frac{da}{dn} = A(\Delta\sigma)^2 a$$

$$\text{or } \frac{da}{dn} = f(\Delta\sigma)^2 a$$

$$= f(\Delta K)^2$$

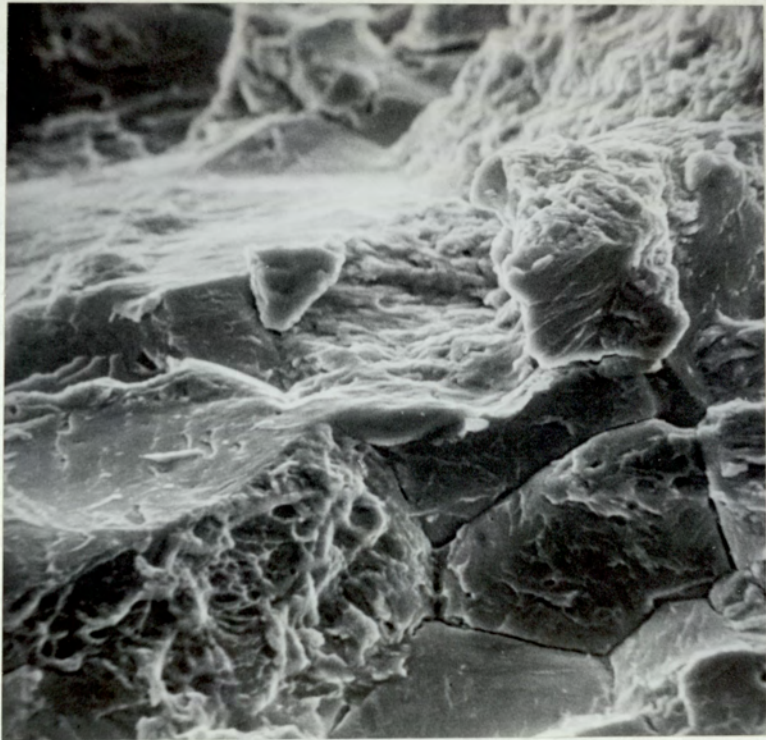


Fig.65. Isolated Regions of Micro-void Coalescence and Intergranular Fracture in QT-A Steel. (x 2000)

$$\Delta K = 22.9 \text{ MNm}^{-3/2}$$

$$K_{\text{max}} = 40 \text{ MNm}^{-3/2}$$

The above relation is consistent with Liu's (38) observation who used an energy criterion for his fatigue crack growth equation.

5.6 Constant ΔK Tests at Constant Mean Load or Maximum Load

In view of the discussion on the results of the constant K condition tests, it could be expected that the crack growth rate at a constant ΔK and at a constant mean load would be constant. Table 7 shows that in the case of high strength QT-A steel, this is true. In fact, the crack growth rates showed slight increases at high crack lengths. Such an increase would be expected if this material is sensitive to high K_{\max} values. Examination of the fracture surfaces showed the evidence of both the intergranular cracking and the micro-void coalescence in isolated areas at high K_{\max} values (Fig. 65).

In the case of low strength IS steel tested at constant mean load, a reduction in the crack growth rate with the increase in crack length was observed. This showed that though the mean load may affect the growth rate, other factors are at work. It was noted that for the low ΔK tests ($\Delta K = 19 \text{ MNm}^{-3/2}$), the higher was the mean load, the bigger was the reduction in growth rates; whereas for the high ΔK tests ($\Delta K = 30 \text{ MNm}^{-3/2}$), the reverse happened. For the latter case where K_{\max} was high ($K_{\max} = 60-70 \text{ MNm}^{-3/2}$), the possibility is that some static modes such as micro-cleavage or micro-void coalescence was contributing to counteract the crack growth reduction. An examination of the fracture surface was not very conclusive, but some micro-void coalescence was observed.

When σ_{\max} was kept constant at constant ΔK , the QT-A material again showed a behaviour similar to that at constant mean load. In the cases of QT-B and IS steels, the crack growth rate was fairly constant up to $a/W = 0.45$, indicating that σ_{\max} is a better crack



(a) Un-etched Fracture Surface. (x 1300)



(b) Etched Fracture Surface. (x 6500)
Etchant-- Nital(2%). Time-- 20 Secs.

Fig.66. Cleaved Region in QT-B Steel.
 $\Delta K=18.4 \text{ MNm}^{-3/2}$ $K_{\text{max}}=35 \text{ MNm}^{-3/2}$

growth controlling factor than σ_{mean} . The slowing down at very high crack lengths in the IS steel could be related to excessive plasticity and crack blunting due to very high K_{mean} values.

5.7 Constant K_{max} with Increasing ΔK

The crack growth curves given in Fig. 32 show that at low value of K_{max} ($= 19 \text{ MNm}^{-3/2}$), the crack growth rates were well inside the scatter-band of the constant load tests. For tests with high K_{max} values, the crack growth rates were faster than the constant load tests in both QT-A and QT-B materials. The fracture surface of the QT-B steel showed isolated patches of cleavage fractures at high K_{max} . The cleaved area, when examined closely, showed particles embedded in the matrix. The fracture surface was etched in nital for twenty seconds and examined under the stereoscan again. The cleaved area now showed up the distribution of some small second phase particles (Fig. 66). These particles are believed to be carbide particles which caused the cleavage fracture. Thus in both QT-A and QT-B steels, the crack growth rates at high K_{max} were influenced by additional modes of fracture.

Though the regression lines have been drawn through the results of the tests for different K_{max} values, it could be noticed that in spite of the increasing ΔK , the crack growth rates showed a slight gradual slowing down. This could be due to the decreasing R value with the progress of the test. Looking at it in another angle, this slowing down could be due to the decreasing maximum stress which has been shown previously to influence the crack growth rates.

5.8 ΔK Interaction Effect

When the testing conditions are such that no slowing down of the crack growth rate occurs at a constant ΔK condition, it would be of

value to find the effect of interaction between different magnitudes of stress intensity ranges. The results of such tests are shown in table 10. No crack growth retardation effect of ΔK reduction was noticed in either QT-A or IS steel up to a ΔK change of 50%. On the other hand, no crack growth acceleration was observed due to the increases of ΔK values. The crack growth rates given in table 10 show some increases as compared to the constant load crack growth rate values, but this is only a reflection of higher maximum stresses used in the present tests. These increases, therefore, do not reflect any genuine ΔK interaction effect. The ΔK interaction effect showed up only when the reduction in ΔK was 60%. Under this circumstance, the crack growth rates became considerably slower with respect to the constant load tests in both the heat-treatments even though R values were higher. It could be argued that in the case of IS steel, for the reasons of crack blunting and excessive plasticity at high K_{max} as discussed in section 5.6, the slowing down has occurred. However, QT-A steel which would be expected to show crack growth acceleration at high K_{max} values, did show a slowing down. Therefore, this slowing down of the crack growth rate above 50% reduction in ΔK is a genuine interaction effect, though in the case of IS steel, part of it could be due to the crack blunting effect. It is thus believed that an interaction effect due to ΔK change occurs only at very high changes and the magnitude of such an effect is very small.

5.9 K_{mean} Reduction Tests

The occurrence of a transient crack growth period in steel after a reduction in K_{mean} agrees generally with similar observations made by other people in aluminium alloys. The number of cycles required at the lower K_{mean} level to return to a stable crack growth rate was

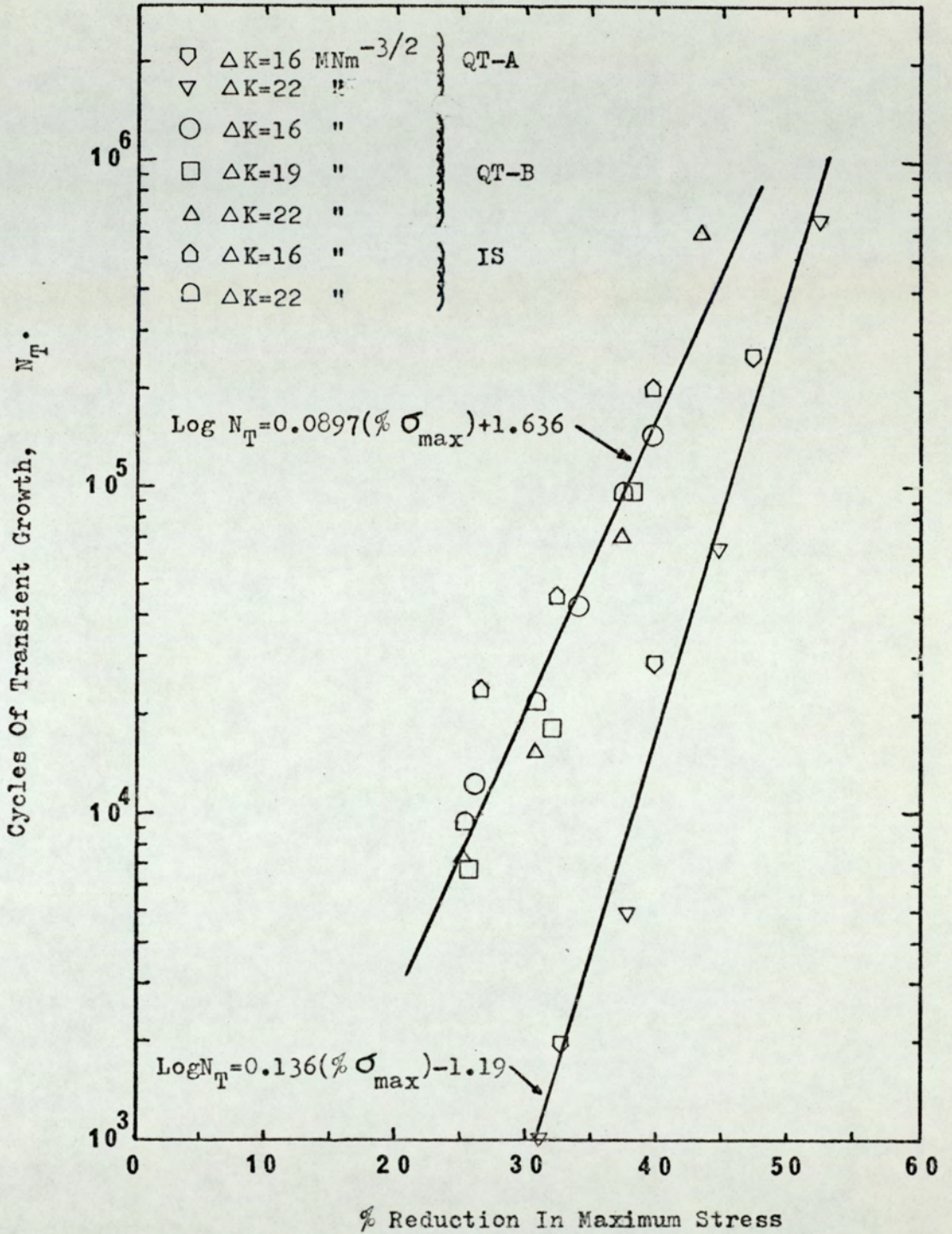


Fig. 67. Relationship Between The Number Of Cycles Of Transient Growth And The Percentage Reduction In Maximum Stress.

found to be a unique function of the percentage reduction in the maximum stress or K_{\max} at the point of load change. Attempts to relate the number of transient growth cycles to the average stress intensity parameters of the load-blocks were not very successful. The functional relationship between the transient growth cycles and the percentage reduction in σ_{\max} is shown in Fig. 67. The two variables can be represented by an equation of the type:

$$\log N_T = B (\% \sigma_{\max}) + C \quad (36)$$

where N_T is the number of cycles of transient growth, $\sigma_{\max} \%$ is the percentage reduction in the maximum stress, and B and C are constants.

The maximum stress is preferred to K_{\max} to establish this relationship because the former has been found to be an important crack growth controlling variable (Sections 5.5 and 5.6). However, σ_{\max} can be replaced by K_{\max} at load change in equation 36 to obtain the same result.

It can be seen that the results of the two low strength ductile steels fell into one scatter-band and are different from the results of the high strength QT-A steel. The co-efficients B and C in equation 36 characterise the two sets of results. Thus the transient crack growth region increases systematically with the increase in σ_{\max} reduction. The transient growth exceeds a million cycles if the percentage reduction in σ_{\max} is about 45% in the case of QT-B and IS steels, and about 55% in the case of QT-A steel. This can be regarded a totally retarded or dormant crack. This observation agrees with the findings of Jonas and Wei ⁽¹⁰⁷⁾ on a titanium alloy.

Material	ΔK MNm ^{-3/2}	K_{max1} MNm ^{-3/2}	K_{max2} MNm ^{-3/2}	$2(\tau_{y1} - \tau_{y2})$ mm	Transient Growth, mm			% σ_{max} Reduction
					Specimen 1	Specimen 2	Average	
QT-B	16	38.70	28.55	0.158	0.025	0.050	0.038	26.20
	16	39.00	25.69	0.188	0.025	0.15	0.088	34.10
	16	38.56	23.26	0.214	0.225	0.325	0.275	39.60
QT-B	19	40.35	29.97	0.166	0.050	0.075	0.063	25.70
	19	40.09	27.24	0.194	0.125	0.075	0.100	32.00
	19	39.38	24.26	0.216	0.350	0.250	0.300	38.30
QT-B	22	42.00	31.40	0.174	0.025	0.075	0.050	25.20
	22	41.62	28.77	0.202	0.125	0.250	0.198	30.80
	22	41.37	25.86	0.234	0.300	0.425	0.363	37.40
	22	42.39	24.04	0.276	0.825	0.650	0.738	43.20
	22	40.29	26.46	0.036	0	0.048	0.024	32.84
QT-A	16	39.75	23.90	0.042	0.119	0.143	0.131	39.81
	16	40.00	21.00	0.046	0.262	0.215	0.239	47.44
	22	42.70	30.30	0.036	0.048	0.048	0.048	31.03
QT-A	22	42.40	26.50	0.044	0.095	0.072	0.084	37.84
	22	43.80	23.94	0.053	0.358	0.239	0.299	44.71
	22	45.57	21.70	0.063	0.978	0.954	0.966	52.38
IS	16	38.86	28.44	0.498	0.092	-	0.092	26.60
	16	38.46	25.96	0.574	0.092	-	0.092	32.50
	16	38.53	23.15	0.674	0.206	-	0.206	39.80
IS	22	42.06	31.31	0.562	0.137	-	0.137	25.50
	22	41.62	28.73	0.646	0.274	-	0.274	30.90
	22	42.15	26.16	0.776	0.435	-	0.435	37.70

Table 16. Transient Crack Growth in Kmean Reduction Tests (Controlling Variables: σ_{max} , σ_{mean})

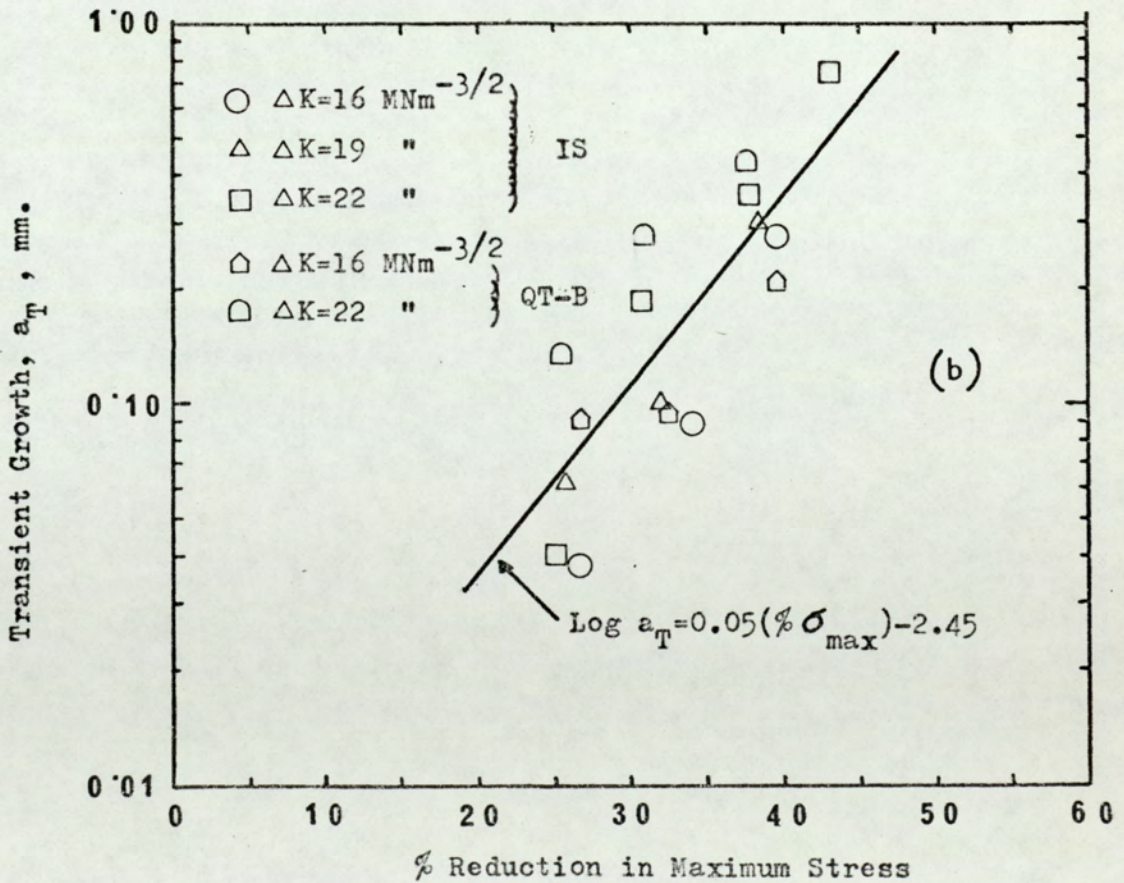
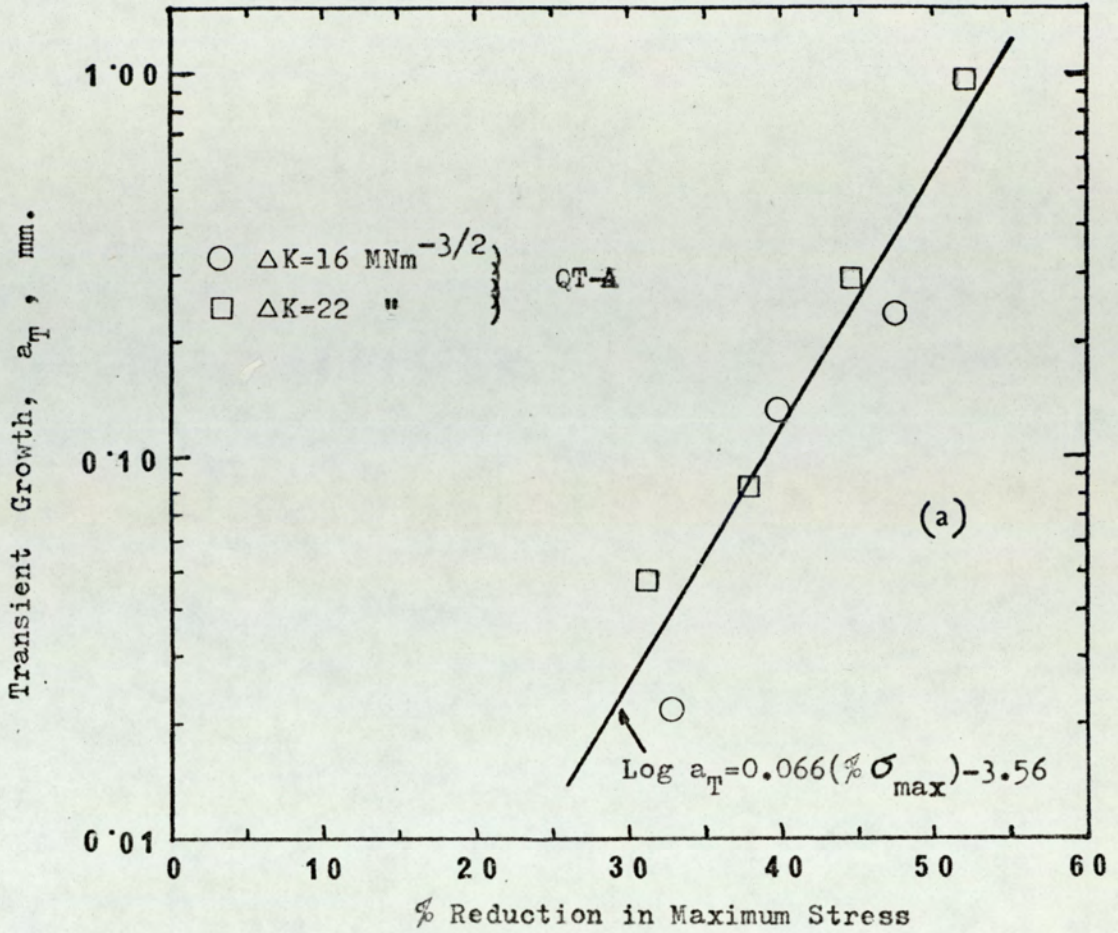


Fig.68. Relationship Between The Amount of Transient Growth And The Percentage Reduction in Maximum Stress.

The table 12a-b shows that the number of transient growth cycles decreases with the increase in ΔK for the same percentage reduction in K_{mean} . Thus in QT-A steel, even a 60% reduction in K_{mean} did not cause crack dormancy at $\Delta K = 22 \text{ MNm}^{-3/2}$, whereas under the same condition a dormant crack occurred at $\Delta K = 16 \text{ MNm}^{-3/2}$. In general, the low strength steels were found to be more susceptible to crack growth delay than the high strength QT-A. Thus a total crack dormancy was obtained with QT-B and IS steels with only 50% reduction in K_{mean} at all values of ΔK tested.

Both the AFFDL model (91) and Wheeler model (92) predict a return to the non-retarded crack growth when the maximum plastic zone boundary at the lower stress level touches the elastic-plastic boundary due to the maximum stress at the previous high load level. It is worthwhile to analyse the results of the present tests in the light of these models.

The plane strain maximum plastic zone radius was calculated (equation 10) at the end of each high load block. The same was calculated for the low load block at the end of the retarded growth region. The difference between the two plastic zone sizes are then calculated. These differences and the actual transient crack growth distances are compared in table 16. No definite relation could be observed between the two parameters. At low changes in σ_{max} , the transient growth is smaller than the plastic zone difference and at high changes, it is bigger. This holds good for all the heat-treatments and all the ΔK levels tested. Thus AFFDL and Wheeler models do not seem fit in the present results. On the other hand, the amount of transient growth can be related to the percentage reduction in σ_{max} as shown in Fig. 68a-b. Again the results of

QT-B and IS steels fell into one scatter-band and those of QT-A in another. The functional relationship between the two variables is given by

$$\log a_T = P (\% \sigma_{max}) + Q \quad (37)$$

where a_T is the amount of transient crack growth in mm; P and Q are constants.

The observation of increasing amount of retarded growth with the increasing amount of percentage overload for a high-low load sequence is consistent with the observations made by Corbly and Packman (91) and Von Euv (93).

If we examine the stabilised crack growth rate data given in table 11a-b, we find that there is a systematic slowing down of the growth rates at constant ΔK for the different heat-treatments. The crack growth rates followed equation 35 generally, but the scatter was found to be bigger than that obtained in tests where ΔK was kept constant uniformly. This scatter arises from the interaction effects of K_{mean} . In general, the crack growth rates obtained in the stabilised growth regions of the test were higher than those in the constant load tests. This increase in growth rates can be attributed to the higher R values used in the K_{mean} reduction tests.

Some variations of the transient growth results could be observed when duplicate specimens are considered. This could be due to the difficulty in locating the exact position of the end of the transient growth period on the potential drop chart. Nevertheless, the trends observed in Figs. 67 and 68 are real and are not invalidated by the drawback mentioned above.

Since it was established that about 50% decrease in K_{mean} could produce a dormant crack in QT-B and IS steels at constant ΔK condition, it was necessary to evaluate the effects of increases in ΔK under such conditions. The table 13 shows that an increase of 20% in ΔK could not counteract the interaction effect of K_{mean} . The reduction of σ_{max} in this case was 44.3%. This decrease can cause the dormancy of the crack as would be obvious from Fig. 67 if cycling for 10^6 cycles is regarded as a measure for total dormancy. A ΔK increase of more than 20% is required to cause the crack growth and more than 50% increase in ΔK is required to totally overcome the effect of 50% reduction in K_{mean} . Thus an increase of just more than $8 \text{ MNm}^{-3/2}$ in ΔK could counteract the effect of K_{mean} reduction by $14 \text{ MNm}^{-3/2}$. It confirms that ΔK is a more important factor than K_{mean} in the fatigue crack growth process. It should be noticed that an increase in ΔK needs to be such that the decrease in σ_{max} is less than 20% so that the crack can grow practically unretarded (Fig. 67) in QT-B and IS steels.

5.10 COD Tests

The crack-tip opening displacement measurements were made to establish whether there is any relation between COD and the slowing down of crack growth rates under constant ΔK condition. For the σ_{max} values used in the constant ΔK tests, the COD values were obtained from Fig. 35. The plane strain COD value for the constant average K_{max} of the test was also calculated.

$\frac{a}{W}$	σ_{\max} MNm ⁻² x 6	Average K_{\max} MNm ^{-3/2}	COD at σ_{\max} x 10 ⁻³ mm	
			Measured	Calculated
0.2 - 0.25	47.6	37.5	7.8	9.5
0.3 - 0.35	36.6	37.5	6.8	9.5
0.4 - 0.45	28.1	37.5	6.8	9.5

Table 17. Comparison of Experimental and Calculated COD

The table 17 shows the comparison of the results. It can be seen that the COD values obtained at different crack lengths were fairly constant and agreed reasonably with the calculated COD. Thus the results did not explain the phenomenon of crack growth slowing down at constant K conditions. In fact, the range of COD values should have been calculated to make a comparison with the crack growth rates. The method employed for COD measurement was not accurate enough at low loads. The COD values below the stress level of ~~6~~ 20 MNm⁻² could be in error.

The second COD measurement test was performed to investigate whether or not a relationship existed between the crack opening displacement and the transient growth rate after a K_{mean} reduction under a constant ΔK fatigue condition. The results given in table 14 show that high values of maximum and minimum COD were obtained at the high K_{mean} block, the COD due to the stress intensity range being 1.49×10^{-3} mm. Keeping ΔK the same, a reduction of K_{mean} by 30% did lower both the maximum and the minimum COD, but the COD range was higher. This higher COD range implies crack blunting. The measurements of COD up to 12,000 cycles showed some

erratic behaviour and after that the values of maximum, minimum and range COD became constant. The range COD value was then the same as that obtained before the K_{mean} change. On the potential chart record, the transient growth period was found to be about 39,000 cycles. The table 14 shows that after 39,000 cycles, the COD values were increasing indicating that the crack tip has grown beyond the points at which the measurements were being taken.

The results given in table 12b show that for the testing conditions as above, the number of cycles the crack remained dormant was 7500 and the number of cycles of slow growth was 39,000. These values are comparable to 12,000 cycles of erratic behaviour in COD and 27,000 cycles of steady values of COD before the crack has grown beyond the COD measurement points. This shows that there is some relationship between the COD and the transient growth after a load change but the picture of it does not become very clear from the present experiment. A more accurate and continuous method of COD measurement in fatigue condition needs to be employed to get a better understanding of the load-interaction process. Nevertheless, the present result indicates that the dormancy of a fatigue crack is related to the crack-tip blunting when a decrease in σ_{max} occurs. The crack-tip then undergoes a process of re-sharpening to attain a particular root-radius before any growth can take place. This result agrees with the view put forward by McMillan and Pelloux (82) who believed that the radius of the crack-tip is characteristic of the stress level; the lower the load level, the sharper the tip is. However, Elber's (89) crack closure concept could be an alternative explanation to the transient growth behaviour observed in programme loading condition. He showed that when a high load cycle is

followed by a low load cycle, the stress at which the crack opens is decreased below the value that should have prevailed should there be no interaction. This would increase the effective value of ΔK . In the case of 50% decrease in the load amplitude at $R = 0$, Elber demonstrated that the crack opening stress then gradually rises reducing ΔK_{eff} until no growth occurs. However, in view of this observation it can be argued that in the case where the load reduction is less than 50% at $R \neq 0$, the crack opening stress is decreased thus increasing ΔK_{eff} which would cause crack blunting. Further cycling would reduce ΔK_{eff} causing crack sharpening until the crack opening stress reaches a stable value so that a normal crack growth consistent to the stress level would occur.

5.11 The Effect of Stress Level

A study of the relevant literature showed that in the field of fracture mechanics it has been well established that the stress intensity range is the predominant factor which controls the fatigue crack growth process. It is generally believed that if ΔK is constant, $\frac{da}{dn}$ will be constant. The findings of the constant K condition tests in the previous investigation do not support this general belief. The crack growth equations containing ΔK and K_{max} listed in the literature survey can thus only be applied to the results of the present investigation where ΔK was not constant. No suitable fracture mechanics equation was available which could take into account the crack growth rate slowing down of the constant ΔK tests. The equations containing stress ratio term, which were meant to account for stress level effect, could neither be applied because all of them imply that $\frac{da}{dn}$ should be constant at constant ΔK . However, since the evidence of stress level effect has been observed

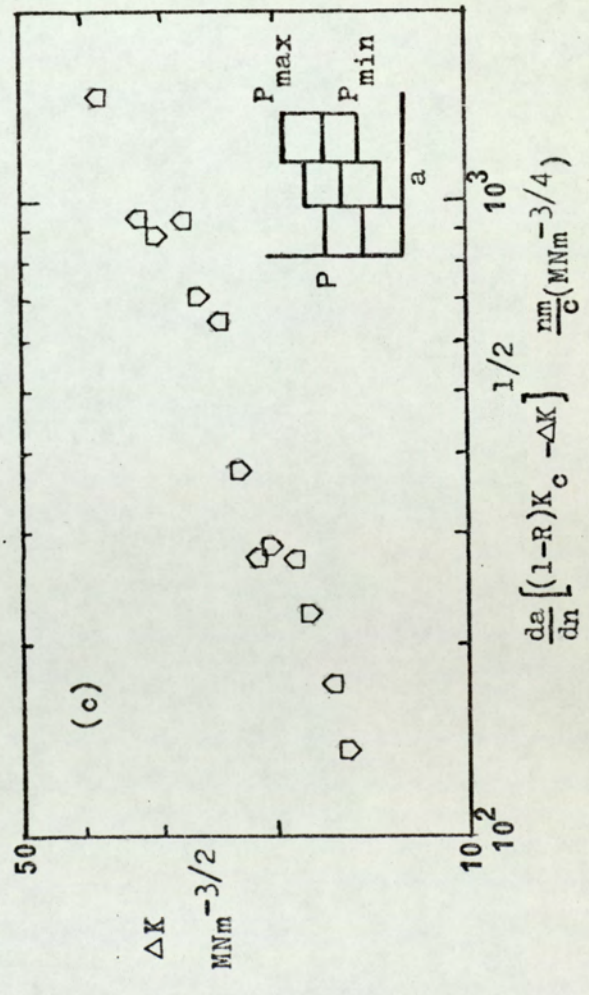
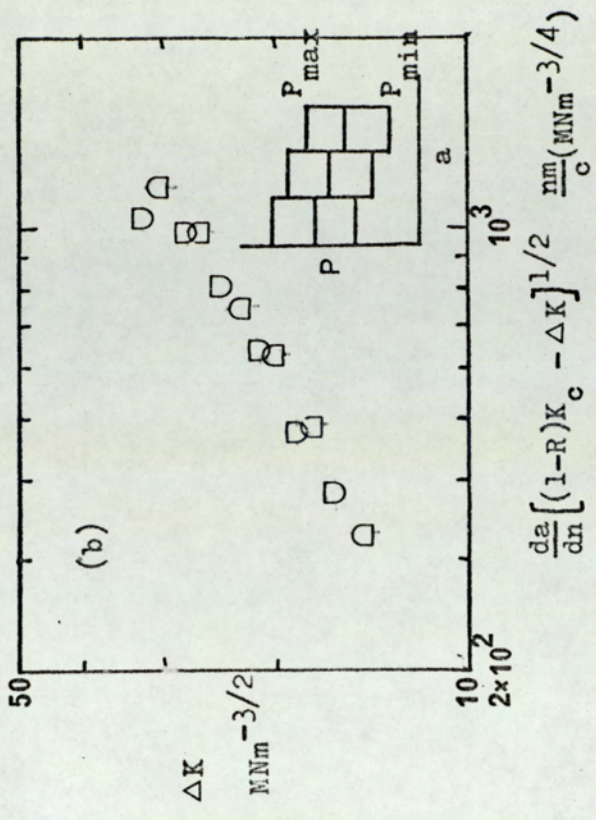
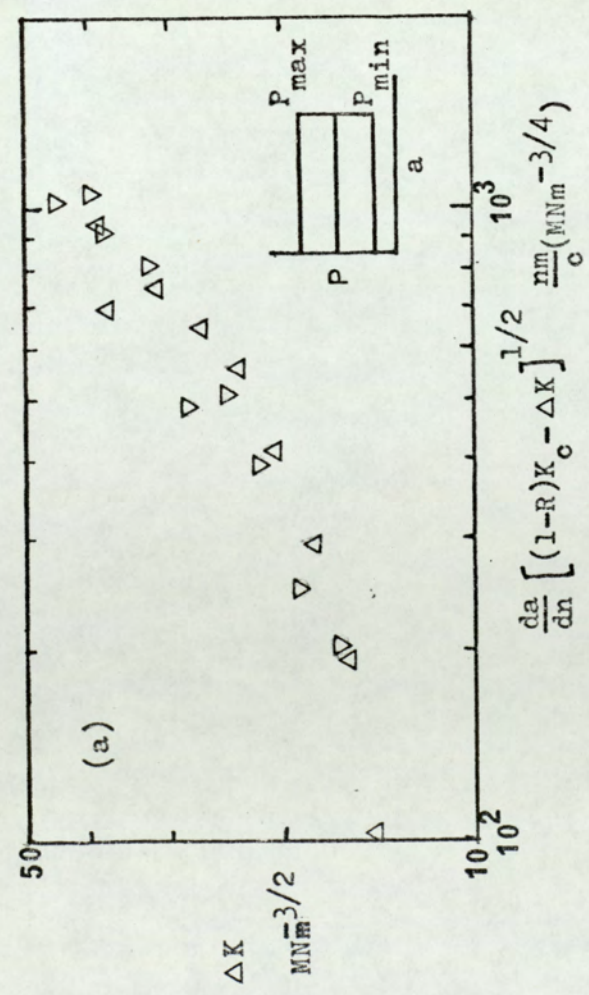


Fig.69. Crack Growth Results Plotted in Terms of Pearson's Equation. QT-A.
 $(K_c = K_{max_{Lt}} = 64 MNm^{-3/2})$
 Each Symbol Represents One Specimen.

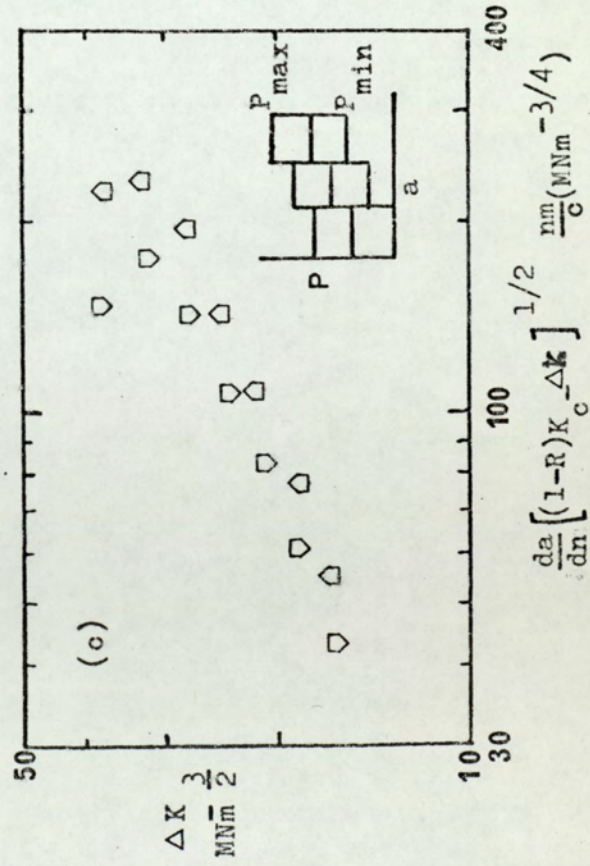
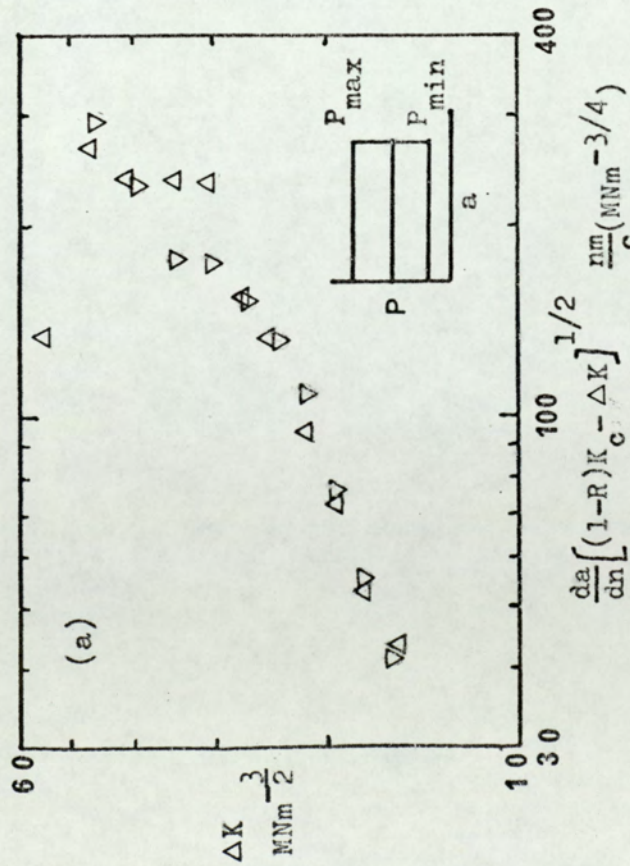
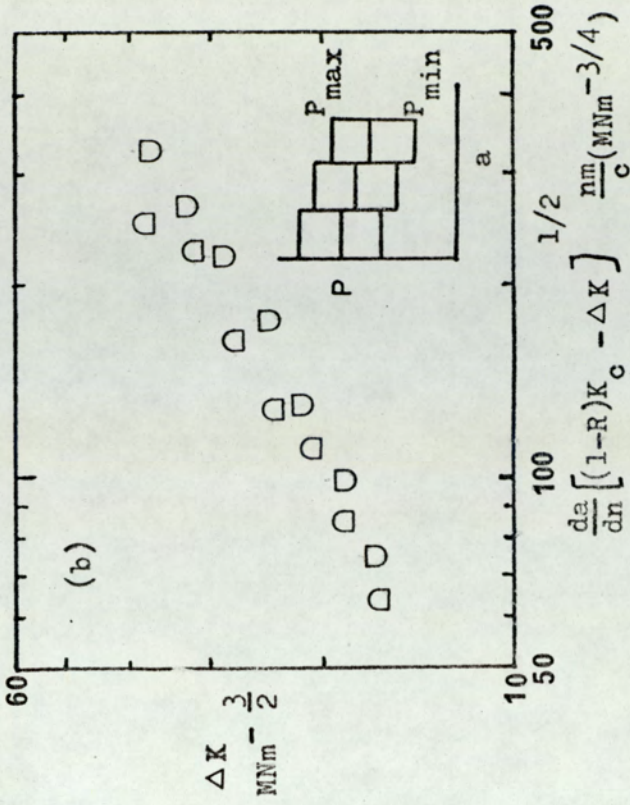


Fig.70. Crack Growth Results Plotted in Terms of Pearson's Equation. IS.

$$(K_c = K_{max_{1,t}} = 70 \frac{1}{2} MNm^{-3/2})$$

Each Symbol Represents One Specimen.

in some of the load controlled programme loading tests, it is necessary to analyse the present results in terms of the existing equations.

Most workers in fatigue have shown that the rate of crack propagation increases as the stress ratio R increases. Some equations were, therefore, put forward to unify the results from different R level tests. The most promising one referred to frequently was given by Forman et al (Equation 18). Recently, Pearson⁽⁴⁴⁾ showed that equation 18 was not a good fit to his crack growth rate results. When the results of the present investigation were analysed, the same conclusion was arrived at. Pearson demonstrated that a better fit to the results could be obtained by modifying Forman's equation. Since Pearson used $K_{\max}(L_t)$ instead of K_c in the modified equation, analysis of the present results was done on the same basis. The results are shown in Fig. 69a-c and Fig. 70a-c. The modified equation fits better in the case of QT-A steel than IS steel. In all the cases, the scatter at high ΔK values is still noticeable instead of the modification done on Forman's equation. Moreover, if the results of the three loading conditions considered in the analysis for each heat-treatment are compared, a scatter between them can be found. Thus it appears that the available equations containing R term could not unify the results from the different tests. On the basis of this observation and the occurrence of gradual slowing down of the crack growth rate at constant K conditions where R was constant, it could be argued that the stress ratio R does not actually reflect the stress level effect on the fatigue crack growth rates.

The observation that the crack growth rate at a constant ΔK

condition was reasonably constant if the maximum stress was kept constant, indicates that it is the maximum stress which plays an important role in the fatigue crack propagation process. McMillan and Pelloux⁽⁸²⁾ also demonstrated the influence of σ_{\max} on crack growth rates in their programme loading tests. Moreover, the evidence of the occurrence of static modes of fracture such as micro-cleavage, micro-void coalescence and intergranular cracking were associated with the high maximum stress of the tests in the present investigation and also elsewhere.⁽⁵⁰⁾ Thus it seems reasonable to believe that it is not the stress ratio R but the actual magnitude of the maximum stress which reflects the stress level effect.

5.12 Microscopic and Fractographic Observations

It has been shown in the results that the rate of fatigue crack propagation could not be associated with the general micro-structural features of the three heat-treatments. On the other hand, the general mechanical properties of the material such as the yield strength and hardness reflect the macroscopic fatigue crack growth characteristic of the materials. The material with high strength and high hardness (QT-A) showed 3 to 5 times higher growth rate than low strength and ductile materials (QT-B and IS). Because of the high ductility, the materials QT-B and IS could accommodate more strain at the crack tip by plastic deformation without fracture than the brittle QT-A steel. In addition to this, more energy was dissipated in ductile steels by extensive crack branching and island formation. Thus the QT-B and IS steels were more resistant to crack growth than QT-A steel.

On the microscopic scale, the QT-A steel had inherent grain boundary weakness which contributed to its faster crack growth rate.

This G.B. weakness has been shown to be due to the segregation of trace elements such as As, Bi, Sn, Sb and due to the precipitation of brittle carbides during quenching.⁽¹⁰⁸⁾ In QT-B steel, on the other hand, the segregation of impurities would have been eliminated by long hours of tempering. The general micro-structural features of the three heat-treatments did not seem to play any important part in the crack growth process. The stringer type MnS inclusions which were perpendicular to the crack growth direction have been found to cause branch cracking in QT-B and IS steels and thus possibly lower the rate of propagation of the main crack. In all the three micro-structures tested, the inclusions and the second phase particles were found to be associated with the static modes of cracking at high maximum stress levels resulting in higher crack growth rates. The second phase particles were also found to be associated with the void coalescence of the static fractures. Thus these particles played a secondary role only at high stress levels.

The occurrence of light and dark bands on the fracture surfaces of the two step load tests agrees with the similar observation made by Hardrath and McEvily⁽⁷⁹⁾ in aluminium alloys. They did not give any explanation to this phenomenon. In the present investigation, the appearance of dark and light bands has been found to be due to the relative difference in the size of the cell structure formed on the fracture surfaces or due to the extent of flow of the material. This difference has been shown to increase with the difference in ΔK , because the size of the cell structure or the extent of flow showed increases with the increases in ΔK (Fig. 57). The appearance of dark and light bands was thus not due to any specific change of the fracture mode but due to the abrupt change in ΔK level. The size of the cell structures observed on the

Material	ΔK MNm ^{-3/2}	K_{max} MNm ^{-3/2}	$2r_y$ Fatigue μm	$2r_y$ Maximum μm	$\frac{2r_{y_{max}}}{\text{Grain Size}}$
QT-A	16	20.0	2.6	15.8	0.564
$\sigma_{ys} =$	19	24.8	3.6	24.2	0.865
1637 MNm ⁻²	22	27.5	4.8	30.0	1.070
Grain Size =	25	31.3	6.2	38.8	1.335
28 μm	30	37.5	9.0	54.6	1.950
QT-B	16	20.0	14.2	90.0	2.30
$\sigma_{ys} =$	19	24.8	20.2	138.2	3.54
687 MNm ⁻²	22	27.5	26.2	170.0	4.36
Grain Size =	25	31.3	35.2	220.2	5.65
39 μm	30	37.5	50.6	316.2	8.10
IS	16	20.0	45.6	284.8	7.12
$\sigma_{ys} =$	19	24.8	64.2	437.8	10.95
386 MNm ⁻²	22	27.5	86.2	538.4	13.46
Grain Size \approx	25	31.3	111.2	697.6	17.44
40 μm	30	37.5	160.2	1001.4	25.04

Table 18. Grain size, plastic zone size and crack growth rates for three heat-treatments

fracture surfaces, because of their lack of definition, could not be related to the stress intensity values. The possibility is that the cell structures are formed due to a non-uniform growth of the crack front in the form of tongues; these tongues increasing in size as the plastic zone size increases at the crack tip. A similar model of fatigue crack growth has been suggested by Robinson and Beevers.⁽¹⁰⁹⁾

Williams and Smith⁽¹¹⁰⁾ showed a kind of 'tide-mark' on the fatigue fracture surfaces of β -brass when the mean stress was changed. This mark was formed by a slight change in the direction of the crack plane. The observation of a ridge-like structure in the present investigation in the region of transient growth after a K_{mean} change (Fig. 58) could be due to the same phenomenon. A slight change of crack growth direction was also noticed in the two-step (40% load change) tests after a load change and this again corroborates the above findings.

Robinson and Beevers⁽¹⁰⁹⁾ have observed that in α -titanium, when the reversed plastic zone size was smaller than the grain size, the fracture process became grain orientation controlled producing more intergranular cracking. When the plastic zone size was bigger than the grain size, K_{max} was playing a prominent role producing furrows running parallel to the crack growth direction. With a view to find the effect of grain size on the fatigue crack growth in the present investigation, the maximum and the fatigue plastic zone radii were calculated by using equations 10 and 11 respectively. The results are shown in table 18.

It can be seen that the fatigue plastic zone size of QT-A steel up to a ΔK value of $30 \text{ MNm}^{-3/2}$ was much smaller than the grain size.

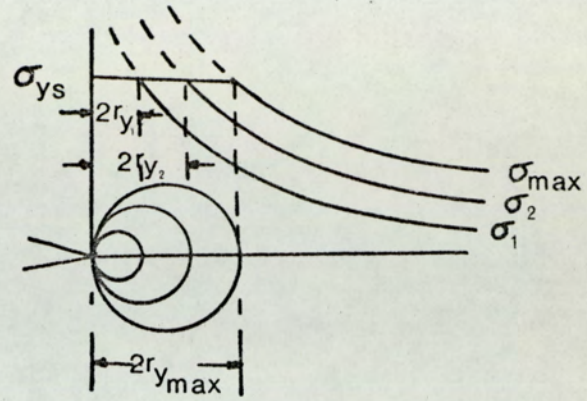
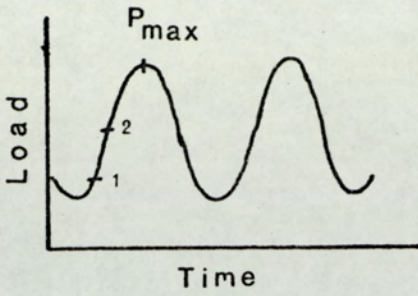
This could explain the occurrence of intergranular cracking in this micro-structure. However, in the QT-B steel, up to a ΔK value of $25 \text{ MNm}^{-3/2}$, the fatigue plastic zone size was smaller than the grain size. One would thus expect the intergranular cracking to occur at low ΔK values. On the contrary, no evidence of intergranular cracking was observed in this micro-structure. In the IS steel, the fatigue plastic zone size was much bigger than the estimate of the grain size. The absence of the intergranular cracking can thus be explained.

When the maximum plastic zone size is examined, it is found to be smaller than the grain size in QT-A steel up to a ΔK value of $19 \text{ MNm}^{-3/2}$. If we consider that the maximum plastic zone size to the grain size ratio is a controlling factor for the intergranular cracking, then the observation of maximum intergranular cracking at ΔK values between $16 - 20 \text{ MNm}^{-3/2}$ can be explained. In cases of QT-B and IS steels, the maximum plastic zone size is much bigger than the grain size and therefore transgranular fracture should predominate. Furrows were observed on transgranular fracture surfaces at high ΔK values which is in agreement with the observation of Robinson and Beevers. (109)

5.13 A Proposed Mechanism of Fatigue Crack Propagation

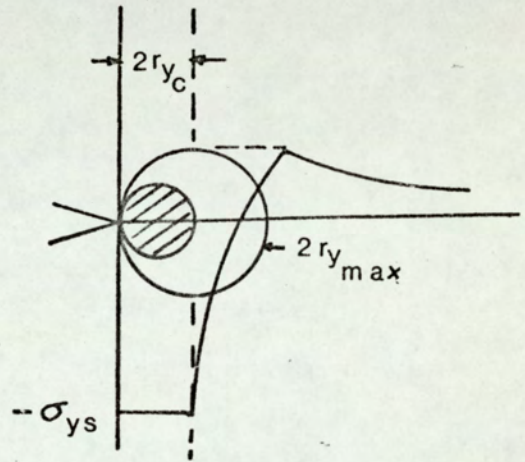
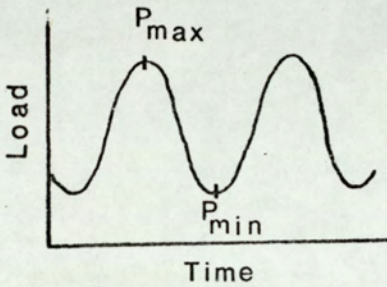
In order to obtain a possible mechanism of fatigue crack propagation, the following assumptions were made:-

- a) The fatigue crack propagation is discontinuous, i.e. the crack increases in length by jumps.
- b) Fatigue is considered to be an accumulation of damage process.
- c) The material in the plastic zone is damaged.



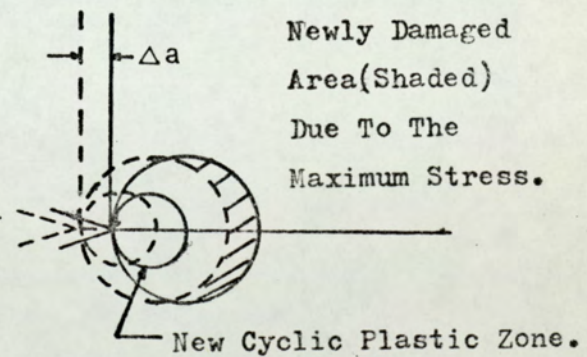
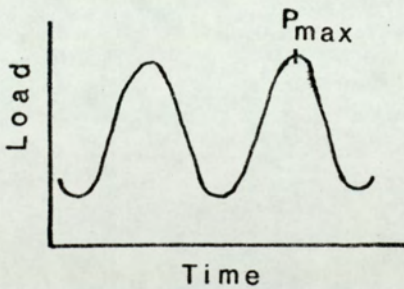
(a) The Formation of The Maximum Plastic Zone During The Rising Part of The First Load Cycle.

$$r_{y_{max}} = \frac{1}{6\pi} \left(\frac{K_{max}}{\sigma_{ys}} \right)^2$$



(b) The Formation of The Cyclic Plastic Zone At The Minimum Load Due To Stress Reversal.

$$r_{y_{cyc}} = \frac{1}{24\pi} \left(\frac{\Delta K}{\sigma_{ys}} \right)^2$$



(c) Crack Extension Due To Damage In The Cyclic Plastic Zone And The Formation of New Cyclic and Maximum Plastic Zones.

Fig.71. Schematic Representation of The Proposed Crack Growth Mechanism.

- d) Two plastic zones are operative in fatigue,
 - i) The zone due to the maximum load,
 - ii) The zone due to the cyclic load.
- e) The yield stress in tension and in compression is the same.

Now we can briefly state the mechanism as follows.

With the first application of the tensile load, a maximum plastic zone is formed at the crack tip. On subsequent cycling, a cyclic plastic zone is formed inside the maximum plastic zone due to the reverse yielding. Damage due to the plastic deformation accumulates inside the plastic zones. It is to be noted that the maximum plastic zone forms only once during cycling if the crack is stationary. When the damage inside the cyclic plastic zone reaches a critical value, the crack extends by a discrete amount inside the damaged material. As soon as the jump occurs, the immediately following rising part of the load cycle causes the maximum plastic zone size to extend beyond the old one by a certain amount. The maximum extension of the maximum plastic zone is on the crack plane and is equal to the crack jump. The cyclic plastic zone forms again and the whole process is repeated with the subsequent crack jump. The crack propagation rate will therefore be mainly dependant on the cyclic plastic zone (i.e. on the cyclic load or ΔK) but as a consequence of crack extension will also be dependant on a fraction of the maximum plastic zone. The extent of the fractional plastic zone will depend on the crack growth rate or in other words, on the crack growth resistance of the material. Schematically, the mechanism is shown in Figs. 71a-c.

The mechanism shown in Fig. 71c will repeat. Hence it can be

argued that the crack growth rate will be dependant, to a minor extent, on the magnitude of the maximum stress. Since the extent of damage ahead of the old maximum plastic zone will also be dependant on the yield stress of the material, it can be assumed that the ratio of σ_{max} to σ_{ys} will be a measure of that damage. Hence

$$\frac{da}{dn} \propto (r_{y \text{ cyclic}} \times \text{Damage due to plasticity on account of } \sigma_{max})$$

$$\text{i.e. } \frac{da}{dn} \propto (\Delta K)^2 \cdot \left(\frac{\sigma_{max}}{\sigma_{ys}} \right)$$

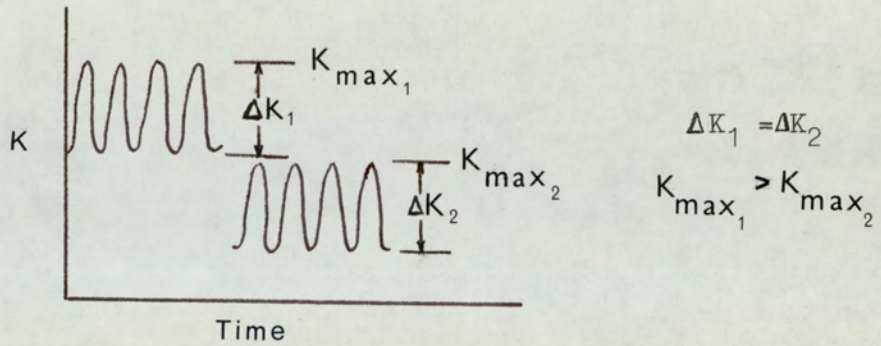
$$\frac{da}{dn} = A(\Delta K)^2 \cdot \left(\frac{\sigma_{max}}{\sigma_{ys}} \right)$$

Generalising the above equation, we can write,

$$\frac{da}{dn} = \frac{A(\Delta K)^m}{R'} \quad (38)$$

$$\text{where } R' = \frac{\sigma_{ys}}{\sigma_{max}}$$

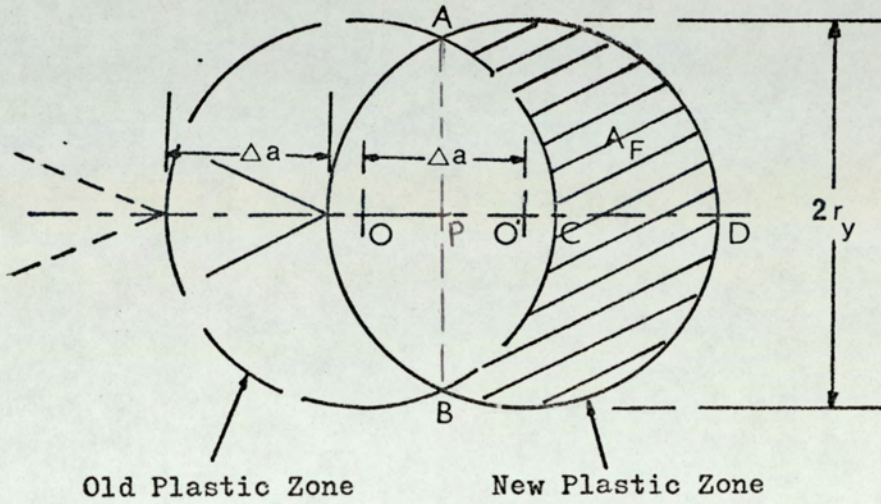
This mechanism can be applied to account for the stress ratio effects. It has been observed that the higher the stress ratio, the faster a fatigue crack grows. Let us consider the two fatigue situations where ΔK values are the same but the stress ratios are different, i.e. one has higher σ_{max} than the other.



We find that the cyclic plastic zone size will be the same in both the cases but the damage due to σ_{\max} will be different. The situation where σ_{\max} is higher will experience more damage than the one with lower σ_{\max} . Hence the growth rate in the higher stress ratio case will be more than that in the lower stress ratio case. The crack growth rates will thus be given by the equation 38.

Let us now estimate the area of the fractional plastic zone formed due to σ_{\max} during a crack jump. For simplification a fatigue situation where K_{\max} is constant is considered here. The size of the plastic zone formed due to the maximum stress intensity will be constant throughout the growth. After a crack jump, the position of the quasi-stationary crack and the associated maximum plastic zones are shown in Fig. 72. The points O and O' are the centres of the old and new plastic zones before and after the jump respectively. The radius of the plastic zone is r_y and the crack jump OO' is considered to be equal to Δa . The area of fractional plastic zone (A_F) will then be given by (see Appendix 2)

$$A_F = 2r_y^2 \left[\sin^{-1} \frac{\Delta a}{2r_y} + \frac{\Delta a}{2r_y} \left\{ 1 - \frac{(\Delta a)^2}{4r_y^2} \right\}^{\frac{1}{2}} \right]$$



Maximum Plastic Zone Radius = r_y

Δa = Crack Jump.

Area A_{DFC} = A_F = Fractional Plastic Zone

Due To Crack Jump.

Fig.72. Schematic Drawing Of The Extension Of Maximum Plastic Zone Due To Crack Jump.

If Δa is very small in comparison to r_y , then neglecting the square term and putting $\sin^{-1} \frac{\Delta a}{r_y} = \frac{\Delta a}{r_y}$, we can write,

$$\begin{aligned} A_F &= 2r_y^2 \cdot \frac{\Delta a}{r_y} \\ &= 2r_y \cdot \Delta a \end{aligned} \tag{39}$$

By using this simplified equation for A_F , the error will be maximum if $\Delta a = 2r_y$, but for small values of Δa , the error will be negligible. In an extreme case where the crack jump will be equal to the diameter of the cyclic plastic zone, the maximum plastic zone formed after the jump will be equal in size to that formed before the jump. In actual situation, the jump will occur by a fraction of the cyclic plastic zone. The residual stresses constraining the crack tip will not allow the size of the maximum plastic zone formed in this condition to equal the old one. Thus the newly formed maximum plastic zone will be smaller. The calculation used to arrive at equation 39 was based on the assumption that the maximum plastic zone before and after the jump are equal in size. This constitutes a limitation to the derivation. Though the area calculated from the simplified equation will be over-estimated by a certain fraction of the actual area formed due to the jump, yet it will be a fairly good approximation for the purpose of discussion.

Let us take the data from six different tests with two heat-treatments QT-A and QT-B. The K_{max} value was kept constant in each case by reducing the σ_{max} value as the crack grew. If we consider the crack jump to take place in each cycle, then $\frac{da}{dn}$ values from the tests can be used as the value of a to calculate the fractional

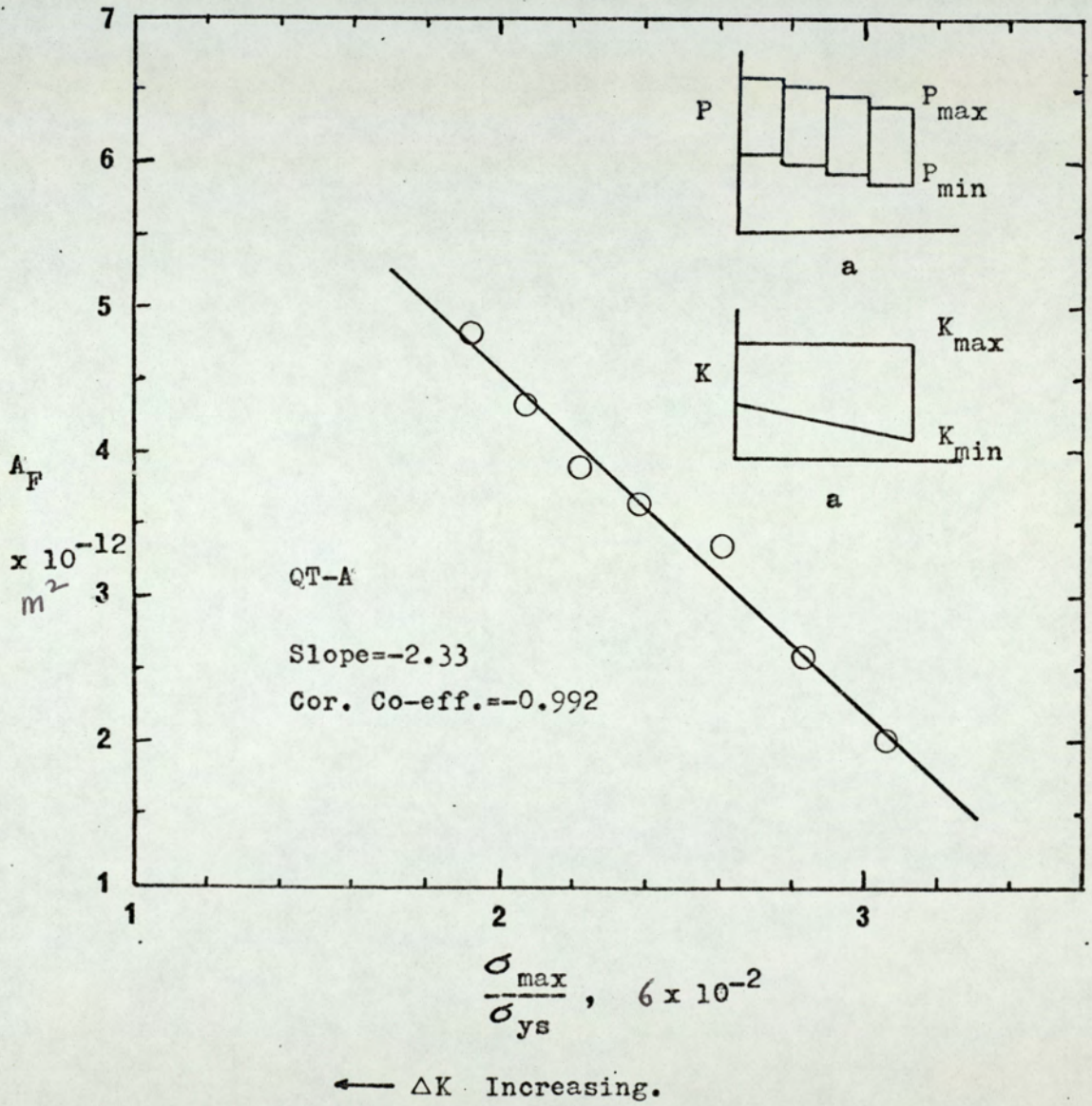


Fig.73. Relationship Between $\frac{\sigma_{max}}{\sigma_{ys}}$ and Fractional Plastic Zones(A_F)

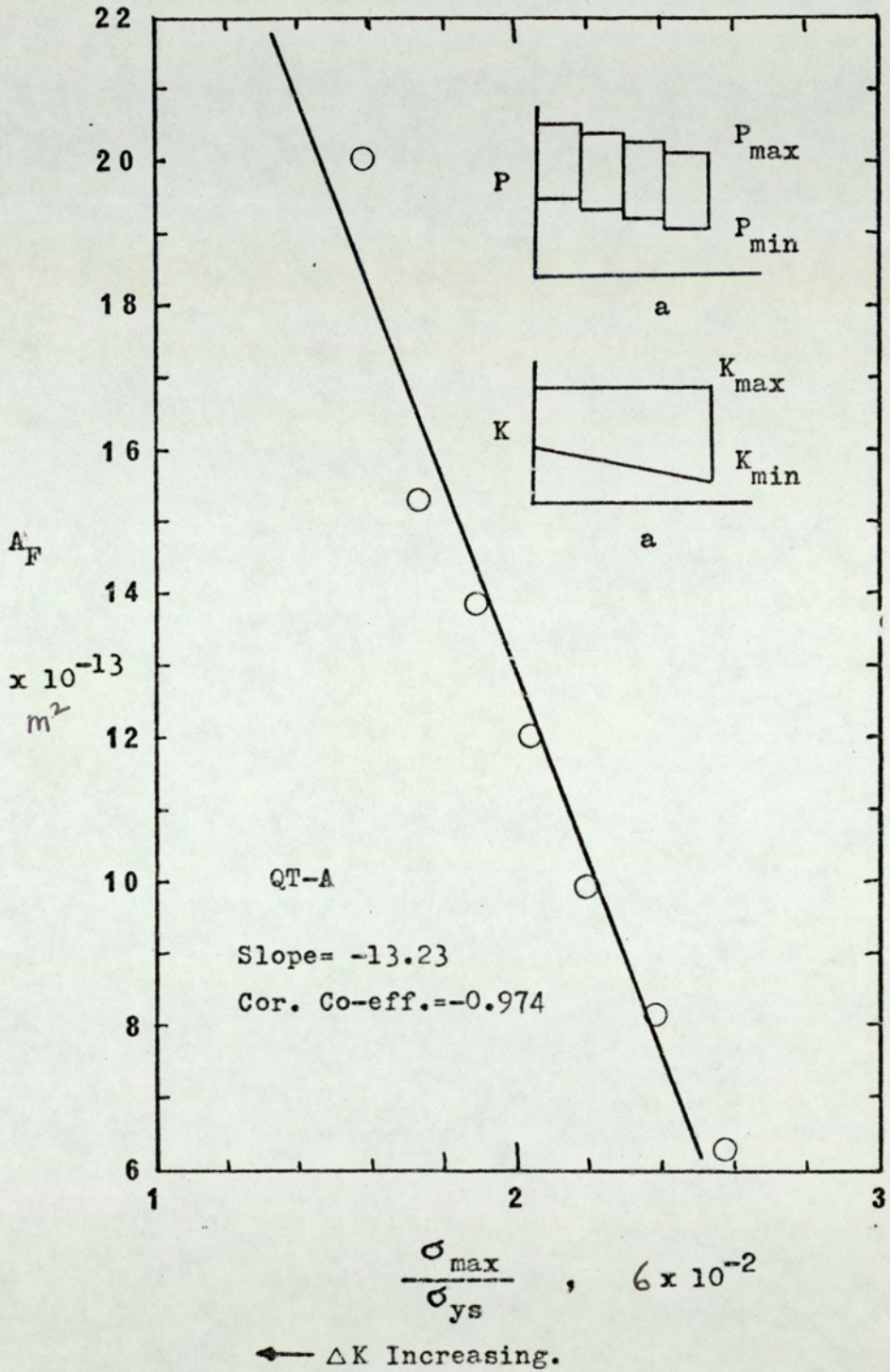


Fig.74. Relationship Between $\frac{\sigma_{max}}{\sigma_{ys}}$ and Fractional Plastic Zones (A_F).

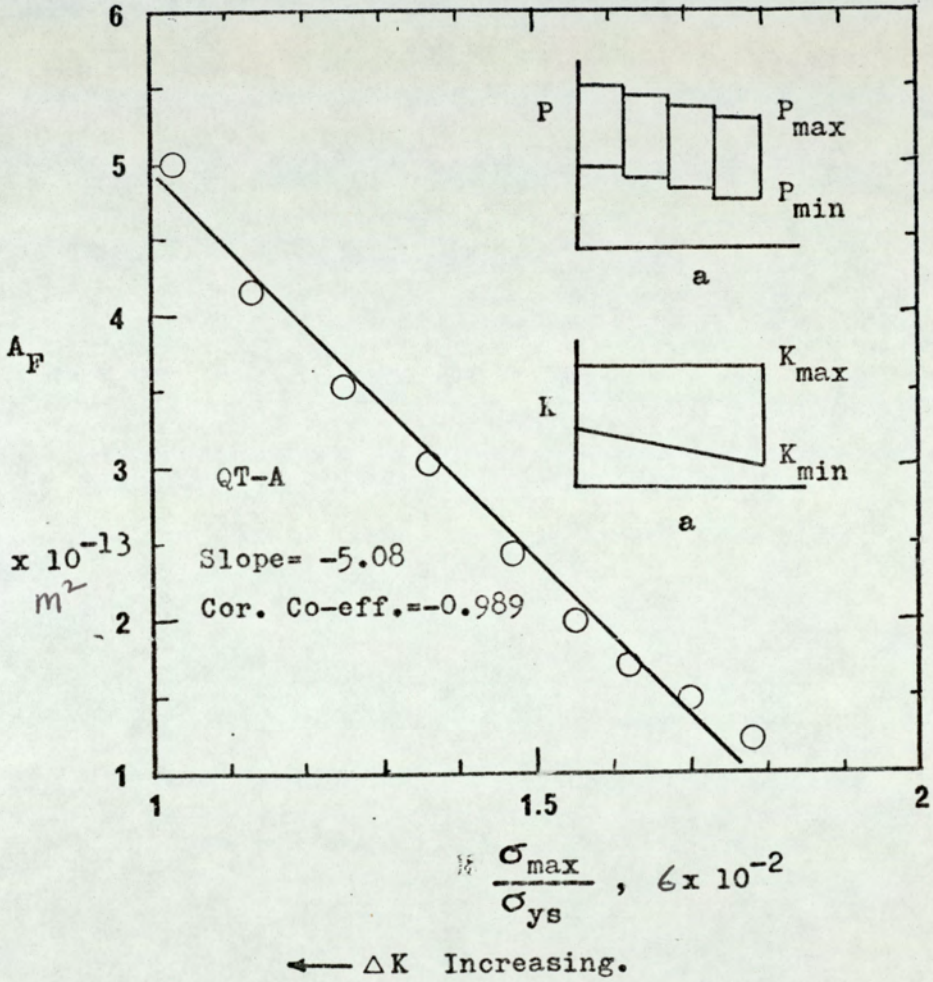


Fig.75. Relationship Between $\frac{\sigma_{max}}{\sigma_{ys}}$ and Fractional Plastic Zones(A_F).

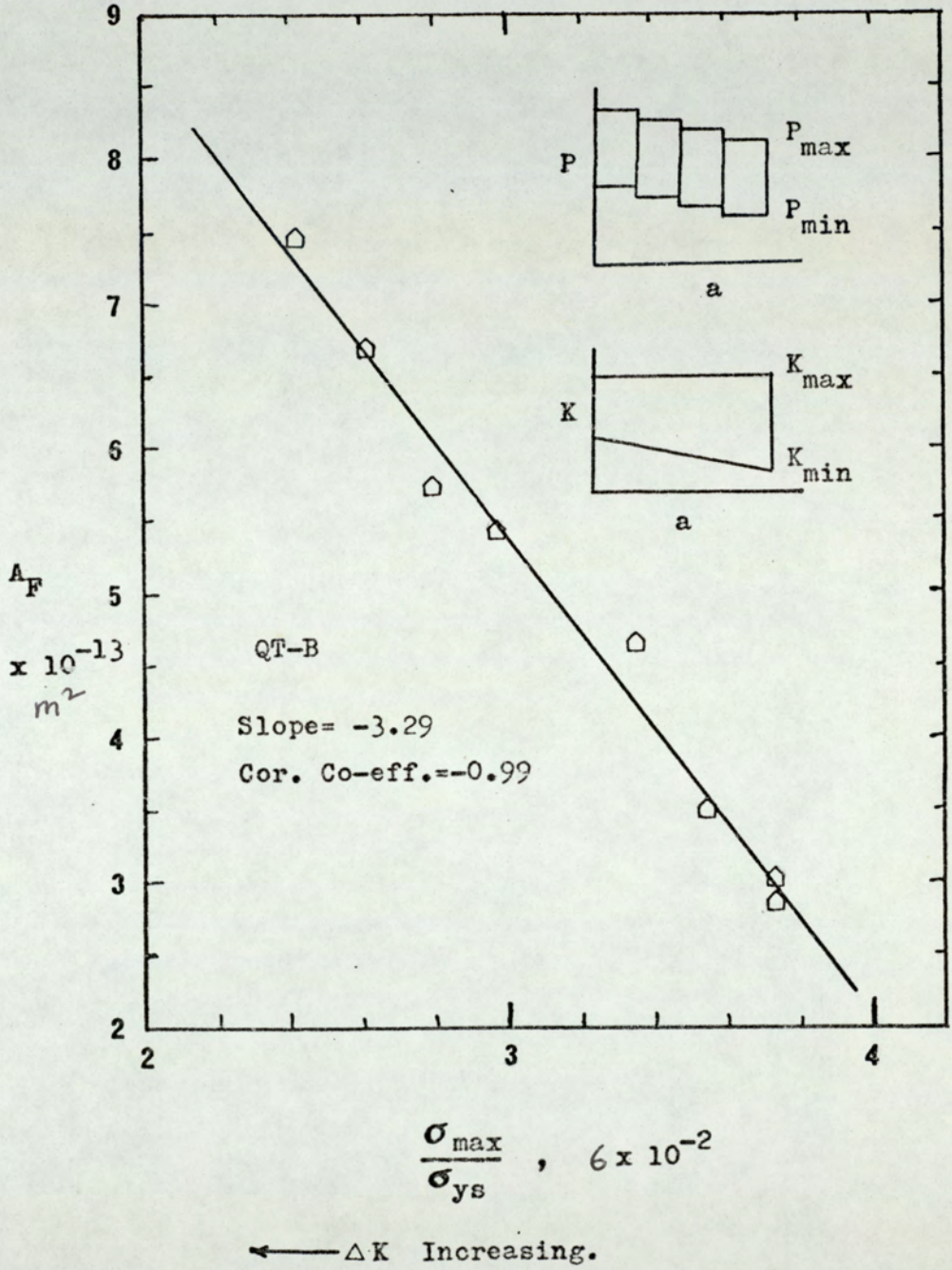


Fig.76. Relationship Between $\frac{\sigma_{max}}{\sigma_{ys}}$ and Fractional Plastic Zones(A_F).

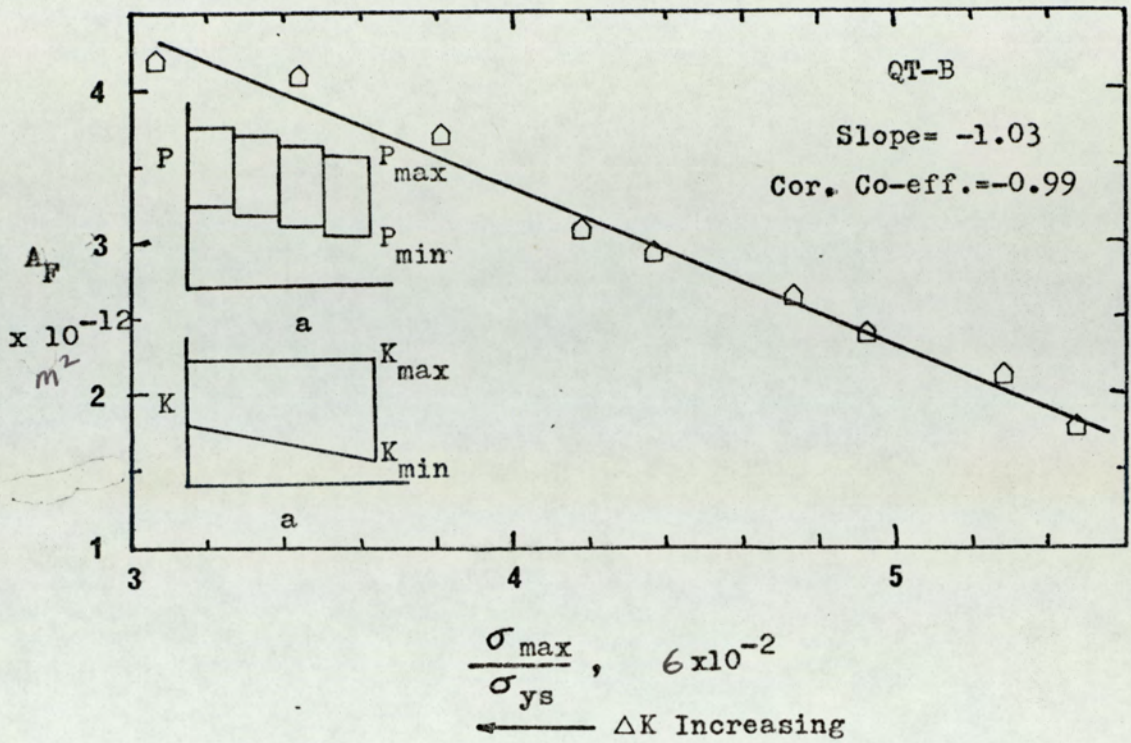


Fig. 77.

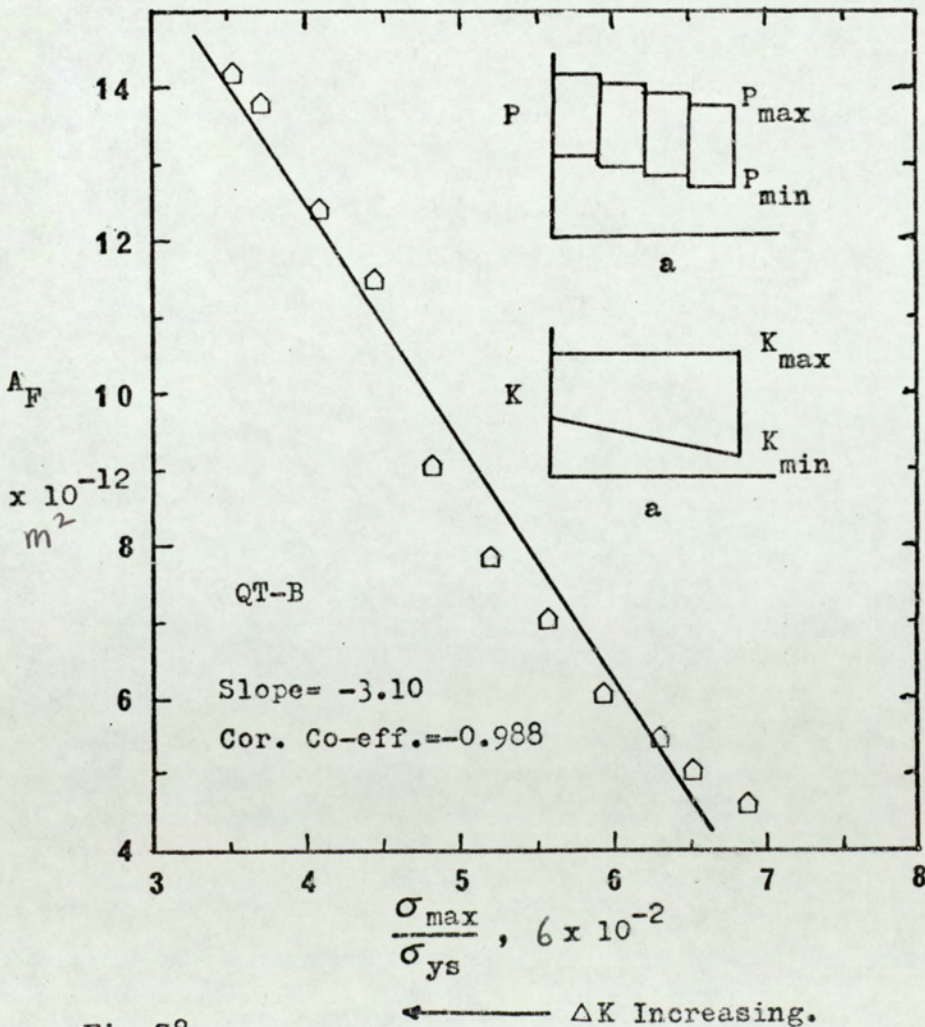


Fig. 78.

Fig. 77/78. Relationship Between $\frac{\sigma_{\max}}{\sigma_{ys}}$ and Fractional Plastic Zones (A_F).

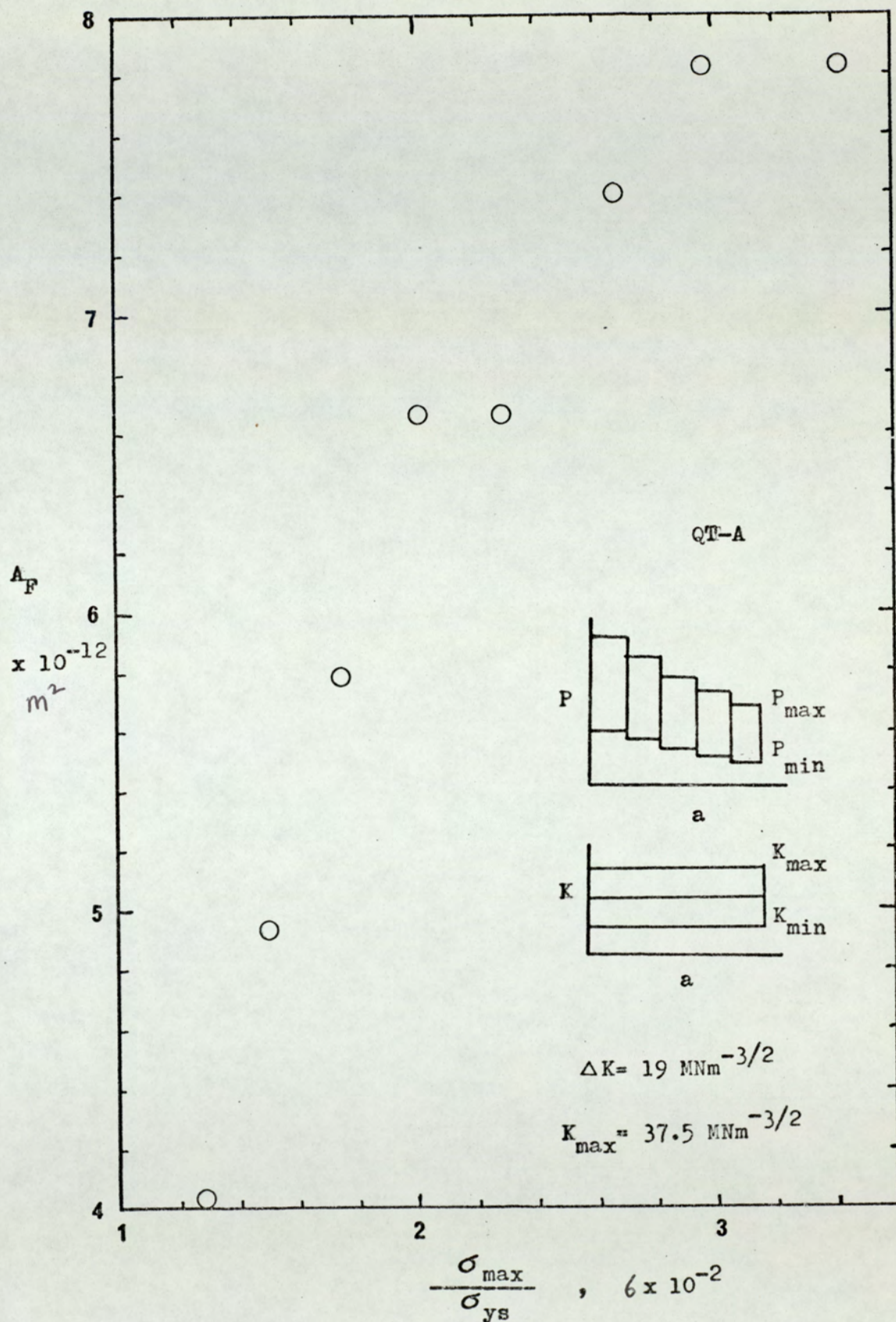


Fig. 79. Relationship Between $\frac{\sigma_{max}}{\sigma_{ys}}$ and Fractional Plastic Zones (A_F).

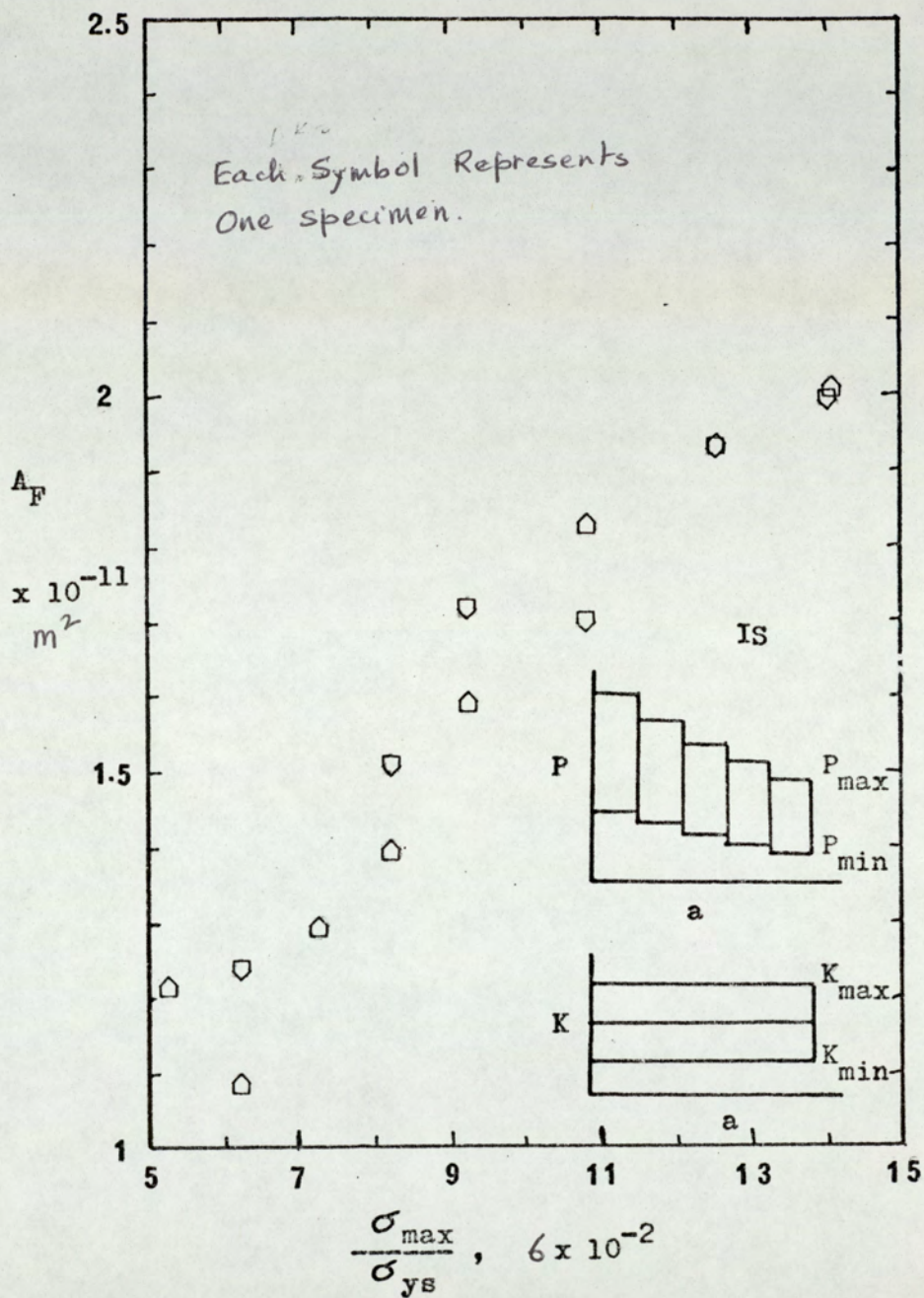


Fig.80. Relationship Between $\frac{\sigma_{max}}{\sigma_{ys}}$ and Fractional Plastic Zones (A_F)

plastic zone areas. The calculated fractional plastic zone areas are then plotted against $\frac{\sigma_{max}}{\sigma_{ys}}$ values of the tests. (Figs. 73-78) Each plot shows a linear relationship between the two variables. Hence it can be concluded that the inclusion of $\frac{\sigma_{max}}{\sigma_{ys}}$ term in the crack growth equation is justified in the light of the proposed mechanism of crack propagation. It can also be seen from these plots that as σ_{max} was decreasing, the fractional plastic zone size was increasing. This happened because the stress intensity range was increasing in these tests thus increasing the amount of the crack jump.

The slowing down of the crack growth rates under constant ΔK and K_{max} condition can be explained by the same mechanism. The fractional plastic zone areas were calculated for these tests and plotted against $\frac{\sigma_{max}}{\sigma_{ys}}$ as shown in Figs. 79 and 80. It can be seen that even under the constant ΔK condition, the fractional plastic zone size was decreasing as the maximum stress was being reduced with the increase in the crack length. Again in these cases, except for the points at the high σ_{max} end where $\frac{da}{dn}$ was fairly constant, the data plotted can be represented by straight lines. If the effect of constant ΔK on the crack growth rate is considered constant, the slowing down occurs due to the progressively lesser damage induced by the maximum stress. It is also worthwhile to note that in the tests where the maximum stress was kept constant under constant ΔK condition, the crack growth rates were virtually constant. This happened because the fractional plastic zone area which is a reflection of the crack growth resistance of the material was constant.

Let us now plot the crack growth rate data obtained from

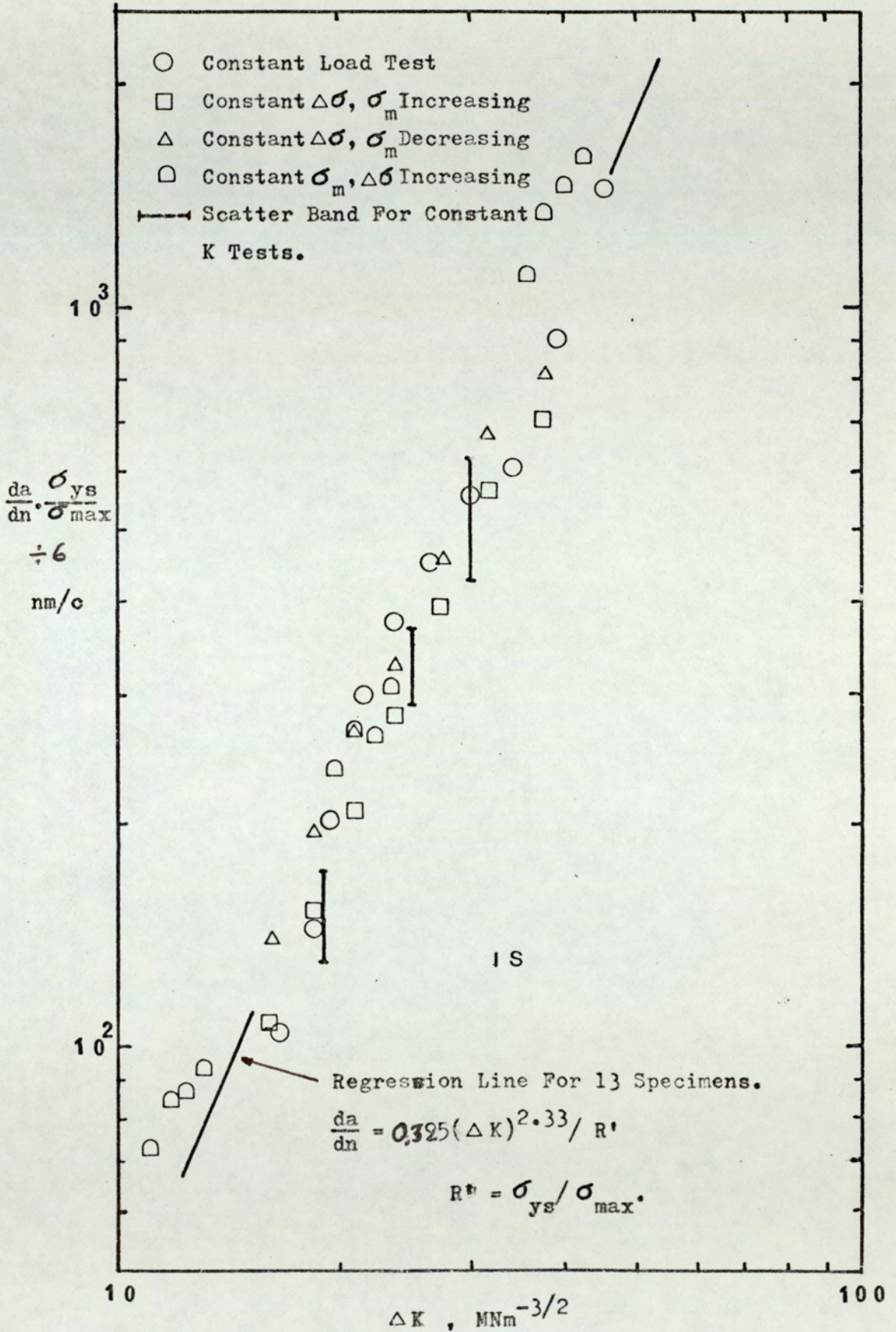


Fig.81a. Crack Growth Results Plotted in Terms of The Proposed Equation.

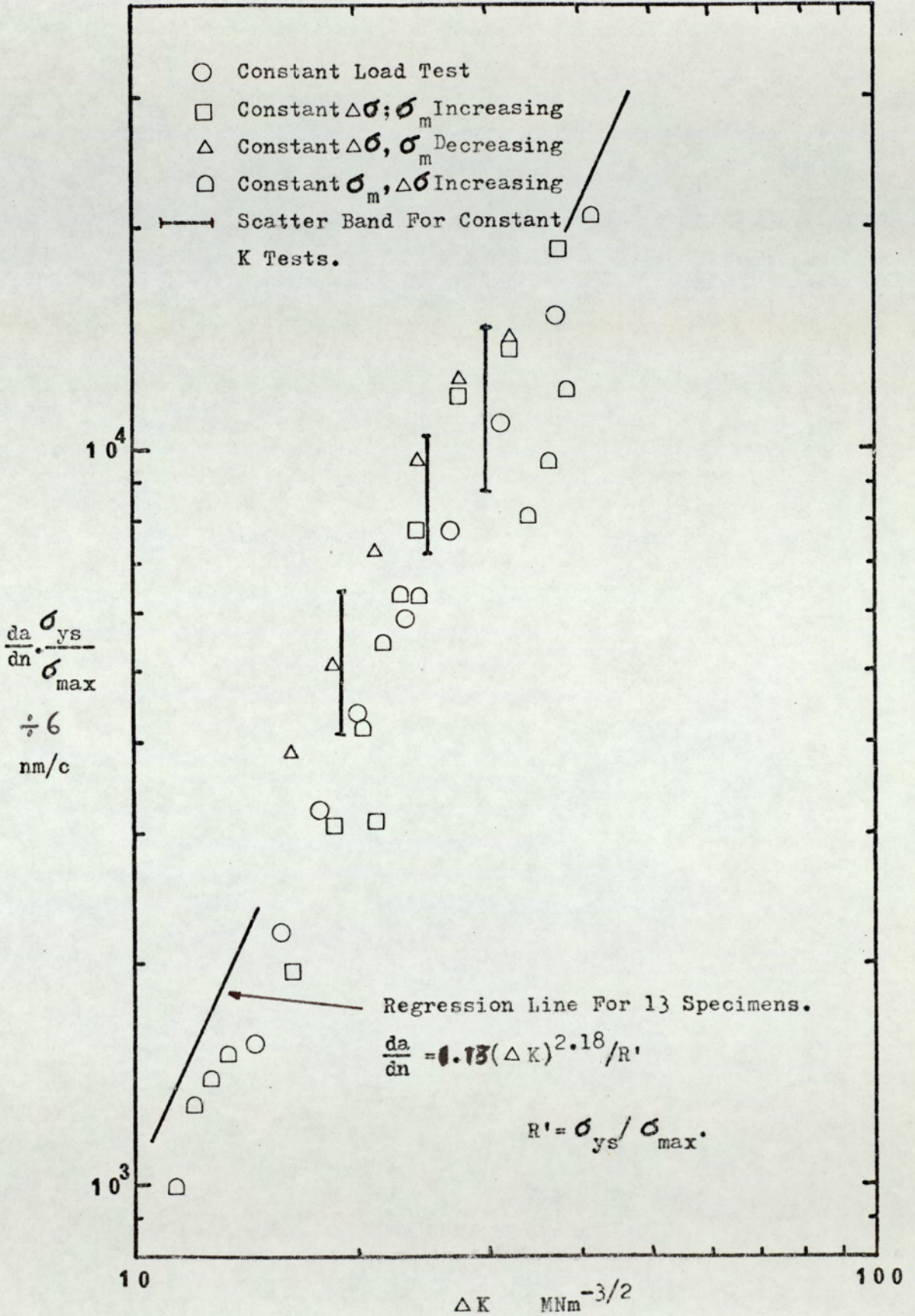


Fig.81b. Crack Growth Results Plotted in Terms of The Proposed Equation. QT-A

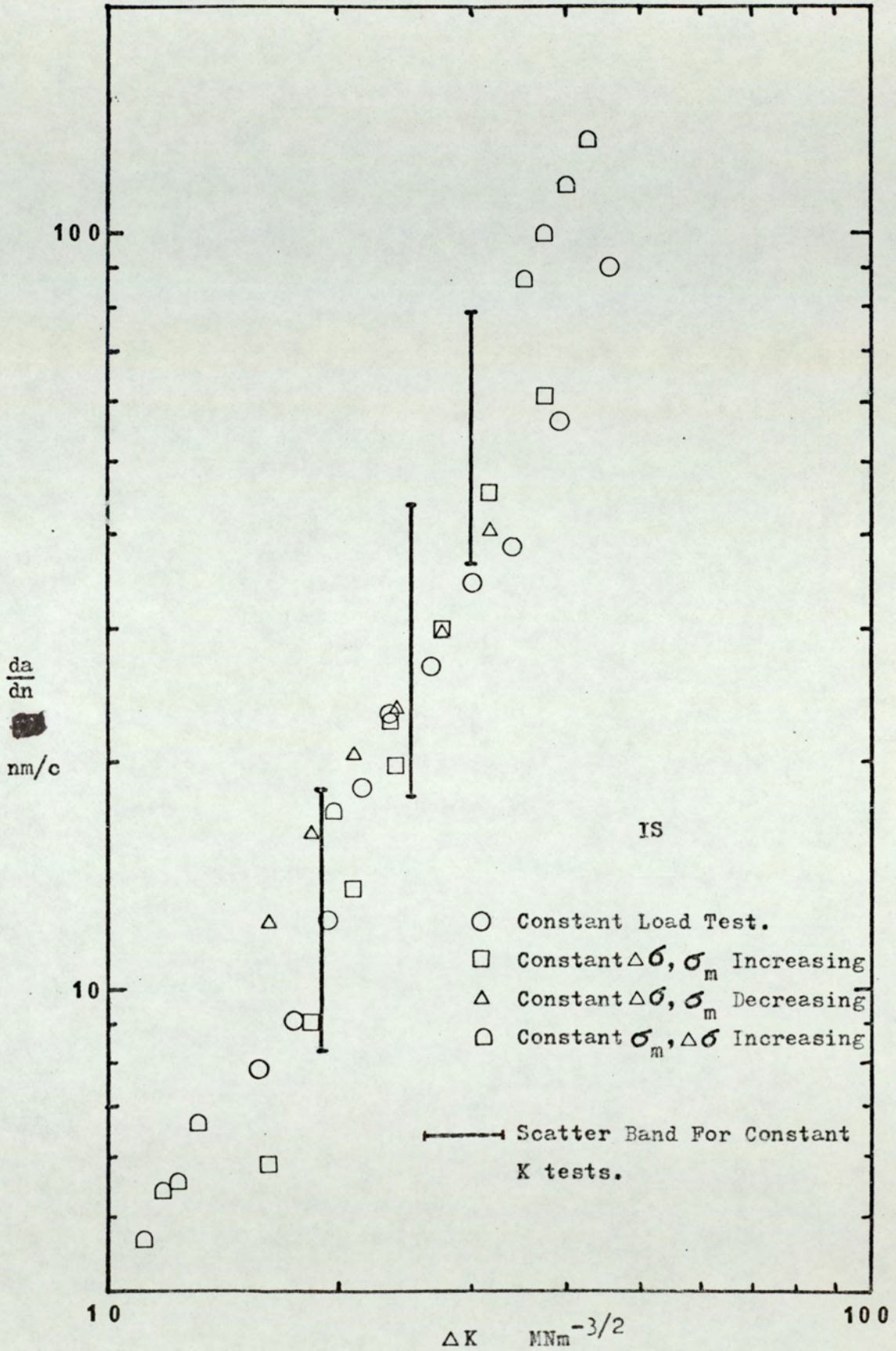


Fig.82. Crack Growth Results Plotted In Terms Of Paris's Equation.

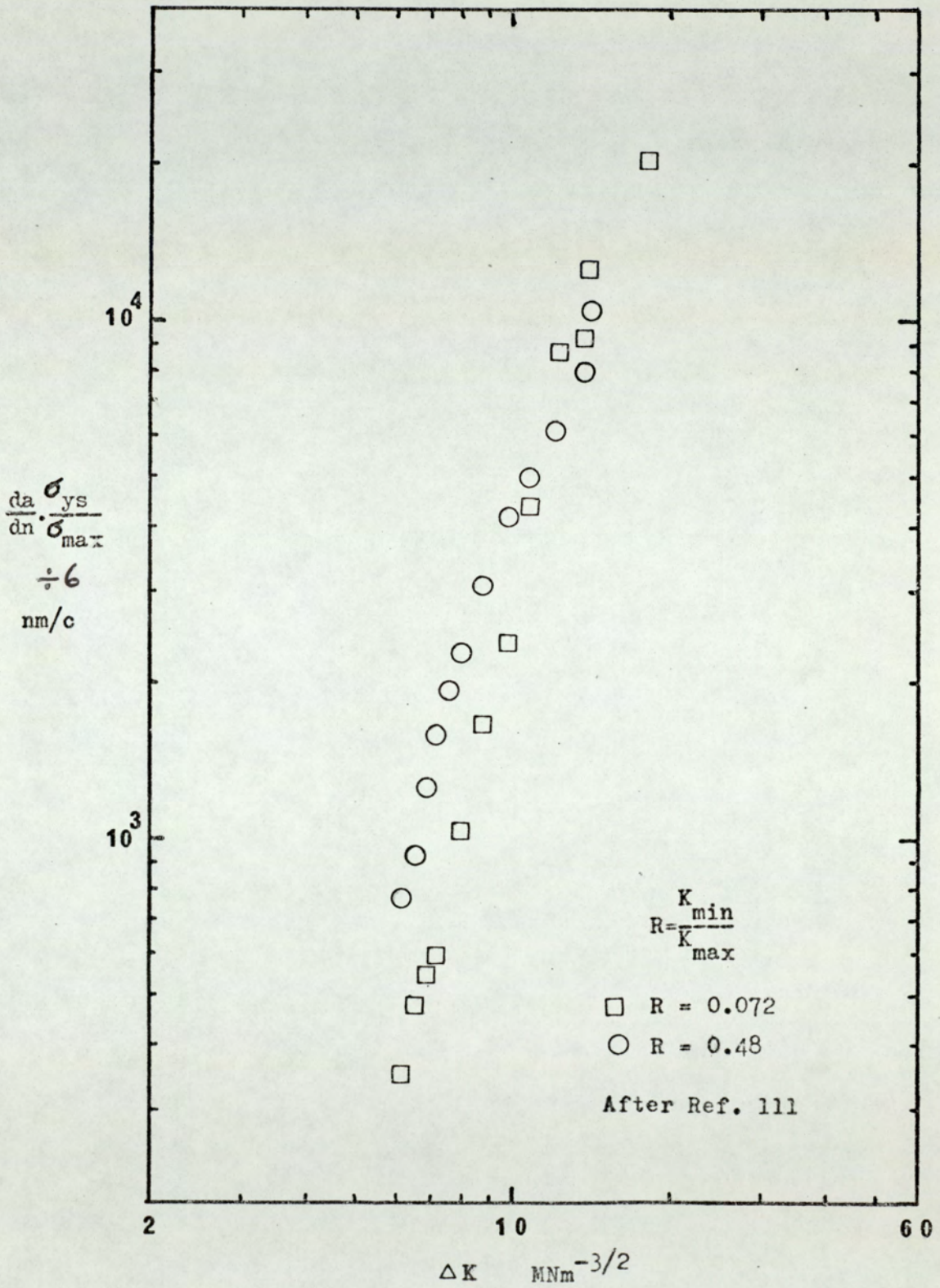


Fig.83. Crack Growth Curve For An Aluminium Alloy Plotted In Terms of The Proposed Equation.

different test programmes including those of constant K conditions in terms of the proposed crack growth equation (Equation 38). The Figs. 81a-b show that very good fit has been obtained with the results of each of the two micro-structures considered. The scatter-band in the case of QT-A steel is a bit large because of the inherent scatter in the crack growth rates observed with this material. For comparison purposes when the data of IS steel was plotted in terms of Paris's equation $\frac{da}{dn} = A(\Delta K)^m$, it shows a bigger scatter and the inadequacy of that equation to encompass the results of constant K condition tests (Fig. 82).

In order to see the usefulness of the proposed equation to other material than steel, the data ⁽¹¹¹⁾ of a high strength Al-Zn-Mg Alloy for tests at two different stress ratios were plotted as shown in Fig. 83. This shows a good fit. The same data when tried with Paris's or Forman's ⁽⁴²⁾ equation did not show a good correlation. Thus it can be concluded that equation 38 can be used adequately to unify the results of fatigue crack propagation in a wide range of loading situations.

5.14 Computer Prediction of Fatigue Life

It has been established that for a high-low load interaction, a transient delayed crack growth rate would occur in a fatigue situation. On the other hand, the interaction effect due to a low-high load change has virtually no effect on the crack growth rate. Thus if the load interaction effects are ignored in calculating the fatigue life of a component, a conservative estimate of life should result. However, it is possible to take the transient crack growth period into account through the use of equations 36 and 37.

Test Programmes and Material	Test Life in Cycles	Prediction of Fatigue Life (cycles) by			
		Paris's Equation from Constant Load Tests	Proposed Equation		
			From Constant Load Tests	From Incr. and Decr. σ_m Tests	From Regression Line in Fig. 81
Two-Step (20% Decr.) QT-A	295,000	298,936	319,832	270,808	243,200
	292,000	297,792	318,439	269,463	242,284
Two-Step (40% Decr.) QT-A	246,000	252,345	258,638	220,468	195,681
	283,000	253,470	259,822	221,286	196,768
Const. $\Delta\sigma$, Incr. σ_m QT-A	111,000	114,758	115,679	90,785	94,525
	141,000	123,380	123,733	98,618	99,584
Const. $\Delta\sigma$, Decr. σ_m QT-A	65,000	114,758	96,435	78,633	83,756
	66,000	123,380	116,957	88,363	91,154
Step ΔP Increase QT-A	167,000	180,537	180,359	155,225	135,237
	177,000	180,537	180,359	155,225	135,237
Two-Step (20% Decr.) IS	786,000	886,909	905,284	796,352	878,644
	800,000	886,909	905,284	796,352	878,644
Two-Step (40% Decr.) IS	1227,000	986,180	1088,187	946,616	1053,076
	1046,500	983,631	1085,628	944,485	1050,663
Const. $\Delta\sigma$, Incr. σ_m IS	576,000	490,882	515,553	455,169	503,375
	464,000	481,328	508,578	448,772	496,407
Const. $\Delta\sigma$, Decr. σ_m IS	379,500	481,328	422,257	373,829	412,964
	319,000	481,328	422,257	373,829	412,964
Step ΔP Increase IS	583,500	709,134	706,823	612,946	682,733
	572,500	709,134	706,823	612,946	682,733

Table 19. Computer Prediction of Fatigue Life

In the present investigation, the beneficial load-interaction effect was ignored to predict the fatigue life of the specimens by using Paris's equation and equation 38. Both the equations were derived from the constant load amplitude data. In addition to this, equation 38 was derived from the results of a variety of test programmes and also from the constant load amplitude tests where σ_m was increasing or decreasing in steps.

The ICL 1900 computer was used to integrate the derived equations to obtain fatigue lives of specimens under different test programmes. The integration was carried out by starting at an initial crack length and increasing it by a very small increment until the final crack length is reached. The life corresponding to this crack length interval is obtained for the actual test. The comparison of the results of the actual test life and the life predicted from the equations are shown in table 19. Based on the constant load amplitude tests, equation 38 gave better life prediction than Paris's equation. In the cases of increasing or decreasing σ_m tests and for the two-step load test with 40% decrease in load amplitude in IS steel, Paris's equation proved inadequate. When the equation 38 obtained from a variety of test programmes was used, the life prediction was conservative or nearly the same as the actual test life. The better prediction resulted from the inclusion of σ_{max} effects of the tests. Since it is practically prohibitive to use a large number of test programmes for life prediction purposes, the results of the increasing and decreasing mean load tests were used to obtain the proposed equation. The prediction based on this equation is mostly conservative and adequate. Hence this simplified programme tests can be used instead of constant amplitude load tests to obtain equation 38 which can then be employed to obtain a

conservative estimate of fatigue life in practical situations. Since an abrupt change of load has not been considered in this prediction, any situation where such load changes exist would yield a more conservative predicted fatigue life. For a more accurate life prediction in the aforementioned situation, equations 36 and 37 can be used in conjunction with equation 38.

6. CONCLUSIONS

Paris's equation $\frac{da}{dn} = A(\Delta K)^m$, which emphasises ΔK as the primary controlling factor for fatigue crack propagation, could be applied to constant load amplitude or increasing load amplitude cases only. In cases where both the load amplitude and mean load were decreased, Paris's equation did not apply.

In programme loading situations, the fatigue crack growth rate was found to be sensitive to the maximum or the mean stress level in the loading spectrum. The maximum stress was an important variable in the case of low strength ductile steels and the mean stress being important for the high strength martensitic steel. In general, for any ΔK level, the higher the mean stress level, the faster was the crack propagation. However, the crack growth rate showed a saturation value at very high mean stress level at low crack lengths under a certain ΔK condition.

At constant ΔK conditions, large reductions in the maximum stress caused a transient growth period comprising of a period of slow growth sometimes preceded by a dormant period depending on the amount of σ_{max} reduction. The stable growth rate obtained after the transient period was slower than the rate obtained before σ_{max} reduction. At a certain ΔK level, a growing fatigue crack could be totally stopped by a sufficiently large reduction in the maximum stress. The amount of reduction required was dependant on the strength and ductility of the steel and the level of ΔK . The dormancy of crack was possibly associated with the blunting of crack-tip. Large increases in σ_{max} did not show any noticeable transient accelerating effect on the fatigue crack propagation rate.

Crack growth equation of the type $\frac{da}{dn} = \frac{A(\Delta K)^m}{[(1-R)K_c - \Delta K]^n}$ which is

meant to account for stress level effect gave considerable scatter at very high and very low ΔK levels but showed good fit at the intermediate range. However, this equation did not apply to constant K condition test results.

The constant ΔK tests generally gave reducing crack growth rate (after a/W 0.3) with decreasing mean stress and increasing $\frac{a}{W}$ even though the stress ratio, R, was constant. The data generated followed an equation of the type $\frac{da}{dn} = A(\Delta\sigma)^m (\sigma_{max})^n \cdot a$ indicating that the stress ratio, R, which is defined as a ratio of K_{min} to K_{max} cannot account for a genuine mean stress effect.

A fatigue crack growth equation of the type $\frac{da}{dn} = \frac{A(\Delta K)^m}{R'}$ where $R' = \frac{\sigma_{ys}}{\sigma_{max}}$ could be applied satisfactorily to the different load programmes examined. This equation is based on a proposed mechanism of fatigue crack propagation. The equation takes the stress level effects into account but does not embrace the high-low load interaction effect which is beneficial to fatigue life of a component.

Fatigue crack propagation in EN24 steel was found to be sensitive to the type of heat-treatments used and the general mechanical properties achieved. The fatigue fracture surfaces of high strength martensitic steel were mixtures of trans and intergranular cracking. The smaller maximum plastic zone size in this material as compared to its grain size was associated with the cracking along the weak grain boundaries. The ductile, low strength steels, on the other hand, showed transgranular fractures which did not correlate well with the micro-structural features. The capacity of these steels to accommodate a large amount of strain at the crack tip by plastic deformation and also their ability to dissipate energy by numerous crack branching and island formation were related to their higher

crack growth resistance as compared to the high strength steels. The inclusions and the second phase particles played a secondary role in the fatigue crack propagation process, enhancing the crack growth rate at high stress levels. The light and dark bands observed on the fracture surface due to a load change were due to the difference in the size of the cell structures formed on the surface, the size increasing with the increase in ΔK .

Ignoring the load-interaction effect which is mostly beneficial to fatigue life, a conservative estimate of crack propagation life could be obtained by integrating equation $\frac{da}{dn} = \frac{A(\Delta K)^m}{R'}$.

RECOMMENDATIONS FOR FURTHER WORK

Most of the programmed and random loading work has been previously done on aluminium alloys and the results analysed in terms of Miner's Rule. Limited amount of work has recently been reported making use of the fracture mechanics as a basis for analysis. Bearing this in mind and basing on the results obtained in the present investigation, the following recommendations can be made for some future work.

1) In order to understand the fatigue behaviour of metals in general under complex loading conditions, basic programme loading work needs to be done on other metals and alloys such as titanium alloy and maraging steel. A fracture mechanics approach should be used.

2) The load-interaction effects need to be evaluated in detail in terms of crack tip opening displacements under programmed fatigue loading conditions. Investigation into the crack closure concept could also be beneficial.

3) Simple block programme loading work should be carried out in an aggressive environment to evaluate the contribution of load-interaction to the corrosion fatigue crack growth behaviour.

4) The crack growth behaviour under random fatigue loading should be investigated and analysed on the basis of fracture mechanics.

5) The fatigue crack growth equation proposed in the present work needs to be verified by using results from other sources on different materials.

ACKNOWLEDGEMENTS

I acknowledge my gratitude to Dr. H.D. Williams for his supervision, advice and guidance during the major part of this research work. I would also like to thank Dr. J.T. Barnby for his supervision and stimulating discussion during the last part of this project.

I wish to thank Professor W. O. Alexander, Head of the Department of Metallurgy, for providing necessary laboratory facilities and all the technicians and members of the staff for helping me at different times during the course of my research. Thanks are also due to my research colleagues for their helpful discussions.

My thanks are due to the Technical Assistance Training Department of the British Government and to the Government of Bangladesh for providing financial support under the Colombo Plan. I would also like to thank the British Council of Birmingham for looking after my welfare during my stay here in the U.K.

Last but not the least, I am very much thankful to my wife, Rini, who extended continuous encouragement to bring my work to a successful completion.

M. Khairuzzaman

Birmingham,
October 1973

V_a Versus $\frac{a}{W}$ Values (Theoretical (102) Calibration).

Appendix :- I

$X=0 \quad Y = \pm 0.16 \sqrt{W}$

V _a /V ₀	0.000	0.001	0.002	0.003	0.004	0.005	0.006	0.007	0.008	0.009
A/W	A/W	A/W	A/W	A/W	A/W	A/W	A/W	A/W	A/W	A/W
0.180	0.0647	0.0654	0.0660	0.0666	0.0673	0.0679	0.0686	0.0692	0.0699	0.0565
0.190	0.0511	0.0518	0.0524	0.0531	0.0537	0.0543	0.0550	0.0556	0.0562	0.0569
0.200	0.0575	0.0581	0.0588	0.0594	0.0600	0.0607	0.0613	0.0619	0.0626	0.0632
0.210	0.0658	0.0665	0.0671	0.0677	0.0683	0.0689	0.0695	0.0701	0.0707	0.0713
0.220	0.0701	0.0707	0.0713	0.0719	0.0725	0.0731	0.0737	0.0743	0.0749	0.0755
0.230	0.0765	0.0771	0.0777	0.0783	0.0789	0.0795	0.0801	0.0807	0.0813	0.0819
0.240	0.0825	0.0831	0.0837	0.0843	0.0849	0.0855	0.0861	0.0867	0.0873	0.0879
0.250	0.0880	0.0886	0.0892	0.0898	0.0904	0.0910	0.0916	0.0922	0.0928	0.0934
0.260	0.0947	0.0953	0.0959	0.0965	0.0971	0.0977	0.0983	0.0989	0.0995	0.1001
0.270	0.1007	0.1013	0.1019	0.1025	0.1031	0.1037	0.1043	0.1049	0.1055	0.1061
0.280	0.1066	0.1072	0.1078	0.1084	0.1090	0.1096	0.1102	0.1108	0.1114	0.1120
0.290	0.1126	0.1132	0.1138	0.1144	0.1149	0.1155	0.1161	0.1167	0.1173	0.1179
0.300	0.1184	0.1190	0.1196	0.1202	0.1208	0.1214	0.1220	0.1225	0.1231	0.1237
0.310	0.1243	0.1249	0.1254	0.1260	0.1266	0.1272	0.1278	0.1283	0.1289	0.1295
0.320	0.1301	0.1306	0.1312	0.1317	0.1324	0.1329	0.1335	0.1341	0.1347	0.1352
0.330	0.1358	0.1364	0.1370	0.1375	0.1381	0.1387	0.1392	0.1398	0.1404	0.1409
0.340	0.1415	0.1421	0.1426	0.1432	0.1438	0.1443	0.1449	0.1455	0.1460	0.1466
0.350	0.1472	0.1477	0.1482	0.1488	0.1494	0.1500	0.1505	0.1511	0.1517	0.1522
0.360	0.1528	0.1533	0.1538	0.1543	0.1549	0.1555	0.1561	0.1567	0.1572	0.1578
0.370	0.1584	0.1589	0.1594	0.1600	0.1606	0.1611	0.1617	0.1622	0.1628	0.1633
0.380	0.1639	0.1644	0.1650	0.1655	0.1661	0.1666	0.1672	0.1677	0.1683	0.1688
0.390	0.1694	0.1699	0.1705	0.1710	0.1716	0.1721	0.1727	0.1732	0.1738	0.1743
0.400	0.1748	0.1754	0.1759	0.1765	0.1770	0.1776	0.1781	0.1786	0.1792	0.1797
0.410	0.1803	0.1808	0.1813	0.1818	0.1824	0.1830	0.1835	0.1840	0.1846	0.1851
0.420	0.1856	0.1862	0.1867	0.1872	0.1878	0.1883	0.1888	0.1894	0.1899	0.1904
0.430	0.1910	0.1915	0.1920	0.1926	0.1931	0.1936	0.1942	0.1947	0.1952	0.1958
0.440	0.1965	0.1970	0.1974	0.1979	0.1984	0.1989	0.1995	0.2000	0.2005	0.2010
0.450	0.2016	0.2021	0.2026	0.2031	0.2037	0.2042	0.2047	0.2052	0.2057	0.2063
0.460	0.2068	0.2073	0.2078	0.2084	0.2089	0.2094	0.2099	0.2104	0.2109	0.2115
0.470	0.2120	0.2125	0.2130	0.2135	0.2141	0.2146	0.2151	0.2156	0.2161	0.2166
0.480	0.2172	0.2177	0.2182	0.2187	0.2192	0.2197	0.2202	0.2207	0.2213	0.2218
0.490	0.2225	0.2228	0.2233	0.2238	0.2243	0.2248	0.2253	0.2259	0.2264	0.2269
0.500	0.2274	0.2276	0.2281	0.2284	0.2289	0.2292	0.2297	0.2300	0.2304	0.2309
0.510	0.2344	0.2346	0.2349	0.2352	0.2355	0.2358	0.2361	0.2364	0.2367	0.2370
0.520	0.2375	0.2378	0.2380	0.2383	0.2385	0.2388	0.2390	0.2392	0.2394	0.2396
0.530	0.2425	0.2428	0.2430	0.2433	0.2435	0.2438	0.2440	0.2442	0.2444	0.2446
0.540	0.2474	0.2476	0.2478	0.2480	0.2482	0.2484	0.2486	0.2488	0.2490	0.2492
0.550	0.2524	0.2526	0.2528	0.2530	0.2532	0.2534	0.2536	0.2538	0.2540	0.2542
0.560	0.2573	0.2575	0.2577	0.2579	0.2581	0.2583	0.2585	0.2587	0.2589	0.2591
0.570	0.2622	0.2624	0.2626	0.2628	0.2630	0.2632	0.2634	0.2636	0.2638	0.2640
0.580	0.2670	0.2672	0.2674	0.2676	0.2678	0.2680	0.2682	0.2684	0.2686	0.2688
0.590	0.2718	0.2720	0.2722	0.2724	0.2726	0.2728	0.2730	0.2732	0.2734	0.2736
0.600	0.2766	0.2768	0.2770	0.2772	0.2774	0.2776	0.2778	0.2780	0.2782	0.2784
0.610	0.2814	0.2816	0.2818	0.2820	0.2822	0.2824	0.2826	0.2828	0.2830	0.2832
0.620	0.2861	0.2863	0.2865	0.2867	0.2869	0.2871	0.2873	0.2875	0.2877	0.2879
0.630	0.2908	0.2910	0.2912	0.2914	0.2916	0.2918	0.2920	0.2922	0.2924	0.2926
0.640	0.2955	0.2957	0.2959	0.2961	0.2963	0.2965	0.2967	0.2969	0.2971	0.2973
0.650	0.3001	0.3003	0.3005	0.3007	0.3009	0.3011	0.3013	0.3015	0.3017	0.3019
0.660	0.3047	0.3049	0.3051	0.3053	0.3055	0.3057	0.3059	0.3061	0.3063	0.3065
0.670	0.3093	0.3095	0.3097	0.3099	0.3101	0.3103	0.3105	0.3107	0.3109	0.3111
0.680	0.3130	0.3132	0.3134	0.3136	0.3138	0.3140	0.3142	0.3144	0.3146	0.3148
0.690	0.3164	0.3166	0.3168	0.3170	0.3172	0.3174	0.3176	0.3178	0.3180	0.3182
0.700	0.3200	0.3202	0.3204	0.3206	0.3208	0.3210	0.3212	0.3214	0.3216	0.3218

0.710	0.3274	0.3270	0.3288	0.3202	0.3207	0.3301	0.3306	0.3310	0.3315
0.720	0.3310	0.3326	0.3332	0.3337	0.3341	0.3346	0.3350	0.3355	0.3359
0.730	0.3343	0.3368	0.3377	0.3381	0.3386	0.3390	0.3394	0.3399	0.3403
0.740	0.3408	0.3441	0.3471	0.3485	0.3490	0.3494	0.3498	0.3502	0.3506
0.750	0.3452	0.3496	0.3526	0.3540	0.3545	0.3549	0.3553	0.3557	0.3561
0.760	0.3495	0.3543	0.3587	0.3601	0.3606	0.3610	0.3614	0.3618	0.3622
0.770	0.3530	0.3582	0.3636	0.3650	0.3655	0.3659	0.3663	0.3667	0.3671
0.780	0.3562	0.3626	0.3680	0.3694	0.3699	0.3703	0.3707	0.3711	0.3715
0.790	0.3608	0.3672	0.3726	0.3740	0.3745	0.3749	0.3753	0.3757	0.3761
0.800	0.3648	0.3712	0.3766	0.3780	0.3785	0.3789	0.3793	0.3797	0.3801
0.810	0.3690	0.3754	0.3808	0.3822	0.3827	0.3831	0.3835	0.3839	0.3843
0.820	0.3732	0.3796	0.3850	0.3864	0.3869	0.3873	0.3877	0.3881	0.3885
0.830	0.3774	0.3838	0.3892	0.3906	0.3911	0.3915	0.3919	0.3923	0.3927
0.840	0.3816	0.3880	0.3934	0.3948	0.3953	0.3957	0.3961	0.3965	0.3969
0.850	0.3858	0.3922	0.3976	0.3990	0.3995	0.3999	0.4003	0.4007	0.4011
0.860	0.3899	0.3963	0.4017	0.4031	0.4036	0.4040	0.4044	0.4048	0.4052
0.870	0.3941	0.4005	0.4059	0.4073	0.4078	0.4082	0.4086	0.4090	0.4094
0.880	0.3982	0.4046	0.4100	0.4114	0.4119	0.4123	0.4127	0.4131	0.4135
0.890	0.4024	0.4088	0.4142	0.4156	0.4161	0.4165	0.4169	0.4173	0.4177
0.900	0.4065	0.4129	0.4183	0.4197	0.4202	0.4206	0.4210	0.4214	0.4218
0.910	0.4106	0.4170	0.4224	0.4238	0.4243	0.4247	0.4251	0.4255	0.4259
0.920	0.4147	0.4211	0.4265	0.4279	0.4284	0.4288	0.4292	0.4296	0.4300
0.930	0.4188	0.4252	0.4306	0.4320	0.4325	0.4329	0.4333	0.4337	0.4341
0.940	0.4229	0.4293	0.4347	0.4361	0.4366	0.4370	0.4374	0.4378	0.4382
0.950	0.4270	0.4334	0.4388	0.4402	0.4407	0.4411	0.4415	0.4419	0.4423
0.960	0.4311	0.4375	0.4429	0.4443	0.4448	0.4452	0.4456	0.4460	0.4464
0.970	0.4352	0.4416	0.4470	0.4484	0.4489	0.4493	0.4497	0.4501	0.4505
0.980	0.4393	0.4457	0.4511	0.4525	0.4530	0.4534	0.4538	0.4542	0.4546
0.990	0.4434	0.4498	0.4552	0.4566	0.4571	0.4575	0.4579	0.4583	0.4587
1.000	0.4475	0.4539	0.4593	0.4607	0.4612	0.4616	0.4620	0.4624	0.4628
1.010	0.4516	0.4580	0.4634	0.4648	0.4653	0.4657	0.4661	0.4665	0.4669
1.020	0.4557	0.4621	0.4675	0.4689	0.4694	0.4698	0.4702	0.4706	0.4710
1.030	0.4598	0.4662	0.4716	0.4730	0.4735	0.4739	0.4743	0.4747	0.4751
1.040	0.4639	0.4703	0.4757	0.4771	0.4776	0.4780	0.4784	0.4788	0.4792
1.050	0.4680	0.4744	0.4798	0.4812	0.4817	0.4821	0.4825	0.4829	0.4833
1.060	0.4721	0.4785	0.4839	0.4853	0.4858	0.4862	0.4866	0.4870	0.4874
1.070	0.4762	0.4826	0.4880	0.4894	0.4899	0.4903	0.4907	0.4911	0.4915
1.080	0.4803	0.4867	0.4921	0.4935	0.4940	0.4944	0.4948	0.4952	0.4956
1.090	0.4844	0.4908	0.4962	0.4976	0.4981	0.4985	0.4989	0.4993	0.4997
1.100	0.4885	0.4949	0.5003	0.5017	0.5022	0.5026	0.5030	0.5034	0.5038
1.110	0.4926	0.4990	0.5044	0.5058	0.5063	0.5067	0.5071	0.5075	0.5079
1.120	0.4967	0.5031	0.5085	0.5099	0.5104	0.5108	0.5112	0.5116	0.5120
1.130	0.5008	0.5072	0.5126	0.5140	0.5145	0.5149	0.5153	0.5157	0.5161
1.140	0.5049	0.5113	0.5167	0.5181	0.5186	0.5190	0.5194	0.5198	0.5202
1.150	0.5090	0.5154	0.5208	0.5222	0.5227	0.5231	0.5235	0.5239	0.5243
1.160	0.5131	0.5195	0.5249	0.5263	0.5268	0.5272	0.5276	0.5280	0.5284
1.170	0.5172	0.5236	0.5290	0.5304	0.5309	0.5313	0.5317	0.5321	0.5325
1.180	0.5213	0.5277	0.5331	0.5345	0.5350	0.5354	0.5358	0.5362	0.5366
1.190	0.5254	0.5318	0.5372	0.5386	0.5391	0.5395	0.5399	0.5403	0.5407
1.200	0.5295	0.5359	0.5413	0.5427	0.5432	0.5436	0.5440	0.5444	0.5448
1.210	0.5336	0.5400	0.5454	0.5468	0.5473	0.5477	0.5481	0.5485	0.5489
1.220	0.5377	0.5441	0.5495	0.5509	0.5514	0.5518	0.5522	0.5526	0.5530
1.230	0.5418	0.5482	0.5536	0.5550	0.5555	0.5559	0.5563	0.5567	0.5571
1.240	0.5459	0.5523	0.5577	0.5591	0.5596	0.5600	0.5604	0.5608	0.5612
1.250	0.5500	0.5564	0.5618	0.5632	0.5637	0.5641	0.5645	0.5649	0.5653
1.260	0.5541	0.5605	0.5659	0.5673	0.5678	0.5682	0.5686	0.5690	0.5694
1.270	0.5582	0.5646	0.5700	0.5714	0.5719	0.5723	0.5727	0.5731	0.5735
1.280	0.5623	0.5687	0.5741	0.5755	0.5760	0.5764	0.5768	0.5772	0.5776
1.290	0.5664	0.5728	0.5782	0.5796	0.5801	0.5805	0.5809	0.5813	0.5817
1.300	0.5705	0.5769	0.5823	0.5837	0.5842	0.5846	0.5850	0.5854	0.5858

X=0
V = ± 0.095 W

VA/V ₀ W	0.000	0.001	0.002	0.003	0.004	0.005	0.006	0.007	0.008	0.009
	A/W									
0.190	0.0454	0.0464	0.0471	0.0477	0.0484	0.0490	0.0497	0.0503	0.0510	0.0517
0.200	0.0523	0.0530	0.0534	0.0543	0.0549	0.0556	0.0562	0.0569	0.0575	0.0581
0.210	0.0586	0.0594	0.0601	0.0607	0.0614	0.0620	0.0627	0.0633	0.0639	0.0646
0.220	0.0652	0.0660	0.0667	0.0671	0.0678	0.0684	0.0691	0.0697	0.0703	0.0710
0.230	0.0716	0.0722	0.0729	0.0735	0.0741	0.0748	0.0754	0.0760	0.0767	0.0773
0.240	0.0779	0.0785	0.0792	0.0798	0.0804	0.0810	0.0817	0.0823	0.0829	0.0835
0.250	0.0842	0.0848	0.0854	0.0860	0.0867	0.0873	0.0879	0.0885	0.0891	0.0898
0.260	0.0904	0.0910	0.0916	0.0922	0.0928	0.0935	0.0941	0.0947	0.0953	0.0959
0.270	0.0965	0.0971	0.0978	0.0984	0.0990	0.0996	0.1002	0.1008	0.1014	0.1020
0.280	0.1026	0.1032	0.1039	0.1045	0.1051	0.1057	0.1063	0.1069	0.1075	0.1081
0.290	0.1087	0.1093	0.1100	0.1105	0.1111	0.1117	0.1123	0.1129	0.1135	0.1141
0.300	0.1147	0.1153	0.1159	0.1165	0.1171	0.1177	0.1183	0.1189	0.1195	0.1200
0.310	0.1206	0.1212	0.1218	0.1224	0.1230	0.1236	0.1242	0.1248	0.1254	0.1260
0.320	0.1265	0.1271	0.1277	0.1283	0.1289	0.1295	0.1301	0.1306	0.1312	0.1318
0.330	0.1324	0.1330	0.1336	0.1341	0.1347	0.1353	0.1359	0.1365	0.1370	0.1376
0.340	0.1382	0.1388	0.1394	0.1399	0.1405	0.1411	0.1417	0.1422	0.1428	0.1434
0.350	0.1440	0.1445	0.1451	0.1457	0.1463	0.1468	0.1474	0.1480	0.1485	0.1491
0.360	0.1497	0.1503	0.1508	0.1514	0.1520	0.1525	0.1531	0.1537	0.1542	0.1548
0.370	0.1554	0.1559	0.1565	0.1570	0.1576	0.1582	0.1587	0.1593	0.1599	0.1604
0.380	0.1610	0.1615	0.1621	0.1627	0.1632	0.1638	0.1644	0.1649	0.1655	0.1660
0.390	0.1666	0.1671	0.1677	0.1682	0.1688	0.1693	0.1699	0.1705	0.1710	0.1716
0.400	0.1721	0.1727	0.1733	0.1738	0.1743	0.1749	0.1754	0.1760	0.1765	0.1771
0.410	0.1776	0.1782	0.1787	0.1793	0.1798	0.1803	0.1809	0.1814	0.1820	0.1825
0.420	0.1831	0.1836	0.1842	0.1847	0.1852	0.1858	0.1863	0.1869	0.1874	0.1879
0.430	0.1885	0.1890	0.1896	0.1901	0.1906	0.1912	0.1917	0.1923	0.1928	0.1933
0.440	0.1939	0.1944	0.1949	0.1955	0.1960	0.1965	0.1971	0.1976	0.1981	0.1987
0.450	0.1992	0.1997	0.2003	0.2008	0.2013	0.2019	0.2024	0.2029	0.2034	0.2040
0.460	0.2045	0.2050	0.2056	0.2061	0.2066	0.2071	0.2077	0.2082	0.2087	0.2092
0.470	0.2098	0.2103	0.2108	0.2113	0.2119	0.2124	0.2129	0.2134	0.2140	0.2145
0.480	0.2150	0.2155	0.2160	0.2166	0.2171	0.2176	0.2181	0.2186	0.2192	0.2197
0.490	0.2207	0.2207	0.2212	0.2217	0.2223	0.2228	0.2233	0.2238	0.2243	0.2248
0.500	0.2253	0.2259	0.2264	0.2269	0.2274	0.2279	0.2284	0.2289	0.2294	0.2299
0.510	0.2305	0.2310	0.2315	0.2320	0.2325	0.2330	0.2335	0.2340	0.2345	0.2350
0.520	0.2355	0.2361	0.2366	0.2371	0.2376	0.2381	0.2386	0.2391	0.2396	0.2401
0.530	0.2406	0.2411	0.2416	0.2421	0.2426	0.2431	0.2436	0.2441	0.2446	0.2451
0.540	0.2456	0.2461	0.2466	0.2471	0.2476	0.2481	0.2486	0.2491	0.2496	0.2501
0.550	0.2506	0.2511	0.2516	0.2521	0.2526	0.2531	0.2536	0.2541	0.2546	0.2551
0.560	0.2555	0.2560	0.2565	0.2570	0.2575	0.2580	0.2585	0.2590	0.2595	0.2600
0.570	0.2605	0.2610	0.2614	0.2619	0.2624	0.2629	0.2634	0.2639	0.2644	0.2649
0.580	0.2653	0.2658	0.2663	0.2668	0.2673	0.2678	0.2683	0.2688	0.2692	0.2697
0.590	0.2702	0.2707	0.2712	0.2717	0.2721	0.2726	0.2731	0.2736	0.2741	0.2745
0.600	0.2755	0.2755	0.2760	0.2765	0.2769	0.2774	0.2779	0.2784	0.2789	0.2793
0.610	0.2803	0.2803	0.2808	0.2813	0.2817	0.2822	0.2827	0.2832	0.2836	0.2841
0.620	0.2846	0.2851	0.2856	0.2860	0.2865	0.2870	0.2874	0.2879	0.2884	0.2888
0.630	0.2893	0.2898	0.2903	0.2907	0.2912	0.2917	0.2921	0.2926	0.2931	0.2936
0.640	0.2940	0.2945	0.2950	0.2954	0.2959	0.2964	0.2968	0.2973	0.2978	0.2982
0.650	0.2997	0.2996	0.2996	0.2996	0.2996	0.2996	0.2996	0.2996	0.2996	0.2996
0.660	0.3034	0.3038	0.3043	0.3047	0.3052	0.3057	0.3061	0.3066	0.3071	0.3075
0.670	0.3080	0.3084	0.3088	0.3092	0.3096	0.3100	0.3104	0.3107	0.3111	0.3115
0.680	0.3126	0.3130	0.3134	0.3138	0.3142	0.3146	0.3150	0.3154	0.3158	0.3162

0.693	0.3171	0.3176	0.3180	0.3185	0.3190	0.3194	0.3199	0.3203	0.3208	0.3212
0.700	0.3217	0.3221	0.3226	0.3230	0.3235	0.3239	0.3244	0.3248	0.3253	0.3257
0.711	0.3262	0.3266	0.3271	0.3275	0.3280	0.3284	0.3289	0.3293	0.3298	0.3302
0.723	0.3307	0.3311	0.3316	0.3320	0.3325	0.3329	0.3334	0.3338	0.3343	0.3347
0.735	0.3351	0.3355	0.3360	0.3365	0.3369	0.3374	0.3378	0.3382	0.3387	0.3391
0.748	0.3396	0.3400	0.3405	0.3409	0.3413	0.3418	0.3422	0.3427	0.3431	0.3435
0.759	0.3440	0.3444	0.3449	0.3453	0.3457	0.3462	0.3466	0.3471	0.3475	0.3479
0.769	0.3484	0.3488	0.3493	0.3497	0.3501	0.3506	0.3510	0.3514	0.3519	0.3523
0.779	0.3527	0.3532	0.3537	0.3541	0.3545	0.3550	0.3554	0.3558	0.3562	0.3566
0.789	0.3571	0.3575	0.3579	0.3584	0.3588	0.3592	0.3597	0.3601	0.3605	0.3610
0.799	0.3614	0.3618	0.3623	0.3627	0.3631	0.3635	0.3640	0.3644	0.3648	0.3653
0.809	0.3657	0.3661	0.3665	0.3670	0.3674	0.3678	0.3682	0.3687	0.3691	0.3695
0.819	0.3694	0.3704	0.3708	0.3712	0.3716	0.3721	0.3725	0.3729	0.3733	0.3738
0.829	0.3742	0.3746	0.3750	0.3755	0.3759	0.3763	0.3767	0.3771	0.3776	0.3780
0.839	0.3784	0.3788	0.3793	0.3797	0.3801	0.3805	0.3809	0.3814	0.3818	0.3822
0.849	0.3826	0.3830	0.3834	0.3839	0.3843	0.3847	0.3851	0.3855	0.3860	0.3864
0.859	0.3868	0.3872	0.3876	0.3880	0.3884	0.3889	0.3893	0.3897	0.3901	0.3905
0.869	0.3909	0.3914	0.3918	0.3922	0.3926	0.3930	0.3934	0.3938	0.3942	0.3947
0.879	0.3951	0.3955	0.3959	0.3963	0.3967	0.3971	0.3975	0.3979	0.3984	0.3988
0.889	0.3992	0.3996	0.4000	0.4004	0.4008	0.4012	0.4016	0.4020	0.4024	0.4029
0.899	0.4035	0.4037	0.4041	0.4045	0.4049	0.4053	0.4057	0.4061	0.4065	0.4069
0.909	0.4073	0.4077	0.4081	0.4085	0.4089	0.4093	0.4098	0.4102	0.4106	0.4110
0.919	0.4114	0.4118	0.4122	0.4126	0.4130	0.4134	0.4138	0.4142	0.4146	0.4150
0.929	0.4154	0.4158	0.4162	0.4166	0.4170	0.4174	0.4178	0.4182	0.4186	0.4190
0.939	0.4194	0.4198	0.4202	0.4206	0.4210	0.4214	0.4218	0.4222	0.4226	0.4230
0.949	0.4234	0.4238	0.4242	0.4246	0.4250	0.4254	0.4258	0.4262	0.4266	0.4269
0.959	0.4273	0.4277	0.4281	0.4285	0.4289	0.4293	0.4297	0.4301	0.4305	0.4309
0.969	0.4313	0.4317	0.4321	0.4325	0.4329	0.4333	0.4337	0.4341	0.4344	0.4348
0.979	0.4352	0.4356	0.4360	0.4364	0.4368	0.4371	0.4375	0.4379	0.4383	0.4387
0.989	0.4391	0.4395	0.4399	0.4403	0.4406	0.4410	0.4414	0.4418	0.4422	0.4426
0.999	0.4430	0.4434	0.4437	0.4441	0.4445	0.4449	0.4453	0.4457	0.4461	0.4464
1.009	0.4468	0.4472	0.4476	0.4480	0.4484	0.4488	0.4491	0.4495	0.4499	0.4503
1.019	0.4507	0.4511	0.4514	0.4518	0.4522	0.4526	0.4530	0.4533	0.4537	0.4541
1.029	0.4549	0.4553	0.4557	0.4561	0.4565	0.4569	0.4573	0.4577	0.4581	0.4585
1.039	0.4588	0.4592	0.4596	0.4600	0.4604	0.4608	0.4612	0.4616	0.4620	0.4624
1.049	0.4658	0.4662	0.4666	0.4670	0.4674	0.4678	0.4682	0.4686	0.4690	0.4694
1.059	0.4699	0.4703	0.4707	0.4711	0.4715	0.4719	0.4723	0.4727	0.4731	0.4735
1.069	0.4753	0.4757	0.4761	0.4765	0.4769	0.4773	0.4777	0.4781	0.4785	0.4789
1.079	0.4796	0.4800	0.4804	0.4808	0.4812	0.4816	0.4820	0.4824	0.4828	0.4832
1.089	0.4867	0.4871	0.4875	0.4879	0.4883	0.4887	0.4891	0.4895	0.4899	0.4903
1.099	0.4884	0.4888	0.4892	0.4896	0.4900	0.4904	0.4908	0.4912	0.4916	0.4920
1.109	0.4926	0.4930	0.4934	0.4938	0.4942	0.4946	0.4950	0.4954	0.4958	0.4962
1.119	0.4988	0.4992	0.4996	0.5000	0.5004	0.5008	0.5012	0.5016	0.5020	0.5024
1.129	0.5023	0.5027	0.5031	0.5035	0.5039	0.5043	0.5047	0.5051	0.5055	0.5059
1.139	0.5094	0.5098	0.5102	0.5106	0.5110	0.5114	0.5118	0.5122	0.5126	0.5130
1.149	0.5129	0.5133	0.5137	0.5141	0.5145	0.5149	0.5153	0.5157	0.5161	0.5165
1.159	0.5164	0.5168	0.5172	0.5176	0.5180	0.5184	0.5188	0.5192	0.5196	0.5200
1.169	0.5199	0.5203	0.5207	0.5211	0.5215	0.5219	0.5223	0.5227	0.5231	0.5235
1.179	0.5235	0.5237	0.5241	0.5245	0.5249	0.5253	0.5257	0.5261	0.5265	0.5269
1.189	0.5267	0.5271	0.5274	0.5278	0.5281	0.5284	0.5288	0.5291	0.5295	0.5298
1.199	0.5302	0.5305	0.5308	0.5311	0.5314	0.5318	0.5321	0.5324	0.5327	0.5330
1.209	0.5335	0.5339	0.5342	0.5345	0.5348	0.5351	0.5354	0.5357	0.5360	0.5363
1.219	0.5369	0.5373	0.5376	0.5379	0.5382	0.5385	0.5388	0.5391	0.5394	0.5397
1.229	0.5403	0.5406	0.5409	0.5413	0.5416	0.5419	0.5423	0.5426	0.5429	0.5433
1.239	0.5436	0.5439	0.5442	0.5445	0.5448	0.5451	0.5454	0.5457	0.5460	0.5463
1.249	0.5469	0.5473	0.5476	0.5479	0.5482	0.5485	0.5488	0.5491	0.5494	0.5497

1.290	0.5502	0.5505	0.5512	0.5519	0.5522	0.5525	0.5528	0.5532
1.300	0.5535	0.5536	0.5541	0.5548	0.5551	0.5554	0.5555	0.5564
1.310	0.5568	0.5571	0.5577	0.5584	0.5587	0.5590	0.5593	0.5597
1.320	0.5600	0.5603	0.5610	0.5613	0.5619	0.5622	0.5625	0.5629
1.330	0.5632	0.5635	0.5640	0.5645	0.5651	0.5655	0.5658	0.5661
1.340	0.5664	0.5667	0.5674	0.5677	0.5683	0.5686	0.5690	0.5693
1.350	0.5696	0.5699	0.5705	0.5712	0.5715	0.5718	0.5721	0.5724
1.360	0.5726	0.5731	0.5734	0.5740	0.5746	0.5750	0.5753	0.5756
1.370	0.5759	0.5762	0.5768	0.5775	0.5778	0.5781	0.5784	0.5787
1.380	0.5790	0.5793	0.5800	0.5803	0.5809	0.5812	0.5815	0.5818
1.390	0.5821	0.5824	0.5831	0.5836	0.5840	0.5842	0.5846	0.5849
1.400	0.5852	0.5855	0.5862	0.5866	0.5874	0.5877	0.5880	0.5884
1.410	0.5885	0.5889	0.5896	0.5898	0.5901	0.5904	0.5907	0.5910
1.420	0.5913	0.5916	0.5922	0.5925	0.5932	0.5935	0.5938	0.5941
1.430	0.5944	0.5947	0.5953	0.5956	0.5962	0.5965	0.5968	0.5971
1.440	0.5974	0.5977	0.5983	0.5986	0.5992	0.5995	0.5998	0.6001
1.450	0.6004	0.6007	0.6013	0.6016	0.6021	0.6024	0.6027	0.6030
1.460	0.6033	0.6036	0.6042	0.6045	0.6051	0.6054	0.6057	0.6060
1.470	0.6063	0.6066	0.6072	0.6075	0.6080	0.6083	0.6086	0.6089
1.480	0.6092	0.6095	0.6101	0.6104	0.6107	0.6113	0.6116	0.6118
1.490	0.6121	0.6124	0.6130	0.6133	0.6136	0.6142	0.6144	0.6147
1.500	0.6150	0.6153	0.6159	0.6162	0.6165	0.6170	0.6173	0.6176
1.510	0.6179	0.6182	0.6188	0.6193	0.6196	0.6199	0.6202	0.6205
1.520	0.6208	0.6211	0.6217	0.6222	0.6225	0.6227	0.6230	0.6233
1.530	0.6236	0.6239	0.6244	0.6246	0.6250	0.6253	0.6258	0.6261
1.540	0.6264	0.6267	0.6273	0.6275	0.6278	0.6281	0.6284	0.6289
1.550	0.6292	0.6295	0.6300	0.6303	0.6306	0.6309	0.6314	0.6317
1.560	0.6320	0.6323	0.6328	0.6331	0.6334	0.6339	0.6342	0.6345
1.570	0.6347	0.6350	0.6354	0.6358	0.6361	0.6367	0.6369	0.6372
1.580	0.6375	0.6378	0.6383	0.6386	0.6388	0.6391	0.6394	0.6399
1.590	0.6402	0.6405	0.6410	0.6413	0.6416	0.6421	0.6424	0.6426
1.600	0.6429	0.6432	0.6437	0.6440	0.6442	0.6448	0.6450	0.6453
1.610	0.6456	0.6459	0.6464	0.6467	0.6469	0.6474	0.6477	0.6480
1.620	0.6482	0.6485	0.6489	0.6493	0.6496	0.6501	0.6504	0.6506
1.630	0.6509	0.6512	0.6517	0.6519	0.6522	0.6527	0.6530	0.6533
1.640	0.6535	0.6538	0.6543	0.6546	0.6551	0.6553	0.6556	0.6559
1.650	0.6561	0.6564	0.6569	0.6572	0.6577	0.6579	0.6582	0.6584
1.660	0.6587	0.6590	0.6595	0.6597	0.6602	0.6605	0.6608	0.6610
1.670	0.6613	0.6615	0.6618	0.6623	0.6625	0.6631	0.6633	0.6636
1.680	0.6638	0.6641	0.6646	0.6648	0.6651	0.6656	0.6658	0.6661
1.690	0.6663	0.6666	0.6671	0.6673	0.6676	0.6681	0.6684	0.6686
1.700	0.6689	0.6691	0.6694	0.6698	0.6701	0.6706	0.6708	0.6711
1.710	0.6713	0.6716	0.6721	0.6723	0.6728	0.6731	0.6733	0.6736
1.720	0.6739	0.6741	0.6747	0.6748	0.6750	0.6755	0.6758	0.6760
1.730	0.6763	0.6765	0.6770	0.6772	0.6775	0.6777	0.6782	0.6785
1.740	0.6787	0.6789	0.6794	0.6797	0.6799	0.6804	0.6806	0.6809
1.750	0.6811	0.6814	0.6818	0.6821	0.6823	0.6828	0.6830	0.6833
1.760	0.6835	0.6837	0.6842	0.6845	0.6849	0.6852	0.6854	0.6856
1.770	0.6859	0.6861	0.6866	0.6868	0.6871	0.6875	0.6878	0.6880
1.780	0.6882	0.6885	0.6889	0.6892	0.6896	0.6899	0.6904	0.6907
1.790	0.6909	0.6911	0.6915	0.6919	0.6921	0.6924	0.6927	0.6929
1.800	0.6929	0.6931	0.6934	0.6938	0.6941	0.6945	0.6947	0.6950
1.810	0.6952	0.6954	0.6957	0.6961	0.6964	0.6968	0.6970	0.6973
1.820	0.6975	0.6977	0.6980	0.6984	0.6986	0.6991	0.6993	0.6995
1.830	0.6998	0.7000	0.7004	0.7007	0.7011	0.7013	0.7016	0.7018
1.840	0.7020	0.7022	0.7025	0.7029	0.7031	0.7034	0.7038	0.7040
1.850	0.7042	0.7045	0.7047	0.7051	0.7054	0.7056	0.7060	0.7062
1.860	0.7065	0.7067	0.7071	0.7074	0.7078	0.7082	0.7084	0.7087
1.870	0.7087	0.7089	0.7093	0.7095	0.7097	0.7102	0.7104	0.7106
1.880	0.7108	0.7111	0.7114	0.7117	0.7119	0.7121	0.7123	0.7126

x=0 v=±0.100W

VA/V0W	0.000	0.001	0.002	0.003	0.004	0.005	0.006	0.007	0.008	0.009
	A/W									
0.200	0.6409	0.6475	0.6482	0.6480	0.0495	0.0502	0.0509	0.0515	0.0522	0.0529
0.210	0.6535	0.6542	0.6549	0.6555	0.0562	0.0568	0.0575	0.0582	0.0588	0.0595
0.220	0.6601	0.6601	0.6614	0.6621	0.0628	0.0634	0.0641	0.0647	0.0654	0.0660
0.230	0.6667	0.6673	0.6680	0.6684	0.0693	0.0699	0.0706	0.0712	0.0719	0.0725
0.240	0.6731	0.6738	0.6744	0.6751	0.0757	0.0764	0.0770	0.0776	0.0783	0.0789
0.250	0.6796	0.6802	0.6808	0.6815	0.0821	0.0828	0.0834	0.0840	0.0847	0.0853
0.260	0.6859	0.6866	0.6872	0.6878	0.0885	0.0891	0.0897	0.0903	0.0910	0.0916
0.270	0.6922	0.6929	0.6935	0.6941	0.0947	0.0954	0.0960	0.0966	0.0972	0.0978
0.280	0.6985	0.6991	0.6997	0.1003	0.1010	0.1016	0.1022	0.1028	0.1034	0.1040
0.290	0.7047	0.7053	0.7059	0.7065	0.1071	0.1077	0.1083	0.1090	0.1096	0.1102
0.300	0.7109	0.7114	0.7120	0.7126	0.1132	0.1138	0.1144	0.1151	0.1157	0.1163
0.310	0.7169	0.7175	0.7181	0.7187	0.1193	0.1199	0.1205	0.1211	0.1217	0.1223
0.320	0.7229	0.7235	0.7241	0.7247	0.1253	0.1259	0.1265	0.1271	0.1277	0.1283
0.330	0.7289	0.7295	0.7301	0.7306	0.1312	0.1318	0.1324	0.1330	0.1336	0.1342
0.340	0.7348	0.7354	0.7360	0.7366	0.1371	0.1377	0.1383	0.1389	0.1395	0.1401
0.350	0.7407	0.7412	0.7418	0.7424	0.1430	0.1436	0.1442	0.1447	0.1453	0.1459
0.360	0.7465	0.7471	0.7476	0.7482	0.1488	0.1494	0.1500	0.1505	0.1511	0.1517
0.370	0.7523	0.7528	0.7534	0.7540	0.1546	0.1551	0.1557	0.1563	0.1568	0.1574
0.380	0.7580	0.7586	0.7591	0.7597	0.1603	0.1608	0.1614	0.1620	0.1625	0.1631
0.390	0.7637	0.7642	0.7648	0.7654	0.1650	0.1655	0.1660	0.1666	0.1672	0.1678
0.400	0.7694	0.7699	0.7704	0.7710	0.1715	0.1721	0.1727	0.1732	0.1738	0.1743
0.410	0.7749	0.7754	0.7760	0.7765	0.1771	0.1777	0.1782	0.1788	0.1793	0.1799
0.420	0.7804	0.7810	0.7815	0.7821	0.1826	0.1832	0.1837	0.1843	0.1848	0.1854
0.430	0.7859	0.7865	0.7870	0.7876	0.1881	0.1887	0.1892	0.1897	0.1903	0.1908
0.440	0.7914	0.7919	0.7925	0.7930	0.1934	0.1941	0.1946	0.1952	0.1957	0.1963
0.450	0.7968	0.7973	0.7979	0.7984	0.1989	0.1995	0.2000	0.2006	0.2011	0.2016
0.460	0.8022	0.8027	0.8032	0.8038	0.2043	0.2048	0.2054	0.2059	0.2064	0.2070
0.470	0.8075	0.8080	0.8086	0.8091	0.2096	0.2102	0.2107	0.2112	0.2117	0.2123
0.480	0.8128	0.8133	0.8138	0.8144	0.2149	0.2154	0.2160	0.2165	0.2170	0.2175
0.490	0.8180	0.8186	0.8191	0.8196	0.2201	0.2207	0.2212	0.2217	0.2222	0.2227
0.500	0.8233	0.8238	0.8243	0.8248	0.2253	0.2259	0.2264	0.2269	0.2274	0.2279
0.510	0.8284	0.8290	0.8295	0.8300	0.2305	0.2310	0.2315	0.2320	0.2326	0.2331
0.520	0.8336	0.8341	0.8346	0.8351	0.2356	0.2361	0.2366	0.2372	0.2377	0.2382
0.530	0.8387	0.8392	0.8397	0.8402	0.2407	0.2412	0.2417	0.2422	0.2427	0.2432
0.540	0.8438	0.8443	0.8448	0.8453	0.2448	0.2453	0.2458	0.2463	0.2468	0.2473
0.550	0.8488	0.8493	0.8498	0.8503	0.2508	0.2513	0.2518	0.2523	0.2528	0.2533
0.560	0.8538	0.8543	0.8548	0.8553	0.2558	0.2563	0.2568	0.2573	0.2578	0.2583
0.570	0.8587	0.8592	0.8597	0.8602	0.2607	0.2612	0.2617	0.2622	0.2627	0.2632
0.580	0.8637	0.8642	0.8647	0.8651	0.2656	0.2661	0.2666	0.2671	0.2676	0.2681
0.590	0.8686	0.8691	0.8695	0.8700	0.2705	0.2710	0.2715	0.2720	0.2725	0.2730
0.600	0.8734	0.8739	0.8744	0.8749	0.2754	0.2759	0.2763	0.2768	0.2773	0.2778
0.610	0.8783	0.8788	0.8792	0.8797	0.2802	0.2807	0.2812	0.2816	0.2821	0.2826
0.620	0.8831	0.8835	0.8840	0.8845	0.2850	0.2855	0.2859	0.2864	0.2869	0.2874
0.630	0.8878	0.8883	0.8888	0.8893	0.2897	0.2902	0.2907	0.2912	0.2916	0.2921
0.640	0.8926	0.8931	0.8935	0.8940	0.2945	0.2950	0.2954	0.2959	0.2963	0.2968
0.650	0.8973	0.8978	0.8982	0.8987	0.2992	0.2996	0.3000	0.3005	0.3010	0.3015
0.660	0.9020	0.9024	0.9028	0.9032	0.3038	0.3043	0.3048	0.3052	0.3057	0.3062
0.670	0.9066	0.9071	0.9075	0.9080	0.3085	0.3090	0.3094	0.3099	0.3103	0.3108

0.680	0.3112	0.3117	0.3122	0.3126	0.3131	0.3135	0.3140	0.3145	0.3149	0.3154
0.690	0.3158	0.3163	0.3167	0.3172	0.3177	0.3181	0.3186	0.3190	0.3195	0.3199
0.700	0.3204	0.3209	0.3214	0.3218	0.3222	0.3227	0.3231	0.3236	0.3240	0.3245
0.710	0.3249	0.3254	0.3258	0.3263	0.3267	0.3272	0.3276	0.3281	0.3285	0.3290
0.720	0.3294	0.3299	0.3303	0.3308	0.3312	0.3317	0.3321	0.3326	0.3330	0.3335
0.730	0.3339	0.3344	0.3348	0.3353	0.3357	0.3362	0.3366	0.3371	0.3375	0.3379
0.740	0.3384	0.3388	0.3392	0.3397	0.3402	0.3406	0.3410	0.3415	0.3419	0.3424
0.750	0.3428	0.3433	0.3437	0.3442	0.3446	0.3450	0.3455	0.3459	0.3463	0.3468
0.760	0.3472	0.3477	0.3481	0.3485	0.3490	0.3494	0.3499	0.3503	0.3507	0.3512
0.770	0.3516	0.3520	0.3525	0.3529	0.3533	0.3538	0.3542	0.3547	0.3551	0.3555
0.780	0.3560	0.3564	0.3568	0.3572	0.3577	0.3581	0.3586	0.3590	0.3594	0.3599
0.790	0.3603	0.3607	0.3611	0.3615	0.3620	0.3624	0.3628	0.3633	0.3637	0.3642
0.800	0.3646	0.3650	0.3654	0.3658	0.3663	0.3667	0.3672	0.3676	0.3680	0.3685
0.810	0.3689	0.3693	0.3697	0.3702	0.3706	0.3710	0.3714	0.3719	0.3723	0.3727
0.820	0.3731	0.3736	0.3740	0.3744	0.3748	0.3753	0.3757	0.3761	0.3765	0.3769
0.830	0.3774	0.3778	0.3782	0.3786	0.3791	0.3795	0.3799	0.3803	0.3807	0.3812
0.840	0.3816	0.3820	0.3824	0.3828	0.3833	0.3837	0.3841	0.3845	0.3849	0.3854
0.850	0.3858	0.3862	0.3866	0.3870	0.3874	0.3879	0.3883	0.3887	0.3891	0.3895
0.860	0.3899	0.3903	0.3907	0.3912	0.3916	0.3920	0.3924	0.3928	0.3932	0.3937
0.870	0.3941	0.3945	0.3949	0.3954	0.3958	0.3962	0.3966	0.3970	0.3974	0.3978
0.880	0.3982	0.3986	0.3990	0.3994	0.3998	0.4002	0.4007	0.4011	0.4015	0.4019
0.890	0.4023	0.4027	0.4031	0.4035	0.4039	0.4043	0.4047	0.4051	0.4056	0.4060
0.900	0.4064	0.4068	0.4072	0.4076	0.4080	0.4084	0.4088	0.4092	0.4096	0.4100
0.910	0.4104	0.4108	0.4112	0.4116	0.4120	0.4124	0.4128	0.4132	0.4137	0.4141
0.920	0.4145	0.4149	0.4153	0.4157	0.4161	0.4165	0.4169	0.4173	0.4177	0.4181
0.930	0.4185	0.4189	0.4193	0.4197	0.4201	0.4205	0.4209	0.4213	0.4217	0.4221
0.940	0.4223	0.4227	0.4231	0.4235	0.4240	0.4244	0.4248	0.4252	0.4256	0.4260
0.950	0.4264	0.4268	0.4272	0.4276	0.4280	0.4284	0.4288	0.4292	0.4296	0.4300
0.960	0.4304	0.4308	0.4312	0.4316	0.4320	0.4324	0.4328	0.4332	0.4336	0.4340
0.970	0.4343	0.4347	0.4351	0.4355	0.4359	0.4363	0.4367	0.4370	0.4374	0.4378
0.980	0.4382	0.4386	0.4390	0.4394	0.4398	0.4402	0.4406	0.4410	0.4414	0.4418
0.990	0.4421	0.4425	0.4429	0.4433	0.4437	0.4441	0.4445	0.4449	0.4453	0.4457
1.000	0.4460	0.4463	0.4467	0.4471	0.4475	0.4479	0.4483	0.4487	0.4490	0.4494
1.010	0.4498	0.4502	0.4506	0.4510	0.4513	0.4517	0.4521	0.4525	0.4529	0.4532
1.020	0.4536	0.4540	0.4544	0.4548	0.4552	0.4555	0.4559	0.4563	0.4567	0.4571
1.030	0.4574	0.4578	0.4582	0.4586	0.4589	0.4593	0.4597	0.4601	0.4605	0.4608
1.040	0.4612	0.4616	0.4620	0.4623	0.4627	0.4631	0.4635	0.4639	0.4642	0.4646
1.050	0.4650	0.4654	0.4657	0.4661	0.4665	0.4669	0.4672	0.4676	0.4680	0.4684
1.060	0.4687	0.4691	0.4694	0.4698	0.4702	0.4706	0.4710	0.4713	0.4717	0.4721
1.070	0.4724	0.4728	0.4732	0.4736	0.4739	0.4743	0.4747	0.4751	0.4754	0.4758
1.080	0.4762	0.4765	0.4769	0.4773	0.4776	0.4780	0.4784	0.4787	0.4791	0.4795
1.090	0.4798	0.4802	0.4804	0.4809	0.4813	0.4817	0.4820	0.4824	0.4828	0.4831
1.100	0.4835	0.4839	0.4842	0.4846	0.4850	0.4853	0.4857	0.4861	0.4864	0.4868
1.110	0.4872	0.4875	0.4879	0.4883	0.4886	0.4890	0.4893	0.4897	0.4901	0.4904
1.120	0.4908	0.4912	0.4914	0.4918	0.4922	0.4926	0.4930	0.4933	0.4937	0.4940
1.130	0.4944	0.4948	0.4951	0.4955	0.4958	0.4962	0.4966	0.4969	0.4973	0.4976
1.140	0.4980	0.4983	0.4987	0.4991	0.4994	0.4998	0.5001	0.5005	0.5008	0.5012
1.150	0.5016	0.5019	0.5023	0.5026	0.5030	0.5033	0.5037	0.5040	0.5044	0.5048
1.160	0.5051	0.5055	0.5058	0.5062	0.5065	0.5069	0.5072	0.5076	0.5079	0.5083
1.170	0.5086	0.5090	0.5093	0.5097	0.5101	0.5104	0.5108	0.5111	0.5115	0.5118
1.180	0.5122	0.5125	0.5129	0.5132	0.5136	0.5139	0.5143	0.5146	0.5150	0.5153
1.190	0.5157	0.5160	0.5164	0.5167	0.5170	0.5174	0.5177	0.5181	0.5184	0.5188
1.200	0.5191	0.5195	0.5198	0.5202	0.5205	0.5209	0.5212	0.5215	0.5219	0.5222
1.210	0.5226	0.5229	0.5233	0.5236	0.5240	0.5244	0.5246	0.5250	0.5253	0.5257
1.220	0.5264	0.5267	0.5270	0.5274	0.5277	0.5281	0.5284	0.5288	0.5291	0.5294
1.230	0.5298	0.5301	0.5304	0.5308	0.5311	0.5315	0.5318	0.5322	0.5325	0.5328
1.240	0.5332	0.5335	0.5338	0.5342	0.5345	0.5349	0.5352	0.5355	0.5359	0.5362
1.250	0.5366	0.5369	0.5372	0.5376	0.5379	0.5382	0.5386	0.5389	0.5392	0.5395
1.260	0.5399	0.5402	0.5405	0.5408	0.5411	0.5414	0.5417	0.5420	0.5423	0.5426
1.270	0.5429	0.5433	0.5436	0.5439	0.5443	0.5446	0.5449	0.5452	0.5455	0.5459

1.280	0.5662	0.5666	0.5669	0.5672	0.5676	0.5679	0.5682	0.5686	0.5689	0.5692
1.290	0.5695	0.5699	0.5702	0.5705	0.5709	0.5712	0.5715	0.5718	0.5721	0.5725
1.300	0.5728	0.5731	0.5734	0.5737	0.5740	0.5743	0.5746	0.5749	0.5752	0.5755
1.310	0.5758	0.5761	0.5764	0.5767	0.5770	0.5773	0.5776	0.5779	0.5782	0.5785
1.320	0.5788	0.5791	0.5794	0.5797	0.5800	0.5803	0.5806	0.5809	0.5812	0.5815
1.330	0.5818	0.5821	0.5824	0.5827	0.5830	0.5833	0.5836	0.5839	0.5842	0.5845
1.340	0.5848	0.5851	0.5854	0.5857	0.5860	0.5863	0.5866	0.5869	0.5872	0.5875
1.350	0.5878	0.5881	0.5884	0.5887	0.5890	0.5893	0.5896	0.5899	0.5902	0.5905
1.360	0.5908	0.5911	0.5914	0.5917	0.5920	0.5923	0.5926	0.5929	0.5932	0.5935
1.370	0.5938	0.5941	0.5944	0.5947	0.5950	0.5953	0.5956	0.5959	0.5962	0.5965
1.380	0.5968	0.5971	0.5974	0.5977	0.5980	0.5983	0.5986	0.5989	0.5992	0.5995
1.390	0.5998	0.6001	0.6004	0.6007	0.6010	0.6013	0.6016	0.6019	0.6022	0.6025
1.400	0.6028	0.6031	0.6034	0.6037	0.6040	0.6043	0.6046	0.6049	0.6052	0.6055
1.410	0.6058	0.6061	0.6064	0.6067	0.6070	0.6073	0.6076	0.6079	0.6082	0.6085
1.420	0.6088	0.6091	0.6094	0.6097	0.6100	0.6103	0.6106	0.6109	0.6112	0.6115
1.430	0.6118	0.6121	0.6124	0.6127	0.6130	0.6133	0.6136	0.6139	0.6142	0.6145
1.440	0.6148	0.6151	0.6154	0.6157	0.6160	0.6163	0.6166	0.6169	0.6172	0.6175
1.450	0.6178	0.6181	0.6184	0.6187	0.6190	0.6193	0.6196	0.6199	0.6202	0.6205
1.460	0.6208	0.6211	0.6214	0.6217	0.6220	0.6223	0.6226	0.6229	0.6232	0.6235
1.470	0.6238	0.6241	0.6244	0.6247	0.6250	0.6253	0.6256	0.6259	0.6262	0.6265
1.480	0.6268	0.6271	0.6274	0.6277	0.6280	0.6283	0.6286	0.6289	0.6292	0.6295
1.490	0.6298	0.6301	0.6304	0.6307	0.6310	0.6313	0.6316	0.6319	0.6322	0.6325
1.500	0.6328	0.6331	0.6334	0.6337	0.6340	0.6343	0.6346	0.6349	0.6352	0.6355
1.510	0.6358	0.6361	0.6364	0.6367	0.6370	0.6373	0.6376	0.6379	0.6382	0.6385
1.520	0.6388	0.6391	0.6394	0.6397	0.6400	0.6403	0.6406	0.6409	0.6412	0.6415
1.530	0.6418	0.6421	0.6424	0.6427	0.6430	0.6433	0.6436	0.6439	0.6442	0.6445
1.540	0.6448	0.6451	0.6454	0.6457	0.6460	0.6463	0.6466	0.6469	0.6472	0.6475
1.550	0.6478	0.6481	0.6484	0.6487	0.6490	0.6493	0.6496	0.6499	0.6502	0.6505
1.560	0.6508	0.6511	0.6514	0.6517	0.6520	0.6523	0.6526	0.6529	0.6532	0.6535
1.570	0.6538	0.6541	0.6544	0.6547	0.6550	0.6553	0.6556	0.6559	0.6562	0.6565
1.580	0.6568	0.6571	0.6574	0.6577	0.6580	0.6583	0.6586	0.6589	0.6592	0.6595
1.590	0.6598	0.6601	0.6604	0.6607	0.6610	0.6613	0.6616	0.6619	0.6622	0.6625
1.600	0.6628	0.6631	0.6634	0.6637	0.6640	0.6643	0.6646	0.6649	0.6652	0.6655
1.610	0.6658	0.6661	0.6664	0.6667	0.6670	0.6673	0.6676	0.6679	0.6682	0.6685
1.620	0.6688	0.6691	0.6694	0.6697	0.6700	0.6703	0.6706	0.6709	0.6712	0.6715
1.630	0.6718	0.6721	0.6724	0.6727	0.6730	0.6733	0.6736	0.6739	0.6742	0.6745
1.640	0.6748	0.6751	0.6754	0.6757	0.6760	0.6763	0.6766	0.6769	0.6772	0.6775
1.650	0.6778	0.6781	0.6784	0.6787	0.6790	0.6793	0.6796	0.6799	0.6802	0.6805
1.660	0.6808	0.6811	0.6814	0.6817	0.6820	0.6823	0.6826	0.6829	0.6832	0.6835
1.670	0.6838	0.6841	0.6844	0.6847	0.6850	0.6853	0.6856	0.6859	0.6862	0.6865
1.680	0.6868	0.6871	0.6874	0.6877	0.6880	0.6883	0.6886	0.6889	0.6892	0.6895
1.690	0.6898	0.6901	0.6904	0.6907	0.6910	0.6913	0.6916	0.6919	0.6922	0.6925
1.700	0.6928	0.6931	0.6934	0.6937	0.6940	0.6943	0.6946	0.6949	0.6952	0.6955
1.710	0.6958	0.6961	0.6964	0.6967	0.6970	0.6973	0.6976	0.6979	0.6982	0.6985
1.720	0.6988	0.6991	0.6994	0.6997	0.7000	0.7003	0.7006	0.7009	0.7012	0.7015
1.730	0.7018	0.7021	0.7024	0.7027	0.7030	0.7033	0.7036	0.7039	0.7042	0.7045
1.740	0.7048	0.7051	0.7054	0.7057	0.7060	0.7063	0.7066	0.7069	0.7072	0.7075
1.750	0.7078	0.7081	0.7084	0.7087	0.7090	0.7093	0.7096	0.7099	0.7102	0.7105
1.760	0.7108	0.7111	0.7114	0.7117	0.7120	0.7123	0.7126	0.7129	0.7132	0.7135
1.770	0.7138	0.7141	0.7144	0.7147	0.7150	0.7153	0.7156	0.7159	0.7162	0.7165
1.780	0.7168	0.7171	0.7174	0.7177	0.7180	0.7183	0.7186	0.7189	0.7192	0.7195
1.790	0.7198	0.7201	0.7204	0.7207	0.7210	0.7213	0.7216	0.7219	0.7222	0.7225
1.800	0.7228	0.7231	0.7234	0.7237	0.7240	0.7243	0.7246	0.7249	0.7252	0.7255
1.810	0.7258	0.7261	0.7264	0.7267	0.7270	0.7273	0.7276	0.7279	0.7282	0.7285
1.820	0.7288	0.7291	0.7294	0.7297	0.7300	0.7303	0.7306	0.7309	0.7312	0.7315
1.830	0.7318	0.7321	0.7324	0.7327	0.7330	0.7333	0.7336	0.7339	0.7342	0.7345
1.840	0.7348	0.7351	0.7354	0.7357	0.7360	0.7363	0.7366	0.7369	0.7372	0.7375
1.850	0.7378	0.7381	0.7384	0.7387	0.7390	0.7393	0.7396	0.7399	0.7402	0.7405
1.860	0.7408	0.7411	0.7414	0.7417	0.7420	0.7423	0.7426	0.7429	0.7432	0.7435
1.870	0.7438	0.7441	0.7444	0.7447	0.7450	0.7453	0.7456	0.7459	0.7462	0.7465
1.880	0.7468	0.7471	0.7474	0.7477	0.7480	0.7483	0.7486	0.7489	0.7492	0.7495
1.890	0.7498	0.7501	0.7504	0.7507	0.7510	0.7513	0.7516	0.7519	0.7522	0.7525

X=0 Y=±0.105W

VA/V0W	0.000	0.001	0.002	0.003	0.004	0.005	0.006	0.007	0.008	0.009
	A/W									
0.210	0.0478	0.0484	0.0491	0.0498	0.0505	0.0512	0.0518	0.0525	0.0532	0.0539
0.220	0.0545	0.0552	0.0559	0.0566	0.0572	0.0579	0.0586	0.0593	0.0599	0.0606
0.230	0.0613	0.0619	0.0626	0.0633	0.0639	0.0646	0.0653	0.0659	0.0666	0.0673
0.240	0.0679	0.0686	0.0692	0.0699	0.0706	0.0712	0.0719	0.0725	0.0732	0.0739
0.250	0.0745	0.0752	0.0758	0.0765	0.0771	0.0778	0.0784	0.0791	0.0797	0.0804
0.260	0.0810	0.0817	0.0823	0.0830	0.0836	0.0843	0.0849	0.0856	0.0862	0.0868
0.270	0.0875	0.0881	0.0888	0.0894	0.0901	0.0907	0.0913	0.0920	0.0926	0.0932
0.280	0.0939	0.0945	0.0952	0.0958	0.0964	0.0971	0.0977	0.0983	0.0990	0.0996
0.290	0.1002	0.1006	0.1015	0.1021	0.1027	0.1034	0.1040	0.1046	0.1052	0.1059
0.300	0.1065	0.1071	0.1077	0.1084	0.1090	0.1096	0.1102	0.1109	0.1115	0.1121
0.310	0.1127	0.1133	0.1139	0.1146	0.1152	0.1158	0.1164	0.1170	0.1176	0.1183
0.320	0.1169	0.1195	0.1201	0.1207	0.1213	0.1219	0.1225	0.1231	0.1238	0.1244
0.330	0.1250	0.1256	0.1262	0.1268	0.1274	0.1280	0.1286	0.1292	0.1298	0.1304
0.340	0.1310	0.1316	0.1322	0.1328	0.1334	0.1340	0.1346	0.1352	0.1358	0.1364
0.350	0.1370	0.1376	0.1382	0.1388	0.1394	0.1400	0.1406	0.1412	0.1418	0.1424
0.360	0.1429	0.1435	0.1441	0.1447	0.1453	0.1459	0.1465	0.1471	0.1477	0.1482
0.370	0.1488	0.1494	0.1500	0.1506	0.1512	0.1518	0.1523	0.1529	0.1535	0.1541
0.380	0.1547	0.1552	0.1558	0.1564	0.1570	0.1576	0.1581	0.1587	0.1593	0.1599
0.390	0.1604	0.1610	0.1616	0.1622	0.1627	0.1633	0.1639	0.1645	0.1650	0.1656
0.400	0.1662	0.1667	0.1673	0.1679	0.1685	0.1690	0.1696	0.1702	0.1707	0.1713
0.410	0.1719	0.1724	0.1730	0.1736	0.1741	0.1747	0.1752	0.1758	0.1764	0.1769
0.420	0.1775	0.1781	0.1784	0.1792	0.1797	0.1803	0.1809	0.1814	0.1820	0.1825
0.430	0.1831	0.1836	0.1842	0.1847	0.1853	0.1859	0.1864	0.1870	0.1875	0.1881
0.440	0.1886	0.1892	0.1897	0.1903	0.1908	0.1914	0.1919	0.1925	0.1930	0.1936
0.450	0.1941	0.1947	0.1952	0.1958	0.1963	0.1969	0.1974	0.1979	0.1985	0.1990
0.460	0.1996	0.2001	0.2007	0.2012	0.2017	0.2023	0.2028	0.2034	0.2039	0.2044
0.470	0.2050	0.2055	0.2061	0.2066	0.2071	0.2077	0.2082	0.2087	0.2093	0.2098
0.480	0.2105	0.2109	0.2114	0.2119	0.2125	0.2130	0.2135	0.2141	0.2146	0.2151
0.490	0.2157	0.2162	0.2167	0.2173	0.2178	0.2183	0.2188	0.2194	0.2199	0.2204
0.500	0.2209	0.2215	0.2220	0.2225	0.2231	0.2236	0.2241	0.2246	0.2251	0.2257
0.510	0.2262	0.2267	0.2272	0.2278	0.2283	0.2288	0.2293	0.2298	0.2304	0.2309
0.520	0.2314	0.2319	0.2324	0.2329	0.2335	0.2340	0.2345	0.2350	0.2355	0.2360
0.530	0.2366	0.2371	0.2376	0.2381	0.2386	0.2391	0.2396	0.2401	0.2407	0.2412
0.540	0.2417	0.2422	0.2427	0.2432	0.2437	0.2442	0.2447	0.2452	0.2458	0.2463
0.550	0.2463	0.2473	0.2478	0.2483	0.2488	0.2493	0.2498	0.2503	0.2508	0.2513
0.560	0.2513	0.2523	0.2528	0.2533	0.2538	0.2543	0.2548	0.2553	0.2558	0.2563
0.570	0.2566	0.2573	0.2578	0.2583	0.2588	0.2593	0.2598	0.2603	0.2608	0.2613
0.580	0.2618	0.2623	0.2628	0.2633	0.2638	0.2643	0.2648	0.2653	0.2658	0.2663
0.590	0.2667	0.2672	0.2677	0.2682	0.2687	0.2692	0.2697	0.2702	0.2707	0.2712
0.600	0.2717	0.2721	0.2724	0.2731	0.2736	0.2741	0.2746	0.2751	0.2756	0.2760
0.610	0.2765	0.2770	0.2775	0.2780	0.2785	0.2790	0.2794	0.2799	0.2804	0.2809
0.620	0.2814	0.2818	0.2823	0.2828	0.2833	0.2838	0.2843	0.2847	0.2852	0.2857
0.630	0.2862	0.2867	0.2871	0.2876	0.2881	0.2886	0.2890	0.2895	0.2900	0.2905
0.640	0.2910	0.2914	0.2919	0.2924	0.2929	0.2933	0.2938	0.2943	0.2947	0.2952
0.650	0.2957	0.2962	0.2966	0.2971	0.2976	0.2981	0.2985	0.2990	0.2995	0.2999
0.660	0.3004	0.3009	0.3013	0.3018	0.3023	0.3028	0.3032	0.3037	0.3042	0.3046
0.670	0.3051	0.3056	0.3060	0.3065	0.3070	0.3074	0.3079	0.3083	0.3088	0.3093

0.680	0.3097	0.3102	0.3107	0.3111	0.3116	0.3121	0.3125	0.3130	0.3134	0.3139
0.690	0.3144	0.3148	0.3153	0.3157	0.3162	0.3167	0.3171	0.3176	0.3180	0.3185
0.700	0.3190	0.3194	0.3199	0.3203	0.3208	0.3212	0.3217	0.3222	0.3226	0.3231
0.710	0.3225	0.3229	0.3234	0.3238	0.3243	0.3247	0.3252	0.3257	0.3261	0.3266
0.720	0.3251	0.3255	0.3260	0.3264	0.3269	0.3273	0.3278	0.3282	0.3287	0.3291
0.730	0.3285	0.3289	0.3294	0.3298	0.3303	0.3307	0.3312	0.3317	0.3321	0.3326
0.740	0.3300	0.3304	0.3309	0.3313	0.3318	0.3322	0.3327	0.3331	0.3336	0.3341
0.750	0.3326	0.3330	0.3335	0.3339	0.3344	0.3348	0.3353	0.3357	0.3361	0.3366
0.760	0.3350	0.3354	0.3359	0.3363	0.3368	0.3372	0.3377	0.3381	0.3386	0.3390
0.770	0.3367	0.3371	0.3375	0.3380	0.3384	0.3388	0.3393	0.3397	0.3401	0.3405
0.780	0.3400	0.3404	0.3408	0.3413	0.3417	0.3421	0.3426	0.3430	0.3434	0.3438
0.790	0.3425	0.3429	0.3433	0.3438	0.3442	0.3446	0.3451	0.3455	0.3459	0.3463
0.800	0.3457	0.3461	0.3465	0.3470	0.3474	0.3478	0.3483	0.3487	0.3491	0.3495
0.810	0.3489	0.3493	0.3497	0.3502	0.3506	0.3510	0.3515	0.3519	0.3523	0.3527
0.820	0.3509	0.3513	0.3517	0.3522	0.3526	0.3530	0.3535	0.3539	0.3543	0.3547
0.830	0.3531	0.3535	0.3539	0.3544	0.3548	0.3552	0.3557	0.3561	0.3565	0.3569
0.840	0.3543	0.3547	0.3551	0.3556	0.3560	0.3564	0.3569	0.3573	0.3577	0.3581
0.850	0.3561	0.3565	0.3569	0.3573	0.3578	0.3582	0.3586	0.3590	0.3594	0.3598
0.860	0.3573	0.3577	0.3581	0.3585	0.3590	0.3594	0.3598	0.4000	0.4004	0.4008
0.870	0.3585	0.3589	0.3593	0.3597	0.3601	0.3605	0.3610	0.4004	0.4008	0.4012
0.880	0.3597	0.3601	0.3605	0.3609	0.3613	0.3617	0.3621	0.4012	0.4016	0.4020
0.890	0.3609	0.3613	0.3617	0.3621	0.3625	0.3629	0.3633	0.4020	0.4024	0.4028
0.900	0.3621	0.3625	0.3629	0.3633	0.3637	0.3641	0.3645	0.4028	0.4032	0.4036
0.910	0.3633	0.3637	0.3641	0.3645	0.3649	0.3653	0.3657	0.4036	0.4040	0.4044
0.920	0.3645	0.3649	0.3653	0.3657	0.3661	0.3665	0.3669	0.4044	0.4048	0.4052
0.930	0.3657	0.3661	0.3665	0.3669	0.3673	0.3677	0.3681	0.4052	0.4056	0.4060
0.940	0.3669	0.3673	0.3677	0.3681	0.3685	0.3689	0.3693	0.4060	0.4064	0.4068
0.950	0.3681	0.3685	0.3689	0.3693	0.3697	0.3701	0.3705	0.4068	0.4072	0.4076
0.960	0.3693	0.3697	0.3701	0.3705	0.3709	0.3713	0.3717	0.4076	0.4080	0.4084
0.970	0.3705	0.3709	0.3713	0.3717	0.3721	0.3725	0.3729	0.4084	0.4088	0.4092
0.980	0.3717	0.3721	0.3725	0.3729	0.3733	0.3737	0.3741	0.4092	0.4096	0.4100
0.990	0.3729	0.3733	0.3737	0.3741	0.3745	0.3749	0.3753	0.4100	0.4104	0.4108
1.000	0.3741	0.3745	0.3749	0.3753	0.3757	0.3761	0.3765	0.4108	0.4112	0.4116
1.010	0.3753	0.3757	0.3761	0.3765	0.3769	0.3773	0.3777	0.4116	0.4120	0.4124
1.020	0.3765	0.3769	0.3773	0.3777	0.3781	0.3785	0.3789	0.4124	0.4128	0.4132
1.030	0.3777	0.3781	0.3785	0.3789	0.3793	0.3797	0.3801	0.4132	0.4136	0.4140
1.040	0.3789	0.3793	0.3797	0.3801	0.3805	0.3809	0.3813	0.4140	0.4144	0.4148
1.050	0.3801	0.3805	0.3809	0.3813	0.3817	0.3821	0.3825	0.4148	0.4152	0.4156
1.060	0.3813	0.3817	0.3821	0.3825	0.3829	0.3833	0.3837	0.4156	0.4160	0.4164
1.070	0.3825	0.3829	0.3833	0.3837	0.3841	0.3845	0.3849	0.4164	0.4168	0.4172
1.080	0.3837	0.3841	0.3845	0.3849	0.3853	0.3857	0.3861	0.4172	0.4176	0.4180
1.090	0.3849	0.3853	0.3857	0.3861	0.3865	0.3869	0.3873	0.4180	0.4184	0.4188
1.100	0.3861	0.3865	0.3869	0.3873	0.3877	0.3881	0.3885	0.4188	0.4192	0.4196
1.110	0.3873	0.3877	0.3881	0.3885	0.3889	0.3893	0.3897	0.4196	0.4200	0.4204
1.120	0.3885	0.3889	0.3893	0.3897	0.3901	0.3905	0.3909	0.4204	0.4208	0.4212
1.130	0.3897	0.3901	0.3905	0.3909	0.3913	0.3917	0.3921	0.4212	0.4216	0.4220
1.140	0.3909	0.3913	0.3917	0.3921	0.3925	0.3929	0.3933	0.4220	0.4224	0.4228
1.150	0.3921	0.3925	0.3929	0.3933	0.3937	0.3941	0.3945	0.4228	0.4232	0.4236
1.160	0.3933	0.3937	0.3941	0.3945	0.3949	0.3953	0.3957	0.4236	0.4240	0.4244
1.170	0.3945	0.3949	0.3953	0.3957	0.3961	0.3965	0.3969	0.4244	0.4248	0.4252
1.180	0.3957	0.3961	0.3965	0.3969	0.3973	0.3977	0.3981	0.4252	0.4256	0.4260
1.190	0.3969	0.3973	0.3977	0.3981	0.3985	0.3989	0.3993	0.4260	0.4264	0.4268
1.200	0.3981	0.3985	0.3989	0.3993	0.3997	0.4001	0.4005	0.4268	0.4272	0.4276
1.210	0.3993	0.3997	0.4001	0.4005	0.4009	0.4013	0.4017	0.4276	0.4280	0.4284
1.220	0.4005	0.4009	0.4013	0.4017	0.4021	0.4025	0.4029	0.4284	0.4288	0.4292
1.230	0.4017	0.4021	0.4025	0.4029	0.4033	0.4037	0.4041	0.4292	0.4296	0.4300
1.240	0.4029	0.4033	0.4037	0.4041	0.4045	0.4049	0.4053	0.4300	0.4304	0.4308
1.250	0.4041	0.4045	0.4049	0.4053	0.4057	0.4061	0.4065	0.4308	0.4312	0.4316
1.260	0.4053	0.4057	0.4061	0.4065	0.4069	0.4073	0.4077	0.4316	0.4320	0.4324
1.270	0.4065	0.4069	0.4073	0.4077	0.4081	0.4085	0.4089	0.4324	0.4328	0.4332
1.280	0.4077	0.4081	0.4085	0.4089	0.4093	0.4097	0.4101	0.4332	0.4336	0.4340
1.290	0.4089	0.4093	0.4097	0.4101	0.4105	0.4109	0.4113	0.4340	0.4344	0.4348
1.300	0.4101	0.4105	0.4109	0.4113	0.4117	0.4121	0.4125	0.4348	0.4352	0.4356
1.310	0.4113	0.4117	0.4121	0.4125	0.4129	0.4133	0.4137	0.4356	0.4360	0.4364
1.320	0.4125	0.4129	0.4133	0.4137	0.4141	0.4145	0.4149	0.4364	0.4368	0.4372
1.330	0.4137	0.4141	0.4145	0.4149	0.4153	0.4157	0.4161	0.4372	0.4376	0.4380
1.340	0.4149	0.4153	0.4157	0.4161	0.4165	0.4169	0.4173	0.4380	0.4384	0.4388
1.350	0.4161	0.4165	0.4169	0.4173	0.4177	0.4181	0.4185	0.4388	0.4392	0.4396
1.360	0.4173	0.4177	0.4181	0.4185	0.4189	0.4193	0.4197	0.4396	0.4400	0.4404
1.370	0.4185	0.4189	0.4193	0.4197	0.4201	0.4205	0.4209	0.4404	0.4408	0.4412
1.380	0.4197	0.4201	0.4205	0.4209	0.4213	0.4217	0.4221	0.4412	0.4416	0.4420
1.390	0.4209	0.4213	0.4217	0.4221	0.4225	0.4229	0.4233	0.4420	0.4424	0.4428
1.400	0.4221	0.4225	0.4229	0.4233	0.4237	0.4241	0.4245	0.4428	0.4432	0.4436
1.410	0.4233	0.4237	0.4241	0.4245	0.4249	0.4253	0.4257	0.4436	0.4440	0.4444
1.420	0.4245	0.4249	0.4253	0.4257	0.4261	0.4265	0.4269	0.4444	0.4448	0.4452
1.430	0.4257	0.4261	0.4265	0.4269	0.4273	0.4277	0.4281	0.4452	0.4456	0.4460
1.440	0.4269	0.4273	0.4277	0.4281	0.4285	0.4289	0.4293	0.4460	0.4464	0.4468
1.450	0.4281	0.4285	0.4289	0.4293	0.4297	0.4301	0.4305	0.4468	0.4472	0.4476
1.460	0.4293	0.4297	0.4301	0.4305	0.4309	0.4313	0.4317	0.4476	0.4480	0.4484
1.470	0.4305	0.4309	0.4313	0.4317	0.4321	0.4325	0.4329	0.4484	0.4488	0.4492
1.480	0.4317	0.4321	0.4325	0.4329	0.4333	0.4337	0.4341	0.4492	0.4496	0.4500
1.490	0.4329	0.4333	0.4337	0.4341	0.4345	0.4349	0.4353	0.4500	0.4504	0.4508
1.500	0.4341	0.4345	0.4349	0.4353	0.4357	0.4361	0.4365	0.4508	0.4512	0.4516
1.510	0.4353	0.4357	0.4361	0.4365	0.4369	0.4373	0.4377	0.4516	0.4520	0.4524
1.520	0.4365	0.4369	0.4373	0.4377	0.4381	0.4385	0.4389	0.4524	0.4528	0.4532
1.530	0.4377	0.4381	0.4385	0.4389	0.4393	0.4397	0.4401	0.4532	0.4536	0.4540
1.540	0.4389	0.4393	0.4397	0.4401	0.4405	0.4409	0.4413	0.4540	0.4544	0.4548
1.550	0.4401	0.4405	0.4409	0.4413	0.4417	0.4421	0.4425	0.4548	0.4552	0.4556
1.560	0.4413	0.4417	0.4421	0.4425	0.4429	0.4433	0.4437	0.4556	0.4560	0.4564
1.570	0.4425	0.4429	0.4433	0.4437	0.4441	0.4445	0.4449	0.4564	0.4568	0.4572
1.580	0.4437	0.4441	0.4445	0.4449	0.4453	0.4457	0.4461	0.4572	0.4576	0.4580
1.590	0.4449	0.4453	0.4457	0.4461	0.4465	0.4469	0.4473	0.4580	0.4584	0.4588
1.600	0.4461	0.4465	0.4469	0.4473	0.4477	0.4481	0.4485	0.4588	0.4592	0.4596
1.610	0.4473	0.4477	0.4481	0.4485	0.4489	0.4493	0.4497	0.4596	0.4600	0.4604
1.620	0.4485	0.4489	0.4493	0.4497	0.4501	0.4505	0.4509	0.4604	0.4608	0.4612
1.630	0.4497	0.4501	0.4505	0.4509	0.4513	0.4517	0.4521	0.4612	0.4616	0.4620
1.640	0.4509	0.4513	0.4517	0.4521	0.4525	0.4529	0.4533	0.4620	0.4624	0.4628
1.650	0.4521	0.4525	0.4529	0.4533	0.4537	0.4541	0.4545	0.4628	0.4632	0.4636
1.660	0.4533	0.4537	0.4541	0.4545	0.					

1.280	0.5455	0.5458	0.5462	0.5465	0.5468	0.5472	0.5475	0.5478	0.5481	0.5485
1.290	0.5468	0.5471	0.5474	0.5478	0.5481	0.5485	0.5488	0.5491	0.5494	0.5498
1.300	0.5521	0.5524	0.5528	0.5531	0.5534	0.5537	0.5540	0.5543	0.5546	0.5550
1.310	0.5554	0.5557	0.5560	0.5564	0.5567	0.5570	0.5573	0.5577	0.5580	0.5583
1.320	0.5566	0.5569	0.5572	0.5576	0.5579	0.5582	0.5585	0.5588	0.5591	0.5594
1.330	0.5619	0.5622	0.5625	0.5628	0.5631	0.5635	0.5638	0.5641	0.5644	0.5648
1.340	0.5651	0.5654	0.5657	0.5660	0.5664	0.5667	0.5670	0.5673	0.5676	0.5680
1.350	0.5653	0.5656	0.5659	0.5662	0.5666	0.5669	0.5672	0.5675	0.5678	0.5681
1.360	0.5715	0.5718	0.5721	0.5724	0.5727	0.5730	0.5734	0.5737	0.5740	0.5743
1.370	0.5746	0.5749	0.5752	0.5756	0.5759	0.5762	0.5765	0.5768	0.5771	0.5775
1.380	0.5778	0.5781	0.5784	0.5787	0.5790	0.5793	0.5796	0.5800	0.5803	0.5806
1.390	0.5809	0.5812	0.5815	0.5818	0.5821	0.5824	0.5828	0.5831	0.5834	0.5837
1.400	0.5840	0.5843	0.5846	0.5849	0.5852	0.5855	0.5858	0.5862	0.5865	0.5868
1.410	0.5871	0.5874	0.5877	0.5880	0.5883	0.5886	0.5889	0.5892	0.5895	0.5898
1.420	0.5901	0.5904	0.5907	0.5911	0.5914	0.5917	0.5920	0.5923	0.5926	0.5929
1.430	0.5932	0.5935	0.5938	0.5941	0.5944	0.5947	0.5950	0.5953	0.5956	0.5959
1.440	0.5962	0.5965	0.5968	0.5971	0.5974	0.5977	0.5980	0.5983	0.5986	0.5989
1.450	0.5992	0.5995	0.5998	0.6001	0.6004	0.6007	0.6010	0.6013	0.6016	0.6019
1.460	0.6022	0.6025	0.6028	0.6031	0.6034	0.6037	0.6040	0.6043	0.6046	0.6049
1.470	0.6052	0.6055	0.6058	0.6061	0.6064	0.6067	0.6070	0.6072	0.6075	0.6078
1.480	0.6081	0.6084	0.6087	0.6090	0.6093	0.6096	0.6099	0.6102	0.6105	0.6108
1.490	0.6111	0.6113	0.6116	0.6119	0.6122	0.6125	0.6128	0.6131	0.6134	0.6137
1.500	0.6140	0.6143	0.6146	0.6148	0.6151	0.6154	0.6157	0.6160	0.6163	0.6166
1.510	0.6169	0.6171	0.6174	0.6177	0.6180	0.6183	0.6186	0.6189	0.6192	0.6194
1.520	0.6197	0.6200	0.6203	0.6206	0.6209	0.6212	0.6215	0.6218	0.6221	0.6223
1.530	0.6226	0.6229	0.6231	0.6234	0.6237	0.6240	0.6243	0.6246	0.6248	0.6251
1.540	0.6254	0.6257	0.6260	0.6263	0.6265	0.6268	0.6271	0.6274	0.6277	0.6279
1.550	0.6282	0.6285	0.6288	0.6291	0.6293	0.6296	0.6299	0.6302	0.6305	0.6307
1.560	0.6310	0.6313	0.6316	0.6318	0.6321	0.6324	0.6327	0.6330	0.6332	0.6335
1.570	0.6338	0.6341	0.6344	0.6346	0.6349	0.6352	0.6354	0.6357	0.6360	0.6363
1.580	0.6365	0.6368	0.6371	0.6374	0.6376	0.6379	0.6382	0.6385	0.6387	0.6390
1.590	0.6393	0.6395	0.6398	0.6401	0.6404	0.6406	0.6409	0.6412	0.6414	0.6417
1.600	0.6420	0.6423	0.6425	0.6428	0.6431	0.6433	0.6436	0.6439	0.6441	0.6444
1.610	0.6447	0.6450	0.6452	0.6455	0.6458	0.6460	0.6463	0.6466	0.6468	0.6471
1.620	0.6474	0.6476	0.6478	0.6481	0.6484	0.6487	0.6490	0.6492	0.6495	0.6498
1.630	0.6503	0.6505	0.6508	0.6511	0.6513	0.6515	0.6518	0.6521	0.6524	0.6527
1.640	0.6532	0.6534	0.6537	0.6539	0.6542	0.6544	0.6547	0.6550	0.6552	0.6555
1.650	0.6558	0.6561	0.6564	0.6566	0.6569	0.6571	0.6574	0.6577	0.6580	0.6583
1.660	0.6586	0.6589	0.6591	0.6594	0.6596	0.6599	0.6602	0.6605	0.6607	0.6610
1.670	0.6614	0.6617	0.6619	0.6622	0.6624	0.6627	0.6630	0.6632	0.6635	0.6638
1.680	0.6641	0.6643	0.6646	0.6648	0.6651	0.6653	0.6656	0.6658	0.6661	0.6663
1.690	0.6666	0.6668	0.6671	0.6673	0.6676	0.6678	0.6681	0.6683	0.6686	0.6688
1.700	0.6691	0.6693	0.6696	0.6698	0.6701	0.6703	0.6706	0.6708	0.6711	0.6713
1.710	0.6716	0.6718	0.6721	0.6723	0.6726	0.6728	0.6731	0.6733	0.6735	0.6738
1.720	0.6740	0.6743	0.6745	0.6748	0.6750	0.6753	0.6755	0.6757	0.6760	0.6762
1.730	0.6765	0.6767	0.6770	0.6772	0.6774	0.6777	0.6779	0.6781	0.6784	0.6786
1.740	0.6789	0.6791	0.6794	0.6796	0.6799	0.6801	0.6803	0.6806	0.6808	0.6811
1.750	0.6814	0.6816	0.6818	0.6821	0.6823	0.6825	0.6828	0.6830	0.6833	0.6835
1.760	0.6838	0.6840	0.6843	0.6845	0.6848	0.6850	0.6853	0.6855	0.6858	0.6860
1.770	0.6863	0.6865	0.6868	0.6870	0.6873	0.6875	0.6878	0.6880	0.6883	0.6885
1.780	0.6888	0.6890	0.6893	0.6895	0.6898	0.6900	0.6903	0.6905	0.6908	0.6910
1.790	0.6913	0.6915	0.6918	0.6920	0.6923	0.6925	0.6928	0.6930	0.6933	0.6935
1.800	0.6938	0.6940	0.6943	0.6945	0.6948	0.6950	0.6953	0.6955	0.6958	0.6960
1.810	0.6963	0.6965	0.6968	0.6970	0.6973	0.6975	0.6978	0.6980	0.6983	0.6985
1.820	0.6988	0.6990	0.6993	0.6995	0.6998	0.7000	0.7003	0.7005	0.7008	0.7010
1.830	0.7013	0.7015	0.7018	0.7020	0.7023	0.7025	0.7028	0.7030	0.7033	0.7035
1.840	0.7038	0.7040	0.7043	0.7045	0.7048	0.7050	0.7053	0.7055	0.7058	0.7060
1.850	0.7063	0.7065	0.7068	0.7070	0.7073	0.7075	0.7078	0.7080	0.7083	0.7085
1.860	0.7088	0.7090	0.7093	0.7095	0.7098	0.7100	0.7103	0.7105	0.7108	0.7110
1.870	0.7113	0.7115	0.7118	0.7120	0.7123	0.7125	0.7128	0.7130	0.7133	0.7135

X=0 Y=±0.110W

VA/VM	0.000	0.001	0.002	0.003	0.004	0.005	0.006	0.007	0.008	0.009
	A/W									
0.220	0.0467	0.0494	0.0501	0.0508	0.0515	0.0522	0.0529	0.0536	0.0543	0.0550
0.230	0.0557	0.0563	0.0570	0.0577	0.0584	0.0591	0.0598	0.0605	0.0611	0.0618
0.240	0.0652	0.0632	0.0630	0.0645	0.0652	0.0659	0.0666	0.0672	0.0679	0.0686
0.250	0.0693	0.0695	0.0704	0.0713	0.0719	0.0726	0.0733	0.0740	0.0746	0.0753
0.260	0.0760	0.0766	0.0773	0.0779	0.0786	0.0793	0.0799	0.0806	0.0813	0.0819
0.270	0.0826	0.0832	0.0830	0.0845	0.0852	0.0859	0.0865	0.0872	0.0878	0.0885
0.280	0.0891	0.0898	0.0904	0.0911	0.0917	0.0924	0.0930	0.0937	0.0943	0.0950
0.290	0.0956	0.0963	0.0969	0.0976	0.0982	0.0988	0.0995	0.1001	0.1008	0.1014
0.300	0.1020	0.1027	0.1033	0.1040	0.1046	0.1052	0.1059	0.1065	0.1071	0.1078
0.310	0.1084	0.1090	0.1097	0.1103	0.1109	0.1116	0.1122	0.1128	0.1134	0.1141
0.320	0.1147	0.1153	0.1160	0.1166	0.1172	0.1178	0.1185	0.1191	0.1197	0.1203
0.330	0.1209	0.1216	0.1222	0.1228	0.1234	0.1240	0.1246	0.1253	0.1259	0.1265
0.340	0.1271	0.1277	0.1283	0.1290	0.1296	0.1302	0.1308	0.1314	0.1320	0.1326
0.350	0.1332	0.1338	0.1344	0.1351	0.1357	0.1363	0.1369	0.1375	0.1381	0.1387
0.360	0.1393	0.1399	0.1405	0.1411	0.1417	0.1423	0.1429	0.1435	0.1441	0.1447
0.370	0.1453	0.1459	0.1465	0.1471	0.1477	0.1483	0.1489	0.1495	0.1501	0.1506
0.380	0.1512	0.1518	0.1524	0.1530	0.1536	0.1542	0.1548	0.1554	0.1559	0.1565
0.390	0.1571	0.1577	0.1583	0.1589	0.1595	0.1600	0.1606	0.1612	0.1618	0.1624
0.400	0.1630	0.1635	0.1641	0.1647	0.1653	0.1659	0.1664	0.1670	0.1676	0.1682
0.410	0.1687	0.1693	0.1699	0.1705	0.1710	0.1716	0.1722	0.1728	0.1733	0.1739
0.420	0.1745	0.1750	0.1756	0.1762	0.1767	0.1773	0.1779	0.1785	0.1790	0.1796
0.430	0.1801	0.1807	0.1813	0.1818	0.1824	0.1830	0.1835	0.1841	0.1847	0.1852
0.440	0.1853	0.1863	0.1869	0.1875	0.1880	0.1886	0.1891	0.1897	0.1903	0.1908
0.450	0.1914	0.1919	0.1925	0.1930	0.1936	0.1941	0.1947	0.1952	0.1958	0.1963
0.460	0.1969	0.1974	0.1980	0.1985	0.1991	0.1996	0.2002	0.2007	0.2013	0.2018
0.470	0.2024	0.2029	0.2035	0.2040	0.2046	0.2051	0.2057	0.2062	0.2067	0.2073
0.480	0.2078	0.2084	0.2089	0.2094	0.2100	0.2105	0.2111	0.2116	0.2121	0.2127
0.490	0.2132	0.2138	0.2143	0.2148	0.2154	0.2159	0.2164	0.2170	0.2175	0.2180
0.500	0.2186	0.2191	0.2196	0.2202	0.2207	0.2212	0.2218	0.2223	0.2228	0.2234
0.510	0.2239	0.2244	0.2249	0.2255	0.2260	0.2265	0.2270	0.2276	0.2281	0.2286
0.520	0.2291	0.2297	0.2302	0.2307	0.2312	0.2318	0.2323	0.2328	0.2333	0.2339
0.530	0.2344	0.2349	0.2354	0.2359	0.2365	0.2370	0.2375	0.2380	0.2385	0.2390
0.540	0.2396	0.2401	0.2406	0.2411	0.2416	0.2421	0.2426	0.2432	0.2437	0.2442
0.550	0.2447	0.2452	0.2457	0.2462	0.2467	0.2473	0.2478	0.2483	0.2488	0.2493
0.560	0.2498	0.2503	0.2508	0.2513	0.2518	0.2523	0.2528	0.2533	0.2539	0.2544
0.570	0.2549	0.2554	0.2559	0.2564	0.2569	0.2574	0.2579	0.2584	0.2589	0.2594
0.580	0.2599	0.2604	0.2609	0.2614	0.2619	0.2624	0.2629	0.2634	0.2639	0.2644
0.590	0.2659	0.2654	0.2659	0.2664	0.2669	0.2674	0.2679	0.2684	0.2689	0.2693
0.600	0.2698	0.2703	0.2708	0.2713	0.2718	0.2723	0.2728	0.2733	0.2738	0.2743
0.610	0.2743	0.2748	0.2752	0.2757	0.2762	0.2767	0.2772	0.2777	0.2782	0.2787
0.620	0.2796	0.2801	0.2806	0.2811	0.2816	0.2821	0.2826	0.2830	0.2835	0.2840
0.630	0.2845	0.2850	0.2855	0.2860	0.2864	0.2869	0.2874	0.2879	0.2883	0.2888
0.640	0.2893	0.2898	0.2903	0.2907	0.2912	0.2917	0.2922	0.2927	0.2931	0.2936
0.650	0.2941	0.2946	0.2950	0.2955	0.2960	0.2965	0.2969	0.2974	0.2979	0.2984
0.660	0.2988	0.2993	0.2998	0.3003	0.3007	0.3012	0.3017	0.3021	0.3026	0.3031
0.670	0.3035	0.3040	0.3045	0.3050	0.3054	0.3059	0.3064	0.3068	0.3073	0.3078
0.680	0.3082	0.3087	0.3092	0.3096	0.3101	0.3106	0.3110	0.3115	0.3120	0.3124

0.690	0.3129	0.3133	0.3138	0.3143	0.3147	0.3152	0.3157	0.3161	0.3166	0.3170
0.700	0.3175	0.3180	0.3184	0.3188	0.3193	0.3198	0.3203	0.3207	0.3212	0.3216
0.710	0.3221	0.3226	0.3230	0.3235	0.3240	0.3244	0.3248	0.3253	0.3258	0.3262
0.720	0.3267	0.3271	0.3276	0.3280	0.3285	0.3289	0.3294	0.3298	0.3303	0.3307
0.730	0.3312	0.3316	0.3321	0.3325	0.3330	0.3335	0.3339	0.3344	0.3348	0.3353
0.740	0.3357	0.3361	0.3366	0.3370	0.3375	0.3379	0.3384	0.3388	0.3393	0.3397
0.750	0.3402	0.3406	0.3411	0.3415	0.3420	0.3424	0.3428	0.3433	0.3437	0.3442
0.760	0.3460	0.3464	0.3469	0.3474	0.3478	0.3483	0.3487	0.3492	0.3496	0.3501
0.770	0.3500	0.3505	0.3510	0.3514	0.3519	0.3524	0.3528	0.3533	0.3537	0.3542
0.780	0.3554	0.3558	0.3563	0.3567	0.3572	0.3576	0.3581	0.3585	0.3590	0.3594
0.790	0.3598	0.3602	0.3607	0.3611	0.3616	0.3620	0.3625	0.3629	0.3634	0.3638
0.800	0.3622	0.3626	0.3631	0.3635	0.3640	0.3644	0.3649	0.3653	0.3658	0.3662
0.810	0.3665	0.3669	0.3674	0.3678	0.3683	0.3687	0.3692	0.3696	0.3701	0.3705
0.820	0.3708	0.3712	0.3716	0.3720	0.3725	0.3729	0.3734	0.3738	0.3743	0.3747
0.830	0.3750	0.3755	0.3759	0.3763	0.3768	0.3772	0.3777	0.3781	0.3786	0.3790
0.840	0.3793	0.3797	0.3801	0.3805	0.3810	0.3814	0.3818	0.3823	0.3827	0.3831
0.850	0.3835	0.3839	0.3843	0.3847	0.3852	0.3856	0.3860	0.3865	0.3869	0.3873
0.860	0.3877	0.3881	0.3885	0.3889	0.3893	0.3898	0.3902	0.3906	0.3910	0.3914
0.870	0.3918	0.3923	0.3927	0.3931	0.3935	0.3939	0.3943	0.3948	0.3952	0.3956
0.880	0.3960	0.3964	0.3968	0.3972	0.3976	0.3981	0.3985	0.3989	0.3993	0.3997
0.890	0.4001	0.4005	0.4009	0.4013	0.4018	0.4022	0.4026	0.4030	0.4034	0.4038
0.900	0.4042	0.4046	0.4050	0.4054	0.4058	0.4063	0.4067	0.4071	0.4075	0.4079
0.910	0.4087	0.4091	0.4095	0.4099	0.4103	0.4107	0.4111	0.4115	0.4119	0.4123
0.920	0.4125	0.4128	0.4132	0.4136	0.4140	0.4144	0.4148	0.4152	0.4156	0.4160
0.930	0.4164	0.4168	0.4172	0.4176	0.4180	0.4184	0.4188	0.4192	0.4196	0.4200
0.940	0.4204	0.4208	0.4212	0.4216	0.4220	0.4224	0.4228	0.4232	0.4236	0.4240
0.950	0.4244	0.4248	0.4252	0.4256	0.4260	0.4264	0.4268	0.4272	0.4276	0.4280
0.960	0.4283	0.4287	0.4291	0.4295	0.4299	0.4303	0.4307	0.4311	0.4315	0.4319
0.970	0.4323	0.4327	0.4331	0.4335	0.4339	0.4343	0.4347	0.4351	0.4355	0.4359
0.980	0.4362	0.4366	0.4370	0.4374	0.4378	0.4382	0.4386	0.4390	0.4394	0.4398
0.990	0.4401	0.4405	0.4409	0.4413	0.4417	0.4421	0.4425	0.4429	0.4433	0.4437
1.000	0.4440	0.4444	0.4448	0.4452	0.4456	0.4460	0.4464	0.4468	0.4472	0.4476
1.010	0.4479	0.4483	0.4487	0.4491	0.4495	0.4499	0.4503	0.4507	0.4511	0.4515
1.020	0.4517	0.4521	0.4525	0.4529	0.4533	0.4537	0.4541	0.4545	0.4549	0.4553
1.030	0.4553	0.4557	0.4561	0.4565	0.4569	0.4573	0.4577	0.4581	0.4585	0.4589
1.040	0.4593	0.4597	0.4601	0.4605	0.4609	0.4613	0.4617	0.4621	0.4625	0.4629
1.050	0.4631	0.4635	0.4639	0.4643	0.4647	0.4651	0.4655	0.4659	0.4663	0.4667
1.060	0.4669	0.4673	0.4677	0.4681	0.4685	0.4689	0.4693	0.4697	0.4701	0.4705
1.070	0.4706	0.4710	0.4714	0.4718	0.4722	0.4726	0.4730	0.4734	0.4738	0.4742
1.080	0.4743	0.4747	0.4751	0.4755	0.4759	0.4763	0.4767	0.4771	0.4775	0.4779
1.090	0.4780	0.4784	0.4788	0.4792	0.4796	0.4800	0.4804	0.4808	0.4812	0.4816
1.100	0.4817	0.4821	0.4825	0.4829	0.4833	0.4837	0.4841	0.4845	0.4849	0.4853
1.110	0.4854	0.4858	0.4862	0.4866	0.4870	0.4874	0.4878	0.4882	0.4886	0.4890
1.120	0.4890	0.4894	0.4898	0.4902	0.4906	0.4910	0.4914	0.4918	0.4922	0.4926
1.130	0.4927	0.4931	0.4935	0.4939	0.4943	0.4947	0.4951	0.4955	0.4959	0.4963
1.140	0.4963	0.4967	0.4971	0.4975	0.4979	0.4983	0.4987	0.4991	0.4995	0.4999
1.150	0.4998	0.5002	0.5006	0.5010	0.5014	0.5018	0.5022	0.5026	0.5030	0.5034
1.160	0.5034	0.5038	0.5042	0.5046	0.5050	0.5054	0.5058	0.5062	0.5066	0.5070
1.170	0.5070	0.5073	0.5077	0.5080	0.5084	0.5088	0.5092	0.5096	0.5100	0.5104
1.180	0.5105	0.5108	0.5112	0.5115	0.5119	0.5122	0.5126	0.5129	0.5133	0.5136
1.190	0.5140	0.5143	0.5147	0.5150	0.5154	0.5157	0.5161	0.5164	0.5168	0.5171
1.200	0.5175	0.5178	0.5182	0.5185	0.5189	0.5192	0.5196	0.5199	0.5203	0.5206
1.210	0.5210	0.5213	0.5217	0.5220	0.5223	0.5227	0.5230	0.5234	0.5237	0.5241
1.220	0.5244	0.5248	0.5251	0.5254	0.5258	0.5261	0.5265	0.5268	0.5272	0.5275
1.230	0.5278	0.5282	0.5285	0.5288	0.5292	0.5295	0.5299	0.5302	0.5306	0.5309
1.240	0.5313	0.5316	0.5319	0.5323	0.5326	0.5330	0.5333	0.5336	0.5340	0.5343
1.250	0.5347	0.5350	0.5353	0.5357	0.5360	0.5363	0.5367	0.5370	0.5374	0.5377
1.260	0.5380	0.5383	0.5387	0.5390	0.5394	0.5397	0.5400	0.5404	0.5407	0.5411
1.270	0.5414	0.5417	0.5421	0.5424	0.5427	0.5431	0.5434	0.5437	0.5441	0.5444
1.280	0.5447	0.5451	0.5454	0.5457	0.5461	0.5464	0.5467	0.5471	0.5474	0.5477

Appendix 2

To Find the Area of the Fractional Plastic Zone

In Fig. 72 we have two co-axial circles with centres at O and O'. The chord AB bisects the line OO'. Let OO' = 2h. Let the radius of the circle be a.

Area of the segment ACB

OP = h and OC = a

$$\begin{aligned} \text{Area} &= 2 \int_h^a (a^2-x^2)^{\frac{1}{2}} dx = 2 \int_0^a (a^2-x^2)^{\frac{1}{2}} dx - 2 \int_0^h (a^2-x^2)^{\frac{1}{2}} dx \\ &= 2 \left(\frac{\pi a^2}{4} \right) - 2 \int_0^h (a^2-x^2)^{\frac{1}{2}} dx \quad h < a \end{aligned}$$

To evaluate $\int_0^h (a^2-x^2)^{\frac{1}{2}} dx$, let $x = a \sin\theta$
 $dx = a \cos\theta d\theta$

$$\begin{aligned} \int_0^h (a^2-x^2)^{\frac{1}{2}} dx &= \int_0^{\sin^{-1} \frac{h}{a}} a^2 \cos^2 \theta \cdot d\theta \\ &= \frac{a^2}{2} \int_0^{\sin^{-1} \frac{h}{a}} (1 + \cos 2\theta) d\theta \\ &= \frac{a^2}{2} \left[\theta + \frac{1}{2} \sin 2\theta \right]_0^{\sin^{-1} \frac{h}{a}} \\ &= \frac{a^2}{2} \left[\theta + \sin\theta \cdot \cos\theta \right]_0^{\sin^{-1} \frac{h}{a}} \\ &= \frac{a^2}{2} \left[\theta + \sin\theta \sqrt{1-\sin^2\theta} \right]_0^{\sin^{-1} \frac{h}{a}} \\ &= \frac{a^2}{2} \left[\sin^{-1} \frac{h}{a} + \frac{h}{a} \left\{ 1 - \frac{h^2}{a^2} \right\}^{\frac{1}{2}} \right] \end{aligned}$$

Area of segment ACB

$$= \frac{\pi a^2}{2} - a^2 \left[\sin^{-1} \frac{h}{a} + \frac{h}{a} \left\{ 1 - \frac{h^2}{a^2} \right\}^{\frac{1}{2}} \right]$$

Area of the shaded region i. e. A_F

$$= \pi a^2 - 2 \left[\frac{\pi a^2}{2} - a^2 \left\{ \sin^{-1} \frac{h}{a} + \frac{h}{a} \left(1 - \frac{h^2}{a^2} \right)^{\frac{1}{2}} \right\} \right]$$

$$= 2a^2 \left[\sin^{-1} \frac{h}{a} + \frac{h}{a} \left(1 - \frac{h^2}{a^2} \right)^{\frac{1}{2}} \right]$$

If we replace a by r_y and h by $\frac{\Delta a}{2}$, then we get

$$A_F = 2r_y^2 \left[\sin^{-1} \frac{\Delta a}{2r_y} + \frac{\Delta a}{2r_y} \left\{ 1 - \frac{(\Delta a)^2}{4r_y^2} \right\}^{\frac{1}{2}} \right]$$

The above expression gives the area of the fractional plastic zone for the loading cases where K_{\max} is held constant.

BIBLIOGRAPHY

1. Gurney, T.R. Fatigue of Welded Structure, Cambridge Univ. Press, 1968
2. Griffith, A.A. Phil. Trans. Roy. Soc. (London), Series A, 221, 1920 pp 163-198
3. Orowan, E. Rep. on Progress in Physics, 12, 1949, pp 185-232
4. Irwin, G.R. Encyclopedia of Physics, Vol. VI, Springer, Heidelberg, 1958, pp 551-590
5. Irwin, G.R. Fracture of Engg. Materials, A.S.M., 1959, pp 211-230
6. Paris, P.C. and Sih, G.C. Fracture Toughness Testing and its Application, ASTM STP 381, 1965
7. Brown, W.F. and Srawley, J.E. ASTM STP 410, Plane Strain Crack Toughness Testing of High Strength Metallic Materials, 1966
8. Irwin, G.R. and Kies, J.A. Welding Journal, 33, 1954, pp 193s-198s
9. Sullivan, A.M. Mat. Res. and Stand., 4, 1964, pp 20-24
10. Winters, R.F. M.Sc. Thesis, Dept. of Met., University of Aston in Birmingham, 1969
11. Johnson, H.H. and Paris, P.C. Engg. Fract. Mech., 1, 1968, pp 3-45
12. Wells, A.A. Crack Prop. Symp., Cranefield, 1, 1961, pp 210-230
13. Cottrell, A.H. 'Steels for Reactor Circuits', I.S.I., 1960, pp 281-296
14. Wells, A.A. British Weld. Journ., 10, 1963, pp 563-570
15. Wells, A.A. Engg. Fract. Mech., 1, No. 3, 1969, p399

16. Terry, P. Ph.D Thesis, University of Aston in Birmingham, 1972
17. Elliot, D., Walker, E.F. and May, M.J. Practical Application of Fract. Mech. to Pressure Vessel Technology, The Inst. of Mech. Engrs. Conf., 1971, pp 217-224
18. Rice, J.R. Fatigue Crack Propagation, ASTM STP 415, 1967, pp 247-311
19. Irwin, G.R. Engg. Fract. Mech., 1, No. 2, 1968, pp 241-257
20. Paris, P.C. Proc. of 10th Sagamore Army Conf., 1964, Syracuse Univ. Press. p107
21. Frost, N.E. and Dugdale, D.S. J. Mech. & Phys. of Solids, 6, 1958, pp 92-110
22. McClintock, F.A. Fracture of Solids, 1962, Eds. Drucker, D.C. & Gilman, J.J. pp 65-102
23. Forsyth, P.J.E. Acta Met., 11, 1963, pp 703-716
24. Plumbridge, W.J. and Ryder, D.A. Metals & Materials, 3, No. 8, 1969, pp 119-142
25. Yokobori, T., Nanbu, M. and Takeuchi, N. Rep. Res. Inst. Strength of Materials, Tohoka University, Japan, 5, No. 1, 1969, p 1
26. Forsyth, P.J.E. Crack Prop. Symp., Cranefield, 1, 1961, p 75
27. Laird, C. and Smith, G.C. Phil. Mag., 8, 1963, pp 1945-1963
28. Laird, C. Fatigue Crack Propagation, ASTM STP 415, 1967, pp 131-180
29. Schijve, J. Fatigue Crack Propagation, ASTM STP 415, 1967, pp 415-459
30. Broek, D. Engg. Fract. Mech., 1, 1970, pp 691-695
31. Pelloux, R.M.N. Engg. Fract. Mech., 1, 1970, pp 697-704

32. Tomkins, B. Phil. Mag., 18, 1968, pp 1041-1066
33. Forsyth, P.J.E. and Metallurgia, 63, 1961, p 117
Ryder, D.A.
34. Christensen, R.H. and Fatigue Crack Prop. ASTM STP 415, 1967,
Harmon, M.B. pp 5-24
35. Paris, P.C. and Trans. A.S.M.E., Ser. D., 85, No. 4,
Erdogan, F. Dec. 1963, pp 528-534
36. Head, A.K. Phyl. Mag., 44, 1953, pp 925-938
37. Frost, N.E., Holden, J. Crack Prop. Symp., Cranefield, 1, 1961
and Phillips, C.E. pp 166-179
38. Liu, H.W. Trans. A.S.M.E., 1963, Ser. D., 85, pp 116-122
39. Hardrath, H.F. and Crack Prop. Symp., Cranefield, 1, 1961,
McEvily, A.J. p 231
40. Miller, G.A. Trans. ASM, 61, 1968, pp 442-448
41. Clark, W.G. (Jr) Metal Progress, 79, 1970, pp 81-86
42. Forman, R.G., Trans. A.S.M.E., Ser. D., 89, 1967, p 459
Kearney, V.E. and
Engle, R.M.
43. Hartman, A. and Engg. Fract. Mech., 1, 1970, No. 4.
Schijve, J. pp 615-631
44. Pearson, S. Engg. Fract. Mech., 4, No. 1, 1972, pp 9-24
45. Heald, P.T., Mat. Sci. Engg., 10, 1972, p 235
Lindley, T.C. and
Richards, C.E.
46. Arad, S., Radon, J.C. J. Mech. Engg. Sci., 13, No. 2, 1971,
and Culver, L.E. pp 75-81
47. Roberts, R. and Trans. A.S.M.E., Ser. D., 89, 1967,
Erdogan, F. pp 885-892
48. Klensil, M. and Engg. Fract. Mech., 4, 1972, pp 77-92
Lukas, P.

49. Cooke, R. J. and Beevers, C.J. 'The Effect of Load Ratio on the Stresses for Fatigue Crack Growth in Medium Carbon Steel', Research Report, Met. Dept., University of Birmingham, 1972
50. Richards, C.E. and Lindley, T.C. Engg. Fract. Mech., 4, 1972, pp 951-978
51. Dover, W.D. Engg. Fract. Mech., 5, 1973, pp 11-21
52. Frost, N.E. and Denton, K. NEL Report No. 260, 1966
53. Frost, N.E. and Greenan, A.F. J. Mech. Engg. Sci., 12, 1970, pp 159-168
54. Gurney, T.R. Metal Construction, British Welding Journal, 1, 1969, No. 2, pp 91-96
55. Newman, J.C. Fatigue Crack Prop., ASTM STP 415, p 380
56. Hudson, C.M. and Scardina, J.T. Engg. Fract. Mech., 1, 1969, pp 429-426
57. Dahlberg, E.P. Trans. ASM Qut., 58, 1965, p 46
58. Ryder, J.T. and Gallahar, J.P. Trans. A.S.M.E., Ser. D., 92, No. 2, 1970 pp 121-125
59. Yokobori et al Rep. Res. Inst. Strength & Fract. of Mat., Tohoko University, Japan, 5, 1969, pp 25-33
60. Carman, C.M. and Katlin, J.M. Trans. A.S.M.E., Ser. D., 88, Dec. 1966, pp 792-800
61. Barsom, J.M. Trans. A.S.M.E., Ser. B., 93, No. 4, Nov. 1971, pp 1190-1196
62. Inckle, A.E. Ph.D Thesis, 1971, University of Aston in Birmingham
63. Kawasaki, T. et al Rep. Res. Inst. Strength & Fract. of Materials, Tohoko University, Japan, 6, No. 1, 1970, pp 25-47

64. Wei, R.P. Trans. ASM, 60, 1967, p 279
65. Griffiths, J.R., Met. Sc. J., 5, 1971, p 150
Mogford, I.L. and
Richards, C.E.
66. Crooker, T.W., Trans. ASM, 61, 1968, p 568
Cooley, L.A., Lange, E.A.
and Freed, C.N.
67. Heiser, F.A. and Trans. A.S.M.E., Ser. D., 93, No.2,
Hertzberg, R.W. June 1971, pp 211-217
68. Broek, D. Int. Conf. on Fracture, Brighton, 1969, p 754
69. Kershaw, J. and Int. J. Fract. Mech., 7, No. 3, Sept. 1971,
Liu, H.W. pp 269-276
70. Pelloux, R.M.N. Trans. ASM, 57, No. 2, 1964, pp 511-518
71. Gerberich, W.W. and Trans. ASM, 65, 1968, pp 184-187
Hartbower, C.E.
72. Miner, M.A. Trans. A.S.M.E., 67, 1945, pp A159-164
73. Swanson, S.R. Mat. Res. Stand., 8, No. 4, 1968, pp 10-44
74. Smith, S.H. Structural Fatigue in Aircraft, ASTM STP 404
1966, pp 74-100
75. Schijve, J. Symp. Fatigue Aircraft Struc., ASTM STP 338,
Oct. 1962, p 193
76. Schijve, J. Current Aeronautical Fatigue Problems, Symp.
in Rome, 1963, Eds., J. Schijve et al, pp 403-428
77. Marco, S.M. and Trans. A.S.M.E., 76, No. 4, 1954, p 627
Starkey, W.L.
78. Christensen, R.H. Crack Prop. Symp., Cranefield, 2, 1961, pp 326-374
79. Hardrath, H.F. and Crack Prop. Symp., Cranefield, 1, 1961,
McEvily, A.J. pp 231-270
80. Donaldson, D.R. and Crack Prop. Symp., Cranefield, 2, 1961,
Anderson, W.E. pp 375-441

81. Schijve, J. and Broek, D. Aircraft Engg., Nov. 1962, pp 314-316
82. McMillan, J.C. and Pelloux, R.M.N. Fatigue Crack Propagation, ASTM STP 415, 1967, pp 505-535
83. Morrow, J.D., Wetzell, R.M. and Topper, T.H. Effects of Environment & Complex Load History on Fatigue Life, ASTM STP 462, 1970 pp 74-91
84. Breyan, W. Effects of Environment & Complex Load History on Fatigue Life, ASTM STP 462, 1970 pp 127-166
85. Impellizzeri, L.F. Effects of Environment & Complex Load History on Fatigue Life, ASTM STP 462, 1970 pp 40-68
86. Swanson, S.R., Cicci, F. and Hoppe, W. Fatigue Crack Propagation, ASTM STP 415, 1967, pp 312-362
87. Schijve, J., Jacobs, F.A. and Tromp, P.J. NLR-TR 68117U, The Netherlands, 1968
88. Elber, W. Engg. Fract. Mech., 2, No. 1, 1970, pp 37-45
89. Elber, W. Damage Tolerance in Aircraft Structure, ASTM STP 486, 1971, pp 230-242
90. Adams, N.J.I. Engg. Fract. Mech., 4, 1972, pp 543-554
91. Corbly, D.M. and Packman, P.F. Engg. Fract. Mech., 5, 1973, pp 479-497
92. Wheeler, O.E. Trans. A.S.M.E., Ser. D., March 1972, pp 181-186
93. Von Euv, E.F.J., Hertzberg, R.W. and Richard, R. Stress Analysis and Growth of Cracks, ASTM STP 513, 1972, pp 230-259
94. Dowling, N.E. J. of Materials, JMLSA, 7, No. 1, 1972, pp 71-87
95. Crooker, T.W. NRL Report 7347

96. Barnby, J.T. Welding & Metal Fab., February 1969, pp 71-75
97. Melcon, M.A. and Current Aeronautical Fatigue Problems, Symp.
McCulloch, A.J. in Rome, 1963, Eds. J. Schijve et al, pp 347-401
98. B.S.I. Methods for Plane Strain Fracture Toughness
Testing, DD3, 1971
99. Srawley, J.E. and ASTM STP 381, pp 133-198, 1965
Brown, W.F.
100. Jack, A.R. and CEGB Report SSD/MID/R/215/70, July 1970
Yeldham, D.E.
101. Ritchie, R.O. Res. Report, Met. Dept., University of
Cambridge, 1972
102. Gilby, D.M. and R.A.E. Tech. Rep. No. 66402, Dec. 1966
Pearson, S.
103. BISRA Open Report, MG/EB/312/67
104. BISRA Open Report, MG/E/307/67
105. Ritchie, R.O. The Practical Implications of Fracture
Mechanics, The Institution of Metallurgists,
Spring Meeting, 1973, pp 73-87
106. Dowse, K.R. and Metal Trans., 2, Feb. 1971, p 599
Richards, C.E.
107. Jonas, O. and Int. J. Fract. Mech., 7, 1971, p 116
Wei, R.P.
108. Tetelman, A.S. and Fracture of Structural Materials, Wiley, 1967
McEvily, A.J.
109. Robinson, J.L. and 'The Effects of Load Ratio, Interstitial Con-
tent & Grain Size on Low Stress Fatigue Crack
Propagation in α -titanium', Research Report,
University of Birmingham, May, 1973
110. Williams, H.D. and Phil. Mag., 13, No. 124, 1966, p 835
Smith, G.C.
111. Pisarski, H.G. Private Communication